

TRANSITION METAL COMPLEXES AS PROBES FOR
HIGHER-ORDER STRUCTURE IN RNA

Thesis by
Christine S. Chow

In Partial Fulfillment of the Requirements
for the Degree of
Doctor of Philosophy

California Institute of Technology

Pasadena, California

1992

(Defended January 20, 1992)

ACKNOWLEDGEMENTS

I wish to express my sincere thanks to my thesis advisor, Jacqueline K. Barton, for her constant enthusiasm and support throughout my five years as a graduate student.

I am indebted to a number of collaborators, particularly Paul Huber and Olke Uhlenbeck, for many helpful discussions. Much of the work presented here would not have been possible without the help of their coworkers, Kevin Hartmann, Steve Rawlings, and Linda Behlen, who supplied me with endless amounts of RNA. I would like to thank Professor N. J. Turro, Vijay Kumar, and Gary Jaycox for assistance with the lifetime studies.

I would like to thank all of the Barton group members, past and present, who have contributed to the completion of this work. Special thanks go to Niranjan Sardesai for reviewing this manuscript. In addition, I would like to thank Eric and Maureen Long, Anna Pyle, Sally White, Tina Voulgaris, Joe Dougherty, and Richard Hartshorn for their advice, friendship, and many unforgettable times. I would like to acknowledge Mike Wong for his hard work and enthusiasm as a summer student at Columbia. Thanks go to the rest of the Barton group: Houg-Yau Mei, Mindy Kirshenbaum, Jeff Bocarsly, Ellen Levy, Alan Friedman, Takashi Morii, Inho Lee, Michael Pustilnik, Louis Kuo, Kiyoshi Uchida, Ayesha Sitlani, Donna Campisi, Tom Shields, Sheila David, Scott Klakamp, Cathy Murphy, Debbie Brown, Susanne Lin, Yonchu Jenkins, Ai Ching Lim, Achim Krotz, Jim Finholt, and Kimberly Waldron. Also many, many thanks go to Mo Rentá for all of her help.

I would like to acknowledge my friends at Columbia and Caltech who have contributed personally to my stay in graduate school. In particular, I thank Adam Gilbert for being a fantastic roommate; Fred Youngs for being a great friend and getting me through my first year, as well as teaching me the joys of skiing; Cindy Jenks for sharing

many long nights with me in the chemistry library at Columbia; William Jenks, Jane Pachter, and Hannah Sevia for moral support and bike rides in Central Park; the Thursday night crew (especially Joe Dougherty, Ric Z., Todd Link, and Paddy Steel) for nights we'd probably like to forget; the very dedicated soccer players for getting me out of bed on Saturday mornings; and the sushi crowd (Kurt, John, Carola, Susanne, and Jon) for making sure I had my fill of raw fish. Thanks go to Harry Gray and Ged Parkin for encouraging me to come to Caltech and to everyone at Caltech who helped me adjust to the move across the country, particularly members of the Lewis group and CNS Department. Finally, I wish to thank Kurt Fleischer and Bill Connick for making life in general a lot more pleasant.

Very special thanks go to Xenia Beebe, Alex Rabinovitch, Dan Rosner, and Kerry Burke for their never-ending support and friendship throughout the years and to my mother, Sharon Dennis, who deserves a lot of credit for her constant encouragement and understanding.

I am grateful to the Ralph M. Parsons Foundation for fellowship support.

ABSTRACT

A series of transition metal complexes were employed to examine higher-order structure in ribonucleic acids. Our results indicate that the complexes $\text{Ru}(\text{phen})_3^{2+}$, $\text{Ru}(\text{TMP})_3^{2+}$, $\text{Rh}(\text{TMP})_3^{3+}$, $\text{Rh}(\text{phen})_2\text{phi}^{3+}$, $\text{Rh}(\text{phi})_2\text{bpy}^{3+}$, and $\text{Rh}(\text{DIP})_3^{3+}$ (phen = 1,10-phenanthroline; TMP = 3,4,7,8,-tetramethyl-1,10-phenanthroline; phi = 9,10-phenanthrenequinone diimine; bpy = bipyridyl; DIP = 4,7-diphenyl-1,10-phenanthroline) have different affinities for tRNA and bind RNA by several different modes of interaction, as shown through a variety of biophysical analyses. These differences in binding have been attributed to the different shapes of the metal complexes. Photolysis of the metal complexes promotes cleavage of native, structured RNA at diverse and novel sites with comparable efficiency and analogous product formation as found with cleavage of double-stranded DNA. As on DNA, RNA strand scission promoted by the complexes of rhodium(III) occurs through an oxidative pathway with the sugar moiety as the target. Reactions with the complexes of ruthenium(II) are consistent with mediation by singlet oxygen with the nucleic acid base as the target. The site selectivity associated with cleavage appears to be based upon the different binding properties and therefore the molecular shapes of the complexes. $\text{Ru}(\text{TMP})_3^{3+}$ cleaves at a subset of solvent accessible sites cleaved by $\text{Ru}(\text{phen})_3^{2+}$. Different sites of cleavage on tRNA are apparent with the rhodium complexes, $\text{Rh}(\text{phen})_2\text{phi}^{3+}$, $\text{Rh}(\text{phi})_2\text{bpy}^{3+}$, and $\text{Rh}(\text{DIP})_3^{3+}$, while $\text{Rh}(\text{TMP})_3^{3+}$ does not promote strand scission of RNA. In particular, $\text{Rh}(\text{phen})_2\text{phi}^{3+}$ targets sites of triple-base interaction, D-T Ψ C loop interactions, and helix-loop junctions in tRNA, where the major groove is open and accessible. $\text{Rh}(\text{DIP})_3^{3+}$ targets RNA loop structures and G-U mismatches that occur within an RNA double-helix. These shape-selective probes, which promote strand scission of tRNA at unique sites, have also been applied to probe mutant tRNAs and to delineate the structure of 5S rRNA. This study demonstrates that small molecules can recognize distinct structures along an RNA strand and suggests that these structures may be utilized for specific recognition by proteins.

TABLE OF CONTENTS

	page
ACKNOWLEDGEMENTS	ii
ABSTRACT	iv
TABLE OF CONTENTS	v
LIST OF FIGURES	x
LIST OF SCHEMES	xiii
LIST OF TABLES	xiii
Chapter 1: Introduction: Features of RNA Tertiary Structure and the Development of New Probes for Higher-Order Structure in RNA	1
1.1. Introduction	1
1.2. Primary and Secondary Structural Features of RNA	2
1.3. Tertiary Structural Features of RNA	6
1.4. Structural Characterization of RNAs: Evidence for Higher-Order Structure in RNA	6
1.5. Biological and Chemical Probes for RNA Structure	8
1.5.1. Biological Probes: Ribonucleases.	9
1.5.2. Chemical Probes.	9
1.6. Transition Metal Complexes as Potential Probes for RNA Structure	11
References	15
Chapter 2: Biophysical Studies of Tris(phenanthroline) and Phenanthrenequinone Diimine Complexes of Ru(II) and Rh(III) Bound to tRNA	18
2.1. Introduction	18
2.2. Experimental	20

2.2.1. Synthesis	20
2.2.2. Methods	22
2.3. Results	26
2.3.1. Synthesis and Characterization	26
2.3.2. Equilibrium Dialysis of Ru(II) Polypyridyl Complexes Against tRNA	31
2.3.3. Equilibrium Dialysis of Rh(III) Complexes Against tRNA	39
2.3.4. Absorption Titrations of Ru(II) and Rh(III) Complexes with tRNA	43
2.3.5. Steady-State Luminescence, Time-Resolved Emission Lifetime and Luminescence-Quenching Measurements of Ru(II) Complexes Bound to tRNA	49
2.4. Discussion	57
References	61
Chapter 3: Shape-Selective Cleavage of tRNA by Tris(phenanthroline) and Phenanthrenequinone Diimine Complexes of Ru(II) and Rh(III)	63
3.1. Introduction	63
3.2. Experimental	65
3.2.1. Methods for Photocleavage by Rhodium and Ruthenium Complexes	65
3.2.2. Methods for Analysis of the RNA Cleavage Products	68
3.3. Results	69
3.3.1. Photocleavage of tRNA by Ru(II) and Rh(III) Complexes	69
3.3.2. Efficiency of Cleavage and Cleavage as a Function of Wavelength and Metal Concentration	76
3.3.3. Cleavage Product Analysis by Gel Electrophoresis and HPLC Analysis	81

3.3.4. High-Resolution Mapping of Cleavage Sites by Ru(II) and Rh(III) Complexes Along a tRNA Fragment	88
3.3.5. Competition Studies of Ru(II) and Rh(III) Mixed Ligand Complexes	92
3.4. Discussion	93
References	102
Chapter 4: Recognition of Tertiary Structures in tRNA by Rh(phen) ₂ phi ³⁺ : Tuning the Recognition with Mutant and Structurally Modified tRNAs	104
4.1. Introduction	104
4.2. Experimental	106
4.3. Results	108
4.3.1. Cleavage of Native tRNAs	108
4.3.2. Cleavage of tRNA Transcripts	123
4.3.3. Cleavage of a Modified tRNA	136
4.4. Discussion	139
References	142
Chapter 5: Applications of Rh(phen) ₂ phi ³⁺ as a Probe for RNA Tertiary Structure: Delineation of Structural Domains in 5S rRNA	144
5.1. Introduction	144
5.2. Experimental	146
5.3. Results	149
5.3.1. Site-Selective Cleavage of 5S rRNA by Rh(phen) ₂ phi ³⁺	149

5.3.2.	Cleavage of a Truncated Fragment of Xenopus Oocyte 5S rRNA (3' Δ 12-5' Δ 64) by Rh(phen) ₂ phi ³⁺	155
5.3.3.	Cleavage of 5S rRNA Mutants by Rh(phen) ₂ phi ³⁺	156
5.4.	Discussion	164
5.4.1.	Recognition Characteristics of Rh(phen) ₂ phi ³⁺ : Support of the Y-Shape Structure	164
5.4.2.	Loop Structures in 5S rRNA	165
5.4.3.	Helix Structures in 5S rRNA	166
5.4.4.	Structural Analysis of the 5S rRNA Loop Region: A Comparison of Chemical Probing and Rh(phen) ₂ phi ³⁺ Cleavage	167
5.4.5.	Implications for Protein Binding to 5S rRNA	170
	References	172
Chapter 6:	Recognition of Unusual RNA Structures by Rh(DIP) ₃ ³⁺	176
6.1.	Introduction	176
6.2.	Experimental	178
6.3.	Results	181
6.3.1.	Site-Selective Cleavage of Native tRNAs by Rh(DIP) ₃ ³⁺	181
6.3.2.	Cleavage of Microhelix RNAs by Rh(DIP) ₃ ³⁺	184
6.3.3.	Cleavage of 5S rRNAs by Rh(DIP) ₃ ³⁺	185
6.4.	Discussion	185
6.4.1.	Recognition of Loop Structures in RNA by Rh(DIP) ₃ ³⁺	191
6.4.2.	Recognition of G-U Mismatches in RNA by Rh(DIP) ₃ ³⁺	192
6.4.3.	Implications for Protein Binding	197

References	198
Chapter 7: Conclusions and Future Directions	200

LIST OF FIGURES

	page
Chapter 1:	
1.1. The numbering system for the bases and ribose.	3
1.2. A selection of modified nucleosides from transfer RNA.	4
1.3. A generalized representation of tRNA in the "cloverleaf" form.	5
1.4. The Λ - and Δ -enantiomers of the parent metal complex, tris(1,10-phenanthroline)ruthenium(II).	12
Chapter 2:	
2.1. Structures of the metal complexes studied.	19
2.2. 200 MHz ^1H NMR spectra of tris(3,4,7,8-tetramethyl-1,10-phenanthroline) complexes of rhodium(III) in D_2O and ruthenium(II) in CDCl_3 .	27
2.3. The UV/visible spectrum of tris(3,4,7,8-tetramethyl-1,10-phenanthroline) rhodium(III), $\text{Rh}(\text{TMP})_3^{3+}$, in H_2O .	29
2.4. Binding of $\text{Ru}(\text{TMP})_3^{2+}$ and $\text{Ru}(\text{phen})_3^{2+}$ to native $\text{tRNA}^{\text{bulk}}$ as determined by equilibrium dialysis.	32
2.5. Binding of $\text{Ru}(\text{TMP})_3^{2+}$ to synthetic, double-stranded polynucleotides and native $\text{tRNA}^{\text{bulk}}$ as determined by equilibrium dialysis.	33
2.6. Binding of $\text{Ru}(\text{TMP})_3^{2+}$ to native $\text{tRNA}^{\text{bulk}}$ under varying salt and temperature conditions as determined by equilibrium dialysis.	34
2.7. Circular dichroism spectrum obtained after the dialysis of $\text{tRNA}^{\text{bulk}}$ against <i>rac</i> - $\text{Ru}(\text{TMP})_3^{2+}$.	37
2.8. Scatchard plots of $\text{Rh}(\text{phen})_2\text{phi}^{3+}$ and $\text{Rh}(\text{phi})_2\text{bpy}^{3+}$ bound to native $\text{tRNA}^{\text{bulk}}$.	40
2.9. Scatchard plot of $\text{Rh}(\text{TMP})_3^{3+}$ bound to native $\text{tRNA}^{\text{bulk}}$.	44
2.10. Absorption hypochromism of $\text{Rh}(\text{phen})_2\text{phi}^{3+}$ in the presence of yeast tRNA^{Phe} .	48
2.11. Absorption titration data of $\text{Rh}(\text{phen})_2\text{phi}^{3+}$ binding to yeast tRNA^{Phe} .	50

2.12.	Luminescence quenching of $\text{Ru}(\text{TMP})_3^{2+}$ with increasing concentrations of $\text{Fe}(\text{CN})_6^{4-}$.	54
Chapter 3:		
3.1.	Cleavage of ^{32}P 3'-end-labeled yeast tRNA^{Phe} by $\text{Ru}(\text{TMP})_3^{2+}$ and $\text{Ru}(\text{phen})_3^{2+}$.	70
3.2.	Cleavage of ^{32}P 3'-end-labeled yeast tRNA^{Phe} by $\text{Rh}(\text{phen})_2\text{phi}^{3+}$ and $\text{Rh}(\text{DIP})_3^{3+}$.	72
3.3.	Cleavage of ^{32}P 3'-end-labeled yeast tRNA^{Phe} by $\text{Rh}(\text{phi})_2\text{bpy}^{3+}$.	74
3.4.	Cleavage of ^{32}P 3'-end-labeled yeast tRNA^{Phe} and a 5'-end-labeled <i>Pvu</i> II- <i>Hind</i> III 141 base-pair fragment from pUC19 by $\text{Rh}(\text{phen})_2\text{phi}^{3+}$.	79
3.5.	HPLC chromatograms of tRNA^{Phe} cleavage products after irradiation in the presence of $\text{Ru}(\text{TMP})_3^{2+}$ and $\text{Ru}(\text{phen})_3^{2+}$.	82
3.6.	HPLC analysis of nucleic acid bases produced with RNA degradation by $\text{Rh}(\text{phen})_2\text{phi}^{3+}$.	84
3.7.	End-product analysis of cleavage of ^{32}P 3'-end-labeled (A) and 5'-end-labeled (B) yeast tRNA^{Phe} by $\text{Rh}(\text{phen})_2\text{phi}^{3+}$.	86
3.8.	Cleavage data for the metal complexes mapped onto the three-dimensional structure of yeast tRNA^{Phe} .	89
Chapter 4:		
4.1.	Schematic illustration of $\text{Rh}(\text{phen})_2\text{phi}^{3+}$.	105
4.2.	Cleavage of ^{32}P 3'-end-labeled native yeast tRNA^{Phe} , the yeast tRNA^{Phe} transcript, G19C mutant, and yeast tRNA^{Asp} by $\text{Rh}(\text{phen})_2\text{phi}^{3+}$.	109
4.3.	$\text{Rh}(\text{phen})_2\text{phi}^{3+}$ cleavage sites on yeast tRNA^{Phe} and the unmodified tRNA^{Phe} transcript mapped on a ribbon diagram adapted from the crystal structure of tRNA^{Phe} .	111
4.4.	Tertiary interactions and cleavage data for $\text{Rh}(\text{phen})_2\text{phi}^{3+}$ are shown in a computer graphic representation of the crystal structures of yeast tRNA^{Phe} and tRNA^{Asp} .	113
4.5.	Illustrations of the basis for recognition of the triply bonded bases by $\text{Rh}(\text{phen})_2\text{phi}^{3+}$.	116

4.6.	Mapped sites of cleavage on the TΨC loop mutants G19C and G18A-U55C.	127
4.7.	Cleavage of several ^{32}P 3'-end-labeled tRNA ^{Phe} mutants by Rh(phen) ₂ phi ³⁺ .	131
4.8.	Mapped sites of cleavage on the triple-base mutants G22A-C13U, G46A-G22A-C13U, G45U, and G10C-C25G.	133
4.9.	Densitometer scans of Rh(phen) ₂ phi ³⁺ cleavage of native tRNA ^{Phe} and the chemically modified tRNA ^{Phe} .	137
Chapter 5:		
5.1.	Cleavage of ^{32}P 3'-end-labeled <i>Xenopus</i> oocyte 5S rRNA and a truncated version by Rh(phen) ₂ phi ³⁺ .	150
5.2.	Schematic illustration of the secondary structure of <i>Xenopus</i> 5S rRNA with designations of the sites of cleavage by Rh(phen) ₂ phi ³⁺ .	153
5.3.	Cleavage of mutants of ^{32}P 3'-end-labeled <i>Xenopus</i> oocyte 5S rRNA by Rh(phen) ₂ phi ³⁺ .	157
5.4.	Schematic illustrations of Rh(phen) ₂ phi ³⁺ cleavage on <i>Xenopus</i> 5S rRNA mutants.	160
Chapter 6:		
6.1.	Schematic illustration of Rh(DIP) ₃ ³⁺ .	177
6.2.	Cleavage of ^{32}P 3'-end-labeled yeast tRNA ^{Phe} , G4:U69 microhelix ^{Phe} , U4:G69 microhelix ^{Phe} , and yeast tRNA ^{Asp} by Rh(DIP) ₃ ³⁺ .	182
6.3.	Cleavage of ^{32}P 3'-end-labeled 5S rRNA from <i>Xenopus</i> oocytes by Rh(DIP) ₃ ³⁺ .	186
6.4.	Schematic illustrations of yeast tRNA ^{Phe} , yeast tRNA ^{Asp} , G4:U69 microhelix ^{Phe} , U4:G69 microhelix ^{Phe} , helix I and helix IV of <i>Xenopus</i> oocyte 5S rRNA, and helix I and helix IV of <i>E. coli</i> 5S rRNA with designations of Rh(DIP) ₃ ³⁺ cleavage sites.	188
6.5.	Stacking of the G4-U69 wobble pair in the middle of the acceptor stem of yeast tRNA ^{Phe} with the G3-C70 base pair and with the A5-U68 base pair.	194

LIST OF SCHEMES

	page
Chapter 3:	
3.1. The proposed mechanism of cleavage by tris(phenanthroline) ruthenium(II) complexes on tRNA.	94
3.2. The proposed mechanism of cleavage by phi complexes of rhodium(III) on tRNA.	97

LIST OF TABLES

	page
Chapter 2:	
2.1. Changes induced in absorbance of metal complexes by the presence of tRNA.	46
2.2. Emission lifetimes of <i>rac</i> -Ru(TMP) ₃ ²⁺ and <i>rac</i> -Ru(phen) ₃ ²⁺ in the presence and absence of tRNA and K ₄ Fe(CN) ₆ ·3H ₂ O.	56
Chapter 3:	
3.1. Optimal conditions for RNA photocleavage by ruthenium(II) and rhodium(III) complexes.	77
Chapter 4:	
4.1. Cleavage of tRNA ^{Phe} mutants by Rh(phen) ₂ phi ³⁺ compared with lead cleavage rates and aminoacylation kinetics.	126
Chapter 5:	
5.1. Cleavage of 5S rRNA mutants by Rh(phen) ₂ phi ³⁺ .	162

Chapter 1:

Introduction: Features of RNA Tertiary Structure and the Development of New Probes for Higher-Order Structure in RNA

1.1. Introduction

It has become clear that the one-dimensional nucleotide sequence of RNA contains an abundance of three-dimensional structural polymorphism. Increasing evidence suggests that the diverse biological functions of RNA, including the storage of genetic information, the transfer of this information into protein synthesis, and the catalysis of biochemical reactions are made possible by RNA tertiary structure. For example, proteins may take advantage of the conformational variability in recognizing specific binding sites along the RNA strand. RNA-binding proteins may distinguish their targets not only through specific hydrogen-bonding interactions with the RNA bases but also through specific electrostatic and van der Waals interactions with the sugar-phosphate backbone and base-pair stacks. Furthermore, through tertiary interactions in the molecule such as unusual bending, looping, stacking, and hydrogen bonding, the RNA bases and backbone can be oriented to interact with different kinds of protein structures. It is therefore important to determine the relationship between the RNA sequence and its three-dimensional structure.

X-ray crystallography has thus far provided the highest resolution views of RNA tertiary structure.¹⁻² Unfortunately, the number of different structures determined by this method has been limited to the small transfer RNAs. In addition, one must consider the effects of crystal packing on these structures, which may differ from the solution structures.³ Therefore, other methods are needed to complement the crystallographic studies. NMR has also provided clues as to the three-dimensional structures of RNA molecules, but has been limited to the study of tRNA⁴ and small RNAs less than 100 nucleotides⁵⁻⁶. Enzymatic and chemical probes of the accessibility of the sugar, base, or

phosphate residues have provided a way to characterize sequence-dependent variations in RNA molecules. However, these studies have been limited in general to secondary structure analysis. Therefore, the development of new probes for RNA tertiary structure is still necessary.

1.2. Primary and Secondary Structural Features of RNA

Depending on their biological functions, naturally occurring RNAs are either completely double-helical like DNA or globular with short double-helical domains connected by single-stranded regions. Transfer RNAs, the best characterized RNAs, are polynucleotide chains 75 to 90 nucleotides long. They contain the four standard bases, as shown in Figure 1.1, but also approximately 10% minor variant nucleotides⁷, some of which are illustrated in Figure 1.2. The primary sequences of the tRNAs are well characterized⁸ and can be arranged in the cloverleaf secondary structure⁹ as depicted in Figure 1.3. The four stem regions of the cloverleaf contain four to seven Watson-Crick base pairs and are called the acceptor, anticodon, D, and T stems. The stems and their adjacent loops are named for their biological function or because their loops contain conserved, modified nucleotides (dihydrouridine(D) and ribothymidine (T)).

Another important consideration of the secondary structure of RNA is that the double-helical regions are generally A-form.^{1,10-11} Compared to B-form DNA, considered to be the most common form, the A-form is also right-handed and contains two distinct and well-defined grooves, termed the major and minor grooves. While the B-form base pairs are stacked in the center of the helix and the average base planes are aligned normal to the helix axis, the A-form bases are pushed outward towards the minor groove direction and are tilted substantially with respect to the helix axis. The resulting helix for an A-form RNA has a very shallow and wide minor groove and a major groove that is pulled deeply into the interior of the molecule. The basis for the A-form conformation is a *C_{3'}-endo*

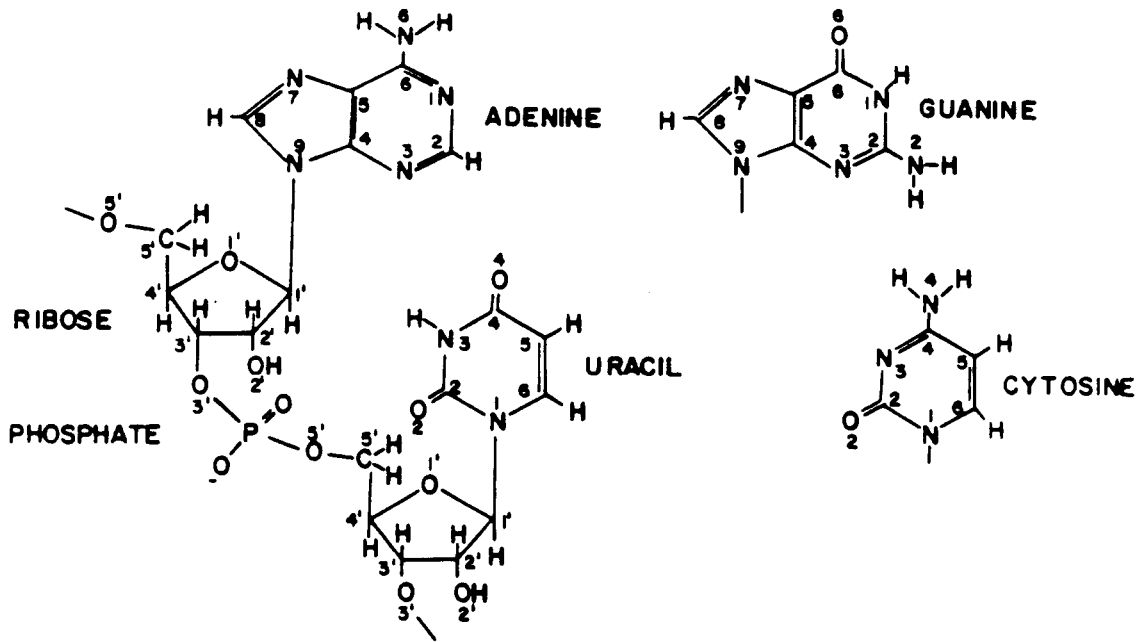
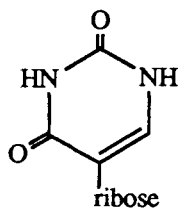
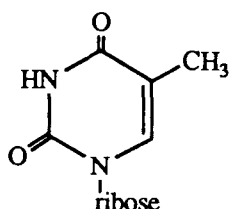
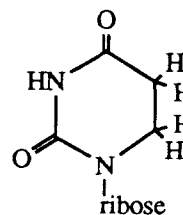


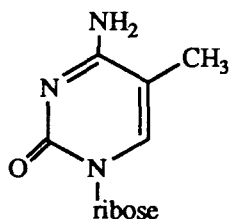
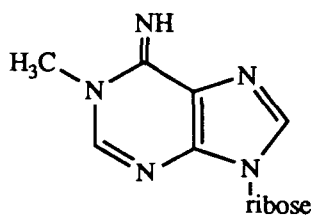
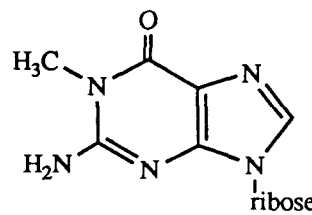
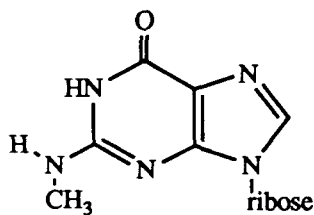
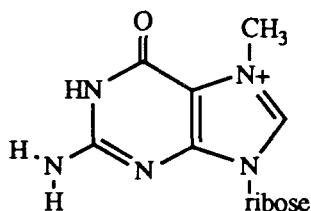
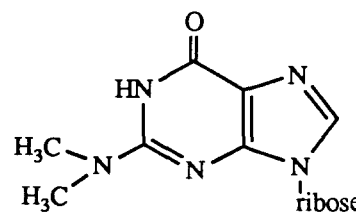
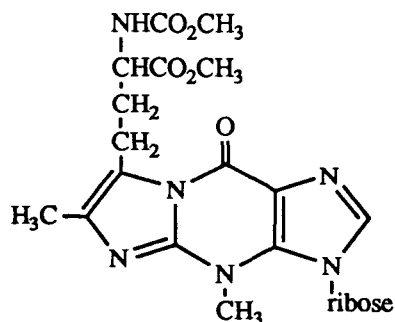
Figure 1.1. The numbering system for the bases and ribose.

1. Pseudouridine (Ψ)

2. Ribothymidine (T)



3. Dihydrouridine (D)

4. 5-Methylcytidine (m^5C)5. 1-Methyladenosine (m^1A)6. 1-Methylguanosine (m^1G)7. N^2 -Methylguanosine (m^2G)8. 7-Methylguanosine (m^7G)9. N^2, N^2 -Dimethylguanosine (m_2^2G)

10. Base "Y"

Figure 1.2. A selection of modified nucleosides from transfer RNA. In the case of base "Y", the ribosyl group is presumably attached to N-9.⁷

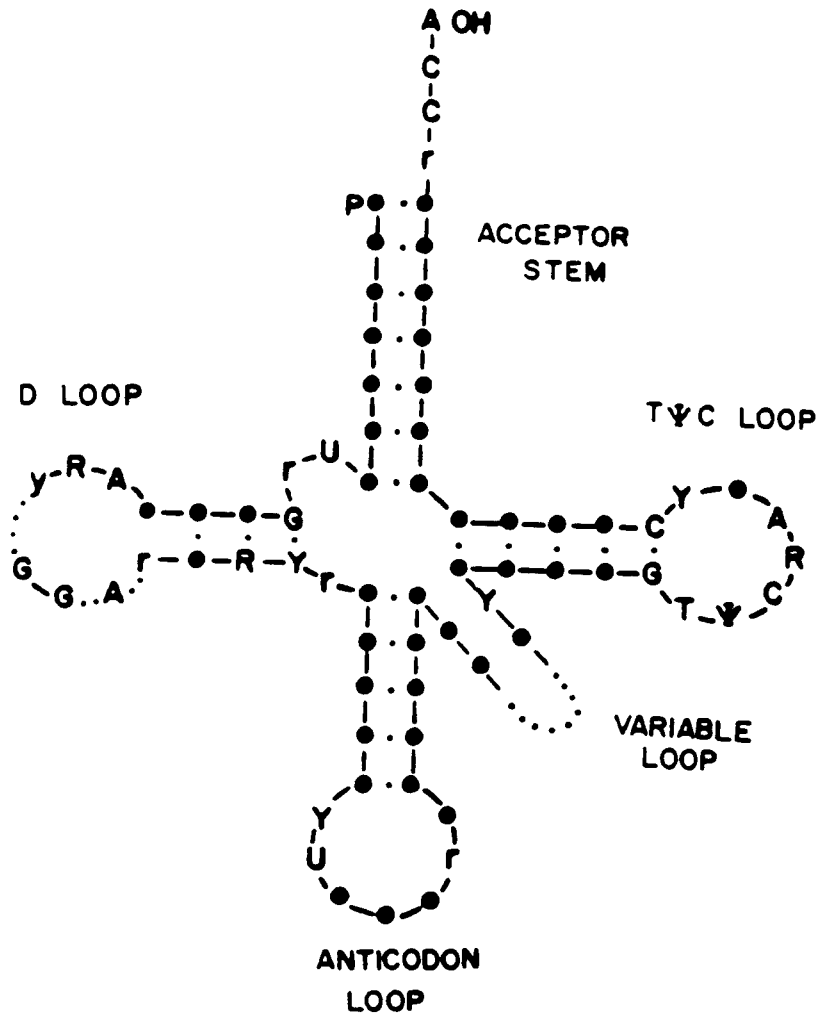


Figure 1.3. A generalized representation of tRNA in the "cloverleaf" form. The bases common to all tRNAs (except initiator tRNAs) are indicated. The symbols are R for conserved purine bases, Y for conserved pyrimidine bases, r for semiconserved purine bases, y for semiconserved pyrimidine bases, p for a 5' terminal phosphate, and OH for a 3' terminal hydroxyl. The large dots indicate variable nucleotides, and the small dots indicate base pairs between nucleotides. The dotted lines are the regions in the chain where the number of nucleotides varies among tRNAs.

sugar pucker, which leads to a phosphate-phosphate distance of $\sim 5.9\text{\AA}$, and stabilization through hydrogen bonding involving the O_2' -hydrogen.

1.3. Tertiary Structural Features of RNA

Tertiary interactions in RNA as defined by Kim et al.^{1a} are taken to mean the hydrogen bonds that occur between the bases (non-Watson-Crick), between bases and the phosphate backbone, and between the backbone residues, except for the interactions in the double-helical stem regions, which are considered secondary interactions. We will also consider mismatched base pairs that occur in double-helical regions to be involved in tertiary interactions. Other tertiary interactions can include stacking of the RNA bases which may contribute to the stability of the molecule. In general, the tertiary interactions serve to stabilize the RNA molecule beyond the secondary hydrogen-bonding interactions found in the purely Watson-Crick double-helical regions.

1.4. Structural Characterization of RNAs: Evidence for Higher-Order Structure in RNA

Evidence for RNA tertiary structure is available from x-ray crystal data of tRNA. Two crystal structures of yeast tRNAs, that of tRNA^{Phe} 1 and of tRNA^{Asp} 2, are known to high resolution. In addition, two crystal structures of RNA synthetases complexed with their cognate tRNAs have been solved recently at high resolution.¹²⁻¹³ The crystal structure analyses have revealed that tRNAs have more or less the same L-shaped configuration. The outer edge of the L corner is occupied by the T loop, while the acceptor and T stems are stacked in a continuous 11-base-pair double helix. Similarly, the anticodon and D stems are stacked on one another, but the helix is kinked by $\sim 26^\circ$ between the two stem axes. In addition to the Watson-Crick base pairs, there are a number of non-standard base pairs in the outer corner of the molecule and base triples, which exist in the

center of the molecule. Extensive base stacking in the center of the molecule is the dominant feature that seems to reinforce the folded structure of the tRNA. The tRNA also exhibits some unusual changes in sugar pucker, phosphate-oxygen torsion angles, and turns or chain reversals in the loops that are stabilized by base-phosphate interactions.

More recently, a crystal structure of an RNA double helix containing non-Watson-Crick base pairs has been determined.¹⁰ The base pairs G-U and U-C were incorporated into a highly regular double helix. Overall, the double helix compared well to a standard A-form RNA helix with only small distortions in the helix. However, small changes were seen locally in which the UUCG-duplex exhibited a widened major groove and variations in the phosphate displacement from the helix axis.

Other evidence for RNA tertiary structure comes from NMR studies. The tRNAs have been studied extensively by NMR.¹⁴ In particular, nuclear Overhauser enhancements (NOEs) can be used to identify the base triples, such as A9-[A23-U12].¹⁵ The amino proton resonance of base A23 in interaction with A9 was seen in the NMR through NOE experiments. This was verified by an additional NOE in the native tRNA from the A23 amino proton to the C₈ proton of A9, as compared to the NOE in a C₈ deuterated sample.

The conformation of an RNA pseudoknot has also been examined by NMR.⁵ The imino protons of the 5'-GCGAUUUCUGACCGCUUUUUUGUCAG-3' RNA were observed, consistent with the formation of two double-helical regions. In addition, NOEs between the imino protons showed that the two stem regions stacked on one another to form a continuous helix. Information regarding the individual nucleotide conformations and internucleotide distances was also available from two-dimensional correlation spectroscopy and two-dimensional NOE spectra to afford a tertiary folding model for this RNA oligonucleotide.

Another three-dimensional structure determined by NMR was the common RNA hairpin, 5'-GGAC(UUCG)GUCC-3'. The tertiary structure for the hairpin was derived

from the interproton distances and scalar coupling constants determined by NMR using distance-geometry calculations.⁶ The G-U base-pair mismatch was important for closing the stem, with the G in a *syn*-conformation. Therefore, the hairpin has a loop of only two nucleotides; both adopt a *C*_{2'}-*endo* sugar pucker. Other tertiary interactions evident from the NMR were a sharp turn in the phosphodiester backbone stabilized by a specific cytosine-phosphate contact and stacking of the cytosine nucleotide on the G-U base pair.

Despite a considerable amount of new information regarding RNA tertiary structures, many elements that stabilize or destabilize RNA structure remain to be identified. The unknown tertiary factors may be related to the long-range interactions such as the triple-base interactions of the type found in tRNA¹⁵, pseudoknot structures⁵, or unusual loop structures such as UUCG⁶. These known structures have revealed the importance of base-phosphate interactions and base-base interactions in the folding and stability of RNA. However, other types of tertiary interactions are likely to exist. Therefore, much work is still needed to determine new types of RNA tertiary structures. Because of the limitations of NMR and x-ray crystallography, other methods are necessary to examine RNA structure in solution.

1.5. Biological and Chemical Probes for RNA Structure

Many laboratories have examined the possibility of using chemical and enzymatic probes to determine RNA structure. These methods have involved the design or applications of molecules that recognize specific RNA structures and promote strand scission of the phosphodiester backbone. Because of the structural complexity of RNA, only a few molecules are known that are capable of recognizing RNA tertiary structure. Although examples exist of sequence-specific recognition of RNA, these reagents generally target single-stranded rather than structured RNA. A few of the chemical and biological

probes of RNA structure have been reviewed by Ehresmann et al.¹⁶; however, more probes have been developed since then and will be discussed below.

1.5.1. Biological Probes: Ribonucleases

The secondary structure of RNA molecules can be probed by nucleases that are specific to single-stranded (S_1 nuclease¹⁷) or double-stranded (RNase V1¹⁸) regions. Unstructured or single-stranded RNA can be probed in a sequence-selective manner with nuclease-DNA hybrids.¹⁹⁻²⁰ For example, a hybrid enzyme ribonuclease S is capable of site-selectively hydrolyzing single-stranded RNA when fused to an oligodeoxyribonucleotide binding site of a defined sequence. Cleavage of the RNA by RNase S, in the absence of the tethered oligonucleotide, occurred relatively nonselectively on a single-stranded RNA substrate. Similarly, tethered oligonucleotides have been used to probe structured RNA in conjunction with RNase H activity.²¹

1.5.2. Chemical Probes

A. Base-Specific Probes. Dimethylsulfate (DMS), diethylpyrocarbonate (DEPC), 1-cyclohexyl-3-(2-morpholinoethyl) carbodiimide metho-p-toluene sulfonate (CMCT), hydrazine, β -ethoxy- α -ketobutyraldehyde (kethoxal), and bisulfite target specific positions on the RNA bases.¹⁶ Therefore, Watson-Crick base pairing as well as non-canonical base interactions can be detected by these compounds. In this manner, the tertiary folding patterns of the RNA molecule can be deduced from studies with these probes. However, these probes cannot give information regarding which nucleotides are base paired with each other or the proximity of the specific nucleotides within the tertiary structure.

The cross-linking reagent 4'-(hydroxy-methyl)-4,5',8-trimethyl psoralen (HMT) has been shown to be useful in mapping base pairing and higher-order structure within

RNA molecules.²² HMT is a planar heterocyclic molecule that can intercalate between the stacked RNA bases. Upon irradiation at 365 nm, the HMT will undergo cyclophotoaddition to the 5,6-double bond of a pyrimidine to form a monoadduct. A second photoaddition reaction occurs with a pyrimidine on the opposite strand at an adjacent base pair. The precise point of cross-linking can then be deduced using a purine-specific ribonuclease that will cleave the cross-linked pyrimidine.

B. Phosphate-Specific Probes. Lead-catalyzed cleavage of RNA depends not upon the preference of a particular secondary structure nor upon solvent accessibility, but instead occurs in tRNA with high specificity at a highly structured region of the molecule.²³⁻²⁴ Cleavage by lead ion has been an extremely sensitive assay of the structural perturbations local to the lead sites. X-ray diffraction studies²⁵ on a cleaved and uncleaved tRNA^{Phe}-lead complex have shown that the lead ions are precisely coordinated with the tRNA bases in a pocket formed by eight residues of the D and T loops. The lead is coordinated in such a way that it can remove the proton from the 2'-hydroxyl of ribose-17 and eventually lead to the production of 2',3'-cyclic phosphate and 5'-hydroxyl termini.

Ethylnitrosourea (ENU) is an N-nitroso alkylation reagent that has an affinity for the phosphate oxygens of RNA. The accessible phosphates will be modified, the resulting phosphotriester will be unstable upon mild alkaline treatment, and the strand will break.²⁶ ENU has been used to monitor the tertiary structure of RNA in solution as well as determine which phosphate groups are in contact with RNA binding proteins.²⁷ Overall, ENU appears to have little preference for secondary structure, but rather has the ability to distinguish between protected and exterior regions of the RNA.

C. Sugar-Specific Probes. Methidiumpropyl-EDTA·Fe(II) (MPE·Fe(II)) is an intercalator moiety tethered to the metal chelating EDTA. Upon the addition of Fe(II) and a reducing agent such as DTT, the ferrous ions bind EDTA and generate short-lived radicals that can promote strand scission of the phosphodiester backbone.²⁸ This reagent has been

shown to bind double-helical regions selectively in preference to single-stranded regions of RNA and when complexed to Fe(II), readily cleaves the RNA backbone.²⁹ In contrast, 1,10-phenanthroline-copper ($\text{Cu}(\text{phen})_2^+$) has been observed to cleave tRNA^{Phe} at single-strand regions and loop structures.³⁰ This probe recognizes predominantly unstructured RNA which is not involved in base-pairing interactions.

$\text{Fe}(\text{EDTA})^{2-}$ has been used successfully to determine regions of an RNA molecule that are less solvent-accessible than others.³¹ Native tRNA contains regions that are not accessible to cleavage by $\text{Fe}(\text{EDTA})^{2-}$. Similarly, when the catalytic intervening sequence from *Tetrahymena* rRNA is subjected to $\text{Fe}(\text{EDTA})^{2-}$ treatment, about 40% of the molecule is protected and remains uncleaved. This probe may therefore be useful to define the interior and exterior regions of RNA molecules, as determined by their folded three-dimensional structures.

Finally, the antitumor agent bleomycin has been shown to cleave a specific tRNA precursor in a highly selective fashion in the presence of Fe(II).³² The RNA cleavage was oxidative and approximately tenfold more selective than DNA cleavage and largely unaffected by nonsubstrate RNAs. The results of these experiments suggested that the Fe(II)-bleomycin is recognizing a specific RNA tertiary structure, rather than a specific sequence. However, the recognition of RNA tertiary structures by this complex has yet to be characterized fully.

1.6. Transition Metal Complexes as Potential Probes for RNA Structure

Towards the development of probes for nucleic acid structure, our laboratory has provided evidence for the interactions of small transition metal complexes with DNA.³³ These complexes are derived from the parent tris(phenanthroline) complex (Figure 1.4) and recognize their DNA binding sites based upon shape considerations.³⁴ By matching the shapes and symmetries of the metal complex to particular variations in local DNA

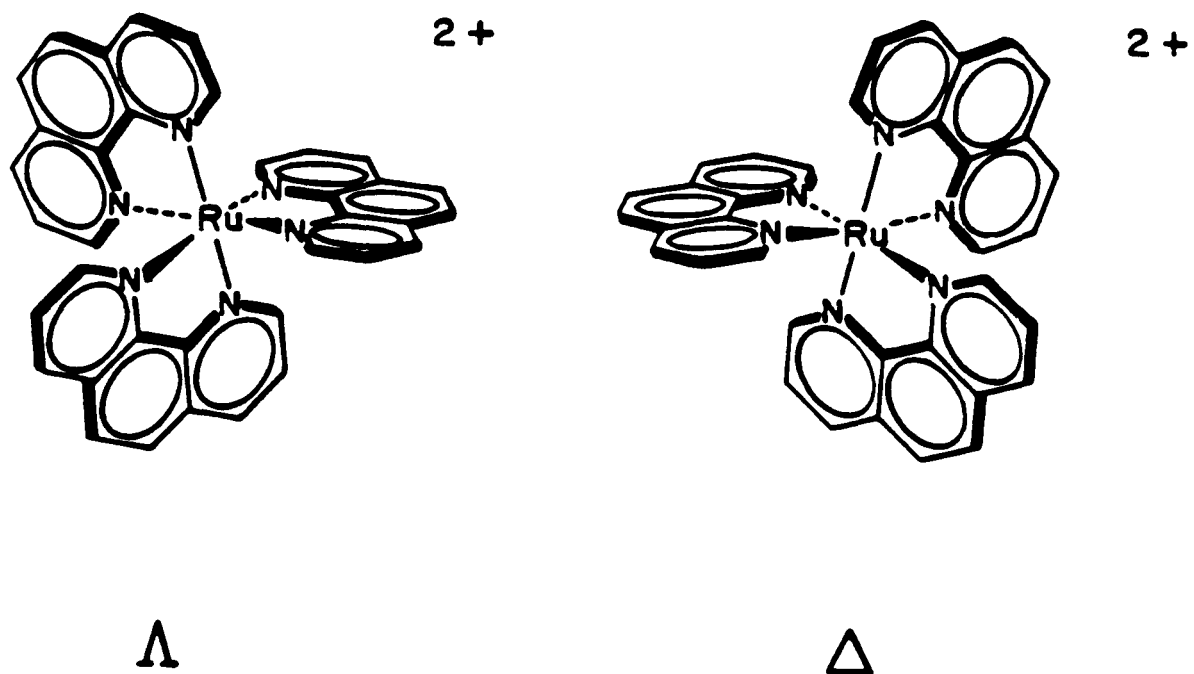


Figure 1.4. The Λ- (left) and Δ- (right) enantiomers of the parent metal complex, tris(1,10-phenanthroline)ruthenium(II).

conformation, a family of molecules that target specific sites along the DNA helix have been developed. Within this family of complexes, the metal centers have been varied so as to change the spectroscopic or reactive characteristics of the complexes. Alternatively, the bidentate ligands can be varied so as to alter the recognition characteristics of the complexes.

There are some important characteristics of the metal complexes that makes them attractive probes of DNA structure. First, the complexes are coordinatively saturated and inert. There can be no direct coordination of the metal center to the nucleic acid. Secondly, the metal complex is rigid and well defined in structure. This is important if conclusions are to be drawn about the structure of the nucleic acid site based upon shape complementarity to the metal complex. Thirdly, these probes all promote strand scission of the DNA at their particular binding sites upon photoactivation. By coupling the photoreactivity with the shape and symmetry constraints of the metal complexes, a family of conformation-specific, and therefore site-specific DNA cleaving molecules has been obtained.

The sequence-neutral DNA cleavage complex, $\text{Rh}(\text{phi})_2\text{bpy}^{3+}$ ($\text{phi} = 9,10$ -phenanthrenequinone diimine), is a useful reagent for high-resolution photofootprinting of DNA.³⁵ A related complex, $\text{Rh}(\text{phen})_2\text{phi}^{3+}$, has been useful as a conformation-specific cleaving agent to probe local DNA structures.³⁶⁻³⁷ Overall, the phi and phen complexes of ruthenium(II) and rhodium(III) have been applied to detect subtle variations in B-DNA conformation³⁶⁻³⁷ or to investigate global secondary structures of a polynucleotide such as a DNA cruciform³⁸, left-handed Z-DNA³⁹, and A-form DNA⁴⁰. In general, these studies have provided a unique and sensitive way to probe the elements of DNA polymorphism in solution.

Given the uniqueness of sites recognized on DNA, these probes should be valuable in assessing the secondary and tertiary structures of RNA as well. In this study we will

first consider the RNA binding properties of the metal complexes using biophysical analyses, then we will examine the ability of these molecules to promote strand scission of RNA. Finally, we will discuss the applications of these probes for examining higher-order structure in the well-characterized tRNAs, tRNA mutants, 5S rRNA, single-nucleotide mutants of 5S rRNA, as well as truncated RNA molecules representing one arm of 5S rRNA or one helix and loop of tRNA.

References

1. a) Kim, S.-H.; Sussman, J. L.; Suddath, F. L.; Quigley, G. J.; McPherson, A.; Wang, A. H.; Seeman, N. C.; Rich, A. *Proc. Natl. Acad. Sci. U.S.A.* **1974**, 71, 4970-4974.
b) Quigley, G. J.; Rich, A. *Science* **1976**, 194, 796-806.
2. Westhof, E.; Dumas, P.; Moras, D. *J. Mol. Biol.* **1985**, 184, 119-145.
3. Romby, P.; Moras, D.; Dumas, P.; Ebel, J. P.; Giege, R. *J. Mol. Biol.* **1987**, 195, 193-204.
4. Patel, D. J.; Shapiro, L.; Hare, D. *Q. Rev. Biophys.* **1987**, 20, 78-90.
5. Puglisi, J. D.; Wyatt, J. R.; Tinoco, I., Jr. *J. Mol. Biol.* **1990**, 214, 437-453.
6. a) Cheong, C.; Varani, G.; Tinoco, I., Jr. *Nature* **1990**, 346, 680-682.
b) Varani, G.; Cheong, C.; Tinoco, I., Jr. *Biochemistry* **1990**, 30, 3280-3289.
7. McCloskey, J. A.; Nishimura, S. *Acc. Chem. Res.* **1977**, 10, 403-410.
8. Sprinzl, M.; Gauss, D. H. *Nucleic Acids Res.* **1982**, 10, r1-r55.
9. Kim, S.-H. *Prog. Nucl. Acid Res. Mol. Biol.* **1976**, 17, 181-216.
10. Holbrook, S. R.; Cheong, C.; Tinoco, I., Jr.; Kim, S.-H. *Nature* **1991**, 353, 579-581.
11. Dock-Bregeon, A. C.; Chevrier, B.; Podjarny, A.; Johnson, J.; de Bear, J. S.; Gough, G. R.; Gilham, P. T.; Moras, D. *J. Mol. Biol.* **1989**, 209, 459-474.
12. Rould, M. A.; Perona, J. J.; Söll, D.; Steitz, T. A. *Science* **1989**, 246, 1135-1142.
13. Ruff, M.; Krishnaswamy, S.; Boeglin, M.; Poterszman, A.; Mitschler, A.; Podjarny, A.; Rees, B.; Thierry, J. C.; Moras, D. *Science* **1991**, 252, 1682-1689.
14. Patel, D. J. *Annu. Rev. Biophys. Bioeng.* **1978**, 29, 337-362.
15. Choi, B. S.; Redfield, A. G. *Nucleic Acids Res.* **1985**, 13, 5249-5254.

16. Ehresmann, C.; Baudin, F.; Mougél, M.; Romby, P.; Ebel, J. P.; Ehresmann, B. *Nucleic Acids Res.* **1987**, *15*, 9109-9128.
17. Wrede, P.; Wurst, R.; Vournakis, J.; Rich, A. *J. Biol. Chem.* **1979**, *254*, 9608-9616.
18. Lowman, H. B.; Draper, D. E. *J. Biol. Chem.* **1986**, *261*, 5396-5403.
19. Zuckermann, R. N.; Schultz, P. G. *Proc. Natl. Acad. Sci. U.S.A.* **1989**, *86*, 1766-1770.
20. Zuckermann, R. N.; Schultz, P. G. *J. Am. Chem. Soc.* **1988**, *110*, 6592-6594.
21. Richardson, P. L.; Schepartz, A. *J. Am. Chem. Soc.* **1991**, *113*, 5109-5111.
22. Garrett-Wheeler, E.; Lockard, R. E.; Kumar, A. *Nucleic Acids Res.* **1984**, *12*, 3405-3422.
23. Werner, C.; Krebs, B.; Keith, G.; Dirheimer, G. *Biochim. Biophys. Acta* **1976**, *432*, 161-175.
24. Behlen, L. S.; Sampson, J. R.; DiRenzo, A. B.; Uhlenbeck, O. C. *Biochemistry* **1990**, *29*, 2515-2523.
25. Brown, R. S.; Hingerty, B. E.; Dewan, J. C.; Klug, A. *Nature* **1983**, *303*, 543-546.
26. Kusmieriek, J. T.; Singer, B. *Biochim. Biophys. Acta* **1976**, *442*, 420-431.
27. Romby, P.; Moras, D.; Bergdoll, M.; Dumas, P.; Vlassov, V. V.; Westhof, E.; Ebel, J. P.; Giege, R. *J. Mol. Biol.* **1985**, *184*, 455-471.
28. Hertzberg, R. P.; Dervan, P. B. *J. Am. Chem. Soc.* **1982**, *104*, 313-315.
29. Kean, J. M.; White, S. A.; Draper, D. E. *Biochemistry* **1985**, *24*, 5062-5070.
30. Murakawa, G. J.; Chen, C. B.; Kuwabara, M. D.; Nierlich, D. P.; Sigman, D. S. *Nucleic Acids Res.* **1989**, *17*, 5361-5375.
31. a) Latham, J. A.; Cech, T. R. *Science* **1989**, *245*, 276-282.
b) Celander, D. W.; Cech, T. R. *Biochemistry* **1990**, *29*, 1355-1361.

32. Carter, B. J.; de Vroom, E.; Long, E. C.; van der Marel, G. A.; van Boom, J. H.; Hecht, S. H. *Proc. Natl. Acad. Sci. U.S.A.* **1990**, *87*, 9373-9377.
33. Pyle, A. M.; Barton, J. K. *Prog. Inorg. Chem.* **1990**, *38*, 413-475.
34. Barton, J. K. *Science* **1986**, *233*, 727-733.
35. Uchida, K.; Pyle, A. M.; Morii, T.; Barton, J. K. *Nucleic Acids Res.* **1989**, *17*, 10259-10279.
36. Pyle, A. M.; Long, E. C.; Barton, J. K. *J. Am. Chem. Soc.* **1989**, *111*, 4520-4522.
37. Pyle, A. M.; Morii, T.; Barton, J. K. *J. Am. Chem. Soc.* **1990**, *112*, 9432-9434.
38. Kirshenbaum, M. R.; Tribolet, R.; Barton, J. K. *Nucleic Acids Res.* **1988**, *16*, 7943-7960.
39. Barton, J. K.; Raphael, A. L. *Proc. Natl. Acad. Sci. U.S.A.* **1985**, *82*, 6460-6464.
40. a) Mei, H.-Y.; Barton, J. K. *J. Am. Chem. Soc.* **1986**, *108*, 7414-7416.
b) Mei, H.-Y.; Barton, J. K. *Proc. Natl. Acad. Sci. U.S.A.* **1988**, *85*, 1339-1343.

Chapter 2:

Biophysical Studies of Tris(phenanthroline) and Phenanthrenequinone Diimine Complexes of Ru(II) and Rh(III) Bound to tRNA

2.1. Introduction

This chapter involves a biophysical analysis of tRNA binding by ruthenium(II) and rhodium(III) polypyridyl and phenanthrenequinone diimine (phi) complexes. Figure 2.1 illustrates the structures of these complexes. They are all coordinatively saturated, inert to substitution, and rigid and well defined in structure. There can be no direct coordination of the metal center to the RNA. Instead, binding to tRNA will be based purely upon noncovalent interactions between the metal complex and the nucleic acid. In addition, by varying the ligands and ligand substituents on the complexes and comparing the binding to tRNA, we may be able to determine the contributions of the ligand functionalities to binding to the structured tRNA molecule. Also, these tris-chelated octahedral complexes are chiral, which may be important in defining the selectivity in binding at particular sites along the RNA polymer. Using a variety of methods such as equilibrium dialysis, absorption titration, steady-state luminescent measurements, and time-resolved emission lifetime measurements, the binding of these transition metal complexes to tRNA may be studied.

The utility of the chiral metal complexes as probes for DNA conformations has been considered.¹ Ruthenium(II) polypyridyl complexes are particularly useful for these studies because of their well-characterized chemical and spectroscopic properties.²⁻³ The interaction of tris(1,10-phenanthroline)ruthenium(II), $\text{Ru}(\text{phen})_3^{2+}$, with nucleic acids has been investigated previously. It has been found that the complex binds to double-stranded DNA through two different noncovalent modes: intercalation and hydrophobic surface

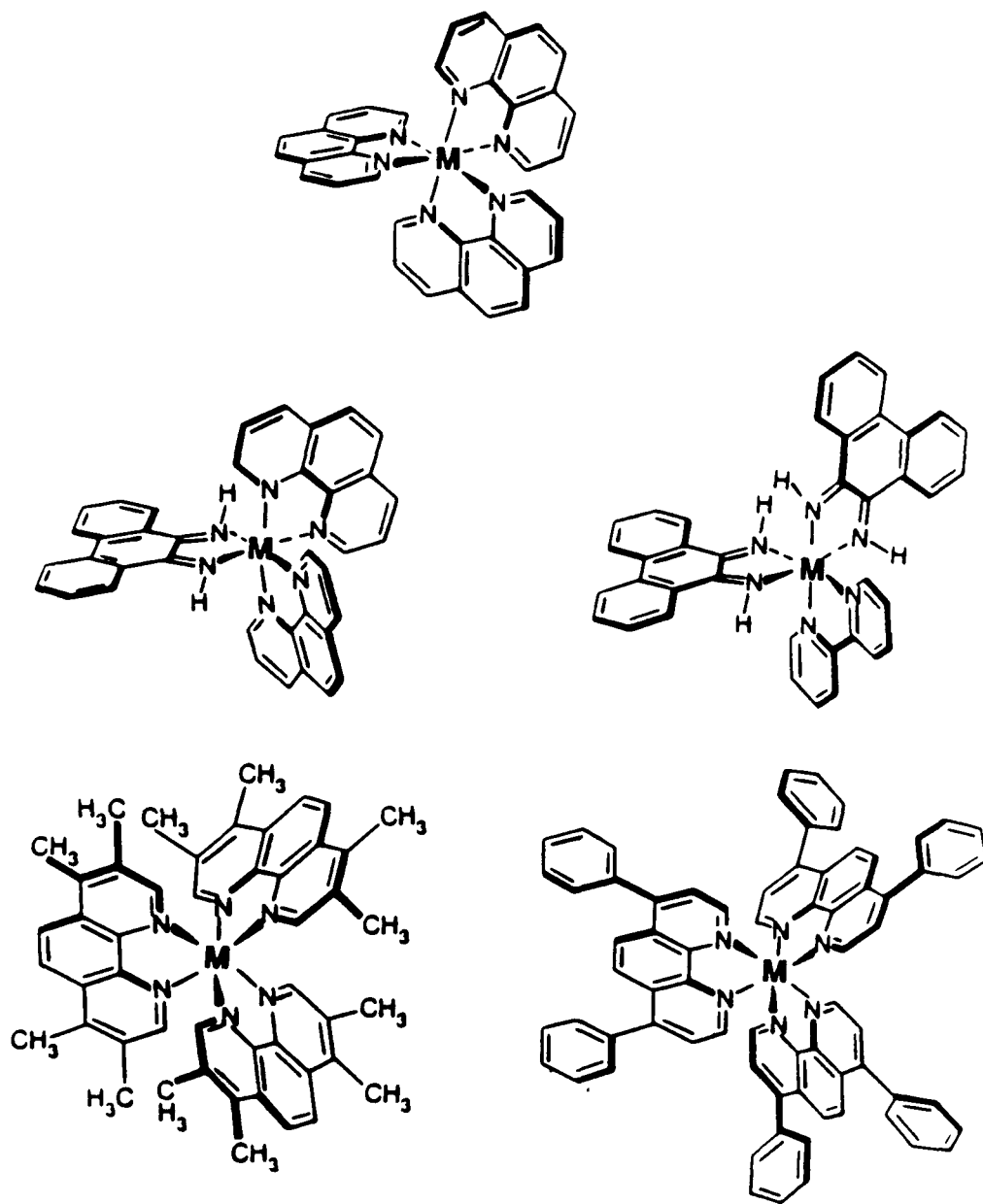


Figure 2.1. Structures of the metal complexes studied: M= Ru(II) or Rh(III). Shown clockwise from the top are $\text{Ru}(\text{phen})_3^{2+}$, $\text{Rh}(\text{phi})_2\text{bpy}^{3+}$, $\text{Rh}(\text{DIP})_3^{3+}$, $\text{Ru}(\text{TMP})_3^{2+}$ or $\text{Rh}(\text{TMP})_3^{3+}$, and $\text{Rh}(\text{phen})_2\text{phi}^{3+}$.

binding.⁴⁻⁵ The intercalative bound mode shows a chiral preference for the Δ -isomer, and the surface bound mode shows a preference for the Λ -isomer. Time-resolved emission measurements of *rac*-Ru(phen)₃²⁺ in the presence of DNA showed two components in the lifetime decay which have been assigned to the intercalative and surface-bound modes. Under the same conditions, phi complexes of rhodium(III) do not exhibit any luminescence properties, but are shown through equilibrium dialysis and absorption titrations to bind strongly to double-stranded DNA, likely through an intercalative binding mode.⁶

The properties of the metal complexes in binding to DNA were promising for the development of new reagents for studying higher-order RNA structures. We would like first to determine the overall binding affinities of each of these complexes to structured RNA. Early studies indicated that Ru(phen)₃²⁺ binds only weakly to tRNA.⁴ In contrast, Ru(TMP)₃²⁺, with bulky methyl substituents on the phenanthroline ligand, binds favorably to the surface of an A-form DNA or RNA minor groove.⁷ The binding of rhodium(III) phi complexes to RNA has not been investigated previously, but the high binding properties of these complexes to DNA suggested that they may serve as useful probes for RNA structure. To investigate further the usefulness of these metal complexes as probes for RNA structure in solution, we have first considered the binding characteristics of these molecules with the structurally well-characterized⁸⁻⁹ tRNA molecule.

2.2. Experimental

2.2.1. Synthesis

Materials: The reagents used in this study were obtained from the following suppliers: RhCl₃ (42.5% Rh, Aesar Johnson Matthey, Seabrook, NH); RuCl₃ (43% Ru, GFS, Columbus, OH); 1,10-phenanthroline (phen), 3,4,7,8-tetramethyl-1,10-phenanthroline (TMP), 9,10-diaminophenanthrene (DAP), AgNO₃, and N₂H₄·HCl (Aldrich, Milwaukee, WI); potassium chloride (Sigma, St. Louis, MO).

NMR chemical shifts are reported in parts per million (ppm). The ppm scale was set using reference lines from the solvent.

[Ru(phen)₃]Cl₂: This complex was made as described in the literature.^{2a} NMR (DMSO): 8.8 (d, H 4,7), 8.7 (d, H 2,9), 8.4 (s, H 5,6), 7.7 (dd, H 3,8). Extinction coefficient: $\epsilon_{447} = 1.9 \times 10^4 \text{ M}^{-1} \text{ cm}^{-1}$.

[Ru(TMP)₃]Cl₂: This complex was made as described in the literature.^{2a} NMR (CDCl₃): 8.20 (s, H 5,6), 7.98 (s, H 2,9), 2.74 (s, CH₃ 4,7), 2.37 (s, CH₃ 3,8). Extinction coefficient: $\epsilon_{438} = 2.45 \times 10^4 \text{ M}^{-1} \text{ cm}^{-1}$. FAB mass spec ion mass: 809, Ru(TMP)₃²⁺; 574, Ru(TMP)₂²⁺. Galbraith elemental analysis of [Ru(TMP)₃]Cl₂·10 H₂O: %C, 54.34 (calc. 54.33), %H, 6.53 (calc. 6.47), %N, 7.95 (calc. 7.92).

[Rh(TMP)₃]Cl₃: This complex was prepared by the reaction of rhodium trichloride and 3,4,7,8-tetramethyl-9,10-phenanthroline (TMP) in the presence of hydrazine catalyst according to the method of Gillard et al.¹⁰ RhCl₃ (0.13 g, 0.54 mmol) was dissolved in 10 mL H₂O with gentle heating to 40°C. 3,4,7,8-tetramethyl-9,10-phenanthroline (TMP) (0.43 g, 1.8 mmol) was dissolved in 6 mL ethanol with heating and added dropwise to the RhCl₃·H₂O solution. Hydrazinium monochloride (0.0038 g, 0.005 mmol) was added, and the solution was brought to reflux. After heating under refluxing conditions under N₂ for 4 days the solution changed from a dark orange-red color to a pale orange-yellow color. The reaction was stopped by cooling to room temperature and quenching with concentrated HCl (2 mL). The volume was reduced and the hot mixture was slowly cooled to room temperature, resulting in a light pink precipitate. The solid material was filtered and washed with cold acetone. NMR (D₂O): 8.36 (s, H 5,6), 7.37 (s, H 2,9), 2.71 (s, CH₃ 4,7), 2.09 (s, CH₃ 3,8). FABMS: 881, [Rh(TMP)₃]Cl₂⁺;

610, $[\text{Rh}(\text{TMP})_2]\text{Cl}_2^+$; 575, $[\text{Rh}(\text{TMP})_2]\text{Cl}^{2+}$; 339, $[\text{Rh}(\text{TMP})]\text{Cl}^{2+}$. Galbraith elemental analysis of $[\text{Rh}(\text{TMP})_3]\text{Cl}_3 \cdot 6 \text{H}_2\text{O}$: %C, 56.35 (calc. 56.17), %H, 5.56 (calc. 5.90), %N, 8.17 (calc. 8.19). UV-visible (H_2O , 25 °C) λ max (ϵ , $\text{M}^{-1} \text{cm}^{-1}$): 282 nm (8.5×10^4), 313 nm (2.3×10^4), 335 nm (6.2×10^3), 352 nm (3.1×10^3).

$[\text{Rh}(\text{phen})_2\text{phi}]\text{Cl}_3$: This complex was synthesized as described in the literature.¹¹ NMR (DMSO): 14.98 ppm (s, N-H phi), 9.25 (d, H 4 phen), 9.12 (d, H 2 phen), 9.03 (d, H 7 phen), 8.94 (d, H 5,6 phen), 8.54 (dd, H 4,5 phi), 8.47 (d, H 1,8 phi), 8.36 (dd, H 3 phen), 8.08 (d, H 9 phen), 7.91 (dd, H 8 phen), 7.84 (t, H 2,7 phi), 7.57 (t, H 3,6 phi) (assignments were made based on COESY experiments, S. S. David, unpublished results). Extinction coefficient: $\epsilon_{362} = 1.94 \times 10^4 \text{ M}^{-1} \text{cm}^{-1}$.

2.2.2. Methods

Materials: tRNA^{Phe} from brewer's yeast and tRNA^{bulk} from baker's yeast (bulk refers to unfractionated tRNA) (Boehringer Mannheim, Indianapolis, IN); Trizma base (Tris), NaOAc, NaCl, Na_2CO_3 , and EDTA (Molecular Biology Grade, if available, Sigma, St. Louis, MO); $\text{K}_4\text{Fe}(\text{CN})_6 \cdot \text{H}_2\text{O}$ and diethylpyrocarbonate (DEPC) (Aldrich, Milwaukee, WI); Sodium dodecyl sulfate (SDS) (Pierce, Rockford, IL). $[\text{Rh}(\text{phi})_2\text{bpy}]\text{Cl}_3$ was a gift from A. M. Pyle in our laboratory. $[\text{Rh}(\text{DIP})_3]\text{Cl}_3$ was a gift from M. R. Kirshenbaum in our laboratory.

Buffers: Buffer 1 (5 mM Tris, 50 mM NaCl, pH 7.0); buffer 2 (25 mM Tris, 100 mM NaCl, pH 7.6); and buffer 3 (50 mM Trizma, 18 mM NaCl, 20 mM NaOAc, pH 7.0). Buffers were made as 10X solutions and stored at 4°C.

Nucleic Acids: tRNAs from Boehringer Mannheim were generally used without purification. The extinction coefficients for tRNA^{Phe} and tRNA^{bulk} at 260 nm were 7790 $\text{M}^{-1} \text{cm}^{-1}$ and 7460 $\text{M}^{-1} \text{cm}^{-1}$ in nucleotides, respectively.¹² The ratio between the

absorbance readings at 260 nm and 280 nm (OD_{260}/OD_{280}) provided an estimate for the purity of the tRNA. The RNA should have OD_{260}/OD_{280} of 2.0 or greater. If this ratio was less than 2.0, the RNA was purified by extraction with phenol/chloroform followed by extraction with water-saturated ether and precipitation with ethanol. The purified tRNAs were stored in 10 mM Tris-HCl, 1 mM EDTA, pH 7.5.

Metal Stock Solutions: The metal complexes were made to approximately 1 mM and stored frozen in the dark for up to two weeks. The concentrations were measured according to the given extinction coefficients.

Precautions Against Ribonucleases: All glassware was baked at 200°C overnight. Plasticware and pipet tips were treated with 0.1% DEPC and autoclaved. Solutions were made with the highest purity reagents and water available. Buffers were filtered through sterile filters and stored in sterile receiving bottles. Dialysis experiments were performed in sterile polypropylene tubes (4 mL).

Equilibrium Dialysis: The binding of the metal complexes was determined by equilibrium dialysis of yeast tRNA^{bulk} and yeast tRNA^{Phe} (300 μ M RNA nucleotides, 1 mL total volume inside bag) versus metal complex (5 to 200 μ M, 3 mL dialysate, 4 mL total volume) in buffer 1 (5 mM Tris, 50 mM NaCl, pH 7.0). Spectra/Por 2 membranes from Fisher Scientific (12000-14000 MW cutoff) were used for the experiment. The membranes were boiled in Na₂CO₃ solution (2.5 g/L H₂O), rinsed with deionized H₂O, boiled in 1% EDTA, rinsed again with deionized H₂O, boiled twice with a 1% solution of SDS, rinsed and boiled twice with deionized distilled H₂O, boiled in a 0.1% solution of diethylpyrocarbonate (DEPC), and stored in a 50% ethanol/ H₂O solution at 4°C.

The RNA was dialyzed first exhaustively in buffer 1 to remove small fragments. Thereafter, each sample was dialyzed against metal complex at 25°C for 3 to 5 days with shaking until the controls containing no RNA were greater than 95% equilibrated. The

concentrations of free and bound metal complex were determined by absorption spectroscopy. Free metal concentrations outside the bags were determined on the basis of absorption readings at the following wavelengths and extinction coefficients: Ru(phen)₃²⁺, $\epsilon_{438}=1.9 \times 10^4 \text{ M}^{-1} \text{ cm}^{-1}$; Ru(TMP)₃²⁺, $\epsilon_{447}=2.45 \times 10^4 \text{ M}^{-1} \text{ cm}^{-1}$; Rh(TMP)₃³⁺, $\epsilon_{282}=8.5 \times 10^4 \text{ M}^{-1} \text{ cm}^{-1}$; Rh(phen)₂phi³⁺, $\epsilon_{362}=1.94 \times 10^4 \text{ M}^{-1} \text{ cm}^{-1}$; Rh(phi)₂bpy³⁺, $\epsilon_{350}=2.36 \times 10^4 \text{ M}^{-1} \text{ cm}^{-1}$. For concentrations of metal complex inside the bag, in the presence of tRNA, readings were obtained at the isosbestic points as given: Ru(phen)₃²⁺, $\epsilon_{438}=1.9 \times 10^4 \text{ M}^{-1} \text{ cm}^{-1}$; Ru(TMP)₃²⁺, $\epsilon_{455}=2.16 \times 10^4 \text{ M}^{-1} \text{ cm}^{-1}$; Rh(TMP)₃³⁺, $\epsilon_{292}=6.6 \times 10^4 \text{ M}^{-1} \text{ cm}^{-1}$; Rh(phen)₂phi³⁺, $\epsilon_{383}=1.58 \times 10^4 \text{ M}^{-1} \text{ cm}^{-1}$; Rh(phi)₂bpy³⁺, $\epsilon_{400}=2.26 \times 10^4 \text{ M}^{-1} \text{ cm}^{-1}$.

The data from the dialysis experiments was plotted in the form of a Scatchard plot (r_b/C_F is plotted against r_b , where r_b is the ratio of the bound concentration of metal complex to the concentration of RNA nucleotides and C_F is the concentration of metal complex free in solution).¹³ The curves were fit using a 2^o polynomial that approximated the fit of the von Hippel equation for anticooperative binding.¹⁴ The intersection of this curve with the y-axis gives the intrinsic binding constant K_b .

Spectroscopic Measurements: Absorption spectra were measured on a Varian Cary 219 spectrophotometer. Absorption titrations of racemic metal complexes in buffer 1 (Rh(DIP)₃³⁺, Ru(phen)₃²⁺, Ru(TMP)₃²⁺, and Rh(TMP)₃³⁺) or buffer 3 (Rh(phen)₂phi³⁺ and Rh(phi)₂bpy³⁺) were performed using a fixed metal concentration (2 to 5 μM) to which increments (1 to 5 μL) of the tRNA stock solution (0.3 to 2 mM in nucleotides) were added. Metal complex (2 to 5 μM) was also added to the tRNA stock to keep the total dye concentration constant during the titration experiment. The percent hypochromicity (%H) was determined by the following equation:

$$\%H = (\epsilon_{\text{free}} - \epsilon_{\text{measured}})/\epsilon_{\text{free}}.$$

The Meehan half-reciprocal plot¹⁵ was used to estimate the binding constant K for the bound metal complex to tRNA. The following equation represents the change in the apparent extinction coefficient of the metal complex vs. RNA nucleotide concentration of the native tRNA (D):

$$(D/\Delta\epsilon_{AP}) = (D/\Delta\epsilon) + (1/\Delta\epsilon K),$$

where $\Delta\epsilon_{AP} = |\epsilon_a - \epsilon_F|$, $\Delta\epsilon = |\epsilon_B - \epsilon_F|$, and ϵ_a , ϵ_B , and ϵ_F are the apparent, free, and bound metal complex extinctions, respectively. A plot of $D/\Delta\epsilon_{AP}$ versus D gives a slope of $1/\Delta\epsilon$ and a y -intercept of $1/\Delta\epsilon K$, which will be used to obtain K . Alternatively, the binding constants were estimated using Scatchard analysis of the titration data.

Circular dichroic measurements were obtained with a Jasco J-500A automatic recording spectropolarimeter in the spectral region of 400 to 230 nm, scan speed 50 nm/min, sensitivity 5 m°/cm, time constant 1 second, and 3.5 ml quartz cells with path length 1 cm. In the equilibrium dialysis experiment of the racemic metal solution against tRNA, the relative binding of the two individual enantiomers to tRNA can be determined on the basis of the degree of optical enrichment of the unbound enantiomer in the dialysate. The degree of chiral discrimination was quantitated with the following equation:

$$S = (1 + (\Delta C/C_B)(V_{tot}/V_{in}))/2,$$

where S is the selectivity, C_B is the concentration of total bound metal, V_{tot} is the total volume inside (V_{in}) and outside the dialysis bag, and ΔC is the difference in free concentrations between the Δ - and Λ -isomers as measured by the intensity in the circular dichroism spectrum ($\Delta C = \text{rotation in m}^\circ/1.8 \times 10^7 \text{ m}^\circ\text{M}^{-1}$).

Steady-state luminescence measurements were conducted by using a Perkin-Elmer LS-5 fluorescence spectrophotometer at room temperature in buffer 1. Ruthenium(II) samples, typically 5 μM concentrations, were excited at 455 nm and emission was observed between 550 and 750 nm, with RNA nucleotide to metal ratios varying from 1 to 50. Emission lifetimes were performed on a PRA single photon counter at room

temperature in buffer 1. The emission lifetimes were obtained on 2 mL samples containing 5 μM ruthenium complex free or in the presence of 225 to 450 μM tRNA in nucleotides. The ruthenium samples were excited at 455 nm and emission was monitored at 600 nm. In all these experiments, small aliquots (1-5 μl) of a concentrated solution of nucleic acid (0.3 to 2 mM in nucleotides) were added. Quenching experiments were conducted by adding small aliquots of a ferrocyanide stock solution ($\text{K}_4\text{Fe}(\text{CN})_6$, 20 mM) to 2 mL samples containing 5 μM metal complex and 250 μM RNA in nucleotides in buffer 1.

2.3. Results

2.3.1. Synthesis and Characterization

Tris(3,4,7,8-tetramethyl-9,10-phenanthroline)rhodium(III), $[\text{Rh}(\text{TMP})_3]\text{Cl}_3$, was synthesized using the method of Gillard et al.¹⁰ The NMR spectrum of *rac*- $[\text{Rh}(\text{TMP})_3]\text{Cl}_3$ is given in Figure 2.2. Proton assignments were made based on the assignments made for $[\text{Rh}(\text{phen})_3]\text{Cl}_3$ ¹⁶ and NOE difference spectroscopy. Steady-state NOEs were measured in D_2O and MeOH at room temperature. Irradiation of the singlet at 8.4 ppm generates an NOE corresponding to the methyl singlet at 2.7 ppm. Similarly, irradiation of the singlet at 7.4 ppm generates an NOE corresponding to the second methyl singlet at 2.1 ppm. These results were used to assign the proton spectrum of *rac*- $[\text{Ru}(\text{TMP})_3]\text{Cl}_2$ as shown in Figure 2.2. The UV-visible spectrum of $[\text{Rh}(\text{TMP})_3]\text{Cl}_3$ in water is shown in Figure 2.3. The UV-visible spectrum has a λ_{max} at 282 nm with an approximate extinction coefficient of $8.5 \times 10^4 \text{ M}^{-1} \text{ cm}^{-1}$ and shoulders at 313 nm ($2.3 \times 10^4 \text{ M}^{-1} \text{ cm}^{-1}$), 335 nm ($6.2 \times 10^3 \text{ M}^{-1} \text{ cm}^{-1}$), and 352 nm ($3.1 \times 10^3 \text{ M}^{-1} \text{ cm}^{-1}$).

Figure 2.2. 200 MHz ^1H NMR spectra of tris(3,4,7,8-tetramethyl-1,10-phenanthroline) complexes of rhodium(III) (top) in D_2O and ruthenium(II) (bottom) in CDCl_3 . The following proton assignments were made based on NOE studies: H_A , H 5,6; H_B , H 2,9; H_C , CH_3 4,7; H_D , CH_3 3,8.

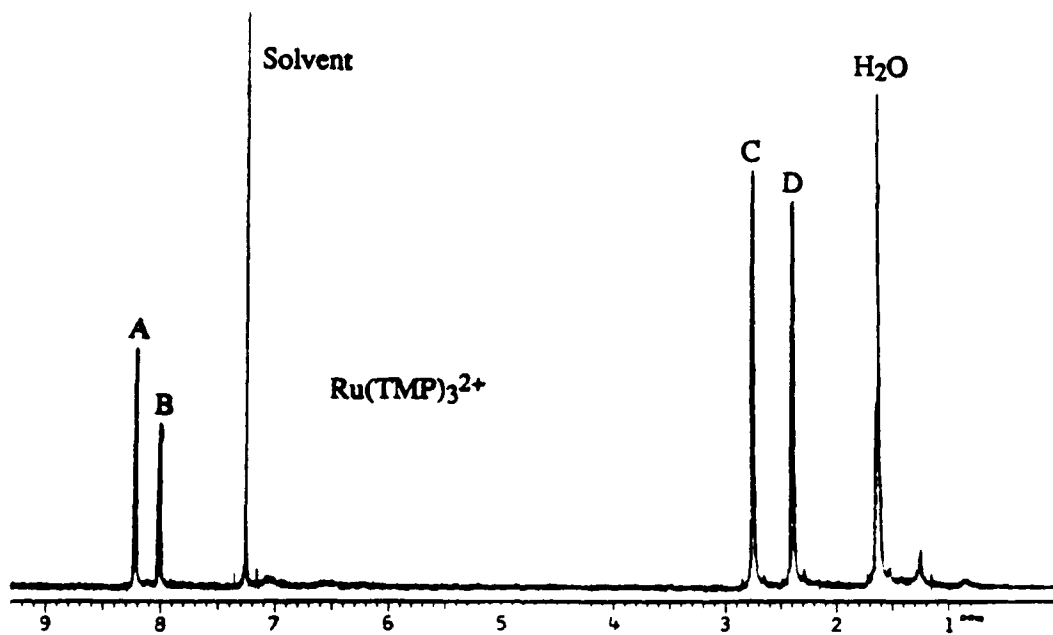
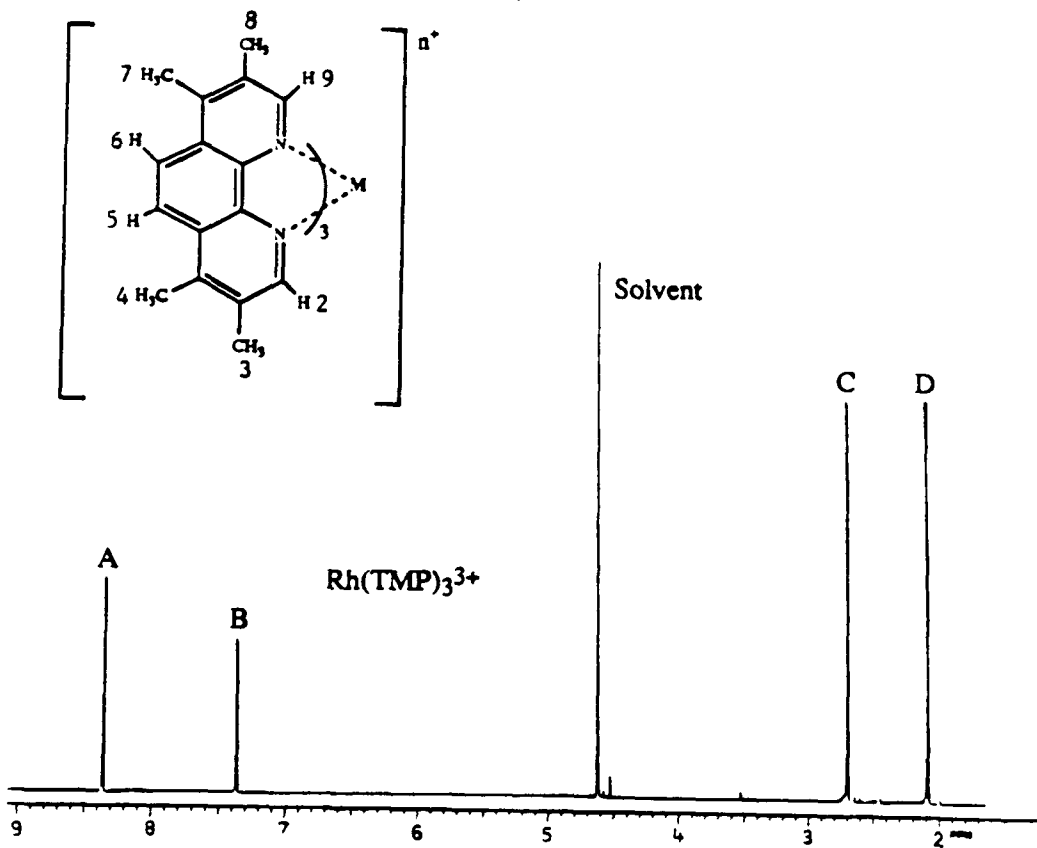
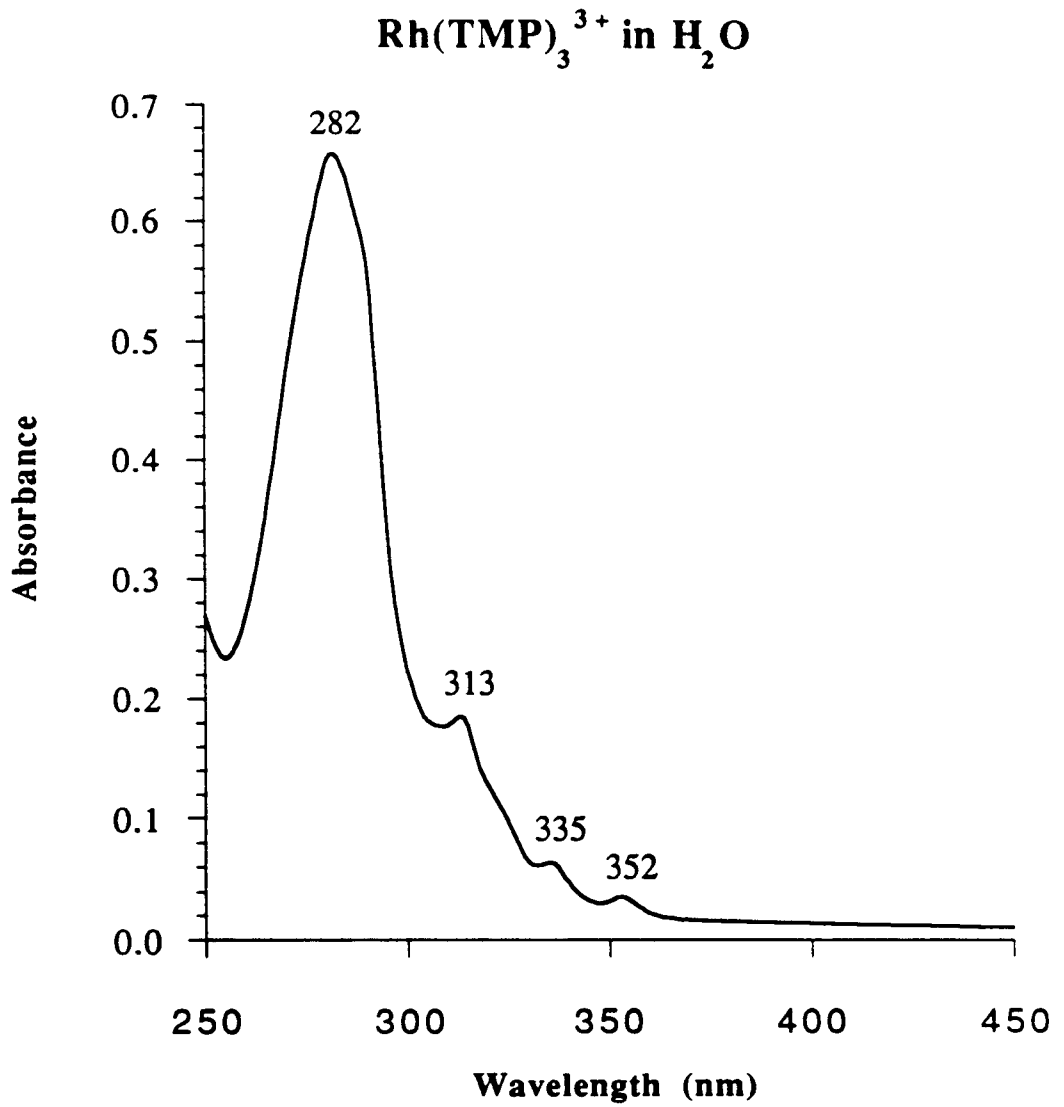


Figure 2.3. The UV/visible spectrum of tris(3,4,7,8-tetramethyl-1,10-phenanthroline) rhodium(III), $\text{Rh}(\text{TMP})_3^{3+}$, in H_2O .



2.3.2. Equilibrium Dialysis of Ru(II) Polypyridyl Complexes Against tRNA

Binding isotherms were determined by equilibrium dialysis of baker's yeast tRNA^{bulk} against *rac*-Ru(phen)₃²⁺ and *rac*-Ru(TMP)₃²⁺. Figure 2.4 shows plots of the ratio of bound ruthenium per nucleotide (r_b) versus the ratio of formal added ruthenium per nucleotide (r_f) for the two ruthenium complexes. Difficulties were encountered using the traditional methods (Scatchard analysis) for measuring binding constants because Ru(phen)₃²⁺ binds only weakly to the tRNA and Ru(TMP)₃²⁺ binds in a cooperative manner. As shown by Figure 2.4, cooperative binding by Ru(TMP)₃²⁺ is greater than that of Ru(phen)₃²⁺. Cooperative binding of Ru(TMP)₃²⁺ to polynucleotides that can adopt an A-like conformation was observed under conditions where little binding was apparent to other forms of nucleic acids.⁷ The preferential association of Ru(TMP)₃²⁺ to A-form helices is evident in Figure 2.5, which compares binding of the metal complex to a synthetic RNA-DNA hybrid, a synthetic double-stranded RNA, and native tRNA. The highest level of binding is seen to the tRNA. The second highest level of binding is seen to double-stranded RNA, poly(rI)-poly(rC), with the lowest amount of binding observed with the RNA-DNA duplex poly(rA)-poly(dT). Some precipitation of the polymers at high r_f values (> 0.1), given the poor solubility of Ru(TMP)₃²⁺, may account for some of the cooperativity seen in the dialysis experiment.

Variations in total binding of Ru(TMP)₃²⁺ to tRNA as a function of ionic strength and temperature have also been considered. Figure 2.6 (panel A) compares the binding of Ru(TMP)₃²⁺ to tRNA in high salt (100 mM NaCl) and lower salt (50 mM NaCl). Under the high salt conditions, no binding to tRNA is evident. Similar results were found with poly(rI)-poly(rC).⁷ It appears that the surface binding of Ru(TMP)₃²⁺ is affected by the electrostatic environment of the RNA backbone. With more sodium ions on the groove surface, the electrostatic association or hydrophobic interaction of the metal complex to the

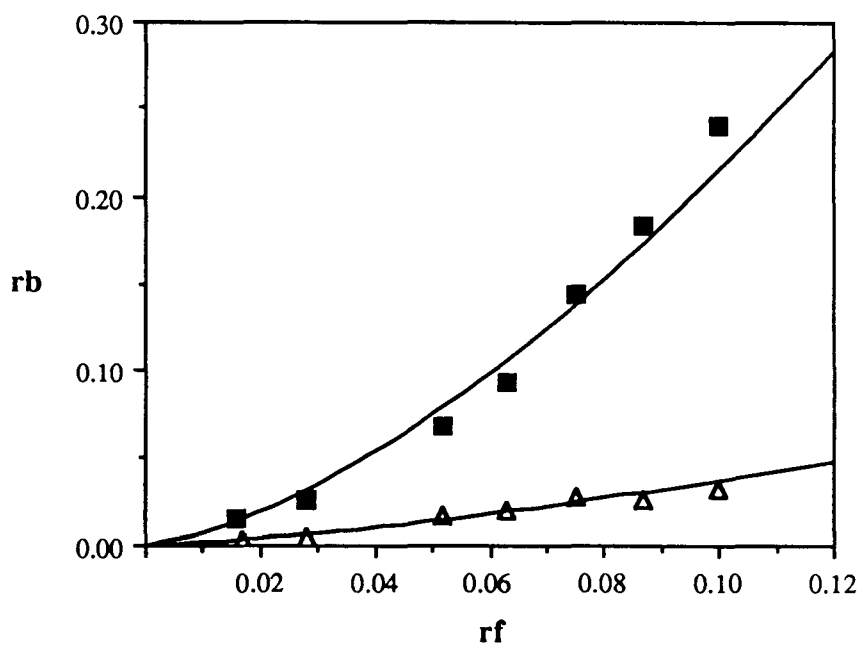


Figure 2.4. Binding of $\text{Ru}(\text{TMP})_3^{2+}$ and $\text{Ru}(\text{phen})_3^{2+}$ to native $\text{tRNA}^{\text{bulk}}$ as determined by equilibrium dialysis. The value of r_b is the ratio of bound ruthenium to nucleotide concentration; the value of r_f is the formal added ratio of metal complex per nucleotide. It can be seen from the plot that cooperative binding of $\text{Ru}(\text{TMP})_3^{2+}$ (closed squares) to tRNA is greater than binding of $\text{Ru}(\text{phen})_3^{2+}$ (open triangles).

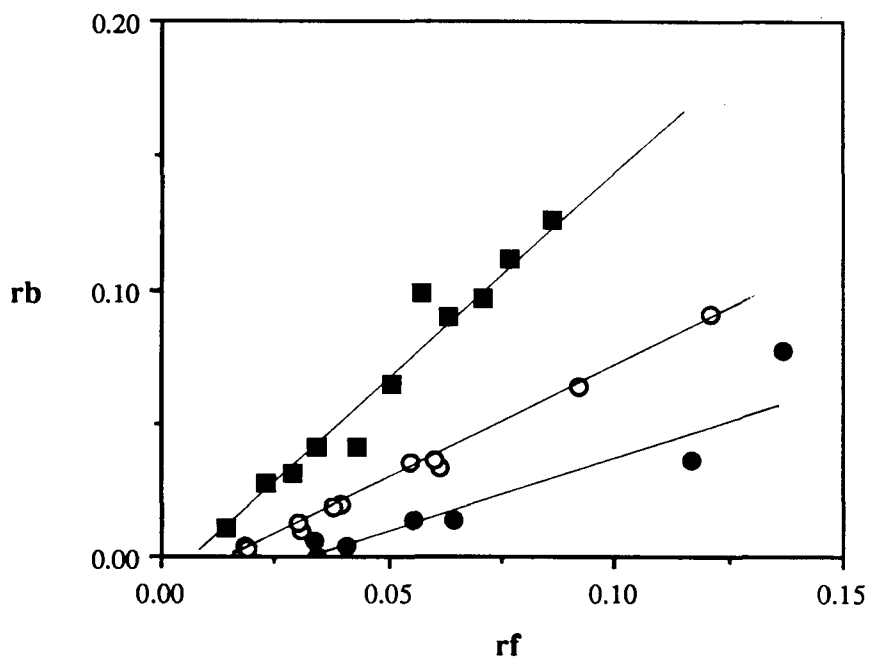
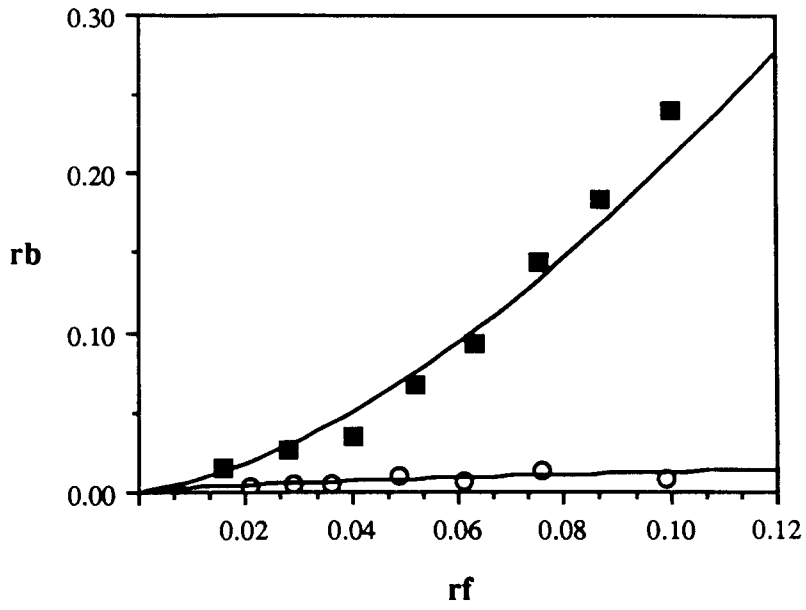
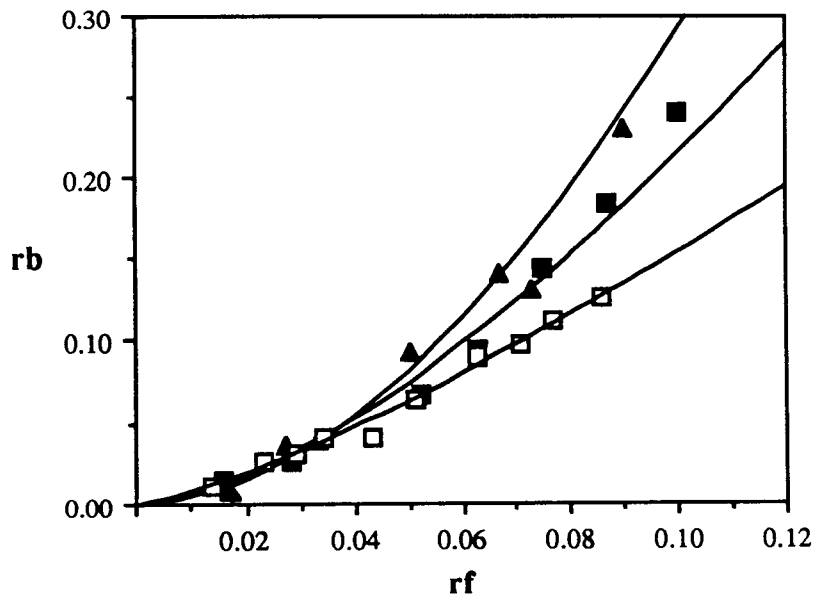


Figure 2.5. Binding of $\text{Ru}(\text{TMP})_3^{2+}$ to synthetic, double-stranded polynucleotides and native $\text{tRNA}^{\text{bulk}}$ as determined by equilibrium dialysis. The value of r_b is the ratio of bound ruthenium to nucleotide concentration; the value of r_f is the formal added ratio of metal complex per nucleotide. The following RNAs are shown in the plot: $\text{tRNA}^{\text{bulk}}$ from baker's yeast (closed squares), $\text{poly}(\text{rI})\cdot\text{poly}(\text{rC})$ (open circles), and $\text{poly}(\text{rA})\cdot\text{poly}(\text{dT})$ (closed circles).

Figure 2.6. Binding of $\text{Ru}(\text{TMP})_3^{2+}$ to native $\text{tRNA}^{\text{bulk}}$ under varying salt and temperature conditions as determined by equilibrium dialysis. (A) The binding of the ruthenium complex under varying salt conditions is shown. In 50 mM NaCl (solid squares), the binding to tRNA is greater than the binding in 100 mM NaCl (open circles). The value of r_b is the ratio of bound ruthenium to nucleotide concentration; the value of r_f is the formal added ratio of metal complex per nucleotide. (B) Small changes in the cooperative binding of $\text{Ru}(\text{TMP})_3^{2+}$ to tRNA under varying temperatures are shown. The following temperatures were used in the dialysis experiments: 37°C (closed triangles), 27°C (closed squares), and 25°C (open squares).

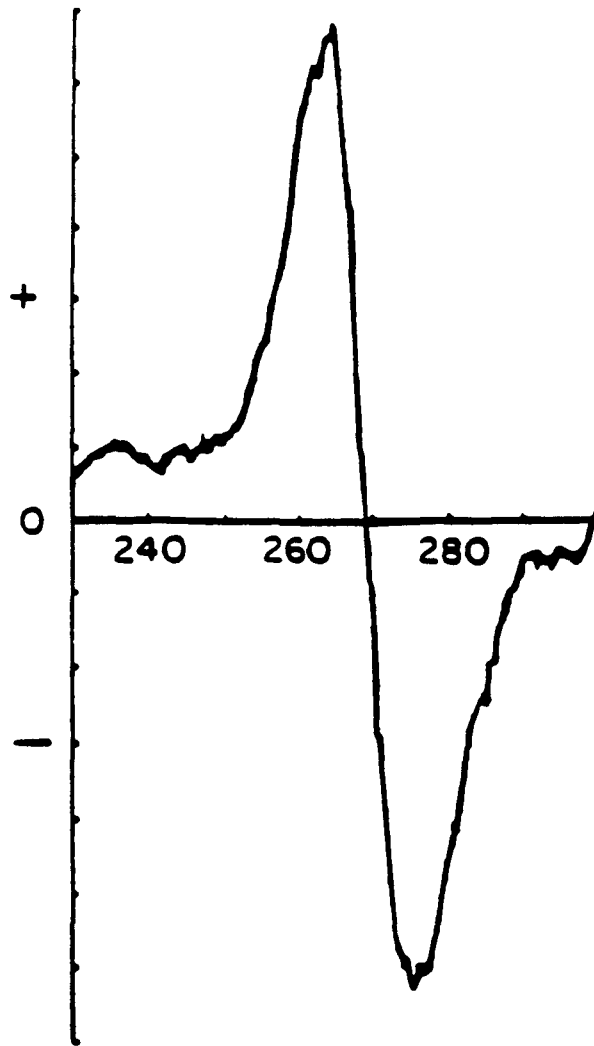
A**B**

RNA may be decreased. Small variations in temperature also lead to changes in the binding of $\text{Ru}(\text{TMP})_3^{2+}$ to tRNA. As shown in Figure 2.6 (panel B), the binding increases slightly as the temperature is raised from 25°C to 37°C. This would be expected for a hydrophobic association of the $\text{Ru}(\text{TMP})_3^{2+}$ with the shallow minor groove of RNA.⁷

For all the dialysis experiments with *rac*- $\text{Ru}(\text{phen})_3^{2+}$ and *rac*- $\text{Ru}(\text{TMP})_3^{2+}$, levels of chiral discrimination were determined through measurement of optical enrichment of the less-favored enantiomer in the dialysate. Figure 2.7 shows the circular dichroism spectrum of the dialysate from the dialysis experiments of tRNA against *rac*- $\text{Ru}(\text{TMP})_3^{2+}$ after equilibrium is established. The circular dichroism spectrum reveals that the dialysate is enriched with the Δ -isomer, indicating a preferential binding of the Δ -isomer to the tRNA under these conditions. Similar chiral preferences were obtained under the same conditions for the dialysis of poly(rI)-poly(rC) and poly(rA)-poly(rU) against *rac*- $\text{Ru}(\text{TMP})_3^{2+}$.^{7a} For tRNA, enrichment of the Δ -isomer in the dialysate varied from 3 to 43%, with the lowest binding levels showing the highest associated discrimination. This is consistent with the cooperativity of binding, in which a loss of enantiomeric discrimination is associated with increased binding of the metal complex. In contrast to the $\text{Ru}(\text{TMP})_3^{2+}$ results, the weakly bound $\text{Ru}(\text{phen})_3^{2+}$ exhibits a slight enrichment in the dialysate for the Δ -isomer that varies from 10 to 35%. At low bound concentrations of $\text{Ru}(\text{phen})_3^{2+}$, the Δ -isomer is favored for binding against the tRNA, while no selectivity is apparent at high bound concentrations

The binding features of $\text{Ru}(\text{TMP})_3^{2+}$ to tRNA are consistent with the results of binding to A-form polymers and are different from that of the intercalation of $\text{Ru}(\text{phen})_3^{2+}$ to B-form polymers. In addition, these studies have shown that $\text{Ru}(\text{phen})_3^{2+}$ binds poorly to the tRNA, which contains several A-form double-helical regions. It is likely that $\text{Ru}(\text{TMP})_3^{2+}$ binds more strongly than $\text{Ru}(\text{phen})_3^{2+}$ to tRNA because the methyl substituents provide more favorable hydrophobic interactions with the surface of the RNA.

Figure 2.7. Circular dichroism spectrum obtained after the dialysis of tRNA^{bulk} against *rac*-Ru(TMP)₃²⁺. Dialysis against the native, folded tRNA leads to the enrichment in the dialysate of the less-favored Δ -isomer as shown. This result demonstrates that the Λ -isomer is preferentially bound to the tRNA.



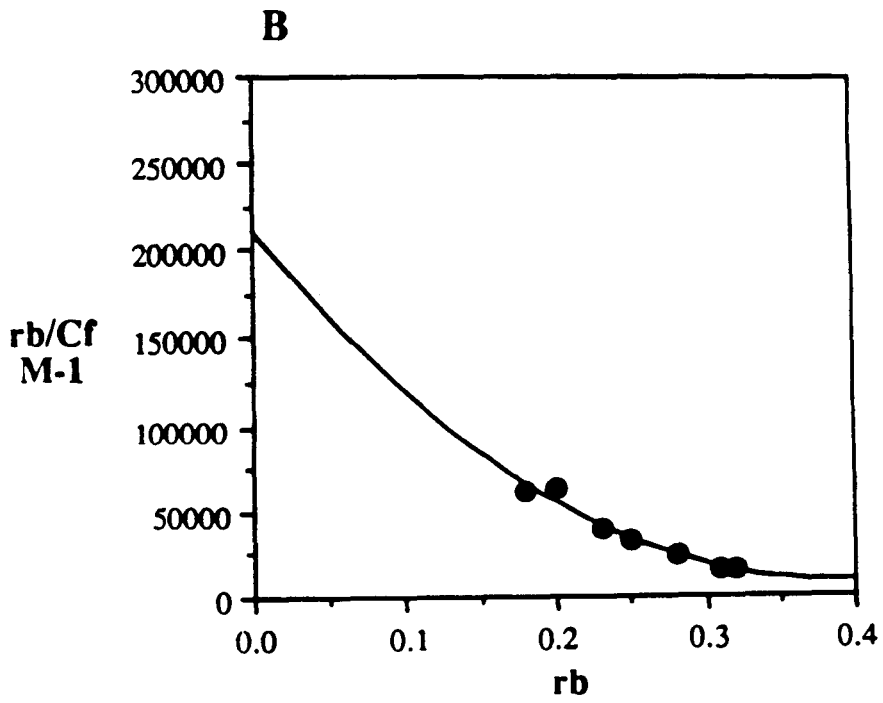
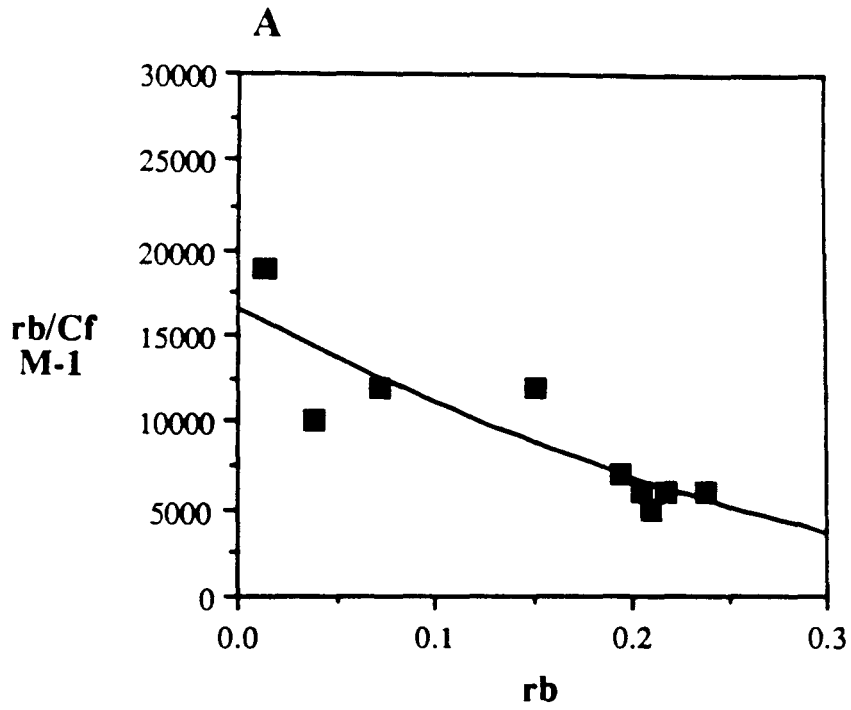
The selectivity for the Λ -isomer also provides evidence for the more favorable binding of the $\text{Ru}(\text{TMP})_3^{2+}$ to the surface of the RNA, rather than through an intercalative mode, based on symmetry requirements. However, the stronger binding of $\text{Ru}(\text{TMP})_3^{2+}$ to the tRNA compared to the synthetic double-stranded RNAs suggests that the complex may bind by other modes on the highly structured, folded tRNA. In addition, the enantiomeric selectivity for the Δ -isomer with $\text{Ru}(\text{phen})_3^{2+}$ indicates that this complex may also bind to the tRNA molecule by an alternative binding mode.

2.3.3. Equilibrium Dialysis of Rh(III) Complexes Against tRNA

The use of equilibrium dialysis and other analyses has established that the phi complexes of rhodium(III) have an unusually high affinity for DNA.⁶ In a similar manner, binding isotherms were determined by equilibrium dialysis of baker's yeast tRNA^{bulk} against *rac*- $\text{Rh}(\text{phen})_2\text{phi}^{3+}$ and *rac*- $\text{Rh}(\text{phi})_2\text{bpy}^{3+}$. Figure 2.8 shows Scatchard plots which were obtained for these two rhodium complexes bound to tRNA. The plot for $\text{Rh}(\text{phen})_2\text{phi}^{3+}$ shows a lot of scatter for the points in the low r_b range. This results because of difficulties measuring the concentration of free metal complex in this range. Because of the high binding of the metal complex to tRNA, all of the metal complex is inside the bag at low concentrations, and the remaining metal concentration outside the bag is below the detection limit by absorption spectroscopy. Therefore, no consistent data points were available at r_b values less than 0.1, thus making it difficult to fit a binding isotherm. Also, the rhodium complex has a tendency to precipitate in the presence of tRNA at high concentrations.

The curve for $\text{Rh}(\text{phen})_2\text{phi}^{3+}$ binding to tRNA was fit using a 2^o polynomial that approximated the fit of the von Hippel equation for anticooperative binding¹⁴. The intersection of this curve with the y-axis gives the approximate intrinsic binding constant K_b , $1.6 \times 10^4 \text{ M}^{-1}$. This is likely to be an underestimate of the binding constant because of

Figure 2.8. Scatchard plots of $\text{Rh}(\text{phen})_2\text{phi}^{3+}$ and $\text{Rh}(\text{phi})_2\text{bpy}^{3+}$ bound to native $\text{tRNA}^{\text{bulk}}$. (A) Plot of the $\text{Rh}(\text{phen})_2\text{phi}^{3+}$ results from the equilibrium dialysis experiments. The curve was fit using a 2^o polynomial, which approximates the fit using the von Hippel equation for anticooperative binding. Intersection of this curve with the y-axis (intrinsic K_b) occurs at $1.6 \times 10^4 \text{ M}^{-1}$ by this method. (B) Plot of the $\text{Rh}(\text{phi})_2\text{bpy}^{3+}$ results from the equilibrium dialysis experiments. The points fall on a curve characteristic of anticooperative binding with an intrinsic K_b of $2 \times 10^5 \text{ M}^{-1}$.



difficulties in measuring the data at low r_b values. If the data is plotted where r_b is the ratio of the bound metal complex to the concentration of tRNA in molecules, rather than nucleotides, an intrinsic binding constant of $1.5 \times 10^6 \text{ M}^{-1}$ is obtained. This higher value for the binding constant is more consistent with the value obtained for $\text{Rh}(\text{phen})_2\text{phi}^{3+}$ bound to calf thymus DNA ($1.97 \times 10^6 \text{ M}^{-1}$).⁶ It is possible that the rhodium complex is very site-selective in its binding to tRNA, whereas on DNA the binding may be less discriminating, thus explaining the difference in binding constants between the polynucleotides.

The Scatchard plot for $\text{Rh}(\text{phi})_2\text{bpy}^{3+}$ was also difficult to obtain because of high precipitation of the complex inside the dialysis bags at high r_b values. It was impossible to obtain r_b values less than 0.2 because the rhodium complex was all bound inside the dialysis bags at low concentrations, and no detectable complex remained outside the bags. However, if the binding curve is extrapolated from the dialysis data, a binding constant of $2 \times 10^5 \text{ M}^{-1}$ is obtained, which is consistent with the binding constant obtained for $\text{Rh}(\text{phi})_2\text{bpy}^{3+}$ to calf thymus DNA ($2.7 \times 10^5 \text{ M}^{-1}$).⁶

The dialysate in the $\text{Rh}(\text{phen})_2\text{phi}^{3+}$ experiment became enriched in the Δ -isomer, indicating a preferential binding of the Λ -isomer to tRNA. These results are similar to the results observed with the dialysis of $\text{Rh}(\text{phen})_2\text{phi}^{3+}$ with double-stranded DNA, in which the Λ -isomer bound more favorably, but only at high metal concentrations.⁶ Once the strong binding sites of the complex on tRNA are saturated, a weaker binding mode may become prevalent in which the Λ -isomer is favored. No chiral discrimination was evident in the binding of $\text{Rh}(\text{phi})_2\text{bpy}^{3+}$ to the tRNA.

Difficulties were encountered using the dialysis method to measure the binding constant of *rac*- $\text{Rh}(\text{DIP})_3^{3+}$ to the tRNA. This complex was too insoluble in water to perform dialysis experiments. *Rac*- $\text{Rh}(\text{TMP})_3^{3+}$ showed less cooperative binding than $\text{Ru}(\text{TMP})_3^{2+}$ in a dialysis experiment performed under the same conditions. Perhaps

the higher solubility of the rhodium complex in water diminishes the cooperative binding effects of the methylated complex. The Scatchard plot, shown in Figure 2.9, gives an intrinsic binding constant K_b of $2 \times 10^4 \text{ M}^{-1}$. Once again, however, these results must be examined with caution because the data points lie far from the y-intercept and the binding curve must be extrapolated to the ordinate of the Scatchard plot.

2.3.4. Absorption Titrations of Ru(II) and Rh(III) Complexes with tRNA

In the absorption titration experiment, perturbations in the electronic spectra of the metal complexes upon binding to tRNA will be considered. Table 2.1 summarizes the spectral properties of the metal complexes and changes observed upon binding to the tRNA^{bulk} from baker's yeast. An absorption hypochromism as well as a large red shift in the intense metal to ligand charge-transfer band (MLCT) of the ruthenium(II) complexes or in the phi-centered π - π^* transition of the rhodium(III) mixed-ligand complexes may accompany binding to the tRNA. The binding to tRNA by Ru(phen)₃²⁺ showed no changes in the absorption spectrum of the complex. This is different from that observed for Ru(phen)₃²⁺ bound to B-DNA, which exhibited a noticeable hypochromism (17%) and isosbestic points at 355 and 364 nm in the absorption spectrum.¹⁷ These spectral changes have been associated with intercalation of the metal complex into the DNA base pairs in the major groove. Since the major groove of an A-form polymer is largely inaccessible to intercalation by the metal complex, the absence of observable changes in the absorption spectrum of Ru(phen)₃²⁺ in the presence of tRNA is reasonable.

The absorption spectrum of Ru(TMP)₃²⁺ with bound tRNA shows a slight hypochromism (9%) with an isosbestic point at 455 nm, where the mole ratio of metal complex to RNA in nucleotides (Ru/RNA) is 0.025. These results differ from Ru(TMP)₃²⁺ bound to poly(rI)·poly(rC), which showed no changes in the absorbance spectrum.⁷ The absence of absorption changes for Ru(TMP)₃²⁺ bound to double-stranded

Figure 2.9. Scatchard plot of $\text{Rh}(\text{TMP})_3^{3+}$ bound to native $\text{tRNA}^{\text{bulk}}$. The data was obtained by equilibrium dialysis. The curve was fit using a 2^o polynomial, which approximates the fit using the von Hippel equation for anticooperative binding. Intersection of this curve with the y-axis (intrinsic K_b) occurs at $2.0 \times 10^4 \text{ M}^{-1}$ by this method.

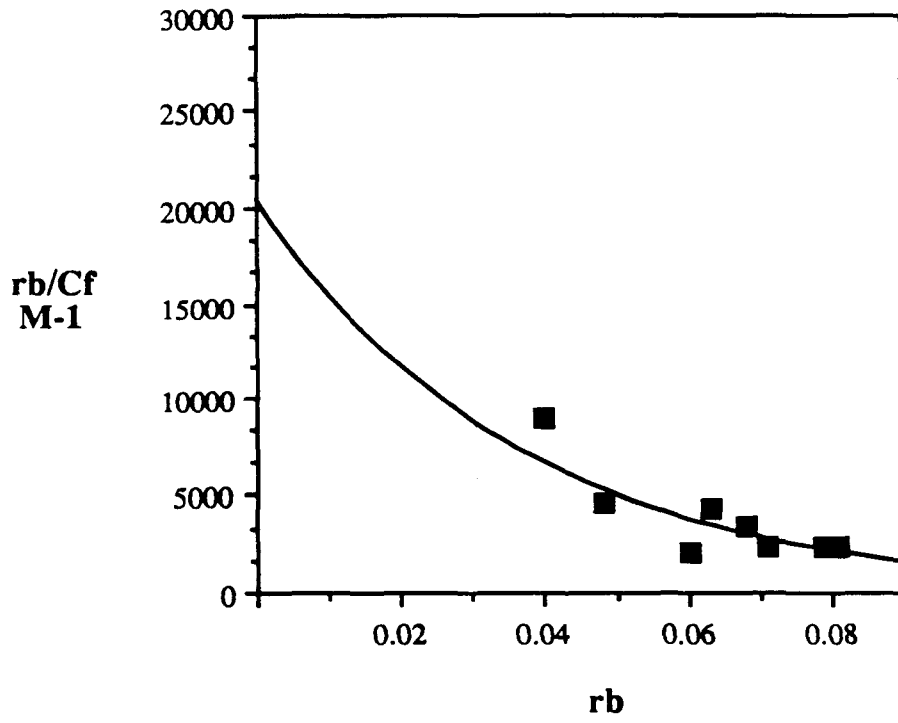


Table 2.1. Changes Induced in Absorbance of Metal Complexes by the Presence of tRNA.

<i>metal complex</i>	<i>Absorption λ_{max} (nm), free</i>	<i>Absorption λ_{max} (nm), bound</i>	$\Delta\lambda$ (nm)	$\%H^a$
Ru(phen) ₃ ²⁺	447	447	0	0
Ru(TMP) ₃ ²⁺	438	438	0	9
Rh(TMP) ₃ ³⁺	282	284	2	9
Rh(DIP) ₃ ³⁺	296	300	4	37
Rh(phen) ₂ phi ³⁺	358	372	14	24
Rh(phi) ₂ bpy ³⁺	375	390	15	15

^a %H represents the percent hypochromicity, $[\epsilon_{free} - \epsilon_{measured}]/\epsilon_{free}$

RNA was expected since the methyl groups on the phenanthroline would prevent this complex from intercalating into the RNA. $\text{Ru}(\text{TMP})_3^{2+}$ likely binds to the minor groove of the A-form RNA or DNA with the ligands orientated against the backbone of the polynucleotide in a way which is unlikely to cause any change in the aromaticity of the ligands, and thus no changes in the absorption spectrum.¹⁸ The hypochromicity observed for $\text{Ru}(\text{TMP})_3^{2+}$ bound to tRNA as compared to double-helical RNA indicates that perhaps a different type of binding interaction exists. Stacking of the bases of the tRNA with the aromatic portion of the $\text{Ru}(\text{TMP})_3^{2+}$ may result because of the unusual tertiary structure of the tRNA.

In the case of $\text{Rh}(\text{DIP})_3^{3+}$, it is difficult to measure the changes in the absorption spectrum because the complex is insoluble at high concentrations in water. In addition, the absorption spectrum of $\text{Rh}(\text{DIP})_3^{3+}$ ($\epsilon_{298} = 1.16 \times 10^5 \text{ M}^{-1} \text{ cm}^{-1}$) overlaps with the tRNA spectrum ($\epsilon_{260} = 7460 \text{ M}^{-1} \text{ cm}^{-1}$) at high concentrations of RNA. However, upon the addition of tRNA (100 μM in nucleotides) to a solution of $\text{Rh}(\text{DIP})_3^{3+}$ in buffer 1 at low concentration (2 μM) ($\text{Rh}/\text{RNA} = 0.02$), a 4 nm red shift in the absorbance maximum is observed with an isosbestic point at 325 nm and a hypochromicity of 37%. In the case of $\text{Rh}(\text{TMP})_3^{3+}$, similar problems are encountered with overlap of the absorption bands ($\epsilon_{282} = 8.5 \times 10^4$ for $\text{Rh}(\text{TMP})_3^{3+}$); however, a 2 nm red shift in the absorbance maximum is observed with an isosbestic point at 292 nm and a hypochromicity of 9% upon the addition of tRNA ($\text{Rh}/\text{RNA} = 0.015$).

The ligand-centered $\pi\text{-}\pi^*$ transition of the $\text{Rh}(\text{phen})_2\text{phi}^{3+}$ complex is strongly affected in the presence of tRNA. The absorption titration spectrum is shown in Figure 2.10. A large red shift (14 nm) and hypochromicity (24%) are associated with the binding of $\text{Rh}(\text{phen})_2\text{phi}^{3+}$ to tRNA ($\text{Rh}/\text{RNA} = 0.04$). The hypochromicity is almost half of the value obtained for the rhodium complex bound to DNA (42.3%), which was associated with a 16 nm red shift.⁶ Similar difficulties were encountered in extracting the binding

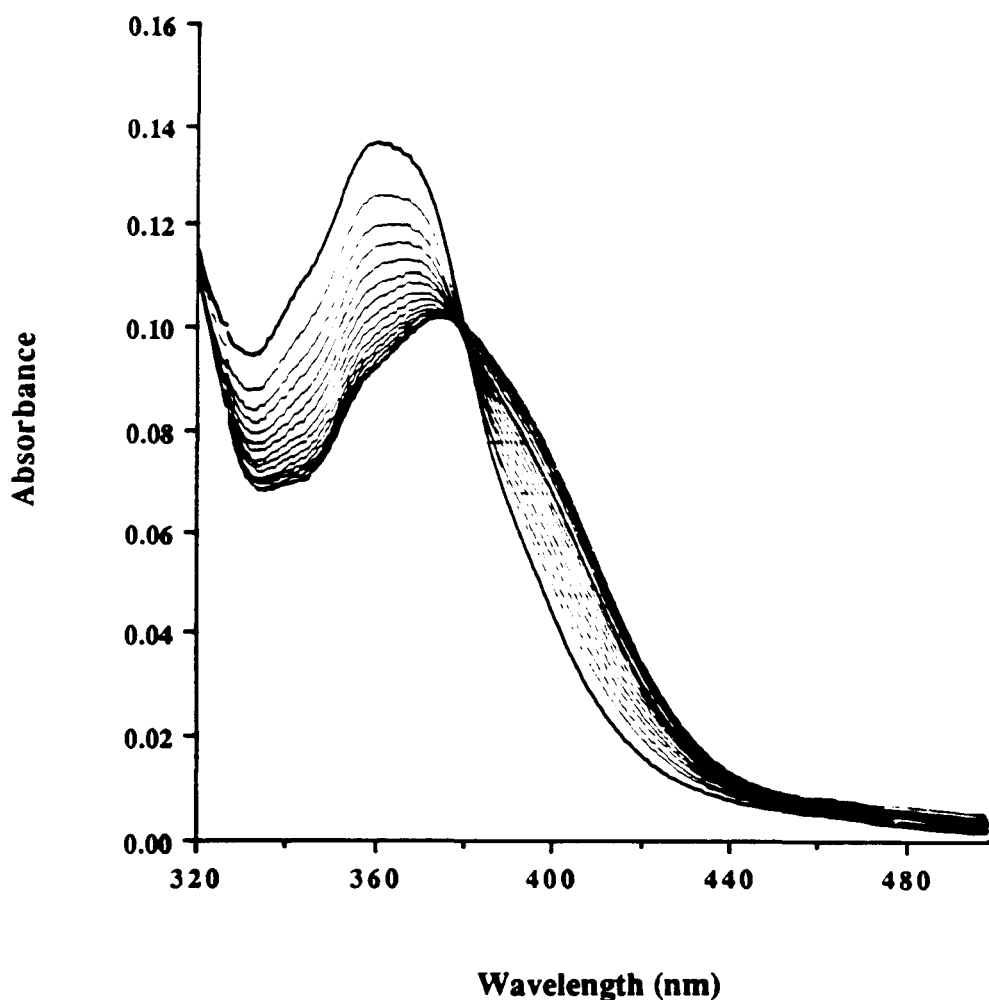


Figure 2.10. Absorption hypochromism of $\text{Rh}(\text{phen})_2\text{phi}^{3+}$ in the presence of yeast tRNA^{Phe} . Attempts were made to obtain many points at low mole ratios of rhodium complex bound to RNA nucleotides (r_b). $[\text{Rh}(\text{phen})_2\text{phi}^{3+}] = 10.3 \mu\text{M}$ for all scans. $[\text{RNA}] = 0, 29.6, 44.1, 59.3, 73.7, 88.9, 103.4, 118.6, 133.0, 148.2, 162.6, 177.8, 192.3, 207.5,$ and $221.9 \mu\text{M}$, respectively, as the scans shift to lower absorbances. Isosbestic points: 383 and 315 nm. $\lambda_{\text{max free}} = 358 \text{ nm}$, $\lambda_{\text{max bound}} = 372 \text{ nm}$ (14 nm red shift). Hypochromicity = 24%.

curve from the titration data as were found in the Scatchard analysis of the dialysis data. It is difficult to obtain data for low r_b values; therefore, the binding curve must be extrapolated from the binding data far from the ordinate of the Scatchard plot. As shown in Figure 2.11, the Scatchard curve using the absorption titration data gives a binding constant of $3.5 \times 10^5 \text{ M}^{-1}$ for $\text{Rh}(\text{phen})_2\text{phi}^{3+}$ bound to tRNA. These results are consistent with those obtained by this method for $\text{Rh}(\text{phen})_2\text{phi}^{3+}$ binding to calf thymus DNA ($3.6 \times 10^5 \text{ M}^{-1}$) when plotted in the form of a Scatchard plot.⁶

In the case of $\text{Rh}(\text{phi})_2\text{bpy}^{3+}$, large changes in the absorbance spectrum ($\%H = 15\%$, $\Delta\lambda_{\text{max}} = 15 \text{ nm}$, $\text{Rh}/\text{RNA} = 0.014$) are indicative of high binding to the tRNA. In an absorption titration experiment, $\text{Rh}(\text{phi})_2\text{bpy}^{3+}$ initially shows a large hypochromism, then only small changes are observed upon the addition of tRNA. This makes the data difficult to interpret in the form of the Scatchard plot because the points will fall over a very narrow range of r_b values. Similarly, in the case of a Meehan half-reciprocal plot, there is a large error in the $\Delta\epsilon_{\text{AP}}$ value.

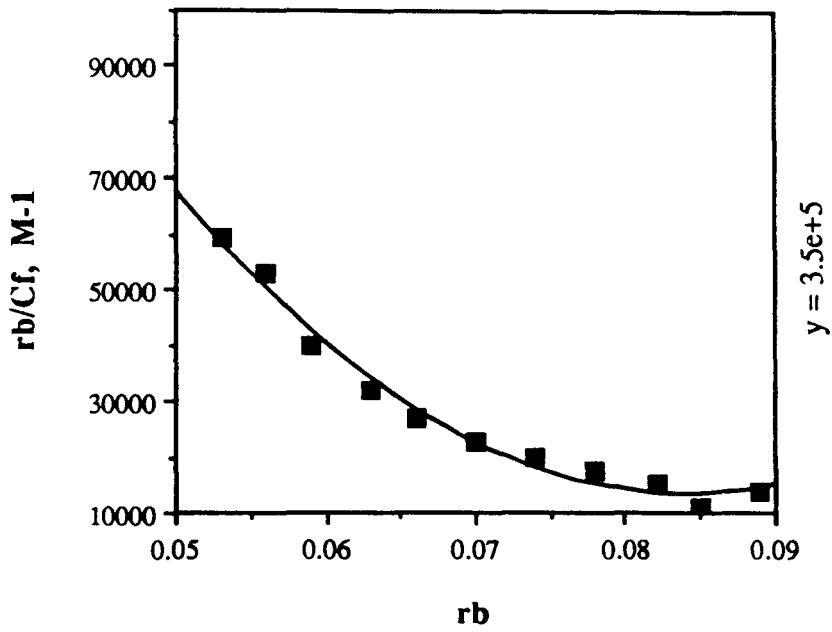
As summarized in Table 2.1, it is evident that the metal complexes interact very differently with tRNA. The phi complexes of rhodium(III) seem to exhibit larger effects on the aromaticity of the ligands, suggestive of stacking interactions with the RNA bases. In contrast, the tetramethyl-phenanthroline ligands seem to interact through hydrophobic interactions on the surface of the RNA, but with other binding interactions present, which also cause small changes in the absorbance spectra.

2.3.5. Steady-State Luminescence, Time-Resolved Emission Lifetime and Luminescence-Quenching Measurements of Ru(II) Complexes Bound to tRNA

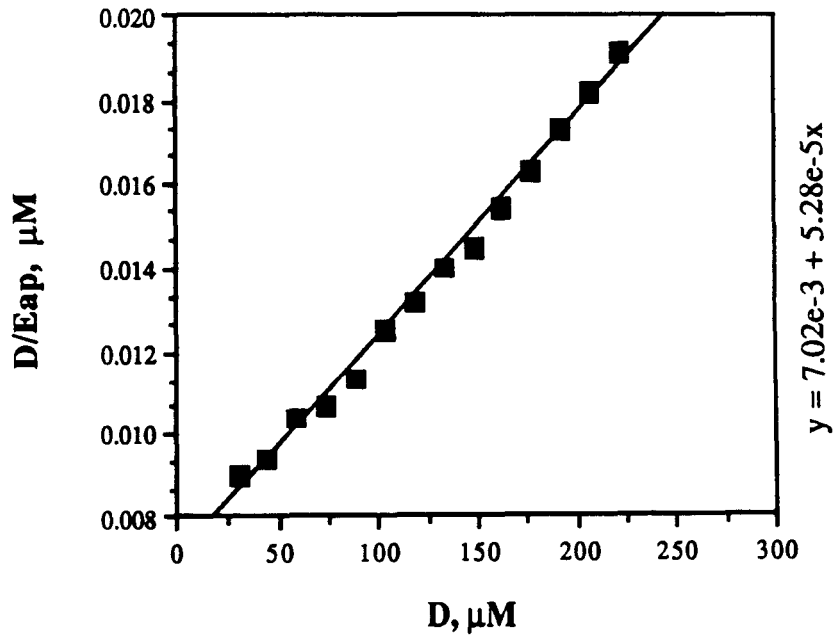
A study of the photophysical properties of the tris(phenanthroline)ruthenium(II) complexes in the presence of $\text{tRNA}^{\text{bulk}}$ was carried out to characterize further the binding

Figure 2.11. Absorption titration data of $\text{Rh}(\text{phen})_2\text{phi}^{3+}$ binding to yeast tRNA^{Phe} . (A) Scatchard plot of $\text{Rh}(\text{phen})_2\text{phi}^{3+}$ bound to yeast tRNA^{Phe} . The curve was fit using a 2^o polynomial, which approximates the fit using the von Hippel equation for anticooperative binding. Intersection of this curve with the y-axis (intrinsic K_b) occurs at $3.5 \times 10^5 \text{ M}^{-1}$ by this method. (B) A Meehan half-reciprocal plot of the same data gives a binding constant of $7.5 \times 10^3 \text{ M}^{-1}$.

A



B



characteristics of these complexes with the native folded tRNA in comparison with double-stranded RNA or DNA. It has been possible to monitor the binding of ruthenium(II) complexes to DNA because of the sensitivity of their photophysical properties to DNA binding.¹⁷ For example, luminescence enhancements in the MLCT band of Ru(phen)₃²⁺ when bound to B-form DNA were observed in steady-state experiments. Luminescence enhancements have been associated with an intercalated mode of binding since a rigidly held and solvent-protected molecule stacked with the base pairs of the DNA helix would experience a slower vibrational quenching of the excited state. In time-resolved luminescence experiments, a biexponential emission decay of the excited state was indicative of two binding modes for Ru(phen)₃²⁺ with DNA.⁴ These binding modes were confirmed by other experiments such as emission polarization and NMR studies.^{4,5} The first binding mode is an intercalative mode with a longer lifetime (~2 μs) in the excited state compared to free ruthenium (~550 ns). The second binding mode is a surface-bound mode that exhibits a lifetime similar to free ruthenium complex.

Steady-state luminescence titrations were performed on *rac*-Ru(TMP)₃²⁺ with tRNA. Samples containing 5 μM Ru(TMP)₃²⁺ in buffer 1 with as much as 450 μM added tRNA were excited at 455 nm and emission was measured at 550 to 750 nm. No increases in the emission intensity were observed upon the addition of tRNA. This result is in contrast to enhancements in the luminescence of Ru(phen)₃²⁺ on binding to duplex DNA.¹⁷ In fact, a slight decrease in the emission intensity was evident with Ru(TMP)₃²⁺ bound to tRNA. This is consistent, however, with studies performed on poly(rI)·poly(rC) and poly(rA)·poly(rU) in which a surface-bound mode of Ru(TMP)₃²⁺ did not lead to enhancements of the emission intensity.¹⁸ The decrease in luminescence may be a result of self-quenching of the ruthenium complex, which binds cooperatively to the RNA.

Steady-state quenching studies were performed on Ru(TMP)₃²⁺ in the presence and absence of tRNA. In a buffer 1 solution containing 5 μM Ru(TMP)₃²⁺ and 225 μM

tRNA, the emission was monitored at 605 nm with the addition of an anionic quencher, $\text{Fe}(\text{CN})_6^{4-}$. One would expect linear behavior for a single-component, donor-quencher system. Alternatively, nonlinear behavior may be indicative of a two- or higher-component system. The anionic quencher is expected to be repelled by the negatively charged RNA phosphate backbone. Therefore, a tightly bound cationic ruthenium complex may be protected from the quencher, while free or surface-bound ruthenium would be quenched rapidly. Figure 2.12 (panel A) shows that the Stern-Volmer plot for $\text{Ru}(\text{TMP})_3^{2+}$ is nonlinear, even in the absence of tRNA. This may be a result of either self-association or precipitation of the metal complex in solution. In the presence of tRNA, the Stern-Volmer plot is also nonlinear and resembles the quenching of free ruthenium complex. However, some points on the plot at low quencher values lie off the curve. This suggests that a ruthenium complex bound to tRNA is distinguished from the free $\text{Ru}(\text{TMP})_3^{2+}$ in solution by the anionic quencher. The unusual curvature at low quencher values suggests differential accessibility of the bound ruthenium species to the quencher, while at high concentrations of quencher, the quenching resembles that of free ruthenium complex.

The emission decay curve of $\text{Ru}(\text{TMP})_3^{2+}$ upon binding to synthetic double-stranded DNA or RNA was found to be a single exponential.^{7a} The emission lifetime of $\text{Ru}(\text{TMP})_3^{2+}$ free in solution or bound to poly(rI)·poly(rC) or calf thymus DNA corresponded to the shorter-lived component of $\text{Ru}(\text{phen})_3^{2+}$, which was assigned to the surface-bound form. Luminescence lifetime studies were performed on the ruthenium(II) complexes in the presence of tRNA, with excitation at 455 nm and emission monitored at 600 nm. Similar results were obtained for $\text{Ru}(\text{phen})_3^{2+}$ in the presence of tRNA, in which a single exponent with a lifetime of 550 ns was obtained. The lifetime of $\text{Ru}(\text{phen})_3^{2+}$ was essentially unchanged upon addition of 225 μM tRNA, showing no evidence of interaction with tRNA by this method. In contrast, the $\text{Ru}(\text{TMP})_3^{2+}$ exhibited biexponential behavior in the presence of tRNA. As summarized in Table 2.2, the decay curves for $\text{Ru}(\text{TMP})_3^{2+}$

Figure 2.12. Luminescence quenching of $\text{Ru}(\text{TMP})_3^{2+}$ with increasing concentrations of $\text{Fe}(\text{CN})_6^{4-}$. (A) The Stern-Volmer plot of free $\text{Ru}(\text{TMP})_3^{2+}$ in solution exhibits nonlinear behavior. (B) The Stern-Volmer plot of $\text{Ru}(\text{TMP})_3^{2+}$ bound to $\text{tRNA}^{\text{bulk}}$ also shows nonlinear behavior, but with nearly the same curvature as the free ruthenium.

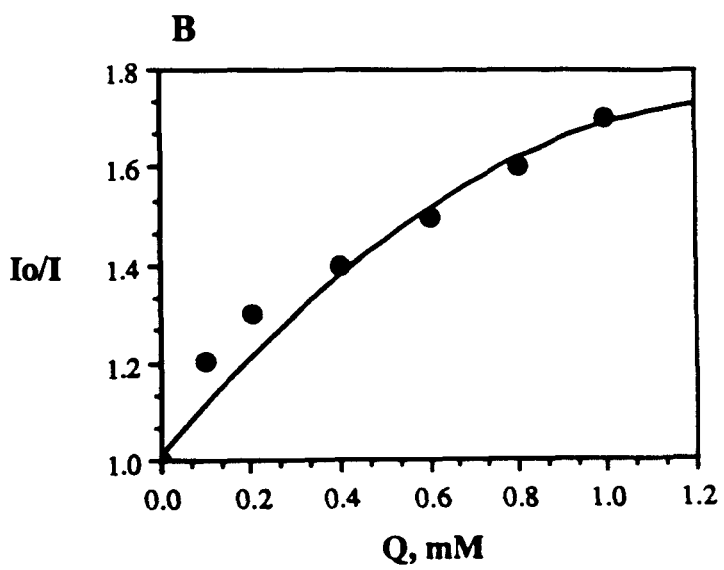
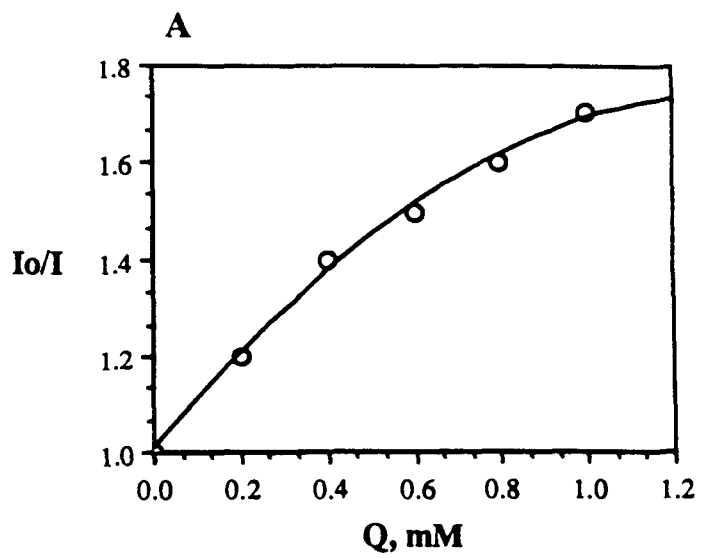


Table 2.2. Emission Lifetimes of *rac*-Ru(TMP)₃²⁺ and *rac*-Ru(phen)₃²⁺ in the Presence and Absence of tRNA and K₄Fe(CN)₆·3H₂O.^a

<i>metal complex</i>	τ_1 (ns)	τ_2 (ns)
Ru(phen) ₃ ²⁺	554 ± 3 ^b	
Ru(phen) ₃ ²⁺ + tRNA ^c	575 ± 2	
Ru(TMP) ₃ ²⁺	635 ± 3	
Ru(TMP) ₃ ²⁺ + tRNA ^c	355 ± 27 (20%)	743 ± 19 (80%)
Ru(TMP) ₃ ²⁺ + tRNA ^d	275 ± 16 (20%)	721 ± 11 (80%)
Ru(TMP) ₃ ²⁺ + Q ^e	461 ± 2	
Ru(TMP) ₃ ²⁺ + tRNA + Q ^f	292 ± 28 (30%)	621 ± 30 (70%)

^a 3500 to 4000 scans were taken on a 6.53 ns timescale using 5 μM metal concentrations in buffer 1.

^b Errors shown are the standard deviations associated with each lifetime measurement. Each value represents an average of at least three lifetime measurements.

^c 5 μM metal complex present with 225 μM tRNA^{bulk}.

^d 5 μM metal complex present with 450 μM tRNA^{bulk}.

^e 5 μM metal complex present with 0.8 mM Fe(CN)₆⁴⁻.

^f 5 μM metal complex present with 225 μM tRNA^{bulk} and 0.8 mM Fe(CN)₆⁴⁻.

upon the addition of 225 μM tRNA can be fit to a biexponential decay with a short-lived component (355 ns) and a longer-lived component (740 ns). Consistent with the absorption titration experiments and the steady-state quenching experiments, the results for $\text{Ru}(\text{TMP})_3^{2+}$ binding to tRNA are indicative of two different binding modes. In the presence of ferrocyanide, which efficiently quenches the free ruthenium, the two components were still present in the decay profile. However, the percentage of each component was changed. The short component is 20% with no quencher, 30% with 0.8 mM quencher, and 75% with 1.6 mM quencher. This suggests that the short-lived emission has contributions from a tightly bound species of the $\text{Ru}(\text{TMP})_3^{2+}$ to tRNA that is not quenched by the anionic ferrocyanide. The longer-lived emission can be quenched by ferrocyanide and is therefore assigned to be free ruthenium or weakly bound ruthenium on the surface of the tRNA. In contrast to studies with DNA and $\text{Ru}(\text{phen})_3^{2+}$, the bulky methyl groups on the phenanthrolines of $\text{Ru}(\text{TMP})_3^{2+}$ would prohibit intercalation between the RNA bases. However, the shorter lifetime component of $\text{Ru}(\text{TMP})_3^{2+}$ bound to tRNA seems to be correlated with a tightly bound species. The short lifetime component may be a result of self-quenching by another bound ruthenium molecule, which would also be consistent with cooperative binding by $\text{Ru}(\text{TMP})_3^{2+}$.

2.4. Discussion

The results of the experiments discussed above demonstrate that there are significant differences in the manner in which the metal complexes bind to tRNA. The differences in binding are likely based on the different shapes of the molecules as well as the different charges of the ruthenium(II) vs. rhodium(III) complexes. The complexes can bind through several possible interactions: intercalation, hydrophobic interactions with the surface of the RNA, or electrostatic interactions to the negatively charged phosphate backbone. Variations in the binding characteristics of the metal complexes suggests that

they interact with the tRNA through several of these modes. It has been established through crystallographic⁸ and NMR⁹ studies that the folded tRNA chain has a rigid three-dimensional structure in which the double-helical regions adopt an A-conformation. This type of structure will restrict intercalation. It has been shown that ethidium bromide, which intercalates into DNA, will bind only several sites on the tRNA molecule.¹⁹ Therefore, both the double-helical regions and the unstacked, single-stranded regions of the tRNA would not be well suited for intercalation by the metal complexes.

In contrast, $\text{Ru}(\text{TMP})_3^{2+}$ was expected to bind the tRNA in a groove-binding interaction. The four methyl substituents on the phenanthroline ligands may sterically hinder the intercalation of the complex to DNA. However, the increased size and hydrophobicity of the complex should be favorable for surface binding in the helical groove. The shallow extended surface in the minor groove of an A-form RNA was expected to provide an ideal binding site for the metal complex. Indeed, stronger binding by $\text{Ru}(\text{TMP})_3^{2+}$ was observed to tRNA than either double-stranded RNA or RNA/DNA hybrids. In addition, the equilibrium dialysis experiments showed an enantiomeric preference for the Λ -isomer of $\text{Ru}(\text{TMP})_3^{2+}$. This is consistent with the results found with synthetic, double-stranded RNAs in which surface binding of the chiral complex to a right-handed helix favored the left-handed isomer.⁷ However, the results of the absorbance titration, the biexponential luminescence decay, and the steady-state luminescence quenching experiments on $\text{Ru}(\text{TMP})_3^{2+}$ bound to tRNA were all in contrast to the results found on synthetic, double-stranded RNA. These results, along with the higher binding to tRNA, suggest that more than one binding mode to tRNA exists. The results obtained with $\text{Ru}(\text{phen})_3^{2+}$ binding to tRNA were also consistent with these studies. Although this complex can surface bind, it is less favorable because of the lack of hydrophobic substituents on the phenanthroline ligands. A racemic mixture of $\text{Ru}(\text{phen})_3^{2+}$ was shown to bind only weakly to tRNA. However, the enantiomeric preference for the Δ -isomer of

$\text{Ru}(\text{phen})_3^{2+}$ at high r_b values was suggestive of an alternative mode of binding for this complex. The unusual binding modes associated with the ruthenium complexes binding to tRNA may exist because of the tertiary folding of the RNA molecule.

The binding of $\text{Rh}(\text{TMP})_3^{3+}$ and $\text{Rh}(\text{DIP})_3^{3+}$ to tRNA was difficult to study because of the overlap in their absorbance spectra with tRNA as well as solubility problems. However, both complexes exhibit absorbance hypochromism and small red shifts, indicative of some kind of interaction with the tRNA in which the aromatic portions of the molecules are perturbed. $\text{Rh}(\text{TMP})_3^{3+}$ exhibits different properties in binding to tRNA than $\text{Ru}(\text{TMP})_3^{2+}$, likely because of differences in the charge and solubility in water. $\text{Rh}(\text{TMP})_3^{3+}$ appears to bind more tightly than $\text{Ru}(\text{TMP})_3^{2+}$ to the tRNA, and in a noncooperative fashion, as determined by Scatchard analysis of the dialysis experiments.

The results of the equilibrium dialysis and absorbtion titration experiments are indicative of strong binding of $\text{Rh}(\text{phen})_2\text{phi}^{3+}$ and $\text{Rh}(\text{phi})_2\text{bpy}^{3+}$ to tRNA. The intrinsic binding constants obtained by Scatchard analysis for the two complexes are consistent with binding to double-stranded DNA. However, these binding constants (on the order of 10^5 M^{-1}) are likely to be underestimates of the true binding constants. Based on cleavage experiments (Chapter 3) with micromolar concentrations of RNA and nanomolar concentrations of the rhodium complex, the binding constants must be greater than or equal to 10^6 M^{-1} . The error in the intrinsic binding constant K_b is likely introduced from the extrapolation of the binding data far from the ordinate of the Scatchard plot. The high curvature of the Scatchard plots, as well as the enantioselectivity for the Λ -isomer, of $\text{Rh}(\text{phen})_2\text{phi}^{3+}$ are also suggestive of more than one binding mode. It is likely that one strong binding mode exists at low r_b values and another exists at high r_b values.

The absorbtion hypochromism and red shifts observed for phi complexes of rhodium(III) when bound to tRNA are suggestive of a strong stacking interaction with the aromatic portion of the metal complex and the RNA bases. Several studies such as helix

unwinding⁶, absorption titration⁶, and cleavage mechanism^{20,21} indicate that rhodium complexes containing phi ligands bind strongly in the major groove of the DNA by an intercalative mode. However, more experiments are necessary to determine if the same type of binding can occur with RNA. Since the double-stranded regions of tRNA are A-form, the RNA bases are pulled into the interior of the helix and are inaccessible for stacking with the metal complexes from the major groove. The tertiary folding of the tRNA molecule must therefore be important for interaction with the rhodium phi complexes. Also, since the phenanthroline complexes were shown to bind only weakly to the tRNA, it is likely that the extended aromatic system of the phi ligand is necessary to obtain stacking of the metal complex with the tRNA bases.

In conclusion, the RNA binding properties of the ruthenium(II) and rhodium(III) complexes are generally consistent with binding to DNA or RNA synthetic polymers. Some differences in tRNA binding occur, and these are likely associated with the more complex tertiary structure of the RNA. In general, the metal complexes exhibit different binding modes from one another, as well as different enantiomeric preferences. The phi complexes of rhodium(III) exhibit strong binding, likely through stacking interactions with the tRNA, while $\text{Ru}(\text{TMP})_3^{2+}$ exhibits surface binding, as well as other hydrophobic interactions with the RNA. The comparison of the photophysical properties and binding characteristics of these metal complexes in the presence of tRNA has afforded a basis for the development of structure-specific probes for RNA. The interactions of the different metal complexes with tRNA illustrates how the different shapes of the molecules may be incorporated into the design of new reagents that may be able to distinguish between different structures of RNA. With these studies in mind, we would like to investigate the photocleavage properties of the metal complexes in order to develop site-selective cleaving agents of RNA.

References

1. Pyle, A. M.; Barton, J. K. *Prog. Inorg. Chem.* **1990**, 38, 413-475.
2. a) Lin, C-T.; Böttcher, W.; Chou, M.; Creutz, C.; Sutin, N. *J. Am. Chem. Soc.* **1976**, 98, 6536-6544.
b) Sutin, N.; Creutz, C. *Pure Appl. Chem.* **1980**, 52, 2717-2738.
3. Balzani, V.; Moggi, L.; Manfrin, M. F.; Bolletta, F.; Laurence, G. S. *Coord. Chem. Rev.* **1975**, 15, 321-433.
4. Barton, J. K.; Goldberg, J. M.; Kumar, C. V.; Turro, N. J. *J. Am. Chem. Soc.* **1986**, 108, 2081-2088.
5. a) Rehmann, J. P.; Barton, J. K. *Biochemistry* **1990**, 29, 1701-1709.
b) Rehmann, J. P.; Barton, J. K. *Biochemistry* **1990**, 29, 1710-1717.
6. Pyle, A. M., Ph. D. Dissertation, Columbia University, New York, 1989.
7. a) Mei, H.-Y.; Barton, J. K. *J. Am. Chem. Soc.* **1986**, 108, 7414-7416.
b) Mei, H.-Y.; Barton, J. K. *Proc. Natl. Acad. Sci. USA* **1988**, 85, 1339-1343.
8. a) Kim, S.-H.; Sussman, J. L.; Suddath, F. L.; Quigley, G. J.; McPherson, A.; Wang, A. H.; Seeman, N. C.; Rich, A. *Proc. Natl. Acad. Sci. U.S.A.* **1974**, 71, 4970-4974.
b) Quigley, G. J.; Rich, A. *Science* **1976**, 194, 796-806.
9. Patel, D. J.; Shapiro, L.; Hare, D. *Q. Rev. Biophys.* **1987**, 20, 78-90.
10. a) Gillard, R. D.; Osborn, J. A.; Wilkinson, G. *J. Chem. Soc., Dalton Trans.* **1965**, 1951-1965.
b) Gidney, P. M.; Gillard, R. D.; Heaton, B. T. *J. Chem. Soc., Dalton Trans.* **1972**, 2621-2628.
11. Pyle, A. M.; Chiang, M. Y.; Barton, J. K. *Inorg. Chem.* **1990**, 29, 4487-4495.
12. Wells, B. D.; Yang, J. T. *Biochemistry* **1974**, 13, 1311-1316.
13. Scatchard, G. *Ann. N. Y. Acad. Sci.* **1949**, 51, 660.

14. McGhee, J. D.; von Hippel, P. H. *J. Mol. Biol.* **1974**, 86, 469-489.
15. Wolfe, A.; Shimer, Jr., G. H.; Meehan, T. *Biochemistry* **1987**, 26, 6392-6396.
16. Rehmann, J. P., Ph. D. Dissertation, Columbia University, New York, 1988.
17. Barton, J. K.; Danishefsky, A. T.; Goldberg, J. M. *J. Am. Chem. Soc.* **1984**, 106, 2172-2176.
18. Mei, H.-Y., Ph. D. Dissertation, Columbia University, New York, 1989.
19. Wells, B. D.; Cantor, C. R. *Nucleic Acids Res.* **1977**, 4, 1667-1680.
20. Long, E. C.; Absalon, M. J.; Stubbe, J.; Barton, J. K., submitted for publication.
21. Sitlani, A.; Long, E. C.; Pyle, A. M.; Barton, J. K. *J. Am. Chem. Soc.* **1992**, in press.

Chapter 3:

Shape-Selective Cleavage of tRNA by Tris(phenanthroline) and Phenanthrenequinone Diimine Complexes of Ru(II) and Rh(III)

3.1. Introduction

One approach for investigating the three-dimensional structure of RNA involves the use of nucleic acid cleaving agents with specific binding properties. Nucleic acid cleavage chemistry can be extremely useful in marking the binding sites of small molecules of defined conformations on the polynucleotides. In particular, the complexes tris(1,10-phenanthroline)ruthenium(II) $\{\text{Ru}(\text{phen})_3^{2+}\}^1$, tris(3,4,7,8-tetramethyl-1,10-phenanthroline)ruthenium(II) $\{\text{Ru}(\text{TMP})_3^{2+}\}^1$, tris(4,7-diphenyl-1,10-phenanthroline)rhodium(III) $\{\text{Rh}(\text{DIP})_3^{3+}\}^2$, bis(1,10-phenanthroline)(9,10-phenanthrenequinone diimine)rhodium(III) $\{\text{Rh}(\text{phen})_2\text{phi}^{3+}\}^3$, and bis(9,10-phenanthrenequinone diimine)(bipyridyl)rhodium(III) $\{\text{Rh}(\text{phi})_2\text{bpy}^{3+}\}^3$ have been shown to target local variations in conformation along DNA, and upon photoactivation, induce DNA strand scission. In order to maximize the information that can be gleaned from these cleavage reactions, studies regarding the mechanism of strand scission of the nucleic acid by these complexes are essential.

The cleavage chemistry of the phenanthrenequinone diimine (phi) complexes of rhodium(III) on DNA has been characterized in some detail.⁴⁻⁵ The quantum yields for nucleic acid base release at 313 nm are 0.0012 for $\text{Rh}(\text{phen})_2\text{phi}^{3+}$ and 0.0003 for $\text{Rh}(\text{phi})_2\text{bpy}^{3+}$. Mechanistic studies indicate that cleavage of DNA results from direct abstraction of the C3'-H atom from the sugar by a delocalized, excited-state radical on the phi ligand. In contrast to the cleavage by $\text{Fe}(\text{EDTA})^{2-}$, the reaction is mediated by a non-diffusible radical, and no secondary reactants such as dithiothreitol are required. Therefore, cleavage of DNA induced by photolysis of the phi complexes of rhodium(III) is

site-specific. In addition, since the reaction originates on the sugar moiety, no base-preference is inherent in the cleavage chemistry. Chemical modification studies, HPLC analyses, and gel electrophoresis have revealed that the primary products of $\text{Rh}(\text{phen})_2\text{phi}^{3+}$ cleavage on a DNA oligomer contain 3'- and 5'-phosphate termini, and nucleic acid bases are released in stoichiometric proportion. These same products are obtained for $\text{Rh}(\text{phi})_2\text{bpy}^{3+}$ cleavage, along with the release of base propenoic acids and termini assigned as 3'-phosphoglycaldehydes. The formation of these additional products was found to depend upon oxygen concentration. These data are consistent with the photoreaction of phi complexes of rhodium(III) intercalated in the major groove of DNA. In addition, there appears to be a relationship between the recognition characteristics of these complexes on DNA and the pathway of strand scission.

The cleavage characteristics of the ruthenium-based complexes differ substantially from the rhodium complexes. Ruthenium(II) polypyridyls have been well characterized⁷ as efficient sensitizers of singlet oxygen in their excited state. Photolysis with visible light of ruthenium complexes bound to DNA promotes strand scission in a reaction mediated by singlet oxygen.¹ In this case, the reaction involves a diffusible species, $^1\text{O}_2$. Therefore, instead of obtaining a single site of cleavage, a region of several bases along the DNA helix is reacted. In addition, the target of singlet-oxygen chemistry is the nucleic acid base rather than the sugar residue. Base treatment with piperidine is therefore required to achieve strand scission. It has also been observed that the singlet oxygen chemistry targets the four bases with different efficiencies with guanine being the most reactive. Gel electrophoresis and HPLC analysis have revealed that the primary products of $\text{Ru}(\text{TMP})_3^{2+}$ or $\text{Ru}(\text{phen})_3^{2+}$ cleavage on DNA contain 3'- and 5'-phosphate termini, and the chemistry proceeds without the release of nucleic acid bases.

In Chapter 2 it was shown that the transition metal complexes are capable of binding to structured RNA and that the binding modes are related to the overall shapes of

the molecules. In this chapter, we describe experiments designed to test the ability of these complexes to induce strand scission of RNA. We will also compare the efficiencies of RNA and DNA cleavage, examine the dependence of cleavage on the irradiation wavelength and metal concentrations, as well as consider the mechanism of RNA cleavage. Most importantly, we have examined the potential of the metal complexes to recognize structured RNA through site-selective cleavage. In order to test the general applicability of these complexes as RNA structural probes, we have first established the individual cleavage selectivities on the structurally characterized yeast tRNA^{Phe}.

3.2. Experimental

3.2.1. Methods for Photocleavage by Rhodium and Ruthenium Complexes

Materials: The reagents used in this study were obtained from the following suppliers: tRNA^{Phe} from brewer's yeast, pUC19, *Hind* III, *Pvu* II, ATP, and dithiothreitol (DTT) (Boehringer Mannheim, Indianapolis, IN); T4 RNA ligase, sonicated calf thymus DNA (Pharmacia, Piscataway, NJ); Trizma base (Tris), NaOAc, NH₄OAc, NaCl, HEPES (free acid), cacodylic acid (sodium salt), MgCl₂, EDTA, polyacrylamide, N,N'-methylene-bis-acrylamide, urea, boric acid, and dimethyl sulfoxide (Molecular Biology Grade if available, Sigma, St. Louis, MO); diethylpyrocarbonate (DEPC), dimethyl sulfate (DMS), hydrazine, sodium borohydride, and aniline (Aldrich, Milwaukee, WI); [γ -³²P]-ATP and [5'-³²P]-pCp (NEN/Du Pont, Wilmington, DE).

DNA and RNA Preparation, Purification, and Labeling: The plasmid DNA (pUC19) was purified by phenol extraction and precipitated with ethanol. The DNA was then digested with a restriction enzyme (*Pvu* II) to linearize and give 5'-termini for dephosphorylation and end labeling⁸ with T4 polynucleotide kinase and [γ -³²P]-ATP. The labeled fragments were treated with *Hind* III to yield three double-stranded fragments. The 141 base-pair fragment was purified by preparative nondenaturing gel electrophoresis and

isolated by electroelution on a Schleicher and Schuell Elutrap system. The linearized, labeled DNA restriction fragment was then used directly for the photocleavage reactions.

Purified tRNA samples were 3'-end labeled⁹ with T4 RNA ligase (the reaction mixture was incubated for 2.5 hours on ice) and [5'-³²P]-pCp or dephosphorylated and 5'-end labeled with T4 polynucleotide kinase and [γ -³²P]-ATP. All the necessary precautions were taken to prevent contamination by RNases. Following the end-labeling procedures, the tRNA samples were precipitated with 95% ethanol, resuspended in loading dye, and gel purified on 40 cm long and 0.8 mm thick denaturing polyacrylamide gels (10 to 20%) for 8 to 12 hours at 600 V, visualized, and electroeluted. The labeled tRNAs were stored at -20°C in 10 mM Tris·HCl (pH 7.5) and were renatured (heated in storage buffer to 70°C for 10 minutes and slow cooled to room temperature) prior to the photocleavage experiments.

Metal Stock Solutions: The synthesis of the metal complexes has been described in Chapter 2. [Rh(phen)₂DIP]Cl₃, [Rh(DIP)₂phen]Cl₃, [Rh(phen)₃]Cl₃, [Ru(DIP)₃]Cl₂, and [Ru(phen)₂phi]Cl₂ were obtained from J. R. Rehm and A. M. Pyle. Metal stock solutions were made to approximately 1 mM and were stored frozen for several weeks. The stock solutions were diluted immediately prior to addition to the cleavage reaction mixtures.

Lamp Irradiations: Irradiations of the DNA/RNA reaction mixtures (20 μ l) were performed in 0.6 ml siliconized polypropylene tubes. The open reaction tubes were fixed such that the reaction mixture was directly in the focal point of a 1000 W Hg/Xe lamp beam focused and filtered with a monochromator (Oriel model 77250) and a glass filter to eliminate the light below 305 nm. The wavelengths typically used for cleavage were 310 to 365 nm for the rhodium complexes and 442 nm for the ruthenium complexes (+/- 6 nm).

Laser Irradiations: Irradiations of the DNA/RNA reaction mixtures were performed using a He/Cd laser (Liconix model 4200 NB, 442 nm, 22 mW). Open reaction tubes (0.6 ml siliconized tubes) were placed in a holder such that the reaction mixture was directly in

the line of the laser light which was filtered with a glass filter to eliminate the light below 400 nm.

Reaction Conditions: A typical reaction mixture for cleavage of RNA (or DNA) by the metal complexes was as follows: 20 μL containing ^{32}P -end-labeled RNA (~20,000 to 30,000 cpm), 100 μM RNA (or DNA) nucleotides (the concentration was adjusted with cold carrier tRNA or calf thymus DNA), 2.5 to 10 μM metal complex, and Tris-acetate buffer (50 mM Tris, 20 mM sodium acetate, 18 mM NaCl, pH 7.0), sodium cacodylate buffer (50 mM NaCacodylate, pH 7.0), or Tris-HCl buffer (5 mM Tris, 50 mM NaCl, pH 7.0). Typical cleavage conditions for the rhodium complexes were: 10 μM $\text{Rh}(\text{phen})_2\text{phi}^{3+}$ at 365 nm for 10 minutes on the lamp (Tris-acetate or sodium cacodylate buffer); 2.5 μM $\text{Rh}(\text{DIP})_3^{3+}$ at 313 nm for 2 to 6 minutes on the lamp (Tris-HCl buffer); 10 μM $\text{Rh}(\text{phi})_2\text{bpy}^{3+}$ at 313 nm for 2 to 8 minutes on the lamp (Tris-acetate buffer). The samples were vortexed, centrifuged briefly, allowed to equilibrate for 15 minutes at ambient temperature, and irradiated. Following irradiation, the samples were precipitated with 4 μL NH_4OAc (5M) and 120 μL ethanol. The resulting pellets were washed several times with 80 μL cold ethanol and dried. For cleavage under denaturing conditions, the RNA was heated to 90°C for 5 minutes, then quickly chilled on ice. The irradiation was then performed with the sample remaining on ice. Alternatively, the irradiation was performed at 90°C or in the presence of 10 mM EDTA.

Cleavage with $\text{Ru}(\text{TMP})_3^{2+}$ or $\text{Ru}(\text{phen})_3^{2+}$ (2.5 μM) was performed at 442 nm for 20 minutes on the laser (Tris-HCl buffer) followed by precipitation, drying, and aniline treatment: the RNA was resuspended in 20 μL of 1.0 M aniline buffered at pH 4.5 with acetic acid and incubated in the dark at 60°C for 20 minutes, the mixtures were frozen at -70°C and lyophilized to dryness, and two 40 μL aliquots of H_2O were added to the pellets and lyophilized to dryness after each addition.

3.2.2. Methods for Analysis of the RNA Cleavage Products

Gel Electrophoresis: DNA or RNA pellets from the photocleavage reactions were dissolved in 1 to 4 μ l of loading buffer and electrophoresed in TBE buffer (90 mM Tris, 90 mM Boric Acid, 2.5 mM EDTA, pH 8.3) on denaturing polyacrylamide gels (19:1 acrylamide: N,N'-methylene-bis-acrylamide, 8 M urea, TBE buffer, 0.08% ammonium persulfate). DNA loading buffer consisted of 80% (v/v) deionized formamide, 50 mM Tris-borate, pH 8.3, 1 mM EDTA, 0.025% (w/v) each xylene cyanol and bromophenol blue. RNA loading dye consisted of TBE buffer, 7 M urea, 0.025% (w/v) each xylene cyanol and bromophenol blue.

Chemical Sequencing Methods and Alkaline Hydrolysis: DNA reaction products were coelectrophoresed with Maxam-Gilbert sequencing reactions.¹⁰ RNA reaction products were coelectrophoresed with Peattie-Gilbert sequencing reactions.¹¹ Alkaline hydrolysis was performed on ³²P end-labeled RNAs in 0.05M Na₂CO₃ in which the samples were heated to 90°C for 5 minutes and quickly chilled on ice. An equivalent amount of loading dye was then added and a small portion of the reaction mixture was loaded on the gel.

Autoradiography, Densitometry, and Data Processing: After removal from the glass plates, the gels were dried and subjected to autoradiography (Kodak X-OMATTMAR) at -60°C with an intensifying screen or at ambient temperature without an intensifying screen. Autoradiographs were scanned on a laser densitometer (LKB model 2222-020 Ultrascan XL and GelScan XL software).

Cleavage of tRNA Substrate and Determination of Base Products Released: High-performance liquid chromatography (HPLC) on a Waters 600E system equipped with a 484 tunable detector was used to determine the product formation after cleavage with the metal complexes. Nucleic acid base release from the tRNA was examined after irradiation (365 nm for 15 minutes to 1 hour for Rh(phen)₂phi³⁺; 442 nm for 2 hours for

$\text{Ru}(\text{TMP})_3^{2+}$ and $\text{Ru}(\text{phen})_3^{2+}$ of a reaction volume of 40 μL containing 0.5 mM (nucleotides) tRNA and 50 μM metal complex in 50 mM sodium cacodylate, pH 7.0 for $\text{Rh}(\text{phen})_2\text{phi}^{3+}$ or 5 mM Tris, 50 mM NaCl, pH 7.0 for the ruthenium complexes. The ruthenium samples were then precipitated, dried, and treated with 20 μL 1.0 M aniline as described under the cleavage reaction conditions. The dried samples were resuspended in 40 μL of 50 mM sodium cacodylate and injected as 20 μL samples onto a Cosmosil 5 μ , 15 cm C-18 column washed with 0.1 M ammonium acetate at a flow rate of 1.5 mL/min. $\text{Rh}(\text{phen})_2\text{phi}^{3+}$ reaction mixtures were injected directly onto the column as 20 μL samples. Products were detected by UV absorbance at 260 nm and compared to peaks generated with commercial standards. Guanine, uracil, and cytosine were eluted with retention times of 3.4, 1.8, and 1.6 minutes, respectively. Adenosine was not detected under these conditions.

3.3. Results

3.3.1. Photocleavage of tRNA by Ru(II) and Rh(III) Complexes

This section describes the general features of photocleavage by the ruthenium(II) and rhodium(III) complexes as assayed on yeast tRNA^{Phe}. All of the complexes studied thus far that cleave DNA upon photoactivation have also been shown to promote strand scission of RNA. The fragmentation patterns for the ruthenium complexes are shown in Figure 3.1. Similarly, the cleavage patterns for $\text{Rh}(\text{phen})_2\text{phi}^{3+}$ and $\text{Rh}(\text{DIP})_3^{3+}$ are shown in Figure 3.2, and $\text{Rh}(\text{phi})_2\text{bpy}^{3+}$ cleavage is shown in Figure 3.3. At added ruthenium concentrations of 2.5 μM and irradiation in the MLCT band (442 nm) for 20 minutes, $\text{Ru}(\text{phen})_3^{2+}$ and $\text{Ru}(\text{TMP})_3^{2+}$ efficiently cleave RNA, but only after treatment with aniline. The reactions with the ruthenium(II) complexes reveal cutting preferentially at guanine bases. Since the reaction of these complexes likely occurs by attack on the RNA

Figure 3.1. Cleavage of ^{32}P 3'-end-labeled yeast tRNA^{Phe} by Ru(TMP) $_3^{2+}$ and Ru(phen) $_3^{2+}$. Cleavage was performed in 5 mM Tris, 50 mM NaCl, pH 7.0 with 2.5 μM metal complex. The samples were treated with weak base to induce strand breakage. To determine the positions of cleavage generated by the complexes, the tRNA was coelectrophoresed with RNA sequencing reactions. Lane 1: alkaline hydrolysis. Lane 2: control; RNA in the absence of metal or light. Lane 3: photolysis of RNA with no added metal. Bands Y37 and m⁷G46 appear due to aniline treatment. Lanes 4-5: Ru(phen) $_3^{2+}$ and Ru(TMP) $_3^{2+}$ photocleavage products, respectively. Lanes 6-8: sequencing reactions; A at 37°C, A at 90°C, and U, respectively. Weak depurination at G's is evident in the A reaction. Singlet-oxygen mediated photocleavage by the ruthenium complexes yields a reaction at guanine residues, as indicated by the arrows at the right. Sites of preferential cleavage by Ru(phen) $_3^{2+}$ that are not guanines are indicated by the arrows at the left.

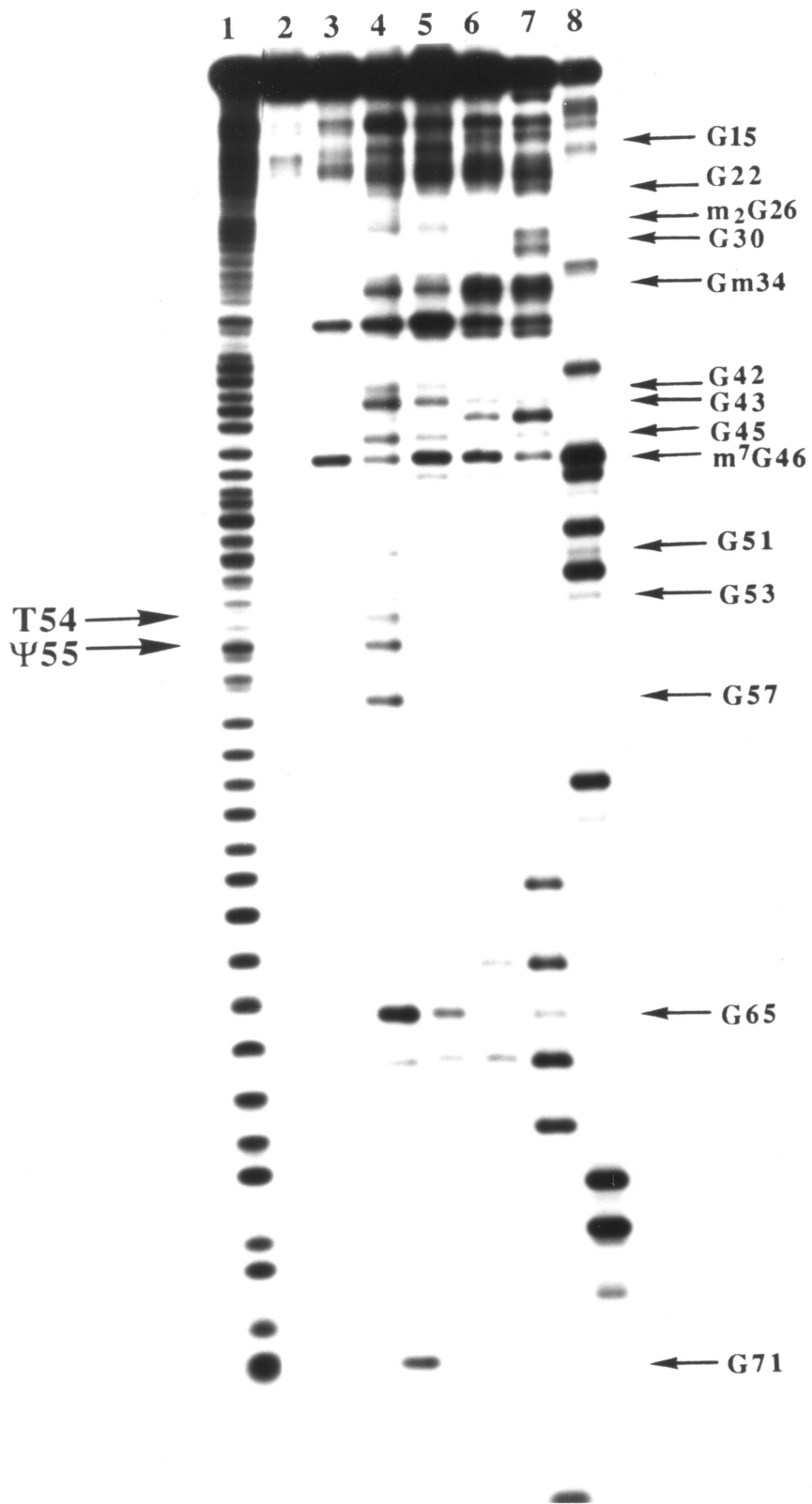


Figure 3.2. Cleavage of ^{32}P 3'-end-labeled yeast tRNA^{Phe} by $\text{Rh}(\text{phen})_2\text{phi}^{3+}$ and $\text{Rh}(\text{DIP})_3^{3+}$. Cleavage was performed in 50 mM Tris, 20 mM NaOAc, 18 mM NaCl, pH 7.0 for $\text{Rh}(\text{phen})_2\text{phi}^{3+}$ and 5 mM Tris, 50 mM NaCl, pH 7.0 for $\text{Rh}(\text{DIP})_3^{3+}$. The metal concentrations employed were 10 μM for $\text{Rh}(\text{phen})_2\text{phi}^{3+}$ and 2.5 μM for $\text{Rh}(\text{DIP})_3^{3+}$. To determine the positions of cleavage generated by the complexes, the tRNA was coelectrophoresed with RNA sequencing reactions. Lane 1: alkaline hydrolysis. Lane 2: control; RNA in the absence of metal or light. Lanes 3 and 8: photolysis of RNA with no added metal; irradiations at 365 nm for 10 minutes and 313 nm for 8 minutes, respectively. Lanes 4-7: specific cleavage by $\text{Rh}(\text{phen})_2\text{phi}^{3+}$ at irradiation times of 4, 6, 8, and 10 minutes at 365 nm. Lanes 9-12: specific cleavage by $\text{Rh}(\text{DIP})_3^{3+}$ at irradiation times of 2, 4, 6, and 8 minutes at 313 nm. Lanes 13-15: sequencing reactions; A at 37°C, A at 90°C, and U, respectively. Arrows on the left indicate $\text{Rh}(\text{phen})_2\text{phi}^{3+}$ cleavage sites and arrows on the right show $\text{Rh}(\text{DIP})_3^{3+}$ cleavage sites.

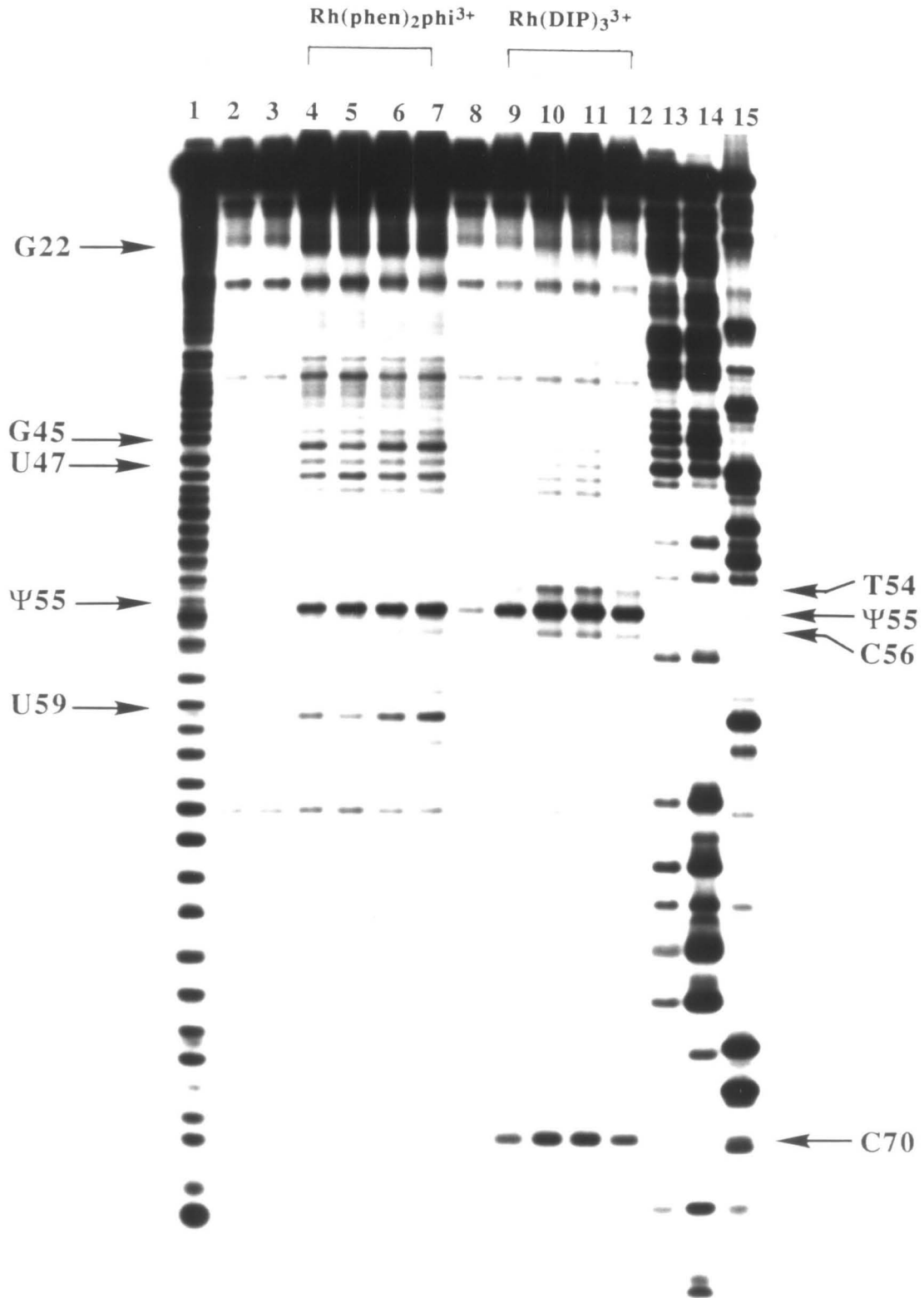
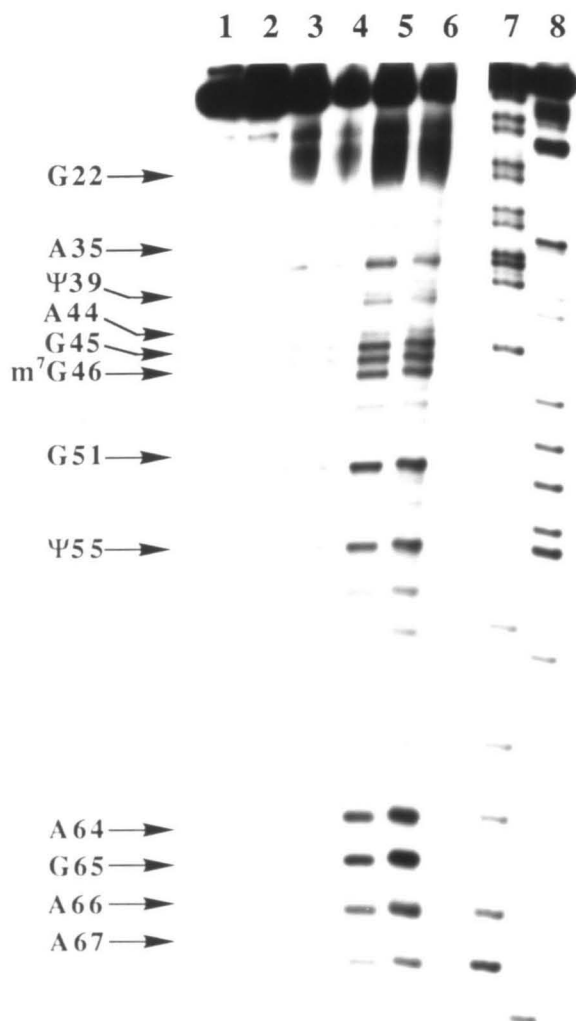


Figure 3.3. Cleavage of ^{32}P 3'-end-labeled yeast tRNA^{Phe} by Rh(phi)₂bpy³⁺. Cleavage was performed in 50 mM Tris, 20 mM NaOAc, 18 mM NaCl, pH 7.0 with 10 μM metal complex. To determine the position of cleavage generated by the complex, the tRNA was coelectrophoresed with RNA sequencing reactions. Lane 1: control; RNA in the absence of metal or light. Lane 2: photolysis of RNA with no added metal; irradiation at 313 nm for 10 minutes. Lanes 3-6: specific cleavage by Rh(phi)₂bpy³⁺ at irradiation times of 2, 4, 6, and 8 minutes at 313 nm. Lanes 7-8: sequencing reactions; A and U, respectively. Arrows on the left indicate Rh(phi)₂bpy³⁺ cleavage sites.



base¹, mild alkaline treatment with buffered aniline is required to convert the lesion to strand breakage.

Photoinduced cleavage of the tRNA was also observed with the rhodium(III) complexes. As shown in Figure 3.2, at 2.5 μM $\text{Rh}(\text{DIP})_3^{3+}$ concentrations, cleavage is observed after only two minutes of irradiation at 313 nm; with 10 μM $\text{Rh}(\text{phen})_2\text{phi}^{3+}$, cleavage is evident after four minutes of irradiation at 365 nm. In this case, no preferred base composition is apparent in cleavage and base treatment is not required for fragmentation. Similarly, as shown in Figure 3.3, at 10 μM concentrations of $\text{Rh}(\text{phi})_2\text{bpy}^{3+}$, cleavage is observed after four minutes of irradiation at 313 nm. For the groove-bound probe, $\text{Rh}(\text{TMP})_3^{3+}$, the site-specific cleavage chemistry that was observed for the other rhodium(III) complexes does not occur. At concentrations ranging from 2.5 to 30 μM , varying wavelengths of irradiation, and varying irradiation times, no cleavage of tRNA was observed with $\text{Rh}(\text{TMP})_3^{3+}$, even after mild base treatment. The photocleavage conditions for the metal complexes with RNA are summarized in Table 3.1. In all cases, no RNA cleavage was observed in the presence of light or metal alone.

3.3.2. Efficiency of Cleavage and Cleavage as a Function of Wavelength and Metal Concentration

Although the rhodium complexes cleave efficiently at their absorbance maxima, 313 and 365 nm irradiations were used because these wavelengths are close to the absorbance maxima and are Hg lines (wavelength of highest intensity light emitted from a Hg/Xe lamp). The most site-selective cleavages were observed, however, with the conditions shown in Table 3.1. In particular, $\text{Rh}(\text{phen})_2\text{phi}^{3+}$ exhibits less cleavage at 365 nm than at 313 nm and at fewer sites. RNA cleavage by the metal complexes increases with increasing concentrations of the complex, increasing irradiation time, and with increasing energy of incident light absorbed. Figures 3.2 and 3.3 demonstrate the extent of RNA

Table 3.1. Optimal Conditions for RNA Photocleavage by Ruthenium(II) and Rhodium(III) Complexes.^a

<i>Metal Complex</i>	<i>λ irradiation (nm)</i>	<i>Concentration (μM)</i>	<i>Time (minutes)</i>	<i>aniline treatment</i>
Ru(TMP) ₃ ²⁺ ^b	442	2.5	20	yes
Ru(phen) ₃ ²⁺ ^b	442	2.5	20	yes
Rh(phen) ₂ phi ³⁺ ^c	365	10	10	no
Rh(phi) ₂ bpy ³⁺ ^d	313	10	8	no
Rh(DIP) ₃ ³⁺ ^b	313	2.5	6	no

^a Cleavage was performed on a 20 μL reaction mixture in the presence of 100 μM RNA nucleotides.

^b The reaction was performed in Tris-HCl buffer; 5 mM Tris, 50 mM NaCl, pH 7.0.

^c The reaction was performed in 50 mM Sodium Cacodylate, pH 7.0.

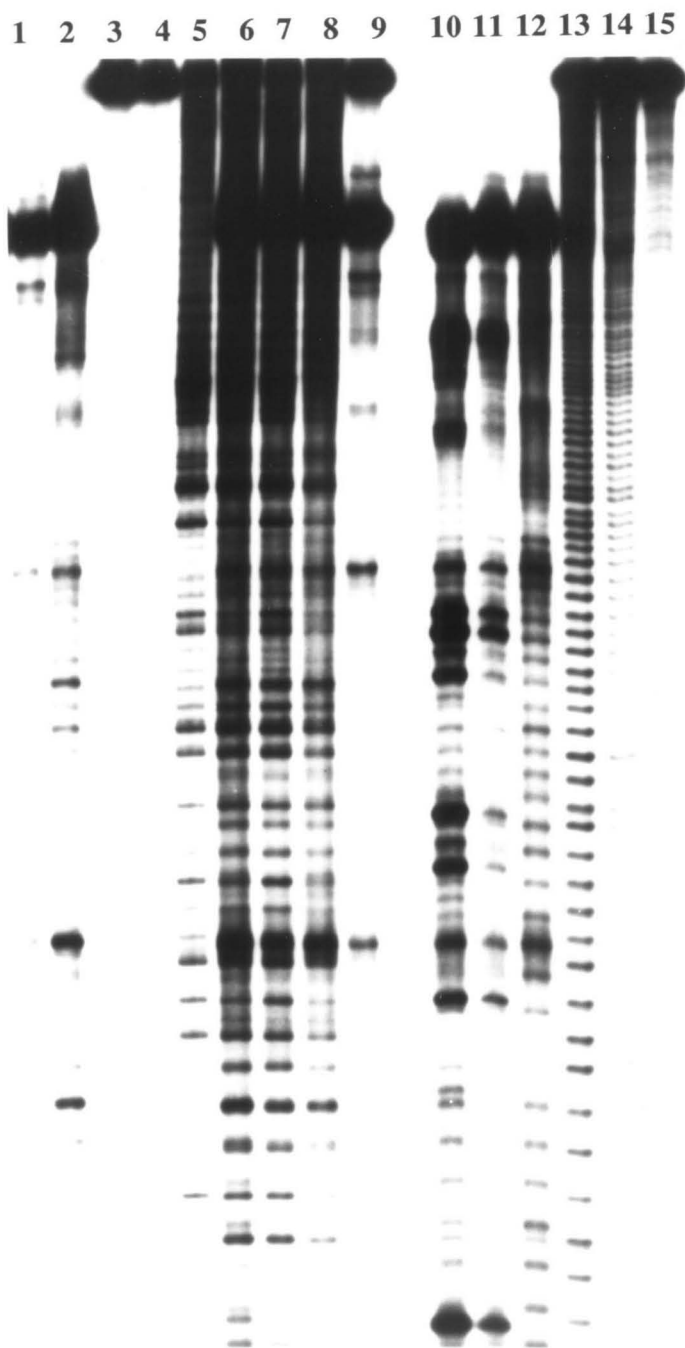
^d The reaction was performed in Tris-acetate buffer; 50 mM Tris, 20 mM NaOAc, 18 mM NaCl, pH 7.0.

photocleavage by the complexes as a function of time with the concentration of rhodium and the irradiation wavelength kept constant. Under these conditions, the amount of cleavage increases with time, but there is no change in site-selectivity of the complex.

Our studies indicate that in general the RNA is a good substrate for the photoactivated cleavage by the metal complexes. However, it was desirable to compare the cleavage efficiency of the complexes on RNA with cleavage of DNA. In most cases, identical conditions as were used on DNA were used to achieve strand scission of RNA. In the case of $\text{Rh}(\text{DIP})_3^{3+}$, the irradiation times on RNA were much longer than the times used for cleavage of supercoiled DNA (2-4 minutes for RNA compared to 20-30 seconds for DNA). However, this may be a reflection of the relative binding of the complex to the different polynucleotides rather than the occurrence of different chemistry.

In order to compare directly the efficiency of RNA strand scission by $\text{Rh}(\text{phen})_2\text{phi}^{3+}$ to that of DNA, we examined cleavage on a mixture of labeled DNA and RNA. As shown in Figure 3.4, the DNA/RNA mixtures (lanes 6-8) gave the same patterns of degradation as the individual DNA (lane 5) or RNA (lane 2). In the absence of any carrier polynucleotide (lane 6), the patterns reflect both RNA and DNA cleavage. In cleavage reactions with carrier DNA (lane 7), the RNA cleavage is slightly diminished. Similarly, with carrier RNA (lane 8), the DNA cleavage is slightly diminished. This experiment indicates that cleavage on tRNA^{Phe} by $\text{Rh}(\text{phen})_2\text{phi}^{3+}$ is comparable in efficiency to cleavage on a DNA fragment under the same conditions. Also shown in Figure 3.4, the cleavage efficiencies of $\text{Rh}(\text{phen})_2\text{phi}^{3+}$ compare well with strand scission generated by $\text{Fe}(\text{EDTA})^{2-}$ (RNA cleavage, lanes 10-12; DNA cleavage, lanes 13-15).¹²⁻¹³ Both of these reagents cleave through an oxidative pathway that targets the sugar moiety. It is interesting to note that while it was possible to cleave RNA with $\text{Fe}(\text{EDTA})^{2-}$ under DNA cleavage conditions¹², the DNA was not cleaved efficiently under RNA cleavage conditions¹³, particularly in the presence of added magnesium.

Figure 3.4. Cleavage of ^{32}P 3'-end-labeled yeast tRNA^{Phe} and a 5'-end-labeled *Pvu* II-*Hind* III 141 base-pair fragment from pUC19 by Rh(phen)₂phi³⁺. Cleavage was performed in 50 mM Tris, 20 mM NaOAc, 18 mM NaCl, pH 7.0 with 10 μM metal complex. Lane 1: RNA control. Lane 2: specific cleavage of RNA by Rh(phen)₂phi³⁺; irradiation at 365 nm for 10 minutes. Lane 3: DNA control. Lane 4: photolysis of DNA with no added metal; irradiation at 365 nm for 10 minutes. Lane 5: specific cleavage of DNA by Rh(phen)₂phi³⁺; irradiation at 365 nm for 10 minutes. Lanes 6-8: specific cleavage of a mixture of DNA and RNA by Rh(phen)₂phi³⁺; irradiation at 365 nm for 10 minutes. Lane 6 contains no carrier polynucleotide, lane 7 contains 100 μM calf thymus DNA as carrier, and lane 8 contains 100 μM tRNA nucleotides as carrier. Lane 9: control; mixture of RNA and DNA. Lanes 10-11: RNA cleavage by Fe(EDTA)²⁻ under the conditions described for RNA¹³ in the absence and presence of 10 mM MgCl₂, respectively. Lane 12: RNA cleavage by Fe(EDTA)²⁻ under the conditions described for DNA¹² in the absence of MgCl₂. Lane 13: DNA cleavage by Fe(EDTA)²⁻ under the conditions described for DNA¹² in the absence of MgCl₂. Lanes 14-15: DNA cleavage by Fe(EDTA)²⁻ under the conditions described for RNA¹³ in the absence and presence of 10 mM MgCl₂.



3.3.3. Cleavage Product Analysis by Gel Electrophoresis and HPLC Analysis

As determined by HPLC analysis, the photoreactions of ruthenium complexes in the presence of tRNA^{Phe} do not show liberation of free nucleic acid bases (Figure 3.5), even after aniline treatment. High-resolution gel electrophoresis points to the production of 5'-phosphate and 3'- or 2'-phosphate termini. The presence of these termini was based on comigration of the cleaved fragments with products of chemical sequencing reactions (diethylpyrocarbonate, dimethylsulfate, or hydrazine followed by aniline treatment)¹¹ and the lack of correspondence to fragment mobility following alkaline hydrolysis (5'-OH) of 3'-end-labeled tRNA.

In contrast, the HPLC analysis (Figure 3.6) of Rh(phen)₂phi³⁺ cleavage of tRNA shows the release of free nucleic acid bases. We were not able to identify some of the peaks in the HPLC. These peaks may correspond to the release of the modified tRNA^{Phe} bases, such as m⁷G46 or Y37. Also, under these experimental conditions we were not able to detect the base adenosine. After cleavage of tRNA with Rh(phen)₂phi³⁺, resolution of the fragments by gel electrophoresis indicated both 5'-phosphate and 3'- or 2'-phosphate termini. As shown on Figure 3.7 (panel A), the cleaved fragments on 3'-end-labeled tRNA^{Phe} comigrate with the chemical sequencing reactions (5'-phosphate) but not with the alkaline hydrolysis fragments (5'-OH), indicating 5'-phosphate termini. Similarly, Figure 3.7 (panel B) shows that the cleaved fragments on 5'-end-labeled tRNA^{Phe} comigrate with the sequencing reactions and the alkaline hydrolysis reactions, indicating 3'- or 2'-phosphate termini. Interestingly, cleavage at G22 yields a single 5'-phosphate terminus but two 3'-termini. A secondary reaction mechanism that is particular to the geometry of the G22 site may account for the mixture of 3'-termini.

Figure 3.5. HPLC chromatograms of tRNA^{Phe} cleavage products after irradiation in the presence of Ru(TMP)₃²⁺ and Ru(phen)₃²⁺. The samples were irradiated at 442 nm for 2 hours followed by aniline treatment. (A) Free base standards U and G with retention times of 1.8 and 3.4 minutes, respectively. (B) RNA control; RNA in the absence of metal or light. (C) Photolysis of RNA with no added metal or aniline treatment. (D) RNA and Ru(TMP)₃²⁺, no irradiation or aniline treatment. (E) RNA and Ru(TMP)₃²⁺ after photolysis at 442 nm for 2 hours. (F) Ru(phen)₃²⁺ and RNA after photolysis at 442 nm for 2 hours. (G) Ru(TMP)₃²⁺ and RNA after photolysis and aniline treatment. (H) Ru(phen)₃²⁺ and RNA after photolysis and aniline treatment.

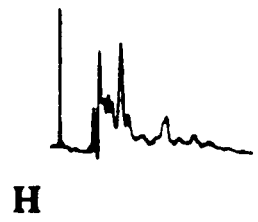
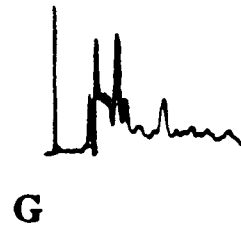
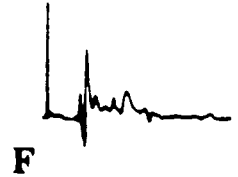
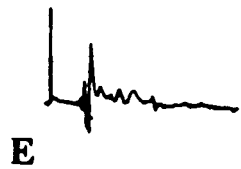
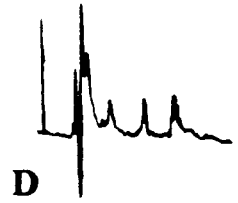
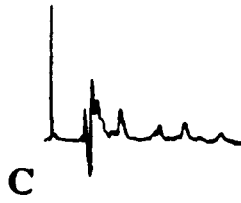
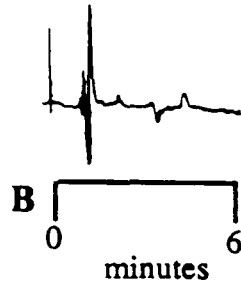
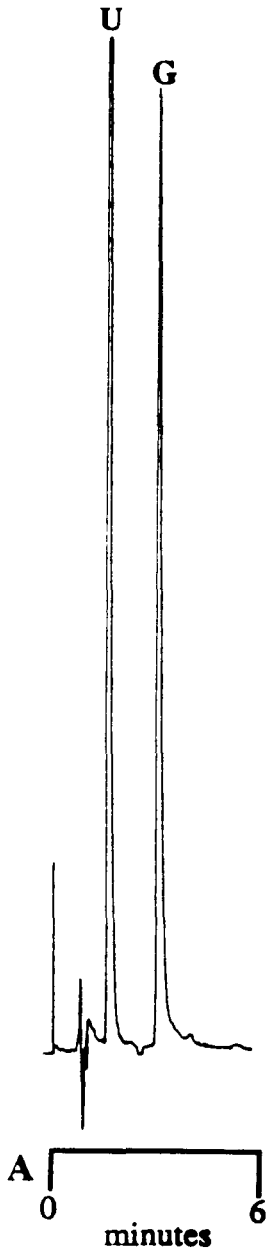


Figure 3.6. HPLC analysis of nucleic acid bases produced with RNA degradation by $\text{Rh}(\text{phen})_2\text{phi}^{3+}$. (A) Free base standards U and G with retention times of 1.8 and 3.4 minutes, respectively. (B) Analysis of the products obtained after irradiation at 365 nm for 1 hour or 15 minutes (C) of a 40 μL reaction mixture containing 50 μM $\text{Rh}(\text{phen})_2\text{phi}^{3+}$ in the presence of 0.5 mM tRNA nucleotides. (D) RNA control; RNA in the absence of metal or light.

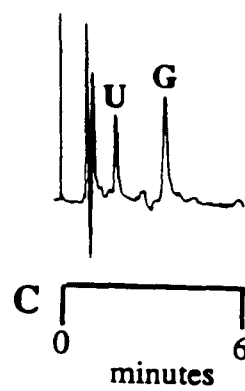
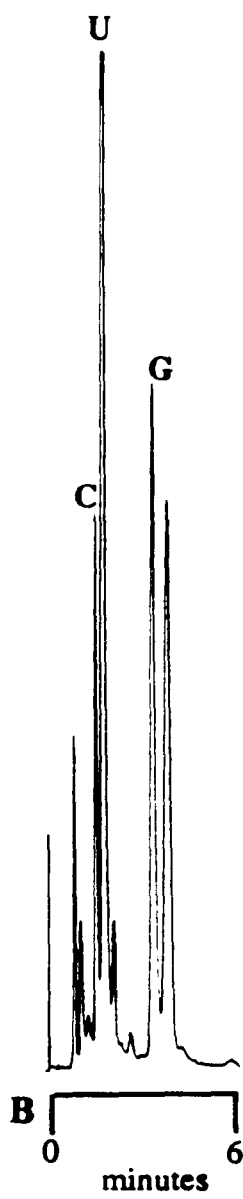
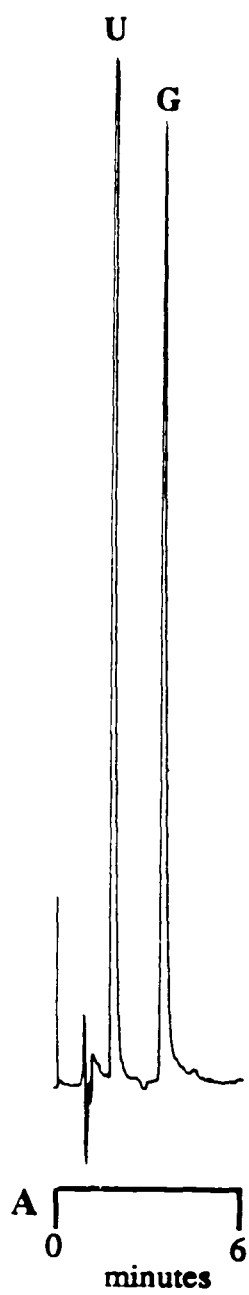
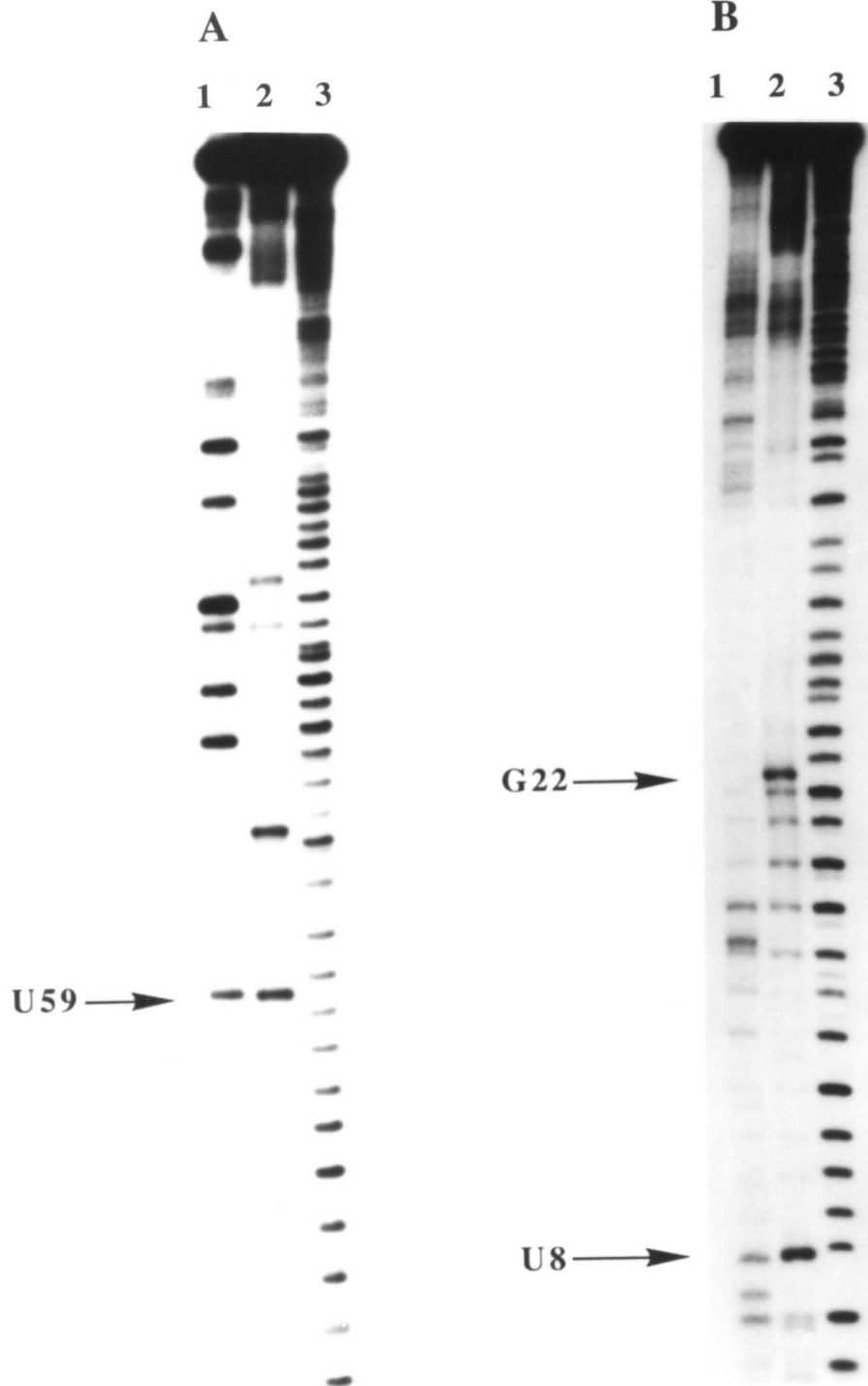


Figure 3.7. End-product analysis of cleavage of ^{32}P 3'-end-labeled (A) and 5'-end-labeled (B) yeast tRNA^{Phe} by Rh(phen)₂phi³⁺. Cleavage was performed in 50 mM Tris, 20 mM NaOAc, 18 mM NaCl, pH 7.0 with 10 μM Rh(phen)₂phi³⁺. To determine the positions of cleavage generated by the complexes, the tRNA was coelectrophoresed with RNA sequencing reactions and alkaline hydrolysis reactions. (A) Lane 1: U-specific reaction. Lane 2: cleavage by Rh(phen)₂phi³⁺; irradiation at 365 nm for 10 minutes. Lane 3: alkaline hydrolysis. The arrow on the left indicates a particular Rh(phen)₂phi³⁺ cleavage site (U59), which demonstrates the comigration with the sequencing reaction, but the lack of migration with the alkaline hydrolysis reaction. (B) Lane 1: U-specific reaction. Lane 2: cleavage by Rh(phen)₂phi³⁺; irradiation at 365 nm for 10 minutes. Lane 3: alkaline hydrolysis. The arrow on the lower left indicates a particular Rh(phen)₂phi³⁺ cleavage site (U8), which demonstrates the comigration with the sequencing reaction and the alkaline hydrolysis reaction. The arrow on the upper left indicates another Rh(phen)₂phi³⁺ cleavage site (G22) with an unusual band migration, indicative of a secondary reaction mechanism that is particular to the geometry of this site.



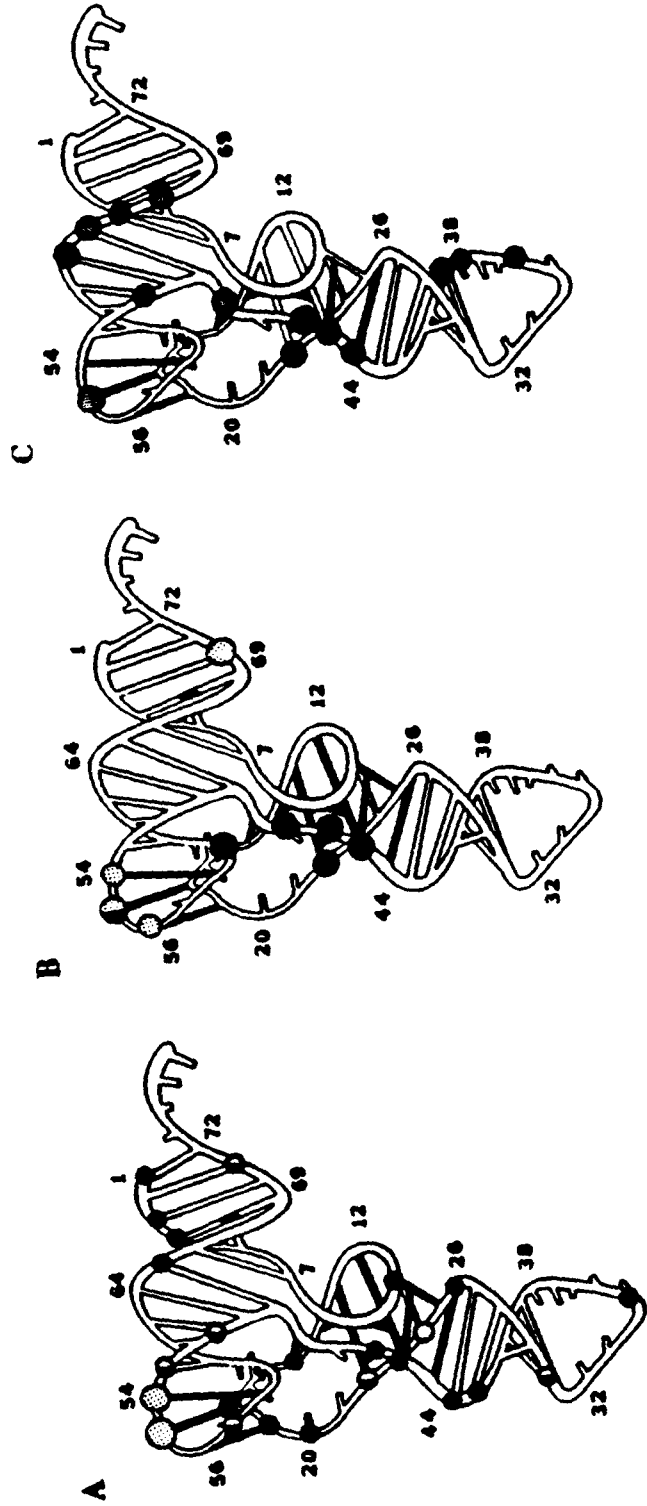
3.3.4. High-Resolution Mapping of Cleavage Sites by Ru(II) and Rh(III) Complexes Along a tRNA Fragment

The site-selectivity associated with the cleavage chemistry of the ruthenium(II) and rhodium(III) complexes can be understood by superimposing the results from the gels (Figures 3.1 to 3.3) onto the three-dimensional structure¹⁴ of yeast tRNA^{Phe}. Figure 3.8A displays the cleavage results for the ruthenium complexes. In experiments performed at low concentrations of metal complex (2.5 μM), somewhat different patterns of cleavage are observed for $\text{Ru}(\text{phen})_3^{2+}$ and $\text{Ru}(\text{TMP})_3^{2+}$, despite the fact that they share a $^1\text{O}_2$ mediated reactivity. However, at high concentrations (greater than 10 μM), the ruthenium complexes cleave with equal intensities at all guanine residues. Understandably, under such conditions the local singlet oxygen concentration becomes greater, therefore increasing the frequency of strand scission at all guanine sites. At low concentrations, however, the different site-selectivities observed must arise because of the different binding characteristics of these molecules, which are governed by their different molecular shapes.

All the guanine residues except G24 are cleaved upon photolysis with $\text{Ru}(\text{phen})_3^{2+}$. The absence of cleavage by the ruthenium complex must reflect the relative accessibility of G24 to attack by $^1\text{O}_2$. In addition, $\text{Ru}(\text{phen})_3^{2+}$ promotes strong cleavage at T54 and $\Psi 55$. It is likely that the complex associates more closely with the tRNA in this region, thereby generating a high local concentration of $^1\text{O}_2$ at these sites. For comparison, $\text{Fe}(\text{EDTA})^{2-}$, which does not itself bind to the polymer, cleaves at all solvent accessible residues in a reaction mediated by a diffusible hydroxyl radical.¹³ In contrast, $\text{Cu}(\text{phen})_2^+$ also cleaves by a reaction mediated by a diffusible species, but preferential cleavage is observed at single-stranded segments of the tRNA.¹⁵

$\text{Ru}(\text{TMP})_3^{2+}$ promotes strand scission at a subset of sites produced by $\text{Ru}(\text{phen})_3^{2+}$ and with somewhat different relative intensities. Guanine residues 22, 24, 30, 51, 53, 57, and 71 are protected from cleavage by $\text{Ru}(\text{TMP})_3^{2+}$. Interestingly, these

Figure 3.8. Cleavage data for the metal complexes mapped onto the three-dimensional structure¹⁴ of yeast tRNA^{Phe}. All bases involved in non-Watson-Crick base pairing, indicative of tertiary interactions, are shown by black lines. (A) Cleavage by Ru(phen)₃²⁺ and Ru(TMP)₃²⁺. Guanine residues cut by both complexes are indicated by black circles. Guanine residues cleaved only by Ru(phen)₃²⁺ are indicated by half black/half white circles. Stippled circles indicate other (non-guanine) residues cleaved by Ru(phen)₃²⁺. G24, protected from cleavage by both complexes is indicated by a white circle. (B) Specific cleavage by Rh(phen)₂phi³⁺ (black circles) and Rh(DIP)₃³⁺ (stippled circles). Note the correspondence between the black lines where tertiary interactions are found and the Rh(phen)₂phi³⁺ cleavage sites. (C) Specific cleavage by Rh(phi)₂bpy³⁺ (stippled circles). A subset of these sites overlaps with the Rh(phen)₂phi³⁺ cleavage sites.



sites appear to mark the edges of the double-helical regions of the tRNA. $\text{Ru}(\text{TMP})_3^{2+}$ is matched in shape to bind against the A-form double helix of RNA¹, but perhaps the shortness of these helical stems in tRNA and the bulkiness of the complex lead to protection from cleavage at the helical borders.

The cleavage patterns with the rhodium complexes (Figure 3.8, B and C) illustrate their particular utility as novel structural probes. Again, the cleavage chemistry for the rhodium complexes is likely the same, but different sites are cleaved. These results indicate that the sites targeted are governed by the shape and binding characteristics rather than by the reactivity of the individual complexes. $\text{Rh}(\text{DIP})_3^{2+}$ induces cleavage at residues $\Psi 55$ and C70, with weaker sites present at T54 and C56. The cleavage at $\Psi 55$ resembles the DNA cleavage observed by $\text{Rh}(\text{DIP})_3^{3+}$ on cruciforms², while cleavage at C70 is adjacent to a G-U mismatch. The site at $\Psi 55$ is also cleaved by $\text{Ru}(\text{phen})_3^{2+}$, $\text{Rh}(\text{phen})_2\text{phi}^{3+}$, and $\text{Rh}(\text{phi})_2\text{bpy}^{3+}$, all of which may intercalate.

$\text{Rh}(\text{phen})_2\text{phi}^{3+}$ induces strong cleavage at residues G22, G45, U47, $\Psi 55$, and U59; weaker sites are observed at A44, m⁷G46, and C48. In addition, under denaturing conditions, no cleavage is observed at these sites, indicating that the native structure is required for interaction with the metal complex. These sites do not correspond to regions of the tRNA that are purely helical or single-stranded. Instead, the major cleavage sites are located in the D and T loops and within the variable loop; these regions are organized uniquely and contain a significant number of tertiary interactions. Cleavage by $\text{Rh}(\text{phi})_2\text{bpy}^{3+}$ on tRNA is evident at residues G22, A35, A38, $\Psi 39$, A44, G45, m⁷G46, G51, $\Psi 55$, A64, G65, A66, A67. A subset of these sites overlaps with the $\text{Rh}(\text{phen})_2\text{phi}^{3+}$ cleavage sites. Perhaps the similar shape of $\text{Rh}(\text{phi})_2\text{bpy}^{3+}$ to $\text{Rh}(\text{phen})_2\text{phi}^{3+}$ allows it to bind to similar sites. However, $\text{Rh}(\text{phi})_2\text{bpy}^{3+}$ appears to be less discriminating than $\text{Rh}(\text{phen})_2\text{phi}^{3+}$ in its binding to tRNA. The higher site-selectivity observed for $\text{Rh}(\text{phen})_2\text{phi}^{3+}$ must depend upon steric factors and the complementarity of

its shape to particular sites along the RNA strand. Overall, the observed sites of cleavage by the rhodium complexes are unique; no other reagents specifically target these regions of the tRNA.

3.3.5. Competition Studies of Ru(II) and Rh(III) Mixed Ligand Complexes

We were interested in increasing the site-selectivity of the complexes through competition with related complexes. For example, $\text{Rh}(\text{phen})_2\text{phi}^{3+}$ and $\text{Rh}(\text{DIP})_3^{3+}$ both exhibited strong cleavage at $\Psi 55$, while $\text{Rh}(\text{phen})_2\text{phi}^{3+}$ cleaved uniquely at a set of sites in the variable loop region of the molecule. Therefore, the cleavage patterns generated by $\text{Rh}(\text{phen})_2\text{phi}^{3+}$ in the presence of $\text{Ru}(\text{DIP})_3^{2+}$ or $\text{Rh}(\text{DIP})_3^{2+}$, which themselves do not promote strand scission of tRNA under $\text{Rh}(\text{phen})_2\text{phi}^{3+}$ cleavage conditions, were expected to be different. It was hoped that a loss or decrease in cleavage by $\text{Rh}(\text{phen})_2\text{phi}^{3+}$ would be apparent at the $\Psi 55$ sites as a result of competitive binding. However, in the presence of equimolar concentrations of $\text{Ru}(\text{DIP})_3^{2+}$ or $\text{Rh}(\text{DIP})_3^{3+}$, no change in the patterns of cleavage was observed for $\text{Rh}(\text{phen})_2\text{phi}^{3+}$. Even at higher concentrations the tris(diphenyl-phenanthroline) complexes did not compete with $\text{Rh}(\text{phen})_2\text{phi}^{3+}$.

In addition, none of the following complexes, $\text{Ru}(\text{phen})_3^{2+}$, $\text{Rh}(\text{phen})_3^{3+}$, $\text{Rh}(\text{phen})_2\text{DIP}^{3+}$, nor $\text{Rh}(\text{DIP})_2\text{phen}^{3+}$, were able to compete with $\text{Rh}(\text{phen})_2\text{phi}^{3+}$. Interestingly, $\text{Ru}(\text{phen})_2\text{phi}^{2+}$ was able to compete with $\text{Rh}(\text{phen})_2\text{phi}^{3+}$, but only at certain sites. It seems that the ruthenium analogue cannot compete with $\text{Rh}(\text{phen})_2\text{phi}^{3+}$ at the $\Psi 55$ site, but can compete efficiently at the variable loop sites (G22, G45, U47, and U59). These results suggest that the binding at $\Psi 55$ has electrostatic contributions, with the higher charged complex binding more strongly. In contrast, the binding at the variable loop sites is not dependent on the charge of the complex. This is consistent with an

intercalative bound mode, which depends on stacking interactions with the complex rather than the positive charge.

3.4. Discussion

The photocleavage experiments were able to provide a great deal of information about the interactions of the metal complexes with tRNA^{Phe}. The most important observation is that all of the complexes that readily cleave DNA in the presence of light can also promote strand scission of RNA. Also, the mechanisms of cleavage as well as the cleavage selectivities are consistent with studies on DNA. The cleavage efficiencies of the metal complexes on RNA are comparable to cleavage on double-stranded DNA. In particular, competition experiments with Rh(phen)₂phi³⁺ on DNA/RNA mixtures indicate that the amount of cleavage on DNA and RNA is comparable. These results are consistent with the binding studies (Chapter 2), which indicated that the rhodium complexes can bind with comparable binding affinities to double-stranded DNA and structured RNA.

The cleavage studies with the ruthenium complexes show the production of 5'-phosphate and 3'- or 2'-phosphate termini without the liberation of free bases after aniline treatment. These cleavage results are equivalent to those obtained on DNA¹ and are consistent with the attack on the nucleic acid base, with guanine being the most reactive. The reaction is likely mediated by singlet oxygen which is generated by photoexcitation of the ruthenium complexes. A general mechanistic scheme for cleavage of RNA by Ru(phen)₃²⁺ and Ru(TMP)₃²⁺ is presented in Scheme 3.1 which is adapted from Ehresmann et al.¹⁷

The cleavage chemistry for the rhodium complexes differs considerably from the ruthenium chemistry. No preferred base composition is observed, aniline is not required for fragmentation, and HPLC analysis shows the release of free nucleic acid bases. After cleavage with the rhodium complexes, high-resolution gel electrophoresis indicates both 5'-

Scheme 3.1. The proposed mechanism of cleavage by tris(phenanthroline)ruthenium(II) complexes on tRNA. The reaction is mediated by singlet oxygen, which is sensitized by the ruthenium complex upon photolysis. Singlet oxygen will react preferentially at guanine residues. A modified guanine is unstable and will be depurinated. The products obtained after aniline treatment are 3'- and 5'-phosphate termini. This scheme has been adapted from Reference 17. The products identified after photocleavage and aniline treatment are boxed. The resulting sugar fragment is likely unstable, so is represented as unknown X. B* represents a modified base.

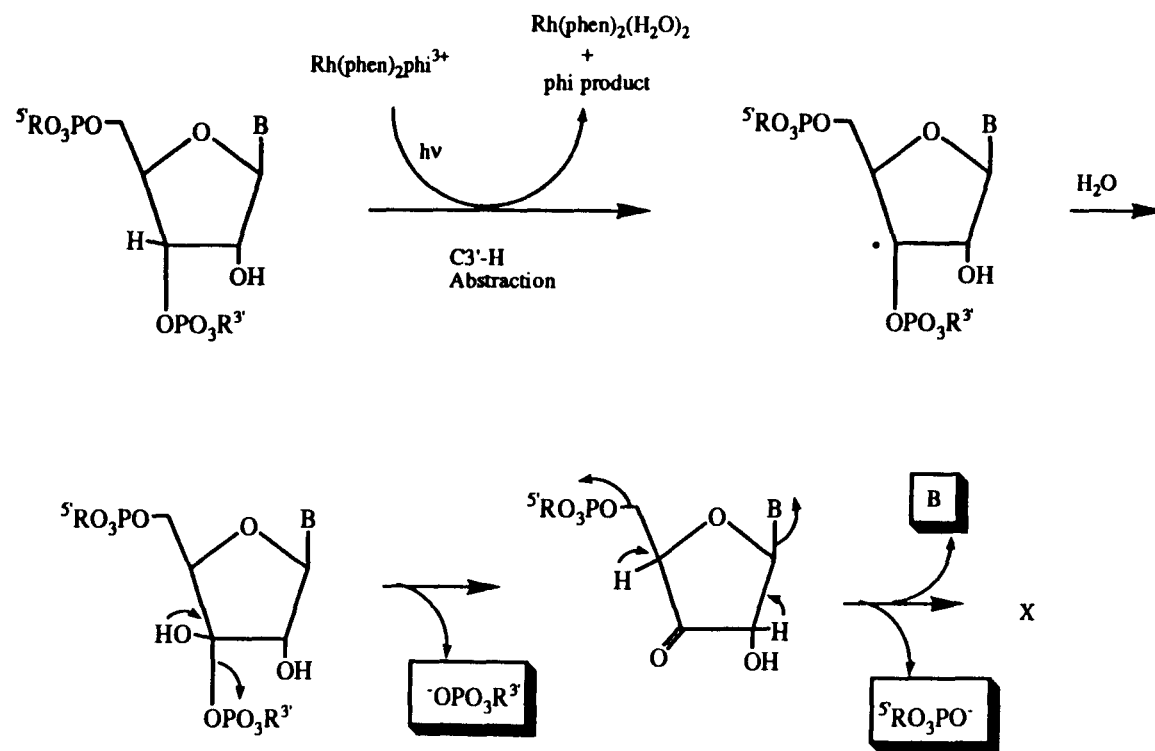
phosphates and 3'- or 2'-phosphate termini. Also, few sites of cleavage on tRNA are evident. Based on these data, photoinduced cleavage by the rhodium complexes appears to occur through a direct oxidative pathway, with the sugar moiety as the target. These results are consistent with results found on DNA.⁴⁻⁵ The proposed mechanism of cleavage, shown in Scheme 3.2 adapted from Stubbe and Kozarich¹⁶, involves abstraction of the C3'-H atom from the sugar, followed by a series of elimination reactions that eventually lead to breakage of the phosphodiester backbone. This mechanism would also be consistent with an intercalated species reacting in the major groove of the RNA.

The lack of reactivity by $\text{Rh}(\text{TMP})_3^{3+}$ was also consistent with the mechanism for cleavage by the phi complexes of rhodium(III). For a groove-bound species, such as $\text{Rh}(\text{TMP})_3^{3+}$, site-specific hydrogen atom abstraction from the major groove is not likely to occur. The bulky methyl groups would prevent this complex from intercalating into the RNA and would instead provide more favorable hydrophobic interactions with the surface of the RNA. $\text{Rh}(\text{TMP})_3^{2+}$ likely binds to the minor groove of the A-form RNA with the ligands orientated against the backbone of the polynucleotide in a way that is unlikely to be favorable for hydrogen abstraction from a sugar residue. In contrast, $\text{Ru}(\text{TMP})_3^{2+}$ is able to promote strand scission because it generates a diffusible species that reacts with the RNA bases.

The site-selectivities associated with the cleavage chemistry on RNA are also consistent with the results obtained on DNA. The ruthenium complexes show preferential cleavage at guanine residues, but with somewhat different patterns of cleavage. The strong cleavage by $\text{Ru}(\text{phen})_3^{2+}$ at T54 and Ψ55 suggests that the complex can associate closely with this region of the tRNA. No strong sites of cleavage other than guanines are evident in the double-stranded or single-stranded regions of the RNA. This was expected since the major groove of A-form helices are for the most part inaccessible for intercalation by the metal complexes. Instead, the strong $\text{Ru}(\text{phen})_3^{2+}$ cleavage sites are centered in a region of

Scheme 3.2. The proposed mechanism of cleavage by phi complexes of rhodium(III) on tRNA. $\text{Rh}(\text{phen})_2\text{phi}^{3+}$ becomes photoexcited, resulting in the abstraction of C3'-H into the excited phi moiety with release of $\text{Rh}(\text{phen})_2(\text{H}_2\text{O})_2^{3+}$ and an altered phi ligand containing the incorporated hydrogen. The resulting C3'-lesion may then solvate, leading to the loss of 3'- and 5'-phosphate termini, direct strand scission, and the release of nucleic acid base. This scheme has been adapted from References 4 and 16. The products identified after photocleavage by $\text{Rh}(\text{phen})_2\text{phi}^{3+}$ are boxed. The resulting sugar fragment is likely unstable, so is represented as unknown X.

Scheme 2



the molecule that exhibits tertiary structure¹⁴; the D and T loop residues interact through long-range hydrogen bonding involving unusual base-pairing schemes.

In contrast, $\text{Ru}(\text{TMP})_3^{2+}$, with its bulky methyl groups, was designed to bind to the open and shallow minor groove of an A-form helix.¹ However, the lack of reactivity at sites other than guanines as well as protection of certain guanine residues at the edges of the helical regions suggested that perhaps tRNA was not a good substrate for site-specific recognition by $\text{Ru}(\text{TMP})_3^{2+}$. Perhaps the shortness of the helical stems in tRNA (4-7 base pairs) and the bulkiness of $\text{Ru}(\text{TMP})_3^{2+}$ lead to protection from cleavage in these regions.

$\text{Rh}(\text{DIP})_3^{3+}$ specifically targets unusual non-B-DNA structures such as Z-DNA¹⁸ and cruciforms.¹ The site-specific cleavage by this complex has also been used to probe other unusual and interesting conformations on DNA, which have yet to be fully characterized.¹⁹ Similarly, $\text{Rh}(\text{DIP})_3^{3+}$ targets a highly structured site ($\Psi 55$) on tRNA, rather than purely double-stranded or single-stranded regions of the molecule. In addition, the complex is able to target an altered conformation within the double-helical region of the acceptor stem of tRNA^{Phe}. Strong cleavage by $\text{Rh}(\text{DIP})_3^{3+}$ is observed at C70, which lies adjacent to a G-U mismatch. The crystal structure¹⁴ of tRNA^{Phe} reveals that a small structural distortion exists in the helix resulting from the mismatched base pair. Apparently the metal complex is able to detect even subtle distortions within the RNA secondary structure.

$\text{Rh}(\text{phen})_2\text{phi}^{3+}$ induces strong cleavage at residues G22, G45, U47, $\Psi 55$, and U59. Once again, these sites do not correspond to regions that are purely helical or single-stranded. Instead, the major sites of cleavage are located in the D and T loops and within the variable loop, a uniquely organized, structured region of the tRNA molecule. In particular, the bases G22, G45, and m⁷G46 (a weak cleavage site) are involved in triple-base interactions, in which normal Watson-Crick base pairs interact with a third base in the major groove of the RNA. The selective targeting of these sites by $\text{Rh}(\text{phen})_2\text{phi}^{3+}$ are

also consistent with the DNA recognition characteristics of the metal complex. Cleavage on DNA occurs at sites that are open in the major groove to permit intercalation by the bulky metal complex.^{4,20} In double-helical regions of RNA, the A-like conformation limits access to the deep and narrow major groove. As is evident from the crystal structure of yeast tRNA^{Phe}¹⁴, however, the addition of the third bases in the major groove distort the usual A-like helix to allow stacking with the rhodium complex. In contrast, MPE-Fe(II), which likely intercalates from the minor groove, shows a high affinity for double-stranded RNA.²¹ Intercalation into A-form helices from the minor groove would not be sterically hindered as it is from the major groove.

The results with Rh(phi)₂bpy³⁺ cleavage on tRNA are also consistent with DNA cleavage studies.³ At high concentrations (10 μM), Rh(phi)₂bpy³⁺ cleaves DNA in a sequence-neutral fashion. Despite the overall similarities in coordination geometries and ligands in Rh(phen)₂phi³⁺ and Rh(phi)₂bpy³⁺, the patterns of cleavage on double-stranded DNA are quite different. Given the strong propensity of the phi ligand to intercalate²², the bound Rh(phen)₂phi³⁺ will likely contain two nonintercalated ancillary phenanthroline ligands. Similarly, Rh(phi)₂bpy³⁺ will contain one phi and one bpy ancillary ligand when the other phi is intercalated. Because of the larger size of the phenanthroline ligands and steric clashes with the DNA bases or backbone, Rh(phen)₂phi³⁺ binds with greater site-selectivity and prefers sites that are open in the major groove.³ In contrast, the ancillary ligands of Rh(phi)₂bpy³⁺ are either smaller in the case of bpy or have an aromatic system that is extended away from the metal center (phi). This will decrease the amount of steric clash with the DNA when the complex is intercalated and thus will allow Rh(phi)₂bpy³⁺ to bind in a less discriminate manner than Rh(phen)₂phi³⁺. Rh(phi)₂bpy³⁺ cleaves at the same sites on tRNA as Rh(phen)₂phi³⁺, but also promotes cleavage at additional sites. Perhaps Rh(phi)₂bpy³⁺ can bind at sites on tRNA which would exhibit steric clashes with Rh(phen)₂phi³⁺. However, cleavage is still not present at double- nor single-stranded

regions. Instead, the additional sites for $\text{Rh}(\text{phi})_2\text{bpy}^{3+}$ occur at other tertiary sites such as helix-helix junctions or stem-loop junctions. These tertiary sites likely have accessible major grooves for interaction with $\text{Rh}(\text{phi})_2\text{bpy}^{3+}$.

In conclusion, it has been shown that the metal complexes developed in our laboratory show a distinctive diversity in site-selective cleavage of tRNA. Photocleavage by the complexes is consistent with reactions on DNA, both in terms of the chemistry and the patterns of recognition. In particular, $\text{Rh}(\text{phen})_2\text{phi}^{3+}$ and $\text{Rh}(\text{DIP})_3^{3+}$ are the most site-selective in cleavage. Both complexes recognize a highly structured folded region of the tRNA where the D and T loops interact through tertiary interactions. In addition, $\text{Rh}(\text{phen})_2\text{phi}^{3+}$ targets triply bonded regions in tRNA^{Phe} , and $\text{Rh}(\text{DIP})_3^{3+}$ targets a G-U mismatch. Given the uniqueness of sites cleaved, these probes should be valuable in assessing the structures of new tRNAs²³. More generally, these complexes may be useful in examining the secondary and tertiary structures in other biologically important RNA molecules. We will explore such applications of these molecules in the following chapters.

References

1. Mei, H.-Y.; Barton, J. K. *Proc. Natl. Acad. Sci. U.S.A.* **1988**, 85, 1339-1343.
2. Kirshenbaum, M. R.; Tribolet, R.; Barton, J. K. *Nucleic Acids Res.* **1988**, 16, 7943-7960.
3. Pyle, A. M.; Long, E. C.; Barton, J. K. *J. Am. Chem. Soc.* **1989**, 111, 4520-4522.
4. Sitlani, A.; Long, E. C.; Pyle, A. M.; Barton, J. K. *J. Am. Chem. Soc.* **1992**, in press.
5. Long, E. C.; Absalon, M. J.; Stubbe, J.; Barton, J. K., submitted for publication.
6. Hertzberg, R. P.; Dervan, P. B. *J. Am. Chem. Soc.* **1982**, 104, 313-315.
7. Juris, A.; Balzani, V.; Barigelletti, F.; Campagna, S.; Belser, P.; von Zelewsky, A. *Coord. Chem. Rev.* **1988**, 84, 85-277.
8. Chaconas, G.; Van de Sande, J. H. *Methods Enzymol.* **1980**, 65, 75-85.
9. England, T. E.; Bruce, A. G.; Uhlenbeck, O. C. *Methods Enzymol.* **1980**, 65, 65-74.
10. Maxam, A. M.; Gilbert, W. *Methods Enzymol.* **1980**, 65, 499-560.
11. Peattie, D. *Proc. Natl. Acad. Sci. U.S.A.* **1979**, 76, 1760-1764.
12. Tullius, T. D.; Dombroski, B. A.; Churchill, M. E. A.; Kam, L. *Methods Enzymol.* **1987**, 155, 537-558.
13. a) Latham, J. A.; Cech, T. R. *Science* **1989**, 245, 276-282.
b) Celander, D. W.; Cech, T. R. *Biochemistry* **1990**, 29, 1355-1361.
14. a) Kim, S.-H.; Sussman, J. L.; Suddath, F. L.; Quigley, G. J.; McPherson, A.; Wang, A. H.; Seeman, N. C.; Rich, A. *Proc. Natl. Acad. Sci. U.S.A.* **1974**, 71, 4970-4974.
b) Quigley, G. J.; Rich, A. *Science* **1976**, 194, 796-806.

15. Murakawa, G. J.; Chen, C. B.; Kuwabara, M. D.; Nierlich, D. P.; Sigman, D. S. *Nucleic Acids Res.* **1989**, *17*, 5361-5375.
16. Stubbe, J.; Kozarich, J. W. *Chem. Rev.* **1987**, *87*, 1107-1136.
17. Ehresmann, C.; Baudin, F.; Mougel, M.; Romby, P.; Ebel, J. P.; Ehresmann, B. *Nucleic Acids Res.* **1987**, *15*, 9109-9128.
18. Kirshenbaum, M. R., Ph. D. Dissertation, Columbia University, New York, 1989.
19. Lee, I., unpublished results.
20. Pyle, A. M.; Morii, T.; Barton, J. K. *J. Am. Chem. Soc.* **1990**, *112*, 9432-9434.
21. Kean, J. M.; White, S. A.; Draper, D. E. *Biochemistry* **1985**, *24*, 5062-5070.
22. Pyle, A. M.; Rehmann, J. P.; Meshoyrer, R.; Kumar, C. V.; Turro, N. J.; Barton, J. K. *J. Am. Chem. Soc.* **1989**, *111*, 3051-3058.
23. See for example Sampson, J. R.; Uhlenbeck, O. C. *Proc. Natl. Acad. Sci. U.S.A.* **1988**, *85*, 1033-1037. Sampson, J. R.; DiRenzo, A. B.; Behlen, L. S.; Uhlenbeck, O. C. *Biochemistry* **1990**, *29*, 2523-2532. Pan, T.; Gutell, R. R.; Uhlenbeck, O. C. *Science* **1991**, *254*, 1361-1364. Hou, Y.-M.; Schimmel, P. *Nature* **1988**, *333*, 140-145.

Chapter 4:

Recognition of Tertiary Structures in tRNA by Rh(phen)₂phi³⁺: Tuning the Recognition with Mutant and Structurally Modified tRNAs[†]

4.1. Introduction

A popular approach towards understanding the relationship between tertiary structure and biological function of RNA involves extensive site-directed or random mutagenesis of the RNA and assay of the mutants *in vitro*. In these studies it is important to distinguish whether a decrease in activity of a mutant is the result of a change in an essential nucleotide or the less interesting consequence of a more general alteration of the overall structure of the RNA. Thus it is important to develop methods to probe rapidly the subtle changes in the conformation of mutant RNA. This chapter involves the study of bis(phenanthroline)phenanthrenequinone diimine rhodium(III) {Rh(phen)₂phi³⁺} (Figure 4.1) as a potential reagent for RNA structure-function mapping.

The recognition characteristics of Rh(phen)₂phi³⁺ are particularly well suited to probing RNA structure. As discussed in Chapter 3, cleavage studies using Rh(phen)₂phi³⁺ and other transition metal complexes have been carried out on tRNA^{Phe}. Rh(phen)₂phi³⁺ is unique among the metal complexes in the sites that it targets. Despite the similar reactivity of the rhodium(III) complexes, different sites are targeted, suggesting that recognition is governed by the different shapes and binding characteristics of these molecules. The sites targeted by Rh(phen)₂phi³⁺ are neither double-helical nor single-stranded. The sites also differ from those marked by other structural probes such as lead ion¹ or psoralen². The double-helical regions of RNA tend to adopt an A-conformation,³⁻⁴

[†] Adapted from Chow, C. S.; Behlen, L. S.; Uhlenbeck, O. C.; Barton, J. K. *Biochemistry* 1992, in press.

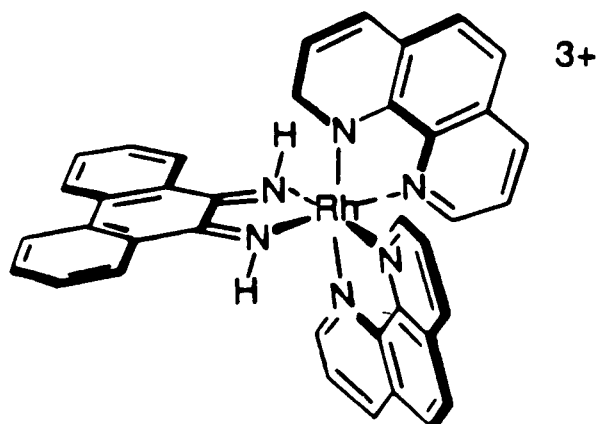


Figure 4.1. Schematic illustration of $\text{Rh}(\text{phen})_2\text{phi}^{3+}$.

where the major groove is pulled deeply into the helix interior; as a result the narrowed major groove becomes inaccessible to intercalation by the metal complex. Thus both the double-helical regions and unstacked, single-stranded regions of RNA are not cleaved by $\text{Rh}(\text{phen})_2\text{phi}^{3+}$. Instead, cleavage by $\text{Rh}(\text{phen})_2\text{phi}^{3+}$ appears to be dependent upon tertiary folding. In particular, $\text{Rh}(\text{phen})_2\text{phi}^{3+}$ targets triply bonded bases in tRNA, where the third base may provide an accessible surface from the major groove for $\text{Rh}(\text{phen})_2\text{phi}^{3+}$ stacking. The complex also cleaves other tertiary structures in tRNA such as D-T loop interactions and helix-loop junctions.

Here we explore further the efficacy of $\text{Rh}(\text{phen})_2\text{phi}^{3+}$ using (i) the two tRNAs that have been crystallographically characterized, tRNA^{Phe} 5-6 and tRNA^{Asp} 7 from yeast, (ii) tRNA^{Phe} containing no base modifications,⁸⁻⁹ (iii) a structurally modified native tRNA^{Phe} ,¹⁰ and (iv) a series of tRNA^{Phe} mutants.¹¹ The goals of these efforts have been to delineate the specificity of this reagent and to evaluate the application of the rhodium complex in detecting structural changes in RNA. The specificity in cleavage by $\text{Rh}(\text{phen})_2\text{phi}^{3+}$ provides a means for identifying conformational changes in RNA tertiary structure upon mutation. Furthermore, the changes in cleavage by $\text{Rh}(\text{phen})_2\text{phi}^{3+}$ can be compared with changes in biological function of the RNA molecule upon mutation.

4.2. Experimental

Materials: The reagents used in this study were obtained from the following suppliers: tRNA^{Phe} from brewer's yeast, ATP, and dithiothreitol (DTT) (Boehringer Mannheim, Indianapolis, IN); T4 RNA ligase (Pharmacia, Piscataway, NJ); Trizma base, NaOAc, NH_4OAc , NaCl, HEPES (free acid), cacodylic acid (sodium salt), MgCl_2 , EDTA, polyacrylamide, N,N'-methylene-bis-acrylamide, urea, boric acid, and dimethyl sulfoxide (Molecular Biology Grade if available, Sigma, St. Louis, MO); diethylpyrocarbonate

(DEPC), dimethyl sulfate (DMS), hydrazine, sodium borohydride, and aniline (Aldrich, Milwaukee, WI); [γ - ^{32}P]-ATP and [5'- ^{32}P]-pCp (NEN/Du Pont, Wilmington, DE).

tRNAs: Unmodified wild type yeast tRNA^{Phe} and mutants, a gift from L. S. Behlen and O. C. Uhlenbeck (Department of Chemistry and Biochemistry, University of Colorado, Boulder, CO) were prepared by *in vitro* transcription by T7 RNA polymerase.¹¹ Yeast tRNA^{Asp} was a gift from D. Moras (Institut de Biologie Moleculaire et Cellulaire du CNRS, Strasbourg, France). Native yeast tRNA^{Phe} (Boehringer Mannheim), yeast tRNA^{Asp}, and the unmodified transcripts were 3'-end labeled with [5'- ^{32}P]-pCp¹² or 5'-end labeled by dephosphorylation with alkaline phosphatase followed by phosphorylation with [γ - ^{32}P]-ATP and polynucleotide kinase. The tRNAs were gel purified on a 10% denaturing polyacrylamide gel, located by autoradiography, excised, and eluted from the gel in 45 mM Tris, 45 mM boric acid, and 1.25 mM EDTA, pH 8.0. The eluted tRNAs were precipitated twice with ethanol and stored in 10 mM Tris-HCl, pH 8.0.

Cleavage Reactions: Rh(phen)₂phi³⁺ stock solutions were freshly prepared. All end-labeled tRNAs were renatured by heating to 70°C for 1 minute in 10 mM Tris-HCl, 10 mM MgCl₂, pH 8.0 and slowly cooling to room temperature prior to use. A typical 20 μL cleavage mixture contained labeled tRNA, 10 μM Rh(phen)₂phi³⁺, the appropriate buffer (50 mM Tris, 20 mM NaAcetate, 18 mM NaCl, 1 mM MgCl₂, pH 7.0 or 50 mM NaCacodylate, 1 mM MgCl₂, pH 7.0), and was brought to a final concentration of 100 μM in nucleotides with carrier tRNA^{Phe}. Irradiation for 10 minutes at 365 nm at ambient temperature using a 1000 W Hg/Xe lamp and monochromator yielded site-specific cleavage of the tRNA samples only in the presence of the rhodium complex. The reaction mixtures were precipitated with ethanol, washed at least three times with 70% ethanol to remove buffer salts, and analyzed on 15% polyacrylamide 8 M urea gels. The full-length tRNA and cleavage products were identified by coelectrophoresing with diethylpyrocarbonate

(DEPC) (A-specific) and hydrazine (U-specific) reactions¹⁰ and viewed by autoradiography.

4.3. Results

4.3.1. Cleavage of Native tRNAs

Cleavage of yeast tRNA^{Phe}: The sites of Rh(phen)₂phi³⁺ cleavage of native tRNA^{Phe} were determined through cleavage of 5'- and 3'-end-labeled tRNA. The rhodium cleavage sites were assigned by comparison with end-labeled products of DEPC and hydrazine reactions, which lead to specific cuts at A and U residues, respectively. As can be seen in Figure 4.2 (lane 5), few and specific cleavage sites are evident on the 3'-end-labeled tRNA. Strong cleavage is observed at residues G22, G45, U47, Ψ55, and U59, with minor cleavage apparent at A44, m⁷G46, and C48. The same sites of cleavage are observed in experiments conducted with 5'-end-labeled tRNA with one additional site evident at U8. The U8 site is not observed on the 3'-end-labeled tRNA because of its closeness to the ³²P label and the poor resolution of the gels in this region. Although most sites produce single 5'- and 3'-termini, cleavage at G22 yields a 5'-phosphate terminus but two 3'-termini. A secondary reaction mechanism that is particular to the geometry of the site may account for the mixture of 3'-termini. Therefore, to avoid ambiguity in assignment, mapping studies were focused primarily on cleavage of 3'-end-labeled RNAs.

A ribbon diagram in Figure 4.3 (panel A), adapted from the crystal structure of tRNA^{Phe},^{5,6} shows the locations of the major and minor Rh(phen)₂phi³⁺ cleavage sites. These sites are different from those observed using other structure-mapping reagents. Figure 4.4 displays the crystal structure of yeast tRNA^{Phe} in a computer graphics representation with the tertiary interactions highlighted in white (4.4A-left) and the cleavage sites for Rh(phen)₂phi³⁺ in yellow (4.4B-left). As can be seen in this figure, there is a strong correlation between cleavage by Rh(phen)₂phi³⁺ and regions of the tRNA exhibiting

Figure 4.2. Cleavage of ^{32}P 3'-end-labeled native yeast tRNA^{Phe}, the yeast tRNA^{Phe} transcript, G19C mutant, and yeast tRNA^{Asp} by Rh(phen)₂phi³⁺. Cleavage was performed in 50 mM Tris, 20 mM NaAcetate, 18 mM NaCl, 1 mM MgCl₂, pH 7.0. Lanes 1, 10 and 14: A-specific reaction on native tRNA^{Phe}, tRNA^{Phe} transcript, and tRNA^{Asp}. Lanes 2, 11, and 15: U-specific reaction on native tRNA^{Phe}, tRNA^{Phe} transcript, and tRNA^{Asp}. Lanes 3, 6, 8, and 12: controls; native tRNA^{Phe}, tRNA^{Phe} transcript, G19C, and tRNA^{Asp}. Lane 4: light control; tRNA^{Phe} irradiated in the absence of metal. Lanes 5, 7, 9, and 13: specific cleavage by Rh(phen)₂phi³⁺ on native tRNA^{Phe}, tRNA^{Phe} transcript, G19C, and tRNA^{Asp}. Arrows indicate reference points along the tRNA sequence. Bars indicate major regions of cleavage by Rh(phen)₂phi³⁺.

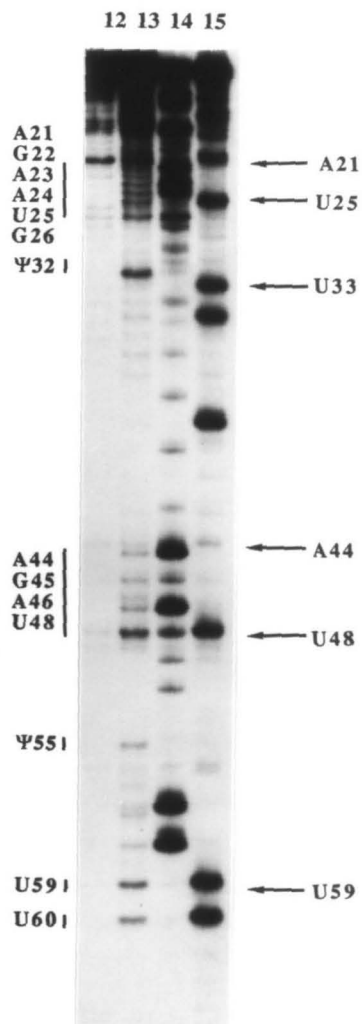
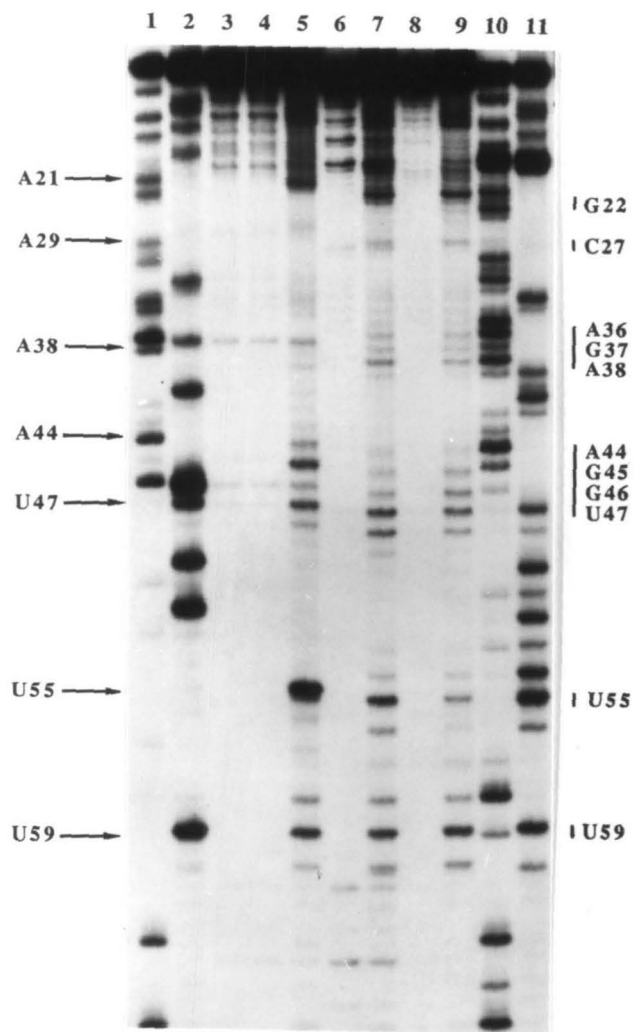


Figure 4.3. Rh(phen)₂phi³⁺ cleavage sites on (A) yeast tRNA^{Phe} and (B) the unmodified tRNA^{Phe} transcript mapped on a ribbon diagram adapted from the crystal structure of tRNA^{Phe}.^{5,6} The solid circles indicate the positions of Rh(phen)₂phi³⁺ promoted strand scission with size corresponding to relative cleavage intensity. Arrows indicate the bases that are modified in the native tRNA^{Phe}.

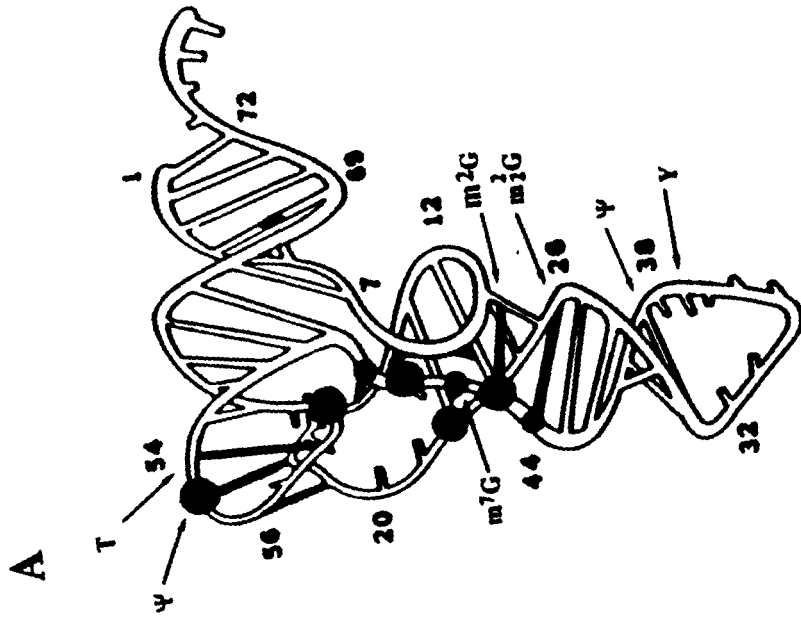
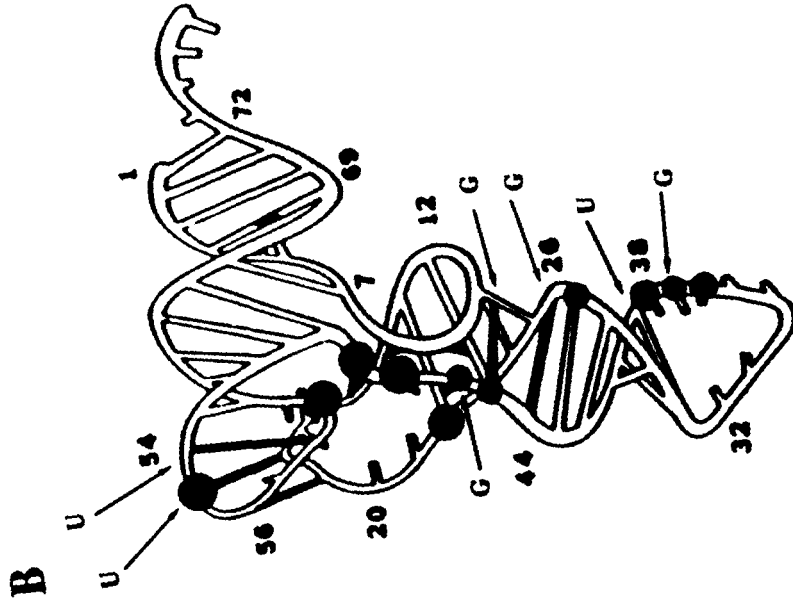
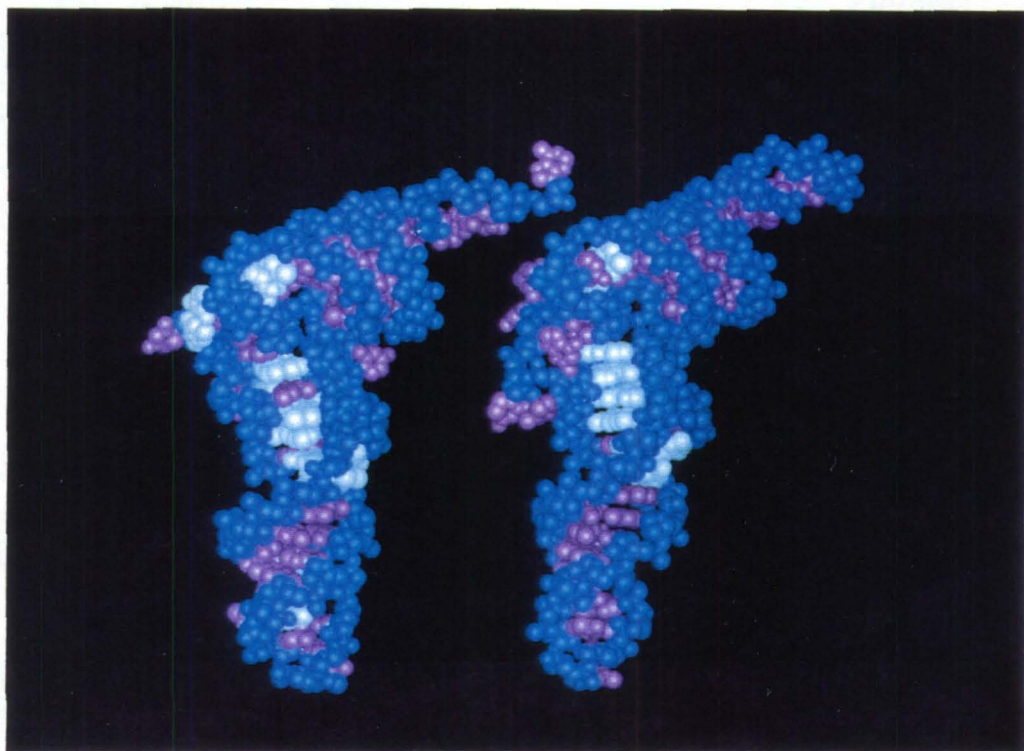
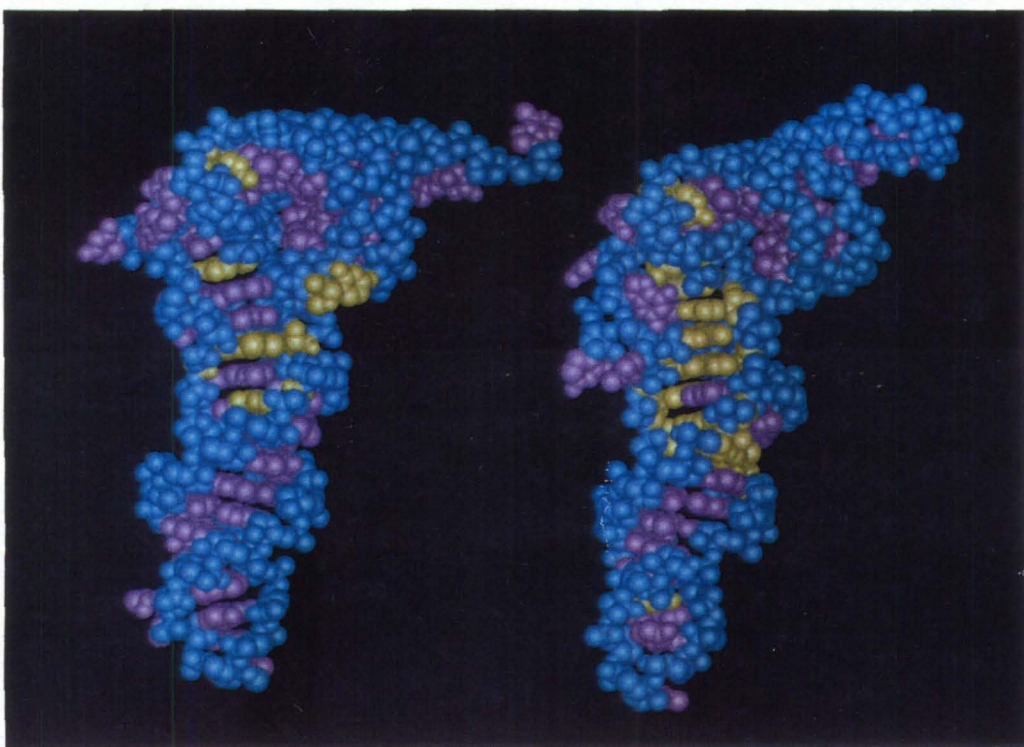


Figure 4.4. Tertiary interactions and cleavage data for $\text{Rh}(\text{phen})_2\text{phi}^{3+}$ are shown in a computer graphic representation of the crystal structures of yeast tRNA^{Phe} and tRNA^{Asp} . The sugar-phosphate backbones are shown in aqua and the nucleic acid bases in purple. (A) The bases involved in tertiary interactions are shown in white for tRNA^{Phe} (left) and tRNA^{Asp} (right). (B) The residues (bases and sugars) that are cleaved by $\text{Rh}(\text{phen})_2\text{phi}^{3+}$ are shown in yellow for tRNA^{Phe} (left) and tRNA^{Asp} (right). Note the correspondence between the white and yellow regions where $\text{Rh}(\text{phen})_2\text{phi}^{3+}$ promotes strand scission.

A



B

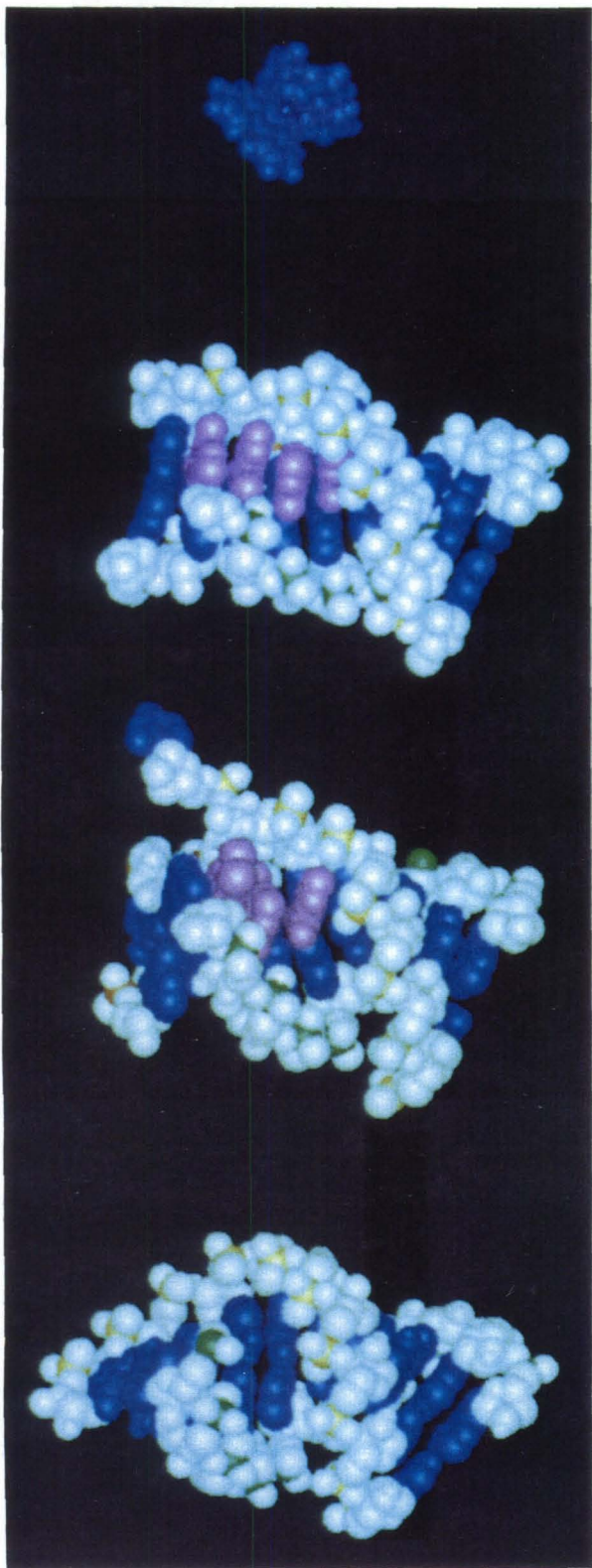


extensive tertiary structure. This finding contrasts cleavage studies with other conventional probes that recognize secondary structural features of the tRNA such as double- or single-stranded regions of the tRNA or regions of greater solvent accessibility.

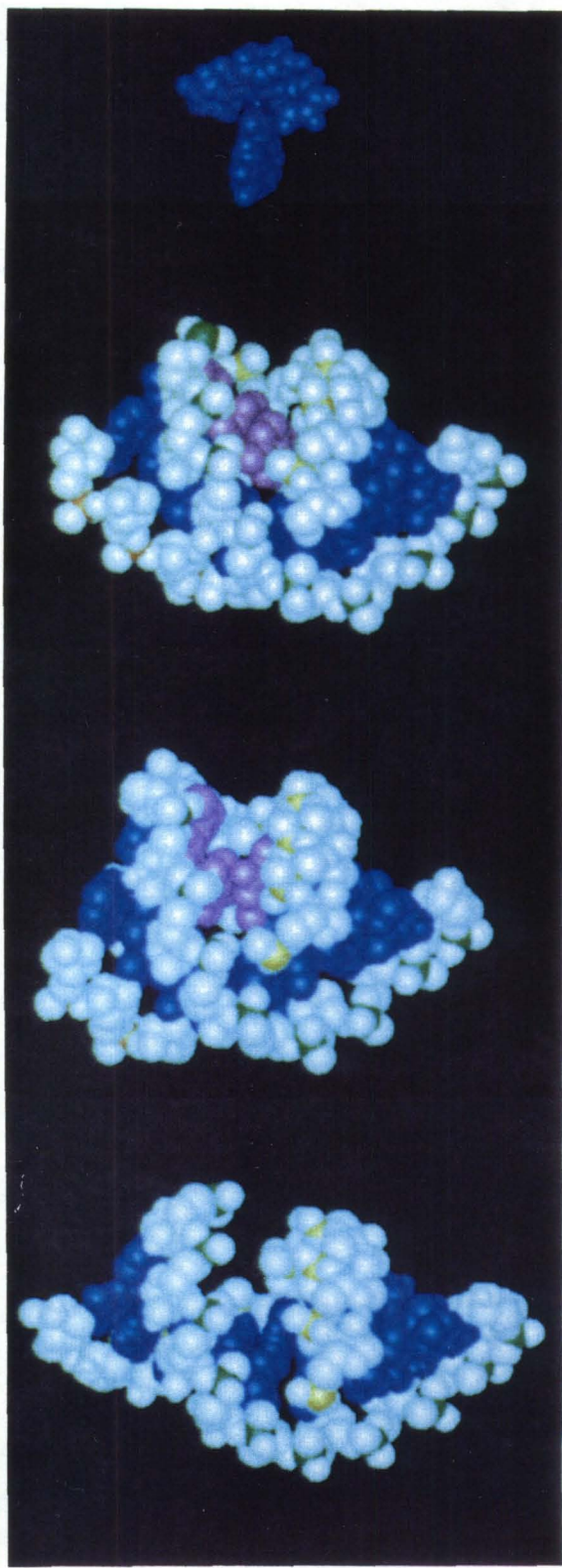
Cleavage at sites that are neither purely single- nor double-stranded may be understood by considering the different structures of an RNA major groove. As can be seen in Figure 4.5, an RNA double helix adopts an A-conformation that contains a deep and narrow major groove; the base pairs are pushed out towards the minor groove of the helix. Thus the base pairs are largely inaccessible from the major groove for stacking with the metal complex. No cleavage by $\text{Rh}(\text{phen})_2\text{phi}^{3+}$ is evident in the double-helical regions of tRNA^{Phe}. However, three of the eight major cleavage sites on tRNA^{Phe} (G22, G45, and m⁷G46) are directly involved in triple interactions in which a third base hydrogen bonds with a normal Watson-Crick base pair in the major groove of the D stem. The interaction of the third base (G45, A9, or G46) in the major groove of the RNA helix creates a structure in which the normally deep and narrow groove is extended towards the surface. As shown in Figure 4.5 (panel B), the filling of the major groove with these third bases (shown in purple) may now provide a platform for stacking with the rhodium complex. Figure 4.5 (panel C) shows an example of a three-base interaction.

Of the three triples (G45-[m²G10-C25], A9-[A23-U12], and m⁷G46-[G22-C13]), the central A9-[A23-U12] shows no cleavage. This lack of cleavage can be rationalized on the basis of the limited accessibility of the sugar-phosphate backbone in this region. The proposed mechanism of cleavage by $\text{Rh}(\text{phen})_2\text{phi}^{3+}$ involves direct hydrogen abstraction from the ribose and therefore necessitates that the complex lie close to the sugar in order for a reaction to occur. Residues G45 and m⁷G46 are located in the variable loop segment and their sugars are quite accessible from the major groove side of the D stem (phosphates of this strand are in yellow in Figure 4.5). Similarly, residue G22 of the D stem has an accessible sugar residue from the major groove (phosphates of this strand are in green).

Figure 4.5. Illustrations of the basis for recognition of the triply bonded bases by $\text{Rh}(\text{phen})_2\text{phi}^{3+}$. (A) A comparison of an A-form RNA double helix (left) and two triple-helix regions based on the crystal structures of yeast tRNA^{Phe} (middle) and tRNA^{Asp} (right). Bases are blue; phosphorous atoms are yellow for strand 1, green for strand 2, and orange for strand 3; the third bases interacting in the major groove are shown in purple (from top to bottom, G45, A9, and G46 for tRNA^{Phe} and A21, G45, A9, and A46 for tRNA^{Asp}); all other atoms are white. For comparison of sizes, the rhodium complex is shown in blue to the far right. Note that the sugar residues of G45 and G46 are accessible from the major groove (yellow strand), while the sugar of A9 is buried within the molecule (orange strand). The view in (A) is perpendicular to the helix axis. The helices in (B) have been rotated 90° and tilted approximately 45° to afford a view into the major groove. Note how the third bases fill the major groove of an A-like helix and are accessible for stacking from the major groove with the metal complex. (C) Structure of a G-C base pair and a G-[G-C] triple-base pair.

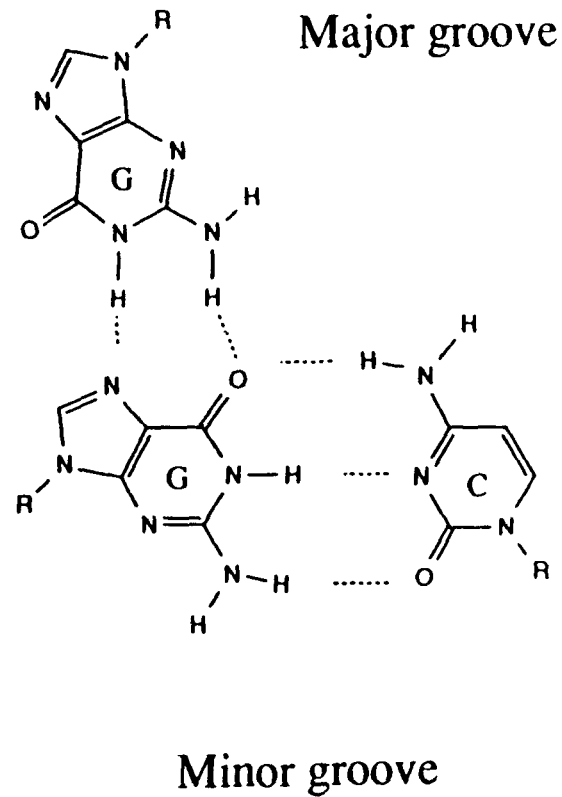
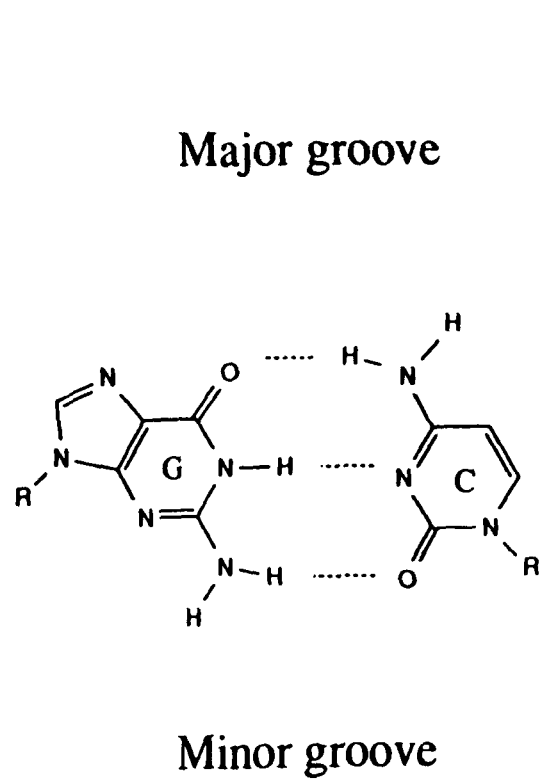


A



B

C



Residue A9 comes from another segment of the polynucleotide chain and intercalates between G45 and m⁷G46 with its backbone buried within the molecule (phosphates of this strand are in orange); as seen in Figure 4.5, although stacking of A9 with the metal complex is feasible, the sugar residue of this nucleotide is not accessible from the major groove side for cleavage.

The strong cleavage by Rh(phen)₂phi³⁺ apparent at the TΨC loop residues, Ψ55 and U59, is not as well understood. As is evident from the crystal structure, this region contains extensive tertiary interactions, and the unusual base interactions between the D and TΨC loops (G18-Ψ55, G19-C56) may provide a structure that facilitates the interaction with the rhodium complex. Cleavage at U59 is also difficult to understand. Although this residue is not base paired, it lies stacked in the core region of the molecule. It is unclear whether the U59 site is recognized uniquely by Rh(phen)₂phi³⁺ or if cleavage here is a result of stacking interactions with the neighboring triply bonded sites.

Effect of salt variation on tRNA^{Phe} cleavage: Cleavage by the rhodium complex varies as a function of magnesium and sodium concentrations as well as buffer conditions. The cleavage experiments shown in Figure 4.2 were performed in sodium acetate buffer (50 mM Tris, 20 mM NaAcetate, 18 mM NaCl, 1 mM MgCl₂, pH 7.0). In 50 mM sodium cacodylate, 1 mM MgCl₂, pH 7.0, additional cleavage sites are observed at residues Y37, A38, and Ψ39 in the anticodon loop. There is also diminished cleavage at U47. However, with increasing concentrations of NaCl (up to 75 mM), a loss in cleavage at the anticodon residues is observed and increased cleavage at U47 is apparent with no change at the other sites. Similarly, a loss of cleavage in the anticodon loop residues is associated with added MgCl₂ (0.5 to 10 mM) as is a loss in cleavage at the triple-base sites. Cleavage at Ψ55 and U59 appears to be independent of magnesium and sodium concentrations. Apparently, the particular orientation of the D and TΨC loops required for recognition by Rh(phen)₂phi³⁺ is not altered in the presence of up to 10 mM MgCl₂ or 75 mM NaCl.

These results suggest that with increasing magnesium ion concentrations, the conformational changes in the tRNA are localized. The overall structure of the tRNA is likely to be unchanged, but a local loosening or tightening of the structure may occur, which is detected by $\text{Rh}(\text{phen})_2\text{phi}^{3+}$. For example, it has been shown through fluorescence studies on the modified base Y37 that the presence of magnesium ion causes the anticodon loop to be more structured, but has little effect on the overall shape of the molecule.¹³ The loss of cleavage by $\text{Rh}(\text{phen})_2\text{phi}^{3+}$ in the anticodon loop and at the triple-base sites may be associated with a tightening of the structure. Alternatively, but less likely given the relative affinities, the magnesium ions may simply be competing with the rhodium complex for binding at these sites.

Cleavage of yeast tRNA^{Asp}: Based upon its crystal structure⁷, the three-dimensional structure of yeast tRNA^{Asp} resembles that of tRNA^{Phe} (Figure 4.4, panel A). Therefore, in order to define further the recognition by $\text{Rh}(\text{phen})_2\text{phi}^{3+}$, we have examined cleavage by the complex on yeast tRNA^{Asp}. There is a striking similarity in cleavage patterns observed on yeast tRNA^{Phe} and tRNA^{Asp} (Figure 4.4, panel B). Strong cleavage, as shown in Figure 4.2 (lane 13), occurs at residues A21 through G26, Ψ 32, and U48. Weaker cleavage is apparent at A44, G45, A46, Ψ 55, U59, and U60. Again, the sites of cleavage appear to mark regions of tertiary folding of the tRNA molecule, as compared in Figure 4.4 (panels A and B, right).

Five of the fourteen cleavage sites in tRNA^{Asp} are directly involved in triple-base interactions and three neighbor and stack with the base triples. Also consistent with tRNA^{Phe} results, the remaining cleavage sites are located in the anticodon and T Ψ C loops. The tertiary interactions found in yeast tRNA^{Asp} are generally analogous to those observed in yeast tRNA^{Phe}, but with some minor differences that may affect cleavage by $\text{Rh}(\text{phen})_2\text{phi}^{3+}$. Most of the differences in cleavage between tRNA^{Asp} and tRNA^{Phe} can be explained by the crystal structure data.

We will first consider the sites of triple-base interaction. The following interactions occur in the major groove of the D stem: G45-[G10-U25], A9-[A23-U12], and A46-[G22-Ψ13]. It appears that the presence of only four bases (A44, G45, A46, U48) in the variable loop of yeast tRNA^{Asp} as compared to five (A44, G45, G46, U47, C48) in yeast tRNA^{Phe} induces a different stacking environment for the base triples, as is revealed when comparing the crystal structures (Figure 4.5, panels A and B). The base triples in tRNA^{Asp} are more evenly stacked on one another compared to the base triples in tRNA^{Phe}. The presence of G-U mismatched base pairs may also contribute to the increased stacking of the base triples in tRNA^{Asp}.⁷ There is a greater uniformity in cleavage observed across the triple sites in tRNA^{Asp} as compared with tRNA^{Phe}; this uniformity may be a function of the evenness or columnar stacking apparent in the triply bonded region of tRNA^{Asp}.

Another structural difference apparent in tRNA^{Asp} is a rotation of the A15-U48 Levitt pair with respect to U8-A14. This rotation leads to an interaction of A21 with the sugar of U8 and base of A14 to form a fourth base triple; A21 of tRNA^{Phe} interacts only with the sugar of U8. Ethylnitrosourea alkylation studies¹⁴ have revealed the differential reactivities of phosphates in the two tRNA species. Phosphate 22 in the D stem is protected in tRNA^{Asp}, yet accessible in tRNA^{Phe}. In contrast, phosphates 23 and 24 are accessible in tRNA^{Asp}, but partially protected in tRNA^{Phe}. The rhodium cleavage results show that sugar residue 22 is most accessible in tRNA^{Phe}, while residues 23, 24, and neighboring residues are accessible in tRNA^{Asp}. We have also observed strong cleavage at position 48 on tRNA^{Asp}, but not on tRNA^{Phe}. This may also be a result of the different conformation of the neighboring U8-A14-A21 triple interaction. Again, Figure 4.5 (panel A) shows the more evenly stacked arrangement for A21 and U48 in tRNA^{Asp}.

The crystal structure of tRNA^{Asp} reveals the absence of G19-C56 base pairing and other interactions between the D and TΨC loops typical of tRNA^{Phe}. Cleavage by Rh(phen)₂phi³⁺ is apparent at the TΨC loop residues Ψ55, U59, and U60 on the

tRNA^{Asp}, but the cleavage associated with this region is much weaker than that observed on tRNA^{Phe}. As revealed in the tRNA^{Asp} crystal structure⁷, C56 remains stacked on G57; however, G19 is displaced by about 4 Å compared to tRNA^{Phe}. As a consequence, the G19-C56 base pair, which is important for maintenance of the D-TΨC loop interactions in tRNA^{Phe}, is disrupted. However, solution studies on tRNA^{Asp} revealed protection from N-3 alkylation by dimethylsulfate at C56, which according to the crystal structure should be reactive.¹⁵ The lack of reactivity of C56 at N-3 suggested the existence of a G19-C56 Watson-Crick base pair correlated with the free state of the molecule in solution. Our results indicate that the rhodium complex is recognizing structure in the TΨC loop, but to a lesser extent than observed for tRNA^{Phe}. Perhaps this region in tRNA^{Asp} is related structurally to tRNA^{Phe}, but is somewhat more flexible.

Other differences in cleavage by Rh(phen)₂phi³⁺ on tRNA^{Asp} and tRNA^{Phe} are seen in the anticodon loops. On tRNA^{Phe}, we observe cleavage of the anticodon residues Y37, A38, and Ψ39 only under certain salt conditions, whereas on tRNA^{Asp} strong cleavage at Ψ32 is apparent. This is consistent with the data of Romby et al.¹⁵, who showed that the loop residues of tRNA^{Asp} are more susceptible to chemical modification under native conditions than those of tRNA^{Phe}, suggesting that the anticodon loop in tRNA^{Asp} has a different structure. This could result from the different stacking interactions in tRNA^{Asp} because of the long-range effects such as the G30-U40 mismatched base pair in the anticodon stem or different base composition in the loop itself.

The effects of magnesium ion on cleavage of tRNA^{Asp} also differ from those seen on tRNA^{Phe}. However, the results on tRNA^{Asp} are consistent with the notion of only localized conformational changes in the tRNA in the presence of magnesium ions. A loss of cleavage is observed at the triple-base sites in 10 mM MgCl₂, consistent with a tightening of the structure in this region so as to inhibit interactions with Rh(phen)₂phi³⁺. In contrast to the tRNA^{Phe} results, increased cleavage is observed in the TΨC loop

residues in tRNA^{Asp}. A magnesium induced structural change may actually enhance interaction with the rhodium complex in the TΨC loop of tRNA^{Asp}. No change in cleavage at the anticodon residue Ψ32 is associated with increased magnesium. In contrast to tRNA^{Phe}, Mg²⁺ seems to have little effect on the structure of the anticodon loop in tRNA^{Asp} and subsequent interaction with Rh(phen)₂phi³⁺.

4.3.2. Cleavage of tRNA Transcripts

Cleavage of unmodified tRNA: Cleavage by Rh(phen)₂phi³⁺ of the yeast tRNA^{Phe} transcript, which lacks all fourteen modified nucleotides but otherwise contains no base substitutions, was examined. Thermal melting profiles of the transcript show that at low magnesium concentrations the transcript possesses a less stable structure in comparison to the native yeast tRNA^{Phe},⁸ even at high magnesium concentrations (8 mM) the transcript exhibits a different melting profile, suggestive of a more flexible structure than the fully modified yeast tRNA^{Phe}. Perhaps the absence of specific base modifications causes an overall destabilization of the tRNA transcript. NMR studies on the tRNA^{Phe} transcript have further indicated that even when the transcript is folded normally (5 mM free MgCl₂), local structural changes may arise because of the absence of base modifications.⁹

Cleavage of unmodified tRNA^{Phe} by Rh(phen)₂phi³⁺ seems to be similar but not identical to that of fully modified tRNA^{Phe}. Strong cleavage, shown in Figure 4.2, is apparent at G22, U47, C48, U55 (Ψ55 in native), and U59 with minor sites at C27, A36, G37 (Y37 in native), A38, G45, and G46 (m⁷G46 in native). The rhodium cleavage results indicate that globally the folded structure of the tRNA is likely the same. Furthermore, the fact that the sites of cleavage are in general the same on the modified and unmodified tRNAs provides evidence that the complex is recognizing a specific shape or structure and that the actual cleavage chemistry is not related to the base modifications.

The differences in cleavage between native and wild type tRNA^{Phe} are shown in a ribbon diagram in Figure 4.3. The figure also indicates the bases that are modified in the native tRNA^{Phe}. Changes in cleavage in the anticodon loop (residues 36 to 38) and the anticodon stem (residue 27) may reflect a loosening or alteration in the structure due to the absence of the modified bases. In contrast to modified native tRNA^{Phe}, cleavage of the anticodon loop residues in the unmodified tRNA transcript is actually enhanced in 10 mM MgCl₂. This may be reflective of the subtle structural differences between the modified and unmodified RNA rather than blocking effects of the bulky modified base Y37. A decrease in cleavage at U55 may also reflect the absence of modified bases at residues 54 and 55. Similarly, the small changes in selectivity by the rhodium complex in the triple-base region could be a result of minor structural variations that arise when modified bases are no longer present to stabilize specific interactions. For example, the hydrogen bonding at the m⁷G46-[G22-C13] base triple by N-1 and the exocyclic N-2 of G46 may be stabilized by the increased positive charge associated with methylation at N-7. The positive charge may also stabilize the interactions of G46 with phosphate 9. The triple G45-[m²G10-C25] is followed by the severely propeller-twisted A44-m²G26 base pair. The m²G10-C25 base pair stacks with m²G26, while A44 stacks with the C27-G43 base pair below. The dimethylation of G26 may contribute to the propeller twisting of the base pair and therefore may stabilize the stacking interaction at the neighboring triple site. These interactions are likely important for recognition by the rhodium complex as seen by changes in cleavage at A44, G45, and G46, as well as at C27.

The salt-dependent changes in cleavage by Rh(phen)₂phi³⁺ have also been considered on the unmodified tRNA^{Phe} transcript. Similar to native tRNA^{Phe}, a gradual loss in cleavage at G22, U47, and C48 with increasing magnesium is observed. With increasing magnesium ion concentrations, no cleavage is apparent at A44, G45, and G46.

This suggests that the unmodified tRNA transcript may be structurally slightly different from native tRNA, rather than simply more flexible, even in the presence of magnesium.

Cleavage of tRNA mutants: In order to characterize further the recognition characteristics of the rhodium complex, cleavage was examined on a series of mutant tRNAs prepared as RNA transcripts. Table 4.1 summarizes the findings obtained. In addition, Table 4.1 shows a comparison of the rhodium cleavage data to assays of mutant structure based upon cleavage by lead ion¹ and rates of aminoacylation¹¹. It has been possible to monitor the folding of tRNA^{Phe} by measuring its specific cleavage reaction with lead ion.¹ In this reaction, lead ion coordinates to the nucleotide bases U59 and C60 in the T loop and promotes cleavage between U17 and G18 in the D loop. Using Table 4.1, rhodium cleavage as an assay for RNA structural perturbations may be compared and contrasted to these current methodologies.

Mutations of tertiary interactions in the D-TΨC loop region: We were interested in exploring how changes in the D-TΨC loop interactions might perturb the overall tertiary structure of the RNA. Figure 4.6 summarizes the cleavage data for two different D-TΨC loop mutants. These mutations occur at neighboring residues and have substantially different effects on the TΨC loop cleavage. These effects are localized, however, and little change in cleavage is observed at the triple-base or anticodon sites.

The crystal structure of yeast tRNA^{Phe} shows that the nucleotides G19-C56 form the only tertiary Watson-Crick base pair in the outermost corner of the tRNA molecule and are important for maintaining interactions between the D and TΨC loops. The G19C mutant leads to a C19-C56 mismatch, which is expected to disrupt partially the D-TΨC loop interaction. An observed 5-fold decrease in the rate of site-specific cleavage by lead indicates that this mutant has an altered tertiary structure in the corner region of the tRNA^{Phe} molecule.¹ Rh(phen)₂phi³⁺ promotes strand scission of G19C (Figure 4.2) at

Table 4.1. Cleavage of tRNA^{Phe} Mutants by Rh(phen)₂phi³⁺ Compared with Lead Cleavage Rates and Aminoacylation Kinetics.

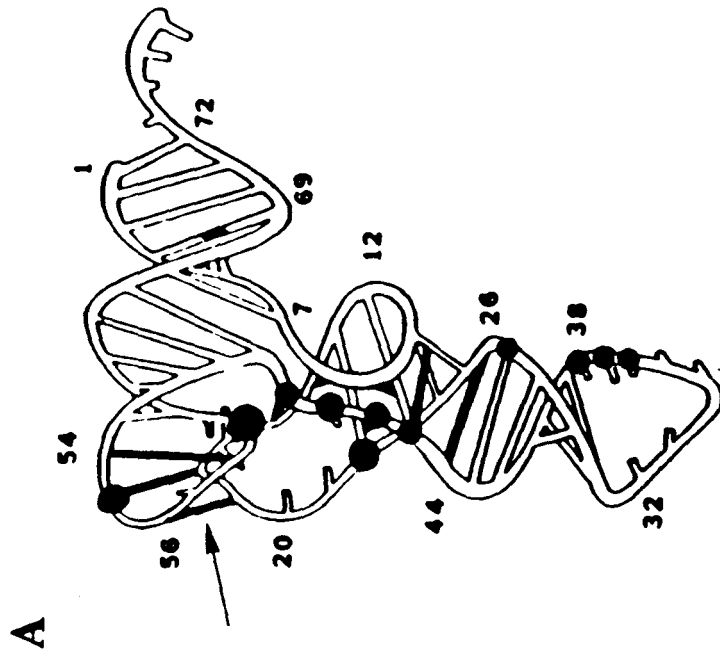
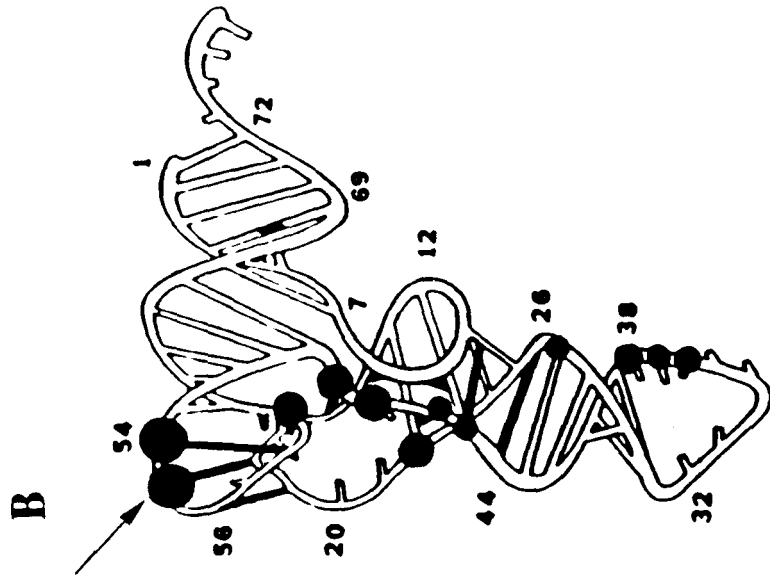
<i>mutant</i>	<i>tertiary interaction</i> ^a	<i>diminished sites</i> ^b	<i>enhanced sites</i> ^b	<i>Pb</i> ^c	<i>amino-acylation</i> ^d
wild type	G19-C56, G18-U55			(1.0)	(1.0)
G19C	C19-C56	48, 55	45, 46	ND ^e	ND
G18A-U55C	A18-C55		54, 55	0.42	0.23
wild type	G46-[G22-C13]			(1.0)	(1.0)
G46C	C46-[G22-C13]	lose 45, 47, 48, 55		0.22	0.40
G22A-C13U	G46-[A22-U13]		45, 46	0.40	0.53
G46A-G22A -C13U	A46-[A22-U13]	48	44, 45, 46	0.44	1.20
wild type	A9-[A23-U12]			(1.0)	(1.0)
A9U	U9-[A23-U12]	36, 37, 38, 46, 47, 59		0.18	0.55
wild type	G45-[G10-C25]			(1.0)	(1.0)
G45U	U45-[G10-C25]		45, 46, 47	0.87	0.95
G10C-C25G	G45-[C10-G25]	27, 36, 37, 38, 48	45, 46, 54, 55, 60	ND	0.88

^a Tertiary interactions for wild type are in regular text and mutations are in bold.

^b Cleavage relative to wild type tRNA^{Phe} transcript. Cleavage mixtures contained 3'-end-labeled tRNA, 10 μM Rh(phen)₂phi³⁺, 100 μM carrier tRNA^{Phe}, 50 mM Tris, 20 mM NaAcetate, 18 mM NaCl, and 1 mM MgCl₂, pH 7.0 at 25°C.

^c Taken from Behlen et al.¹ ^d Taken from Sampson et al.¹¹ ^e ND is not detected.

Figure 4.6. Mapped sites of cleavage on the TΨC loop mutants (A) G19C and (B) G18A-U55C. Arrows point to the sites of mutation.



U59 and the anticodon residues to the same extent as in the wild type transcript, but there are small changes in cleavage at the triple-base sites and a noticeable decrease in cleavage at U55. This result is consistent with cleavage results on yeast tRNA^{Asp}; the disrupted G19-C56 base pair that is evident in the crystal structure seems to have only small long-range effects on cleavage by Rh(phen)₂phi³⁺ at the triple-base sites, but less cleavage at the TΨC loop site (U55) with less selectivity is apparent.

The mutant G18A-Ψ55C (data not shown) shows overall patterns of cleavage by Rh(phen)₂phi³⁺, which are similar to wild type, but with greatly enhanced cleavage at U54 and C55. This mutation is expected to have significant effects on the interaction between the D and TΨC loops. The aminoacylation kinetics of this mutant indicate that the hydrogen bonding interactions between G18 and Ψ55 are important for interaction with the cognate yeast phenylalanyl-tRNA synthetase.¹¹ In addition, decreased lead cleavage suggests that this mutant has an altered tertiary structure.¹ The cleavage results with Rh(phen)₂phi³⁺ indicate that the tRNA is still folded with its overall structure the same, but a significant structural change has occurred in the D-TΨC loop region. Together with the tRNA^{Asp} cleavage data, these results point to the importance of the TΨC loop structure for the recognition by the rhodium complex.

Mutations of the G46-[G22-C13] tertiary interaction: In the core region of the tRNA molecule, the G22-C13 base pair in the D stem interacts with G46 of the variable loop. This triple-base scheme is stabilized by seven hydrogen bonds (four tertiary) in tRNA^{Phe} and three hydrogen bonds (one tertiary) in tRNA^{Asp}. Mutations in this tertiary interaction were constructed to maintain the conserved pyrimidine 13-purine 22 motif and vary at position 46. These mutations exhibit relatively small differences in aminoacylation kinetics and only slight reductions in lead cleavage (Table 4.1). Importantly, Rh(phen)₂phi³⁺ targets the same sites in these mutants, verifying that the complex recognizes structural features of the RNA rather than individual nucleotides.

Besides having the ability to target the triple-base structure in tRNA, Rh(phen)₂phi³⁺ is able to distinguish small variations in the backbone structure around the base triples. As shown in Figure 4.7 (lane 7), a one-base change to C46-[G22-C13] leads to a large change in cleavage at residues G45 through C48. This mutant appears to be unstable since the overall cleavage is much weaker and less specific at both the triple sites and the D loop sites. A relative lead cleavage of 0.22 compared to wild type cleavage is also indicative of some structural change for this mutation.¹

We have also examined a two-base change at the D stem base pair to G46-[A22-U13] and a three-base change to A46-[A22-U13], a common base triple found among tRNAs. Figure 4.7 (lanes 9 and 11) shows cleavage patterns similar to those on the wild type transcript, but with strong cleavage at G46 for both mutants. These data are compared in ribbon diagrams in Figure 4.8 (panels A and B). Changes in cleavage at the triple-base sites for these mutants may be understood by considering variations in the base-stacking interactions. As was evident in the tRNA^{Asp} cleavage data, the rhodium complex is sensitive to variations in base stacking of the triples, as would be expected if the rhodium complex intercalates in this region. Perhaps the greater change in cleavage for the mutant C46-[G22-C13] results from a greater change in stacking, since the mutation involves a purine to pyrimidine base change at residue 46. In contrast, mutants G46-[A22-U13] and A46-[A22-U13] involve only semiconservative base changes. The conservation of a purine at position 22 and a pyrimidine at position 13 may help to maintain proper stacking interactions within these triple-base regions. Not surprising, the stacking may actually be more important than hydrogen bonding interactions among bases in determining the interactions with an intercalator such as Rh(phen)₂phi³⁺.

Mutations of the A9-[A23-U12] tertiary interaction: A reverse Hoogsteen pair with A9 occurs in the major groove of the A23-U12 base pair of the D stem. This base triple is flanked by two other base triples (G46-[G22-C13] and G45-[G10-C25]) and the A9

Figure 4.7. Cleavage of several ^{32}P 3'-end-labeled tRNA^{Phe} mutants by $\text{Rh}(\text{phen})_2\text{phi}^{3+}$. Cleavage was performed in 50 mM Tris, 20 mM NaAcetate, 18 mM NaCl, 1 mM MgCl_2 , pH 7.0. Lanes 1 and 18: A-specific reaction on the tRNA^{Phe} transcript. Lanes 2 and 19: U-specific reaction on the tRNA^{Phe} transcript. Lanes 3, 6, 8, 10, 12, 14, and 16: controls without metal or irradiation; tRNA^{Phe} transcript, G46C, G22A-C13U, G46A-G22A-C13U, A9U, G45U, and G10C-C25G. Lane 4: light control; tRNA^{Phe} transcript irradiated in the absence of metal. Lanes 5, 7, 9, 11, 13, 15, and 17: specific cleavage by $\text{Rh}(\text{phen})_2\text{phi}^{3+}$ on the tRNA^{Phe} transcript, G46C, G22A-C13U, G46A-G22A-C13U, A9U, G45U, and G10C-C25G. Arrows indicate reference points along the tRNA sequence. Bars indicate major regions of cleavage by $\text{Rh}(\text{phen})_2\text{phi}^{3+}$.

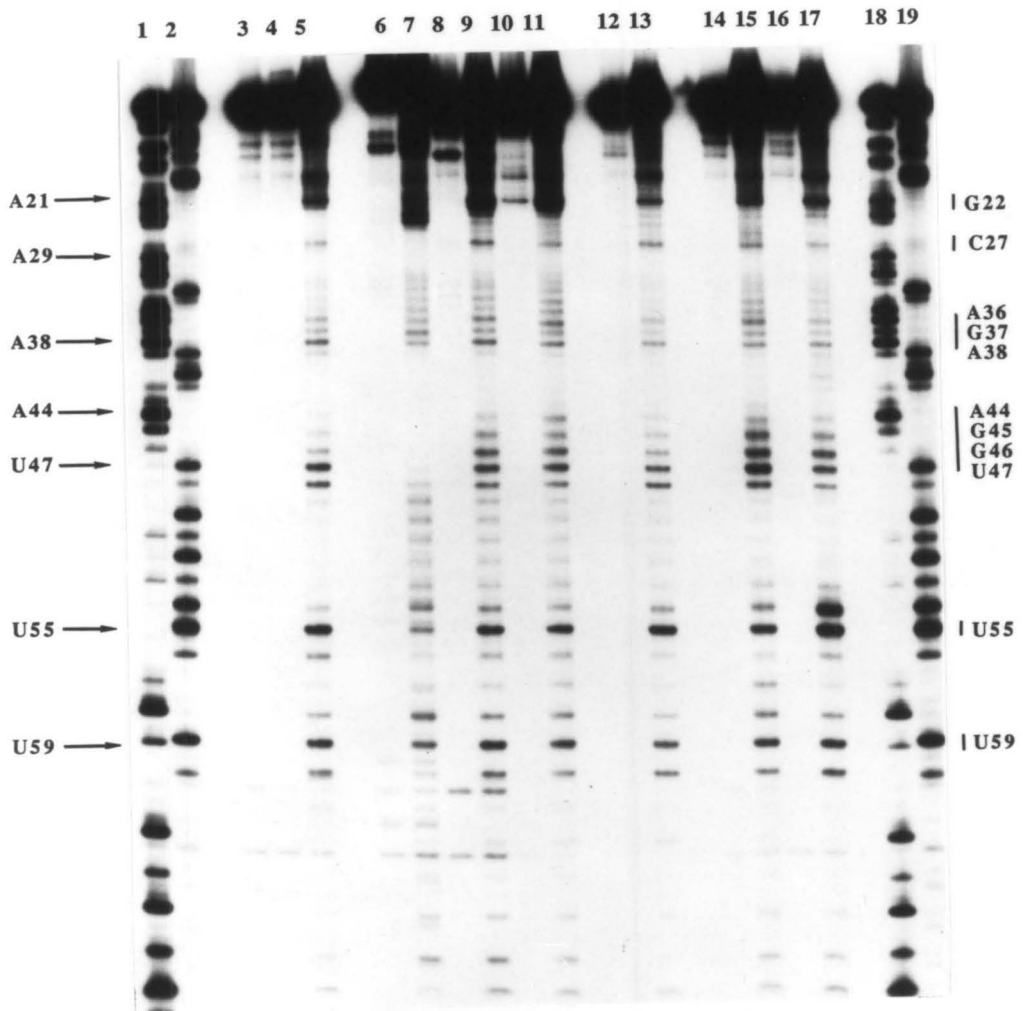
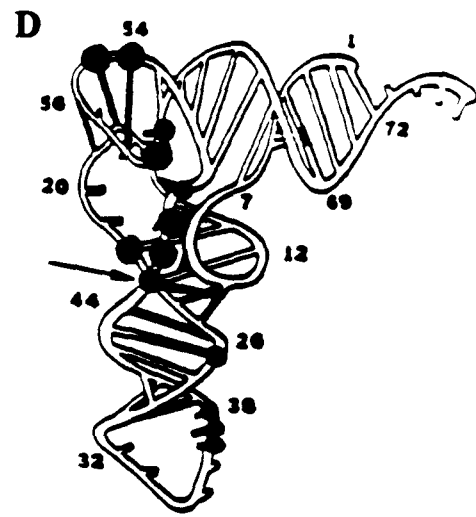
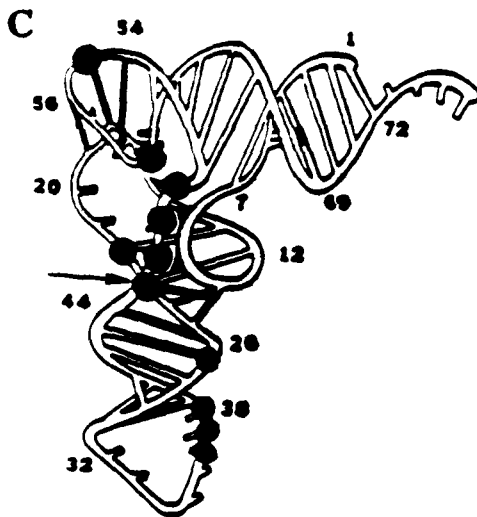
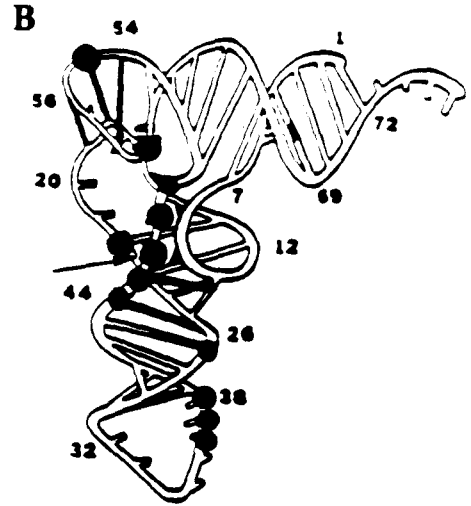
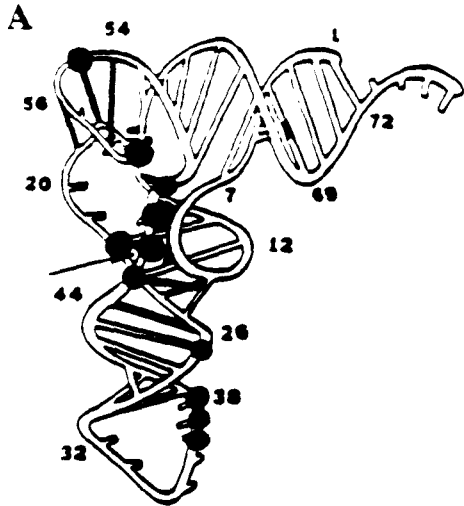


Figure 4.8. Mapped sites of cleavage on the triple-base mutants (A) G22A-C13U, (B) G46A-G22A-C13U, (C) G45U, and (D) G10C-C25G. Arrows point to the sites of mutation.



residue is stabilized by stacking interactions with the G45 and G46 residues. The mutant that involves a one-base change of the third base U9-[A23-U12] exhibits only small changes in the cleavage patterns, as shown in Figure 4.7 (lane 13). We have observed a small decrease in $\text{Rh}(\text{phen})_2\text{phi}^{3+}$ cleavage at all sites except U55. A large decrease in the relative lead cleavage rate (0.18) was associated with this mutant.¹ Although this mutant maintains only one hydrogen bond between U9 and A23, which may be important for interaction with lead ion, the bases may be stacked such that the triple sites are still recognized by the rhodium complex.

Mutations of the G45-[G10-C25] tertiary interaction: The crystal structure of tRNA^{Phe} shows that the variable loop nucleotide G45 is involved in an unusual tertiary interaction. G45 has a single hydrogen bond between its exocyclic amine and the O-6 of G10 in the major groove of the D stem and is tilted and stacked over A44. Furthermore, A44 stacks with the first base of the anticodon stem, while the G10-C25 base pair stacks over G26. The propeller-twisted A44-G26 base pair maximizes stacking with its neighboring nucleotides. The mutations G45U and G10C-C25G, which should form the base triples U45-[G10-C25] and G45-[C10-G25], respectively, exhibit normal aminoacylation kinetics compared with wild type, but, as seen in Table 4.1, show very different rates of cleavage with lead. As with the other triple-base mutants, the overall patterns of cleavage by $\text{Rh}(\text{phen})_2\text{phi}^{3+}$ are the same as wild type (Figure 4.7, lanes 15 and 17; Figure 4.8, panels C and D), again supporting the notion that the rhodium complex recognizes the triple-base structure rather than individual nucleotides. However, one can observe differences within these regions of cleavage. Cleavage at A44, U45, and G46 on G45U is unusually strong compared to cleavage on the wild type transcript. Once again, stacking interactions may be more important than hydrogen bonding interactions in determining binding by the rhodium complex. Hydrogen bonding between G10 and U45 is unlikely, but it seems that the presence of residue 45 in the major groove of the D stem is

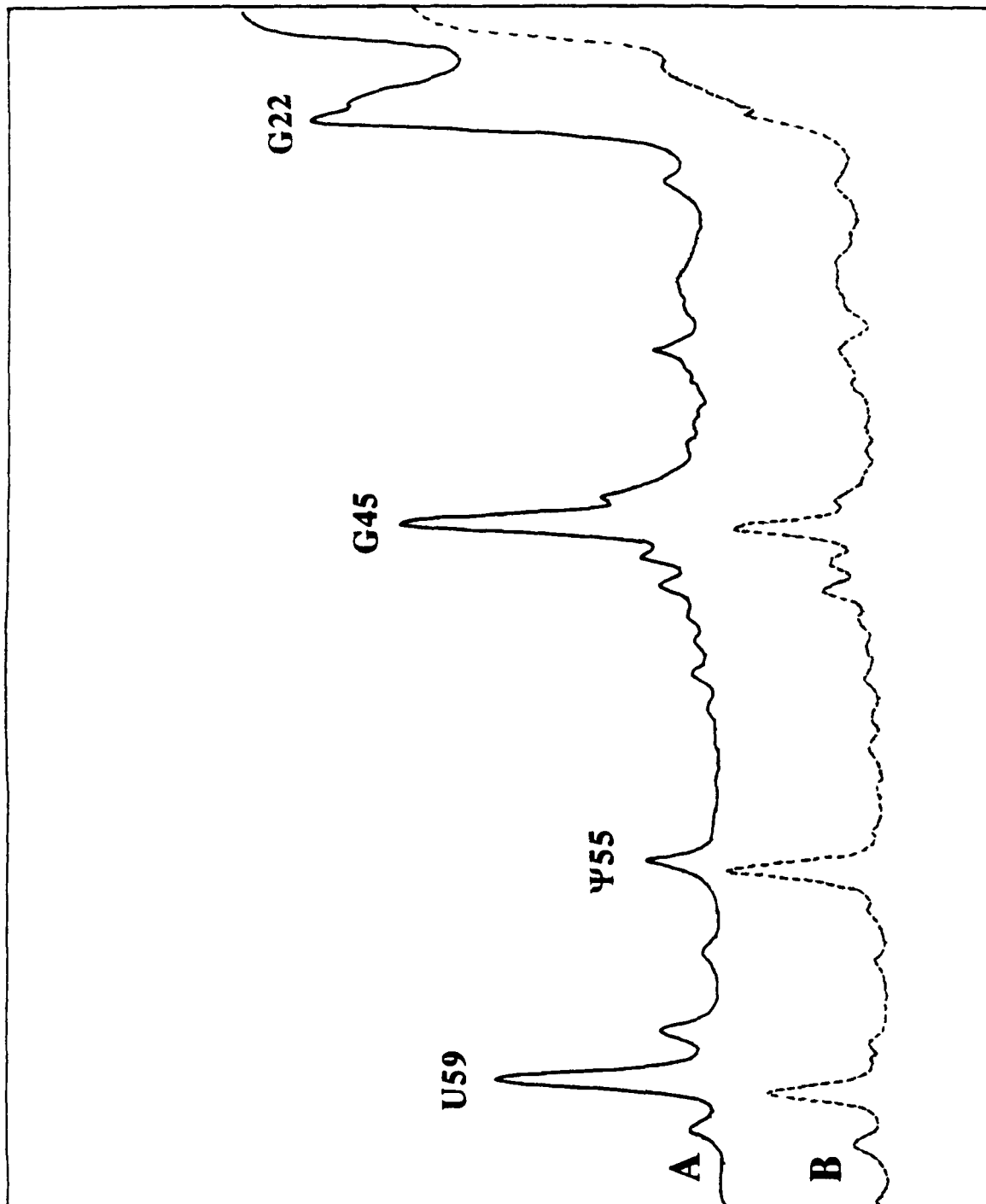
sufficient for recognition by the rhodium complex. The presence of the two neighboring base triples may also help to maintain stacking in this mutant, although stacking of a pyrimidine (U45) is less favored than stacking of a purine (G45).

The double mutant G10C-C25G shows small changes in cleavage at the triple sites and a diminished intensity of cleavage in the anticodon loop and at residue C27. These variations seem to indicate a more global change in structure of the mutant. Unusually strong cleavage is evident in the D-TΨC loop region. Consistent with the rhodium cleavage data, this mutation showed a pronounced effect on the lead cleavage at a site far from the mutation.¹

4.3.3. Cleavage of a Modified tRNA

Chemical modification in which a triple-base interaction is destroyed without substantial effect elsewhere in the molecule is also useful in delineating the recognition of the triple-base sites by $\text{Rh}(\text{phen})_2\text{phi}^{3+}$. Upon sodium borohydride treatment of the native tRNA^{Phe} , residue G46, which is methylated at the N-7 position, is selectively depurinated.¹⁰ This depurination leads to a loss of the third-base interaction in the major groove for the triple G46-[G22-C13]. As shown in Figure 4.9, the cleavage by $\text{Rh}(\text{phen})_2\text{phi}^{3+}$ on the still intact, folded, depurinated tRNA indicates a large reduction in the cleavage intensity at the triple-base sites (G45 and G22) and neighboring site (U59) relative to the other sites of cleavage (Ψ55), which are far from the mutation. However, it is difficult to bring both the borohydride reduction and aniline treatment to completion to permit quantitation of the effect. Additionally, other base modifications, such as depurination at Y37, may occur, which may also cause structural perturbations in the tRNA. Nonetheless, with these caveats, it appears that deletion of the triply bonded base strongly affects cleavage by the rhodium complex on the folded tRNA. These results indicate that the triply bonded base interaction is necessary for binding by $\text{Rh}(\text{phen})_2\text{phi}^{3+}$.

Figure 4.9. Densitometer scans of $\text{Rh}(\text{phen})_2\text{phi}^{3+}$ cleavage of (A) native tRNA^{Phe} and (B) the chemically modified tRNA^{Phe} . Cleavage reactions were performed in 50 mM sodium cacodylate, pH 7.0. The native tRNA^{Phe} was modified with sodium borohydride as described by Peattie¹⁰ prior to cleavage by the metal complex. The major sites of cleavage are marked.



4.4. Discussion

We have shown that $\text{Rh}(\text{phen})_2\text{phi}^{3+}$ is a sensitive probe of the tertiary structure of tRNAs. There is a strong correlation evident between regions of the RNA that are involved in tertiary interactions and sites that are specifically targeted by the rhodium complex. The sites differ from those targeted by other cationic metal complexes which differ in their shape. Mutations that preserve the structure of the triply bonded region of the tRNA are still cleaved by $\text{Rh}(\text{phen})_2\text{phi}^{3+}$, indicating that it is the structure rather than the individual nucleotides that are being targeted. Selective depurination of $\text{m}^7\text{G46}$, the third base involved in the triple in the native, folded tRNA, results in the reduction of cleavage by the metal complex. These results are consistent with the DNA recognition characteristics of $\text{Rh}(\text{phen})_2\text{phi}^{3+}$.¹⁶⁻¹⁷ While the complex binds by an intercalative mode in the open major groove of DNA, binding by the complex in the deep and narrow major groove of double-helical RNA is not expected on the basis of steric considerations. Indeed, no cleavage is observed in double-helical regions of tRNA. Additionally, the complex requires structure in order to intercalate, and thus purely single-stranded regions of the RNA are not targeted by the complex. Furthermore, since the complex cleaves by direct hydrogen abstraction, rather than through a diffusible intermediate, close contact with the RNA is required to achieve strand scission. We have proposed that cleavage by $\text{Rh}(\text{phen})_2\text{phi}^{3+}$ occurs preferentially at regions of tertiary structure in the tRNA because these regions are structured so that the major grooves are open and accessible to stacking by the complex.

The rhodium complex is not specific for one particular tertiary structure. Instead, given the cleavage results on yeast tRNA^{Phe}, yeast tRNA^{Asp}, and structurally modified tRNA mutants, it appears that a variety of tertiary structures are recognized by $\text{Rh}(\text{phen})_2\text{phi}^{3+}$. These structures include triple-base interactions, stem-loop junctions such as in the anticodon stem-loop region, or the structured loop regions such as the TΨC loop. Furthermore, as summarized in Table 4.1, the rhodium complex provides a sensitive

probe for structural perturbations within these regions. One- or two-base changes can affect cleavage at neighboring residues which may be a result of different base stacking interactions for purines versus pyrimidines (i.e. G45U) or local structural distortions created by altered hydrogen bonding interactions between the bases (G18A-U55C). As is also shown from Table 4.1, mutations that disrupt certain tertiary interactions in tRNA can affect cleavage far away from the actual mutation. For example, a change from A9 to U9 affects cleavage at residues 36 to 38 in the anticodon loop. Similarly, a change from G10-C25 to C10-G25 leads to changes in the TΨC loop residues. These results suggest that structural alterations caused by the mutations in these folded regions of tertiary interaction can be propagated through the stacked nucleotides to affect structure at a distance.

Cleavage results with $\text{Rh}(\text{phen})_2\text{phi}^{3+}$ correlate well with lead cleavage data¹ as shown in Table 4.1. Mutations that produced substantial effects on rhodium cleavage, in particular G46C and G10C-C25G, also showed large decreases in lead cleavage rates. In contrast, the A9U yielded only small changes in rhodium cleavage, yet large changes in lead cleavage. It should be noted, however, that there was a change in cleavage by $\text{Rh}(\text{phen})_2\text{phi}^{3+}$ in this mutant at U59. This may be significant since residue 59 is important for coordination by lead ion. In general, lead cleavage requires a high degree of stereochemical constraint and is therefore sensitive to local structure near the lead binding site. The rhodium complex is also sensitive to local structural perturbations, but given that $\text{Rh}(\text{phen})_2\text{phi}^{3+}$ binds at several sites on the polymer, the complex provides a probe for several different regions of the RNA. Furthermore, since $\text{Rh}(\text{phen})_2\text{phi}^{3+}$ appears to probe tertiary interactions, perturbations at a distance from the binding sites that affect tertiary folding of the RNA can be sensitively assayed. Rhodium cleavage data on the tRNA^{Phe} mutants do not seem to correlate with the aminoacylation data.¹¹ This is not surprising, since the rhodium complex does not seem to interact with regions of the tRNA that are

important for making contacts with the tRNA synthetase.¹⁸ However, the cleavage by $\text{Rh}(\text{phen})_2\text{phi}^{3+}$ may correlate with other biological functions of the tRNA.

In conclusion, we have demonstrated through tRNA cleavage that $\text{Rh}(\text{phen})_2\text{phi}^{3+}$ targets sites of tertiary interactions. The results obtained on yeast tRNA^{Asp} and tRNA mutants indicate that cleavage patterns on yeast tRNA^{Phe} may reflect generally the recognition pattern of the complex for all tRNAs. Few and unique sites are cleaved on tRNAs, and the observed cleavage patterns vary sensitively with subtle changes in nucleic acid structure. Therefore, $\text{Rh}(\text{phen})_2\text{phi}^{3+}$ should provide a powerful probe in characterizing the folded structure of different tRNA mutants.

It appears that $\text{Rh}(\text{phen})_2\text{phi}^{3+}$ may also be useful in characterizing other RNA structures. The complex has the ability to target uniquely a few sites within an RNA polymer. Regions that are double-helical or single-stranded are not preferentially bound. Furthermore, given the cleavage chemistry, which involves no diffusible intermediate, the reaction is specific to the site of binding. The cleavage patterns by the rhodium complex may provide a sensitive and specific fingerprint to monitor structural changes in an RNA polymer as a function of different perturbations, substitutions, or reactions. On the basis of the tRNA cleavage data, it appears also that the complex is not specific for a single tertiary interaction. Sites cleaved by the rhodium complex mark a range of tertiary structures. Therefore, used in concert with other structural experiments, $\text{Rh}(\text{phen})_2\text{phi}^{3+}$ may be a powerful and unique probe in characterizing the tertiary structures of other RNAs.

References

1. Behlen, L. S.; Sampson, J. R.; DiRenzo, A. B.; Uhlenbeck, O. C. *Biochemistry* **1990**, *29*, 2515-2523.
2. Garrett-Wheeler, E.; Lockard, R. E.; Kumar, A. *Nucleic. Acids Res.* **1984**, *12*, 3405-3422.
3. Arnott, S.; Hukins, D. W. L.; Dover, S. D.; Fuller, W.; Hodgson, A. R. *J. Mol. Biol.* **1973**, *81*, 107-122.
4. Dock-Bregeon, A. C.; Chevrier, B.; Podjarny, A.; Johnson, J.; de Bear, J. S.; Gough, G. R.; Gilham, P. T.; Moras, D. *J. Mol. Biol.* **1989**, *209*, 459-474.
5. Kim, S.-H.; Sussman, J. L.; Suddath, F. L.; Quigley, G. J.; McPherson, A.; Wang, A. H.; Seeman, N. C.; Rich, A. *Proc. Natl. Acad. Sci. U.S.A.* **1974**, *71*, 4970-4974.
6. Quigley, G. J.; Rich, A. *Science* **1976**, *194*, 796-806.
7. Westhof, E.; Dumas, P.; Moras, D. *J. Mol. Biol.* **1985**, *184*, 119-145.
8. Sampson, J. R.; Uhlenbeck, O. C. *Proc. Natl. Acad. Sci. U.S.A.* **1988**, *85*, 1033-1037.
9. Hall, K. B.; Sampson, J. R.; Uhlenbeck, O. C.; Redfield, A. G. *Biochemistry* **1989**, *28*, 5794-5801.
10. Peattie, D. A. *Proc. Natl. Acad. Sci. U.S.A.* **1979**, *76*, 1760-1764.
11. Sampson, J. R.; DiRenzo, A. B.; Behlen, L. S.; Uhlenbeck, O. C. *Biochemistry* **1990**, *29*, 2523-2532.
12. England, T. E.; Uhlenbeck, O. C. *Nature* **1978**, *275*, 560-561.
13. Beardsley, K.; Tao, T.; Cantor, C. R. *Biochemistry* **1970**, *9*, 3524-3532.
14. Romby, P.; Moras, D.; Bergdoll, M.; Dumas, P.; Vlassov, V. V.; Westhof, E.; Ebel, J. P.; Giege, R. *J. Mol. Biol.* **1985**, *184*, 455-471.

15. Romby, P.; Moras, D.; Dumas, P.; Ebel, J. P.; Giege, R. *J. Mol. Biol.* **1987**, 195, 193-204.
16. Pyle, A. M.; Long, E. C.; Barton, J. K. *J. Am. Chem. Soc.* **1989**, 111, 4520-4522
17. Pyle, A. M.; Morii, T.; Barton, J. K. *J. Am. Chem. Soc.* **1990**, 112, 9432-9434.
18. Sampson, J. R.; DiRenzo, A. B.; Behlen, L. S.; Uhlenbeck, O. C. *Science* **1989**, 243, 1363-1366.

Chapter 5:**Applications of Rh(phen)₂phi³⁺ as a Probe for RNA Tertiary Structure: Delineation of Structural Domains in 5S rRNA[†]****5.1. Introduction**

The ribosomal 5S RNA is an essential component of the cell's machinery for protein synthesis. Despite extensive study, many aspects of the individual function and the higher-order structure of this small RNA (120 nucleotides) remain unknown. A great deal of work has been concerned with the structure of *Xenopus* oocyte 5S rRNA and its interaction with the transcription factor IIIA (TFIIIA). TFIIIA from *Xenopus* is one of three factors that must bind to the internal control region of the 5S RNA gene in order to initiate transcription by RNA polymerase III.¹⁻⁴ In addition, TFIIIA binds to the 5S rRNA transcripts in the cytoplasm of immature oocytes, forming a ribonucleoprotein particle (7S RNP) that stabilizes the 5S rRNA until it is required for ribosome assembly.⁵⁻⁶ The unique ability of TFIIIA to interact specifically with both DNA and RNA provides an interesting basis for regulation. Because of its biological significance, the 5S rRNA-TFIIIA complex provides an attractive model for studying RNA-protein interactions, which are ultimately governed by the tertiary structure of the RNA.

The tertiary structure of 5S rRNA has been the subject of many biochemical and biophysical investigations. On the basis of comparative sequence Fox and Woese⁷ first suggested a minimal secondary structure for prokaryotic 5S rRNA containing four helices, two internal loops, and two external loops. The same strategy was used later to arrive at a similar model for eukaryotic 5S rRNA but with the addition of a fifth helix and an added

[†] Adapted from Chow, C. S.; Hartmann, K. M.; Rawlings, S. L.; Huber, P. W.; Barton, J. K. *Biochemistry* 1992, in press.

internal loop.⁸ Chemical and enzymatic assays of polymer structure as well as several spectroscopic studies are all consistent with this basic model for the secondary structure of prokaryotic and eukaryotic 5S rRNAs.⁹⁻¹¹ Certain regions of the RNA molecule have nonetheless remained refractory to analysis, and the overall three-dimensional structure of the molecule remains ill-defined.

Secondary structure maps for *Xenopus* oocyte 5S rRNA suggest that the RNA should contain several bulged and unusual mismatched residues in helices II, III, and V. Several tentative models for 5S rRNA tertiary structure have proposed a folded structure containing long-range interactions between loop C and either the internal loop E or external loop D¹²⁻¹⁵ or pseudoknot structures¹⁶. There is also evidence that suggests that 5S rRNAs are flexible and can undergo conformational switches that may have functional importance.¹⁷⁻¹⁸ This flexibility may account for some of the discrepancies between the various models for tertiary folding proposed. Westhof et al.¹⁹ have developed a model for higher-order structure that can accommodate both a eubacterial (spinach chloroplast) and a eukaryotic (*Xenopus*) 5S rRNA. This structure does not possess any long-range tertiary interactions between the loops, but involves instead short-range interactions within the internal loop regions. In this model, the 5S rRNA adopts a distorted Y-shape structure with three independent domains that contain several noncanonical base pairs (A-A, U-U, and A-G) within the internal loop regions and bulged nucleotides within the helical regions. Interestingly, growing evidence indicates the importance of RNA structural variations, such as loop structures and bulged nucleotides, as key elements in the recognition of RNA by proteins.²⁰⁻²⁶

We have shown in Chapter 3 that photoactivation of the transition metal complex bis(phenanthroline)phenanthrenequinone diimine rhodium(III) $\{\text{Rh}(\text{phen})_2(\text{phi})^{3+}\}$ promotes strand cleavage at accessible sites in the major groove of DNA and RNA. The rhodium complex, which binds to double-helical DNA by intercalation in the major

groove²⁷⁻²⁸, yields no cleavage in the double-helical regions of tRNA, nor in unstructured single-stranded regions. Instead, Rh(phen)₂(phi)³⁺ appears to target preferentially regions of tRNAs that exhibit extensive tertiary interactions and are structured so that the major grooves are open and accessible to stacking by the complex. As described in Chapter 4, this complex has proven to be a valuable probe for higher-order structure in RNA.

Rh(phen)₂(phi)³⁺ is used here to examine the three-dimensional structure of *Xenopus* oocyte 5S rRNA. As with tRNA, we have observed site-selective cleavage of the 5S rRNA at unique sites marked by tertiary interactions. We have synthesized a truncated 5S rRNA representing one arm of the molecule and have introduced site-specific mutations in the full length 5S rRNA to test the involvement of the loop regions in possible long-range interactions. The results do not support models that involve long-range tertiary interactions. However, cleavage by Rh(phen)₂phi³⁺ at specific sites indicates that the apposition of several noncanonical bases found in 5S rRNA as well as in stem-loop junctions may result in intimately stacked structures with opened major grooves. These distinctive structures with accessible bases may be utilized for specific recognition by RNA-binding proteins, such as the transcription factor TFIIIA.

5.2. Experimental

Materials: The reagents used in this study were obtained from the following suppliers: tRNA^{Phe} from brewer's yeast and dithiothreitol (DTT) (Boehringer Mannheim, Indianapolis, IN); T7 RNA polymerase, T4 RNA ligase, nucleotide triphosphates (NTP's, sodium salts), and DNA synthesis reagents (Pharmacia, Piscataway, NJ); Trizma base, NaOAc, NH₄OAc, NaCl, HEPES (free acid), cacodylic acid (sodium salt), MgCl₂, KCl, bovine serum albumin, spermidine, Triton X-100, EDTA, polyacrylamide, N,N'-methylene-bis-acrylamide, urea, boric acid, and dimethyl sulfoxide (Molecular Biology Grade if available, Sigma, St. Louis, MO); diethylpyrocarbonate (DEPC), dimethyl sulfate

(DMS), hydrazine, sodium borohydride, and aniline (Aldrich, Milwaukee, WI); [γ - ^{32}P]-ATP, [$5'$ - ^{32}P]-pCp, and Nensorb purification columns (NEN/Du Pont, Wilmington, DE).

5S rRNAs: The purified 5S rRNA from *Xenopus* oocytes as well as the 5S rRNA mutants were generously provided by K. M. Hartmann, S. L. Rawlings, and P. W. Huber (Department of Chemistry and Biochemistry, University of Notre Dame, IN).

Synthesis and Purification of a Truncated Fragment of Xenopus Oocyte 5S rRNA (3' Δ 12-5' Δ 64): The oligoribonucleotide (45-mer) based on domain 3 of the *Xenopus* oocyte 5S rRNA (3' Δ 12-5' Δ 64) was synthesized by using T7 RNA polymerase and synthetic DNA templates following the procedure of Milligan et al.²⁹ DNA templates were synthesized on a Pharmacia Gene Assembler using the phosphoramidite method. The DNA templates were purified by the Nensorb preparative purification method³⁰ followed by polyacrylamide gel electrophoresis (8 M denaturing). The purified DNA was stored in 10 mM Tris-HCl, pH 7.0 at -20°C. The DNA templates were freshly annealed by heating the two strands together to 100°C for 10 minutes and slowly cooling over a 6-hour period to +4°C. The following DNA templates were used:

5'- TAATA CGACT CACTA TAG -3'

3'- ATTAT GCTGA GTGAT ATCCG GACCA ATCAT GGACC

TACCC TCTGG CGGAC CCTTA TGGTC CA -5'.

The transcript reaction mixture contained 40 mM Tris-HCl (pH 8.1 at 37°C), 2 mM spermidine, 5 mM dithiothreitol, 50 $\mu\text{g}/\text{mL}$ bovine serum albumin, 0.01% (v/v) Triton X-100, 1 mM NTPs, 6 mM MgCl_2 , 200 nanomoles DNA template, and 30 units/ μL T7 RNA polymerase and was incubated for 2 hours at 37°C. Following the transcription reaction, the synthesized RNA 45-mer was purified by the Nensorb purification method³¹ and stored in 10 mM Tris-HCl, pH 7.5.

Preparation of Labeled Wild-Type and Mutant 5S rRNAs: The RNAs were labeled either at the 3'-end with cytidine 3',5'-[$5'$ - ^{32}P]-bisphosphate using T4 RNA ligase³² or at

the 5'-end with [γ - ^{32}P]-ATP using T4 polynucleotide kinase³³. The radioactive RNAs were gel purified on 15% denaturing polyacrylamide gels, located by autoradiography, excised, and eluted from the gel slices in 45 mM Tris, 45 mM boric acid, and 1.25 mM EDTA, pH 8.0. The eluted RNAs were precipitated twice with ethanol and stored in 10 mM Tris-HCl, pH 7.5.

Cleavage of 5S rRNAs by Rh(phen)₂phi³⁺: Rh(phen)₂phi³⁺ stock solutions were freshly prepared. All end-labeled rRNAs were renatured by heating to 65°C for 10 minutes in 10 mM Tris-HCl, 10 mM MgCl₂, 300 μM KCl, pH 7.5 and slowly cooling to room temperature prior to use. A typical 20 μL reaction mixture contained 50 mM sodium cacodylate, pH 7.0, labeled 5S rRNA, and 10 μM Rh(phen)₂phi³⁺. The final concentration of nucleotides was adjusted to 100 μM by the addition of carrier tRNA. Irradiation for 10 minutes at 365 nm at ambient temperature using a 1000 W Hg/Xe lamp and monochromator yielded site-specific cleavage of the 5S rRNA samples only in the presence of the rhodium complex. The reaction mixtures were precipitated with ethanol and washed several times with 70% ethanol to remove traces of salt before analysis on sequencing gels.

Sequencing Gels: The rhodium cleavage products were analyzed on 15% polyacrylamide gels containing 8 M urea. The full length 5S rRNAs and cleavage products were identified by coelectrophoresing the appropriate chemical-sequencing reactions³⁴ and viewed by autoradiography. Reactions with dimethyl sulfate followed by NaBH₄ treatment, diethylpyrocarbonate, and hydrazine yield specific cleavages at G, A, and U residues, respectively, with 5'- and 3'-phosphate termini. Fragments produced by Rh(phen)₂phi³⁺ cleavage also possess 5'- and 3'-phosphate termini and may therefore be compared directly with the chemical sequencing lanes.

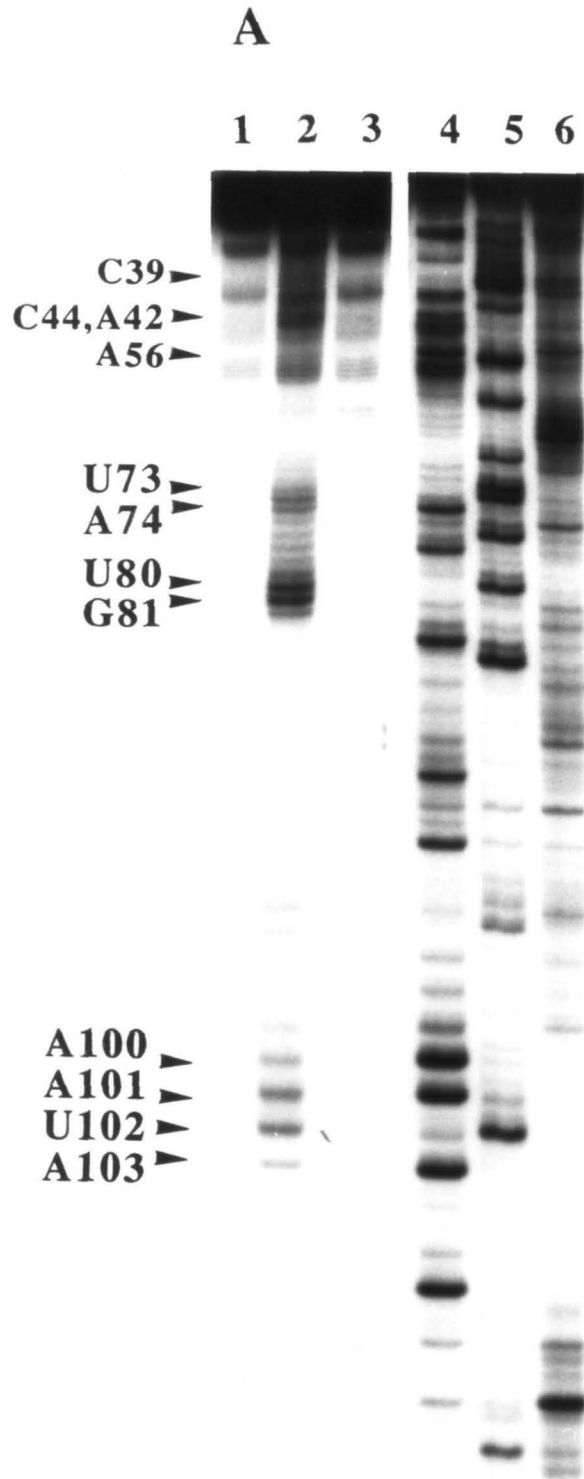
5.3. Results

5.3.1. Site-Selective Cleavage of 5S rRNA by Rh(phen)₂phi³⁺

Cleavage of Xenopus oocyte wild-type 5S rRNA by Rh(phen)₂phi³⁺: The sites of Rh(phen)₂phi³⁺ induced strand scission of wild-type 5S rRNA from *Xenopus* oocytes were determined using 5'- and 3'-end-labeled RNAs. As can be seen in Figure 5.1 (panel A), few and specific sites of cleavage by the rhodium complex are evident on the 3'-end-labeled 5S rRNA. Strong cleavage occurs at residues U73, A74, A101, U102 in the E loop, and U80 and G81 in helix IV; weak cleavage occurs at A100 in loop E and A103 in helix V. In polyacrylamide gels that are further resolved, additional sites are evident at A22 and A56 in the B loop, C29 and A32 in helix III, and C34, C39, A42, and C44 in the C loop. Identical sites of cleavage are observed in experiments conducted with 5'-end-labeled 5S rRNA. Identical sites are also observed in experiments conducted with higher salt (300 mM KCl). Figure 5.2 displays sites of rhodium cleavage on the secondary structure map of *Xenopus* oocyte 5S rRNA.

With the exception of C39, the rhodium cleavage sites occur exclusively at stem-loop junctions, mismatched base pairs, or bulged residues. These results are consistent with cleavage results found earlier on tRNA^{Phe} in which the rhodium complex does not cleave in double-helical regions nor in unstructured single-stranded regions of the RNA. Instead, cleavage on tRNA^{Phe} and tRNA^{Asp} is limited to sites involved in tertiary interactions such as triple-base interactions, stem-loop junctions, or structured loop regions. The rhodium cleavage results on 5S rRNA support the minimal secondary structure model proposed by Luehrsen and Fox⁸, since no cleavage by Rh(phen)₂phi³⁺ is apparent in the proposed double-stranded regions. In addition, since the rhodium complex does not promote strand scission at purely single-stranded regions, the cleavage data suggests that the loop regions of the 5S rRNA must be structured, involving either non-Watson-Crick base pairing within the loops or long-range tertiary interactions between the

Figure 5.1. Cleavage of ^{32}P 3'-end-labeled *Xenopus* oocyte 5S rRNA and a truncated version by $\text{Rh}(\text{phen})_2\text{phi}^{3+}$. (A) Autoradiogram showing cleavage of the full 5S rRNA in 50 mM NaCacodylate, pH 7.0. Lane 1: labeled RNA without metal or irradiation. Lane 2: cleaved RNA after incubation with $\text{Rh}(\text{phen})_2\text{phi}^{3+}$ and irradiation. Lane 3: labeled RNA irradiated in the absence of metal complex. Lanes 4-6: A-, U-, and G-specific reactions, respectively. (B) Autoradiogram showing cleavage of the truncated 5S rRNA (3' Δ 12-5' Δ 64) by $\text{Rh}(\text{phen})_2\text{phi}^{3+}$ in 50 mM NaCacodylate, pH 7.0. Lane 1: labeled RNA without metal or irradiation. Lanes 2 and 3: cleaved RNA after incubation with $\text{Rh}(\text{phen})_2\text{phi}^{3+}$ and irradiation. Lanes 4 and 5: G-specific reaction. Lanes 6 and 7: A- and U-specific reactions, respectively. Major sites of cleavage are marked.



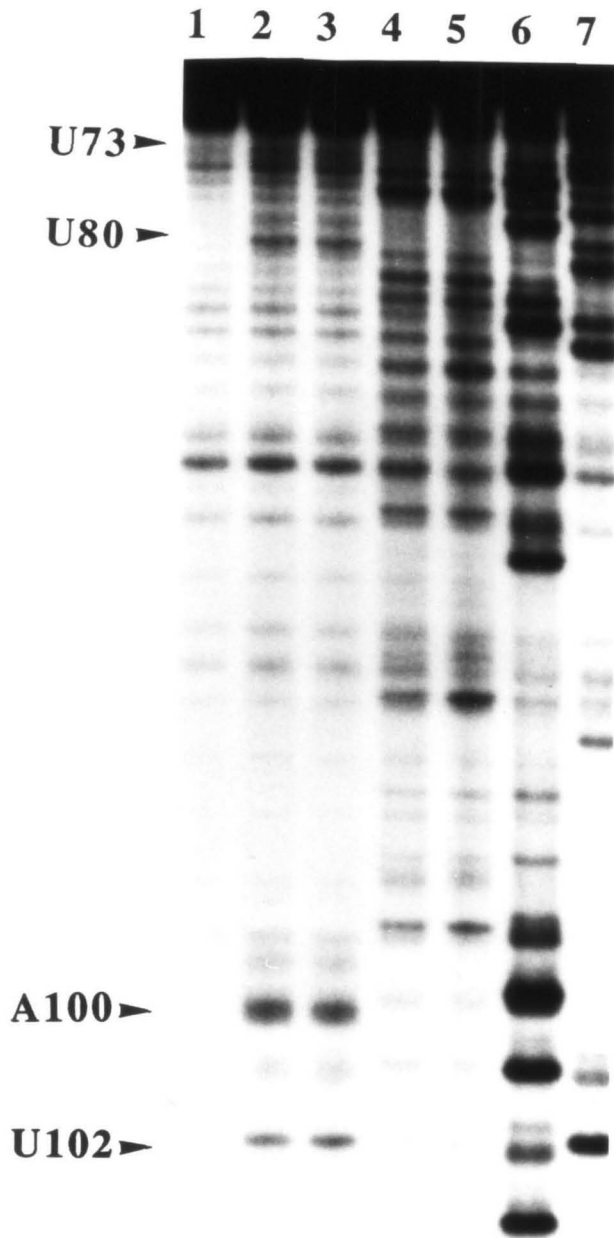
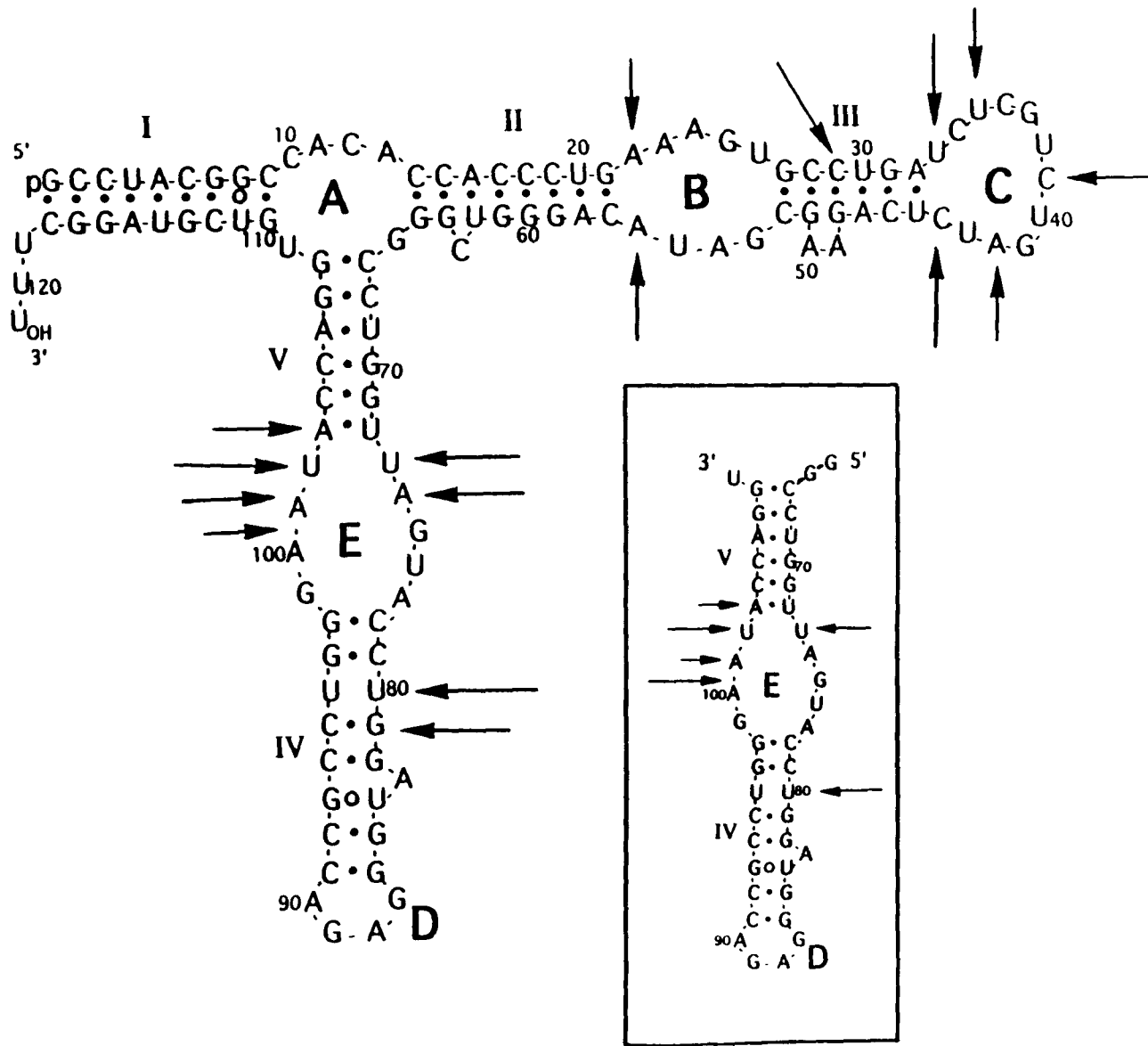
B

Figure 5.2. Schematic illustration of the secondary structure of *Xenopus* 5S rRNA with designations of the sites of cleavage by $\text{Rh}(\text{phen})_2\text{phi}^{3+}$. The arrows indicate the positions of $\text{Rh}(\text{phen})_2\text{phi}^{3+}$ promoted strand scission with length corresponding to relative cleavage intensity. The boxed insert illustrates cleavage on the truncated *Xenopus* oocyte 5S rRNA (3' Δ 12-5' Δ 64) by $\text{Rh}(\text{phen})_2\text{phi}^{3+}$.



loop regions. Cleavage at the U-U mismatch and at the site adjacent to an AA bulge are also suggestive of structures that are different from canonical A-form RNA double helices.

5.3.2. Cleavage of a Truncated Fragment of *Xenopus* Oocyte 5S rRNA (3' Δ 12-5' Δ 64) by Rh(phen)₂phi³⁺

Because several models for the tertiary structure of 5S rRNA include long-range contacts between the two "arms" of the molecule, it became necessary to establish whether such contacts might account for the cleavage pattern obtained with Rh(phen)₂phi³⁺. A smaller fragment of the 5S rRNA (deletion of 5'-residues 1-64 and 3'-residues 110-121), constituting a single "arm" was synthesized (Figure 5.2, insert), and cleavage by the rhodium complex was examined and compared to that on the full 5S rRNA. If Rh(phen)₂phi³⁺ is recognizing long-range tertiary interactions between the loop regions, as in tRNA, then deletion of loops B and C should lead to an altered cleavage by the rhodium complex. Conversely, if loop E has some intrinsic structure that is independent of the rest of the molecule, then the cleavage specificity of the rhodium complex should remain the same.

The truncated RNA fragment corresponding to residues G65 to U109 of the full-length 5S rRNA was synthesized by *in vitro* transcription by T7 RNA polymerase from a synthetic DNA template.²⁹ As shown in Figure 5.1 (panel B), the cleavage pattern for the truncated 5S rRNA is nearly identical to that obtained for wild-type 5S rRNA. Strong cleavage by Rh(phen)₂phi³⁺ on the 3' Δ 12-5' Δ 64 mutant is observed at U80, A100, and U102 with minor cleavage at U73, A74, A101, and A103. Changes in rhodium cleavage at G81, A100, and A101 are evident. Nonetheless, it is clear from these results that despite subtle differences, the same regions on the truncated fragment as on the full 5S rRNA are recognized. The 5S rRNA fragment is likely to adopt the same conformation as the corresponding region in the full-length 5S rRNA. These results are consistent with a

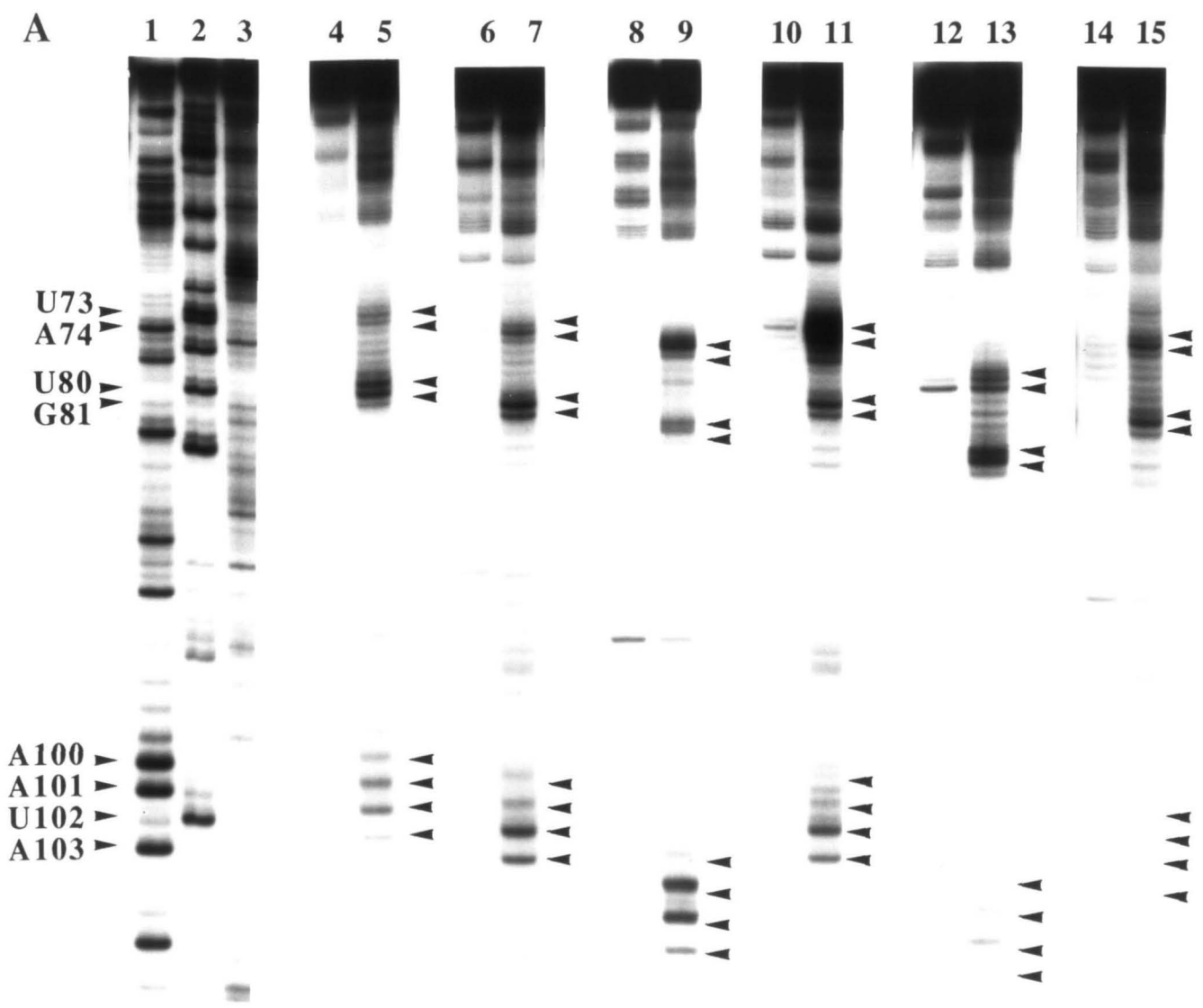
structure for helix IV and loop E, which is independent of the rest of the 5S rRNA molecule.

5.3.3. Cleavage of 5S rRNA Mutants by $\text{Rh}(\text{phen})_2\text{phi}^{3+}$

The preceding results indicate the absence of long-range tertiary interactions in the molecule and suggest instead that cleavage by $\text{Rh}(\text{phen})_2\text{phi}^{3+}$ arises from the recognition of tertiary structures generated more locally by flanking and opposing bases. To confirm the absence of long-range tertiary interactions in the 5S RNA and to probe further the sites recognized by the metal complex, several substitutions at positions in helix IV and loops C and E were made, and their effects on cleavage by $\text{Rh}(\text{phen})_2\text{phi}^{3+}$ were determined. A series of 5S rRNA mutants were prepared by *in vitro* transcription with T7 RNA polymerase by K. M. Hartmann and S. L. Rawlings according to the methods described by Rawlings and Huber.³⁵ The cleavage data given in Figure 5.3, obtained on 3'-end-labeled 5S rRNA, show the effects of mutations on cleavage in loops C and E as well as helix IV. Cleavage data for loops B and C were obtained on 5'-end-labeled RNA (data not shown). The results for all mutations are shown schematically in Figure 5.4 and summarized in Table 5.1.

The substitutions in loop C produce no changes in cleavage by the rhodium complex in loops B and E nor in helices III and IV relative to the cleavage observed on wild-type 5S rRNA. However, there are variations in cleavage by $\text{Rh}(\text{phen})_2\text{phi}^{3+}$ observed within the C loop. The mutation U43A-C44G leads to diminished cleavage in loop C at sites A32 and G44 and complete loss at C34 and C39. Similarly, the mutant A42C exhibits diminished cleavage at C42, with complete loss at C34, C39, and C44, but enhanced cleavage at A32 and an additional cleavage site at C36. Loop E mutants yield no long-range changes in cleavage in loops B or C nor in helices III and IV. The mutation

Figure 5.3. Cleavage of mutants of ^{32}P 3'-end-labeled *Xenopus* oocyte 5S rRNA by $\text{Rh}(\text{phen})_2\text{phi}^{3+}$. Cleavage was performed in 50 mM NaCacodylate, pH 7.0. (A) Effects of mutations on cleavage in the E and C loops. Lanes 1-3: A-, U-, and G-specific reactions on wild-type (WT) 5S rRNA. Lanes 4, 6, 8, 10, 12, and 14: control end-labeled RNAs in the absence of metal and light; WT, U43A-C44G, A100C, A101U, A74C, and A74G, respectively. Lanes 5, 7, 9, 11, 13, and 15: cleavage by $\text{Rh}(\text{phen})_2\text{phi}^{3+}$ of WT, U43A-C44G, A100C, A101U, A74C, and A74G, respectively. Major sites of cleavage are marked. The mutant RNAs were electrophoresed on separate gels next to sequencing lanes, which explains the different mobilities, but are shown here together for comparison. For ease of comparison, only the cleavage lanes and control lanes are shown. (B) Effects of mutations on cleavage in helix IV. Lanes 1, 5, 9, 13, 17, and 21: control end-labeled RNAs without metal or irradiation; ΔA83 , U96A- ΔA83 , U96G- ΔA83 , G18C-C95G, U96A, and WT, respectively. Lanes 2, 6, 10, 14, 18, and 23: specific cleavage by $\text{Rh}(\text{phen})_2\text{phi}^{3+}$ on ΔA83 , U96A- ΔA83 , U96G- ΔA83 , G18C-C95G, U96A, and WT, respectively. Lanes 3, 7, 12, 15, 19, and 24: A-specific reactions on ΔA83 , U96A- ΔA83 , U96G- ΔA83 , G18C-C95G, U96A, and WT, respectively. Lanes 4, 8, 11, 16, 20, and 25: U-specific reactions on ΔA83 , U96A- ΔA83 , U96G- ΔA83 , G18C-C95G, U96A, and WT, respectively. Lane 22: end-labeled WT irradiated in the absence of metal. Major sites of cleavage are marked. Filled circles indicate cleavage in helix IV (U80, G81). These sites have different mobilities for each mutant due to the difference of one nucleotide for the deletion mutants. The open circles indicate the lack of cleavage at the same sites (U80, G81) in helix IV.



B

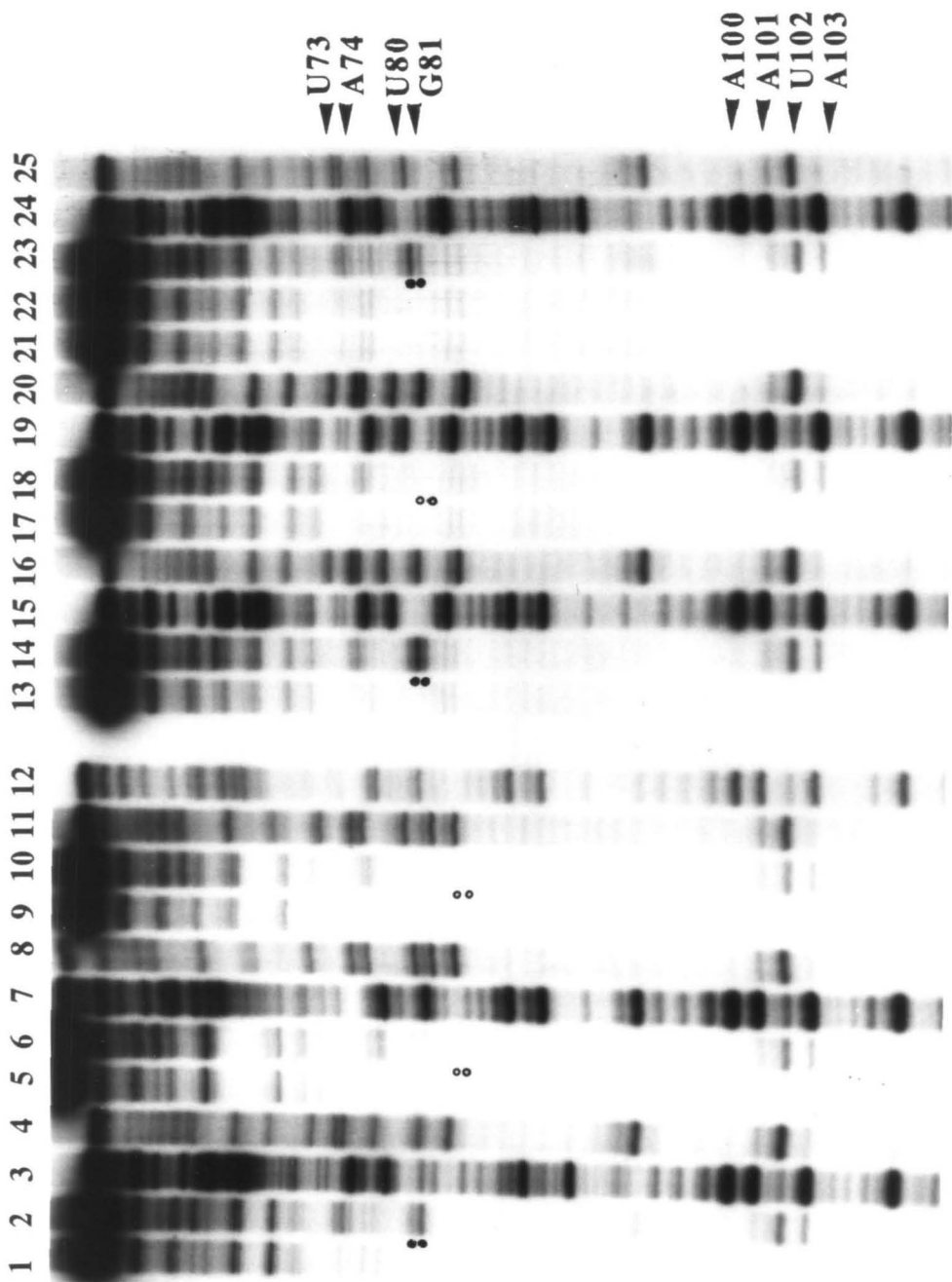


Figure 5.4. Schematic illustrations of $\text{Rh}(\text{phen})_2\text{phi}^{3+}$ cleavage on *Xenopus* 5S rRNA mutants. The arrowheads indicate the positions of strand scission promoted by $\text{Rh}(\text{phen})_2\text{phi}^{3+}$. The cleavage intensity at the marked site is the same as with wild type unless noted by (*). A large (*) indicates that cleavage is enhanced relative to wild type, while a small (*) indicates that cleavage is diminished relative to wild type.

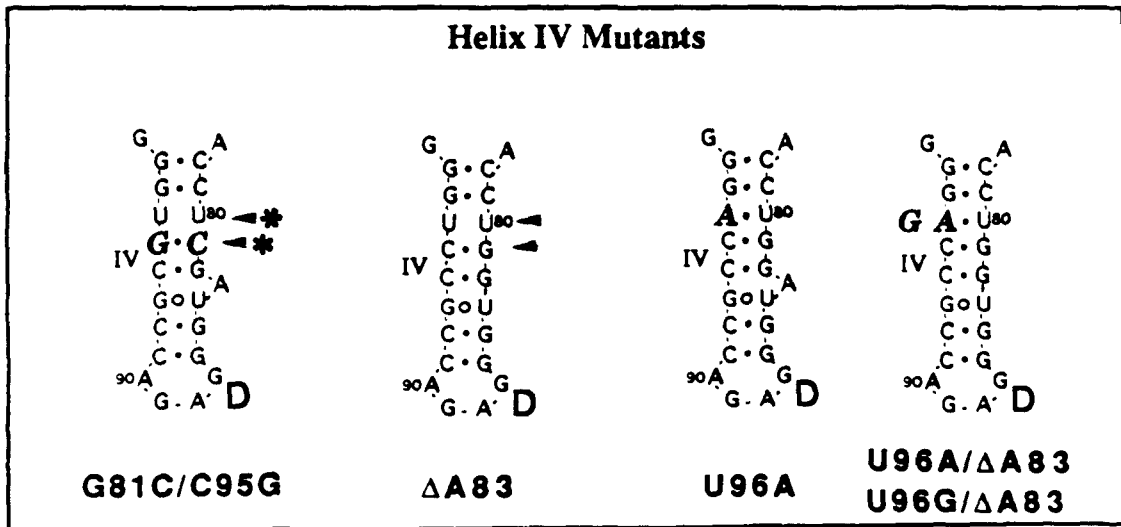
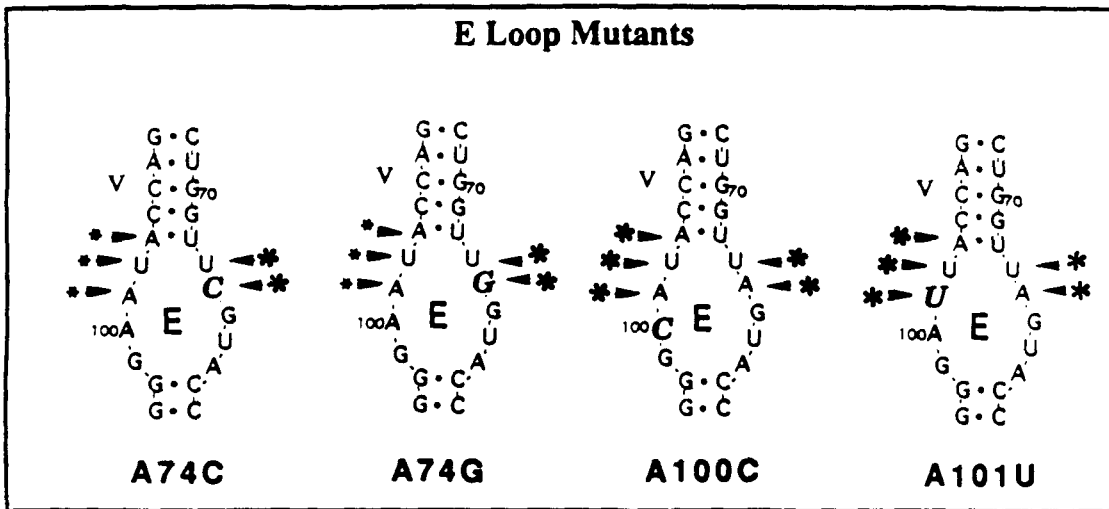
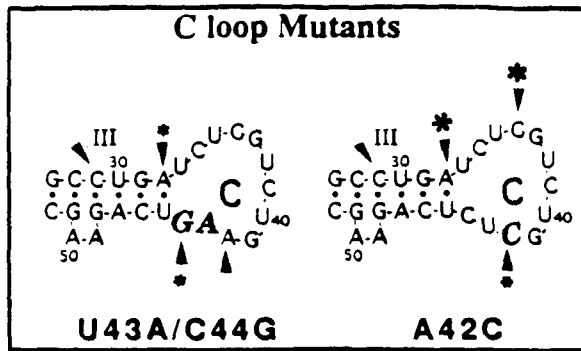


Table 5.1. Cleavage of 5S rRNA Mutants by Rh(phen)₂phi³⁺.

<i>mutant</i>	<i>diminished sites</i> ^a	<i>enhanced sites</i> ^a	<i>no change</i> ^a
U43A-C44G	A32, C34,C39,G44		B loop, E loop, helix IV
A42C	C34, C39, C42, C44	A32, C36	B loop, E loop, helix IV
A100C		A101, U102, A103 U73, A74	B loop, C loop, helix IV
A101U		U101, U102, A103 U73, A74	B loop, C loop, helix IV
A74C	A101, U102, A103	U73, C74	B loop, C loop, helix IV
A74G	A101, U102, A103	U73,G74	B loop, C loop, helix IV
ΔA83			B loop, C loop, E loop, helix IV
U96A	U80, G81		B loop, C loop, E loop
U96G-ΔA83	U80, G81		B loop, C loop, E loop
U96A-ΔA83	U80, G81		B loop, C loop, E loop
G81C-C95G		U80, G81	B loop, C loop, E loop
Δ1-64, Δ110-121			E loop, helix IV

^a Cleavage relative to wild type 5S RNA from *Xenopus* oocytes.

A100C exhibits enhanced cleavage at U73, A74, A101, U102, and A103. Similarly, the mutation A101U leads to enhanced cleavage by the rhodium complex at U73, A74, U101, U102, and A103. Mutations made on the 5'-side of the E loop (A74C and A74G) lead to a diminished cleavage on the opposite side of the loop at A101, U102, and A103, but exhibit a concomitant increase in cleavage at U73, adjacent to the site of mutation, as well as residue 74. The changes observed in cleavage by the rhodium complex with mutations in loops E and C of the 5S rRNA establish that the loop regions of the molecule contain intrinsic structures that are recognized by $\text{Rh}(\text{phen})_2\text{phi}^{3+}$. These data indicate that no long-range interactions exist between loops C and E and helix IV.

Lastly, the introduction of mutations in helix IV leads to alterations in cleavage by $\text{Rh}(\text{phen})_2\text{phi}^{3+}$, which are restricted to helix IV. No changes in rhodium cleavage are observed in the loop regions or in helix III for these mutants. Inspection of the secondary structure map for the wild type 5S rRNA would suggest that cleavage by the rhodium complex at U80 and G81 of helix IV might arise owing to a structural deformation in the helix caused by the bulged nucleotide at position 83 and/or the U-U mismatch. A deletion of the bulged residue A83 results in a cleavage pattern for the rhodium complex, which is identical at all sites to that found on the wild type 5S rRNA. In contrast, if the U-U mismatch is changed to an A-U Watson-Crick base pair, cleavage is no longer observed at either U80 or G81. If the U-U mismatch is changed to either a G-U mismatch or an A-U base pair with the deletion of A83, no cleavage is evident at U80 or G81. Interestingly, if the neighboring C95-G81 base pair is switched to a G95-C81 base pair, cleavage at U80 and C81 is enhanced compared to the wild type 5S rRNA cleavage. These results indicate that the U-U mismatch rather than the bulged A residue leads to the structural distortion recognized by the rhodium complex. In addition, the flanking C-G base pair has an effect on the specific structure that is recognized; the change in cleavage intensity at the U-U

mismatch seen by inverting the flanking base pair may reflect subtle modifications in the nucleotide stacking interactions.

5.4. Discussion

5.4.1. Recognition Characteristics of Rh(phen)₂phi³⁺: Support of the Y-Shape Structure

The reaction of Rh(phen)₂phi³⁺ with *Xenopus* oocyte 5S rRNA does not occur at double-helical regions of the molecule nor within purely single-stranded regions or canonical stem structures. Instead, cleavage by the rhodium complex on 5S rRNA is apparent in loop regions, stem-loop junctions, base-pair mismatches, and bulged residues. These results may be understood on the basis of the DNA recognition characteristics of Rh(phen)₂phi³⁺.²⁷⁻²⁸ Since the rhodium complex interacts in the major groove of DNA by intercalation, stacking by the complex in the deep and narrow major groove of double-helical RNA is not expected, given the steric considerations. The complex could stack easily, however, at sites that are more opened in the major groove. As discussed in Chapter 4, it has been found that Rh(phen)₂phi³⁺ cleaves preferentially at regions of tertiary interactions in crystallographically characterized tRNAs; these regions of the tRNA are structured so as to provide a major groove that is open and accessible to stacking by the metal complex. Cleavage by Rh(phen)₂phi³⁺ on 5S rRNA appears to be consistent with the sites of cleavage found earlier on tRNA. However, the sites which are recognized on 5S rRNA do not appear to be involved in long-range tertiary folding. Instead, the sites recognized on *Xenopus* oocyte 5S rRNA represent several families of localized tertiary interactions, including stem-loop junctions, structured loops, and sites with mismatched bases.

We have examined cleavage on a series of 5S rRNA mutants and a truncated 5S rRNA in order to test the involvement of the cleaved regions in long-range tertiary

interactions; such recognition by the rhodium complex was found to be important on tRNA as shown in Chapter 4. These data, summarized in Figures 5.2 and 5.4 as well as Table 5.1, indicate that the domains of the *Xenopus* oocyte 5S rRNA are independently organized. Mutations in either the loop regions or helical region affect the structure near the site of substitution, but there are no long-range effects found at distant positions. In addition, the cleavage pattern on the truncated 5S rRNA (3' Δ 12-5' Δ 64) is nearly identical to that of the native molecule in loop E and helix IV. Our data support the Y-model structure proposed by Westhof et al.¹⁹, in which the 5S rRNA is made up of three independent structural domains.

5.4.2. Loop Structures in 5S rRNA

Cleavage of 5S rRNA by Rh(phen)₂phi³⁺ occurs at the junctions between loop E and helix V, loop B and helix II, and loop C and helix III. Similarly, we have observed cleavage by the rhodium complex at the anticodon stem-loop region of tRNA^{Phe} and tRNA^{Asp} from yeast. The crystal structures of the two tRNAs reveal that the anticodon stem-loop regions are single-stranded, yet the bases in the loop continue stacking in an A-like helical manner.³⁶⁻³⁸ The major groove of these regions is opened because of the absence of base-pair hydrogen bonds. A broadening of the major groove at analogous stem-loop junctions in the 5S rRNA would facilitate interactions with the rhodium complex.

Westhof and coworkers¹⁹ have proposed noncanonical base pairing of the types A-A, U-U, and A-G in the internal E loop. However, the NMR data is inconsistent with structures of loop E containing the proposed A-G mismatched base pairs.³⁹ Instead, the NMR structure revealed that extensive stacking occurs in loop E and to some extent at the stem-loop junction. We have shown that mutations on one side of the stem-loop structure can alter cleavage by Rh(phen)₂phi³⁺ on the opposite strand of the loop. For example, the

mutations A74C and A74G lead to changes in cleavage at residues A101, U102, and A103 and the mutations A100C or A101U lead to changes at residues U73 and A74. These results suggest that the internal E loop contains an intrinsic structure in which the two strands of the E loop interact in an intimate fashion. This interaction may be due either to unusual base pairing or to the stacking of the nucleotides following the helical structure of the stem.

Mutations in loop C show similar effects as the loop E mutations. The double mutation U43A-C44G leads to a loss in cleavage by $\text{Rh}(\text{phen})_2\text{phi}^{3+}$ at C39 and C34, and diminished cleavage at A32 and G44. The mutation A42C leads to even more significant changes in loop C cleavage at residues A32, C34, C36, C39, and C44. These data are consistent with an intrinsic structure for loop C, which favors interaction with the rhodium complex. Mutations in loop C seem to have significant effects on the folding of the C loop and subsequent recognition by $\text{Rh}(\text{phen})_2\text{phi}^{3+}$. It is likely, based on cleavage by $\text{Rh}(\text{phen})_2\text{phi}^{3+}$ in the tRNA anticodon stem-loop junction, that these stem-loop regions of the 5S rRNA have opened major grooves and stacked structures in the single-stranded regions that are recognized by the metal complex.

5.4.3. Helix Structures in 5S rRNA

Cleavage by $\text{Rh}(\text{phen})_2\text{phi}^{3+}$ does not occur in the canonical helical regions of the 5S rRNA, but rather at regions that display unusual base pairing or multiple bulged residues. On the basis of chemical modification and enzymatic degradation, there is a bulge in helix III with two A residues. Interestingly, Weeks and Crothers²⁶ have proposed that bulges of two or three U residues (but not one) widen the RNA major groove significantly. Similarly, the bulged AA residues in the 5S rRNA may cause an opening of the major groove of helix III and therefore may facilitate stacking interactions with $\text{Rh}(\text{phen})_2\text{phi}^{3+}$.

It is also noteworthy that the rhodium complex does not exhibit cleavage at the proposed single-nucleotide bulges at residues A83 and C63.

We have shown that cleavage in helix IV is dependent on the U-U mismatch, but not the bulged A83. The deletion of the bulged residue A83 has no effect on the cleavage in the middle of helix IV at U80 and G81. In contrast, conversion of the mismatch to either an A-U or a G-U base pair leads to a loss in cleavage at both U80 and G81. The rhodium complex does not appear to target G-U mismatches, and we have not yet tested the interactions of $\text{Rh}(\text{phen})_2\text{phi}^{3+}$ with mismatches of the A-A or A-G type. It seems that the structural distortion of the helix created by the U-U mismatch is sufficient to allow interactions with the metal complex. It is noteworthy that structural distortions in the major groove at a U-C mismatch are evident in the crystal structure of an RNA dodecamer.⁴⁰ It is also interesting that cleavage observed by $\text{Rh}(\text{phen})_2\text{phi}^{3+}$ is asymmetric about the U-U mismatch. Although the helix appears to be symmetrical based on sequence composition, the rhodium complex exhibits strong cleavage only on one side of the U-U mismatch. Furthermore, when the flanking G81-C95 base pair is changed to a C81-G95 base pair, cleavage is enhanced at U80 and C81, but still no cleavage is observed on the opposite strand. The flanking sequences must be important in determining how the mismatched U residues interact.

5.4.4. Structural Analysis of the 5S rRNA Loop Region: A Comparison of Chemical Probing and $\text{Rh}(\text{phen})_2\text{phi}^{3+}$ Cleavage

Romaniuk et al.¹¹ and Westhof et al.¹⁹ have used chemical modifications, such as dimethyl sulfate and diethylpyrocarbonate⁴¹, as well as enzymatic probing to examine in detail the specific structures in the loop regions of *Xenopus* oocyte 5S rRNA. The effects of mutations on the structural organizations of loops B and C⁴² and loop E⁴³ have also been considered. In loop B, most of the nucleotides are accessible to chemical modification

and susceptible to enzymatic degradation by single-stranded ribonucleases. The rhodium cleavage data would be consistent with an open, unstacked structure in this loop, which is not targeted by the metal complex, with binding by $\text{Rh}(\text{phen})_2\text{phi}^{3+}$ being limited instead to the stem-loop junction where stacking is evident.

In contrast, chemical modification studies reveal that loop C contains unreactive pyrimidine residues at U33, C34, U43, and C44. These residues likely stack inside the loop without making any hydrogen bonding contacts. Furthermore, it was proposed that the neighboring residues are base paired by a *trans* Hoogsteen arrangement (U35-A42) and a Watson-Crick arrangement (C36-G41).⁴² $\text{Rh}(\text{phen})_2\text{phi}^{3+}$ may recognize such stacked structures within the C loop. It was shown in Chapter 3 that the rhodium complex promotes strand scission in the TΨC loop of tRNA, in which residues are intimately stacked. Changes in rhodium cleavage associated with the mutant U43A-C44G may be a result of changes in stacking of the purine residues (A43 and G44) inside the loop, since purines would stack differently than pyrimidines. Differences in cleavage in the C-loop region for the mutant A42C may result from a loss of the proposed A42-U35 base pair which could also be important for maintaining stacking of the neighboring pyrimidine residues. The fact that the rhodium complex still cleaves in loop C of mutant A42C, however, would suggest that the C loop is intrinsically structured. It is interesting to note that cleavage by $\text{Rh}(\text{phen})_2\text{phi}^{3+}$ is symmetric about a structure represented as a helix

³¹GAUCUC with mismatched pyrimidine bases and with recognition by $\text{Rh}(\text{phen})_2\text{phi}^{3+}$
CUCUAG⁴¹

at its center.

Chemical modification studies have shown that the E loop is highly structured through noncanonical hydrogen bonding interactions. As seen in the C loop, mutants that destroy the potential for hydrogen bonding in the E loop result in an increased reactivity to probes for chemical accessibility at residues 74 to 77 and 99 to 102 at both the Watson-

Crick and the N-7 positions.⁴³ In this study we have considered only single-nucleotide mutations which can alter the proposed base pairs in loop E. Mutants A74C and A74G, which should disrupt the noncanonical base pairs in loop E, show only slight enhancements in cleavage at U73 by $\text{Rh}(\text{phen})_2\text{phi}^{3+}$ and diminished cleavage at residues 101 to 103 on the opposite strand. The overall patterns of cleavage by $\text{Rh}(\text{phen})_2\text{phi}^{3+}$ are the same for both of these mutants. Similarly, the mutations A100C and A101U should alter the proposed base-pairing schemes and cause structural deviations within the loop. However, the overall rhodium cleavage patterns are identical for these mutants, with enhancements in the cleavage intensities compared to cleavage on wild-type 5S rRNA. It seems that the stacking interactions in the loop are again more important than the hydrogen bonding capabilities with respect to interaction with the metal complex. The proposed structure for loop E in wild-type 5S rRNA shows only slight distortions from an A-form helix.¹⁹ However, we have shown previously that the metal complex cannot interact in the deep and narrow groove of an A-form double helix. Given the recognition characteristics of $\text{Rh}(\text{phen})_2\text{phi}^{3+}$, we would propose that loop E has a significantly more open structure than an A-form helix in which the bases are stacked, but not closely associated by hydrogen bonding. Mutations on one side of the stem-loop structure which alter cleavage by $\text{Rh}(\text{phen})_2\text{phi}^{3+}$ on the opposite side demonstrate that even in the absence of base pair hydrogen bonds, the structure of the loop is determined by the close interaction of bases that are opposite one another. This could be a result of continued stacking from the helical regions of the molecule.

Given the data described here and elsewhere, some general conclusions can be made about the structures in the loop regions. All the results support the notion that these regions contain unusual structures that are not purely double-helical nor single-stranded. Loops C and E of the wild-type 5S rRNA are resistant to both single-strand specific and double-strand specific nucleases.^{42,43} In addition, chemical modification studies reveal

that the bases in loops E and C are inaccessible to chemical probing. This lack of reactivity could be the result of unusual hydrogen bonding or close stacking in the strands that makes the bases inaccessible to solvent. Similarly, $\text{Rh}(\text{phen})_2\text{phi}^{3+}$ exhibits strong cleavage in the loop regions of 5S rRNA. These data indicate that within both loops C and E the strands constituting each loop are not independent of one another but are intimately and intrinsically structured, either by non-canonical base pairing or by the stacking of the bases. Further studies are necessary to determine the exact structures of these regions.

5.4.5. Implications for Protein Binding to 5S rRNA

$\text{Rh}(\text{phen})_2\text{phi}^{3+}$ targets unique sites on 5S rRNA, which are neither double-helical nor single-stranded. Our results indicate that the rhodium complex binds preferentially to regions of the molecule containing more complex tertiary structure in which the major groove has become open and accessible. A broadening of the major groove at stem-loop junctions facilitates interaction with the metal complex. Similarly, multiple bulged nucleotides and base-pair mismatches in the helical regions appear to cause a widening of the major groove, which better accommodates the rhodium complex.

This specific targeting of open, structured major grooves may correlate with site-recognition by proteins that bind 5S rRNA. Recent studies have suggested that structural variations in the major groove of the RNA may be critical in making contacts with protein.^{25,26} A recent crystal structure has revealed that yeast aspartyl-tRNA synthetase interacts with the end of the acceptor stem and at the anticodon stem-loop junction of tRNA^{Asp} in the major groove;²⁵ this major groove interaction is made possible by the increased accessibility of the bases in a helix-loop junction. Similarly, a model for RNA-protein recognition developed by Weeks and Crothers²⁶ involves the distortion of an A-form helix by bulged nucleotides, which permits protein binding in the opened major groove of the RNA.

Interestingly, regions of the 5S rRNA that are recognized by $\text{Rh(phen)}_2\text{phi}^{3+}$ appear to be critical for binding by the *Xenopus* transcription factor IIIA. TFIIIA binds to 5Ss rRNA to form a ribonucleoprotein particle that stabilizes the nucleic acid until it is required for ribosome assembly.^{5,6} Mutagenesis experiments reveal that specificity in binding by the factor is conferred by several independent interactions dispersed over the RNA binding site that depend upon the higher-order structure of the nucleic acid.^{35,44-48} Nuclease and chemical protection experiments¹⁰ as well as hydroxyl radical footprinting,⁴⁶ have revealed that a substantial portion of the RNA molecule interacts with TFIIIA with close association between the factor and the arm of the RNA composed of helix IV-loop E-helix V. It appears that the junctions between the helical stems and internal loops of 5S rRNA provide the primary binding sites for TFIIIA. Missing nucleoside experiments have been performed in which the RNA is modified by Fe(EDTA)^{2-} and is allowed to exchange with TFIIIA.⁴⁶ After separation of the bound and unbound RNA's, it was revealed that missing nucleoside positions enriched in the unbound fraction of RNA are located in the two strands that comprise loop E. Thus, these results have established that the strands of loop E constitute an important recognition site for TFIIIA.⁴⁶ At this time it is not clear if the sequence-dependent association of TFIIIA with loop E is a result of specific contacts between the factor and the RNA bases or if local tertiary structures are important for interaction with the protein. Nonetheless, an interesting correlation is evident between the regions targeted by $\text{Rh(phen)}_2\text{phi}^{3+}$ and the determinants for recognition by TFIIIA, particularly in helix IV and loop E. The opened structures in the major groove that are recognized by $\text{Rh(phen)}_2\text{phi}^{3+}$ may be important for specific binding by the protein. It is noteworthy in this context that on the 5S rRNA gene, $\text{Rh(phen)}_2\text{phi}^{3+}$ appears to mark sites of binding of the individual fingers of TFIIIA.⁴⁹ Overall, $\text{Rh(phen)}_2\text{phi}^{3+}$ may be generally useful in marking potential sites for protein recognition in the major groove of RNA as well as offering structural information regarding the tertiary folding of the RNA.

References

1. Sakonju, S.; Bogenhagen, D. F.; Brown, D. D. *Cell* **1990**, 19, 13-25.
2. Sakonju, S.; Brown, D. D.; Engelke, D.; Ng, S.-Y.; Shastry, B. S.; Roeder, R. G. *Cell* **1981**, 23, 665-669.
3. Bogenhagen, D. F.; Sakonju, S.; Brown, D. D. *Cell* **1980**, 19, 27-35.
4. Engelke, D. R.; Ng, S.-Y.; Shastry, B. S.; Roeder, R. G. *Cell* **1990**, 19, 717-728.
5. Picard, B.; Wegnez, M. *Proc. Natl. Acad. Sci. U.S.A.* **1979**, 76, 241-245.
6. Pelham, H. R. B.; Brown, D. D. *Proc. Natl. Acad. Sci. U.S.A.* **1980**, 77, 4170-4174.
7. Fox, G. E.; Woese, C. R. *Nature* **1975**, 256, 505-506.
8. Luehrsen, K. R.; Fox, G. E. *Proc. Natl. Acad. Sci. U.S.A.* **1981**, 78, 2150-2154.
9. Andersen, J.; Delihias, N.; Hanas, J. S.; Wu, C.-W. *Biochemistry* **1984**, 23, 5752-5759.
10. Christiansen, J.; Brown, R. S.; Sproat, B. S.; Garrett, R. A. *EMBO J.* **1987**, 6, 453-460.
11. Romaniuk, P. J.; Leal de Stevenson, I.; Ehresmann, C.; Romby, P.; Ehresmann, B. *Nucleic Acids Res.* **1988**, 16, 2295-2312.
12. Böhm, S.; Fabian, H.; Venyaminov, S. Y.; Matveev, S. V.; Lucius, H.; Welfle, H.; Filimonov, V. V. *FEBS Lett.* **1981**, 132, 357-361.
13. Hancock, J.; Wagner, R. *Nucleic Acids Res.* **1982**, 10, 1257-1269.
14. Pieler, T.; Erdmann, V. A. *Proc. Natl. Acad. Sci. U.S.A.* **1982**, 79, 4599-4603.
15. Nazar, R. N. *J. Biol. Chem.* **1991**, 266, 4562-4567.
16. Göringer, H. U.; Wagner, R. *Nucleic Acids Res.* **1986**, 14, 7473-7485.

17. Kao, T. H.; Crothers, D. M. *Proc. Natl. Acad. Sci. U.S.A.* **1980**, *77*, 3360-3364.
18. Kime, M. J.; Moore, P. B. *Nucleic Acids Res.* **1982**, *10*, 4973-4983.
19. Westhof, E.; Romby, P.; Romaniuk, P. J.; Ebel, J.-P.; Ehresmann, C.; Ehresmann, B. *J. Mol. Biol.* **1989**, *207*, 417-431.
20. Peattie, D. A.; Douthwaite, S.; Garrett, R. A.; Noller, H. F. *Proc. Natl. Acad. Sci. U.S.A.* **1981**, *78*, 7331-7335.
21. Christiansen, J.; Douthwaite, S. R.; Christensen, A.; Garrett, R. A. *EMBO J.* **1985**, *4*, 1019-1024.
22. Mougel, M.; Eyermann, F.; Westhof, E.; Romby, P.; Expert-Bezancon, A.; Ebel, J.-P.; Ehresmann, B.; Ehresmann, C. *J. Mol. Biol.* **1987**, *198*, 91-107.
23. Rould, M. A.; Perona, J. J.; Söll, D.; Steitz, T. *Science* **1989**, *246*, 1135-1142.
24. Calnan, B. J.; Tidor, B.; Biancalana, S.; Hudson, D.; Frankel, A. D. *Science* **1991**, *252*, 1167-1171.
25. Ruff, M.; Krishnaswamy, S.; Boeglin, M.; Poterszman, A.; Mitschler, A.; Podjarny, A.; Rees, B.; Thierry, J. C.; Moras, D. *Science* **1991**, *252*, 1682-1689.
26. Weeks, K. M.; Crothers, D. M. *Cell* **1991**, *66*, 577-588.
27. Pyle, A. M.; Long, E. C.; Barton, J. K. *J. Am. Chem. Soc.* **1989**, *111*, 4520-4522.
28. Pyle, A. M.; Morii, T.; Barton, J. K. *J. Am. Chem. Soc.* **1990**, *112*, 9432-9434.
29. Milligan, J. F.; Groebe, D. R.; Witherell, G. W.; Uhlenbeck, O. C. *Nucleic Acids Res.* **1987**, *15*, 8783-8798.
30. Johnson, B. A.; McClain, S. G.; Doran, E. R.; Tice, G.; Kirsch, M. A. *BioTechniques* **1990**, *8*, 424-429.

31. Johnson, M. T.; Read, B. A.; Monko, A. M.; Pappas, G.; Johnson, B. A. *BioTechniques* **1986**, 4, 64-70.
32. England, T. E.; Uhlenbeck, O. C. *Nature* **1978**, 275, 560-561.
33. Silberklang, M.; Gillum, A. M.; RajBhandary, U. L. *Nucleic Acids Res.* **1977**, 4, 4091-4108.
34. Peattie, D. A. *Proc. Natl. Acad. Sci. U.S.A.* **1979**, 76, 1760-1764.
35. Rawlings, S. L.; Huber, P. W., submitted for publication.
36. Kim, S.-H.; Sussman, J. L.; Suddath, F. L.; Quigley, G. J.; McPherson, A.; Wang, A. H. J.; Seeman, N. C.; Rich, A. *Proc. Natl. Acad. Sci. U.S.A.* **1974**, 71, 4970-4974.
37. Quigley, G. J.; Rich, A. *Science* **1976**, 194, 796-806.
38. Westhof, E.; Dumas, P.; Moras, D. *J. Mol. Biol.* **1985**, 184, 119-145.
39. Varani, G.; Wimberly, B.; Tinoco, I., Jr. *Biochemistry* **1989**, 28, 7760-7772.
40. Holbrook, S. R.; Cheong, C.; Tinoco, I., Jr.; Kim, S.-H. *Nature* **1991**, 353, 579-581.
41. Ehresmann, C.; Baudin, F.; Mougel, M.; Romby, P.; Ebel, J.-P.; Ehresmann, B. *Nucleic Acids Res.* **1987**, 15, 9109-9128.
42. Brunel, C.; Romby, P.; Westhof, E.; Romaniuk, P. J.; Ehresmann, B.; Ehresmann, C. *J. Mol. Biol.* **1990**, 215, 103-111.
43. Leal de Stevenson, I.; Romby, P.; Baudin, F.; Brunel, C.; Westhof, E.; Ehresmann, C.; Ehresmann, B.; Romaniuk, P. J. *J. Mol. Biol.* **1991**, 219, 243-255.
44. Huber, P. W.; Wool, I. G. *Proc. Natl. Acad. Sci. U.S.A.* **1986**, 83, 1593-1599.
45. Timmins, P. A.; Langowski, J.; Brown, R. S. *Nucleic Acids Res.* **1988**, 16, 8633-8644.
46. Darsillo, P.; Huber, P. W. *J. Biol. Chem.* **1991**, 266, 21075-21082.

47. Romby, P.; Baudin, F.; Brunel, C.; Leal de Stevenson, I.; Westhof, E.;
Romaniuk, P. J.; Ehresmann, C.; Ehresmann, B. *Biochimie* **1990**, 72, 437-452.
48. You, Q.; Veldhoen, N.; Baudin, F.; Romaniuk, P. J. *Biochemistry* **1991**, 30,
2495-2500.
49. Huber, P. W.; Morii, T.; Mei, H.-Y.; Barton, J. K. *Proc. Natl. Acad. Sci.*
U.S.A., in press.

Chapter 6:

Recognition of Unusual RNA Structures by $\text{Rh}(\text{DIP})_3^{3+}$

6.1. Introduction

The occurrence of the noncomplementary G-U base pair was initially envisioned by Crick in his wobble hypothesis¹ for RNA codon-anticodon interactions and was later confirmed after the three-dimensional x-ray structure²⁻³ for yeast tRNA^{Phe} was solved. A single G-U wobble pair occurs in the amino acid acceptor stem of tRNA^{Phe}. Similarly, the elucidation of the crystal structure of yeast tRNA^{Asp} revealed the existence of one G-Ψ and three G-U base pairs in three of its four helical stems.⁴ Both of the tRNA crystal structures show that the G-U pair has features that distinguish it from the regular Watson-Crick base pairs, C-G and U-A. Upon examination of the tRNA crystal data, Mizuno and Sundaralingam⁵ noticed that the geometry of the G-U wobble pair results in unusual stacking of its bases with the neighboring bases. Interestingly, two independent groups have discovered that a single G3-U70 base pair within the amino acid acceptor helix is a major determinant of the identity of tRNA^{Ala}.⁶⁻⁹ Thus the presence of G-U base pairs at conserved positions in RNA molecules suggests that these mismatches may play a defined structural or functional role.

In our studies on the photocleavage of RNA with transition metal complexes (Chapter 3), we discovered that cleavage by tris(4,7-diphenyl-1,10-phenanthroline) rhodium(III) $\{\text{Rh}(\text{DIP})_3^{3+}\}$ (Figure 6.1) is extremely site-selective. In particular, two distinct sites of cleavage are observed on yeast tRNA^{Phe}. One of these sites, Ψ55, is also recognized by other related transition metal complexes and is marked by tertiary interactions between the D and TΨC loops. The second strong cleavage site occurs at C70. Interestingly, this residue lies to the 3'-side of U69, which is involved in a mismatched base pair with G4. No other reagent targets the C70 site on tRNA^{Phe} with such high

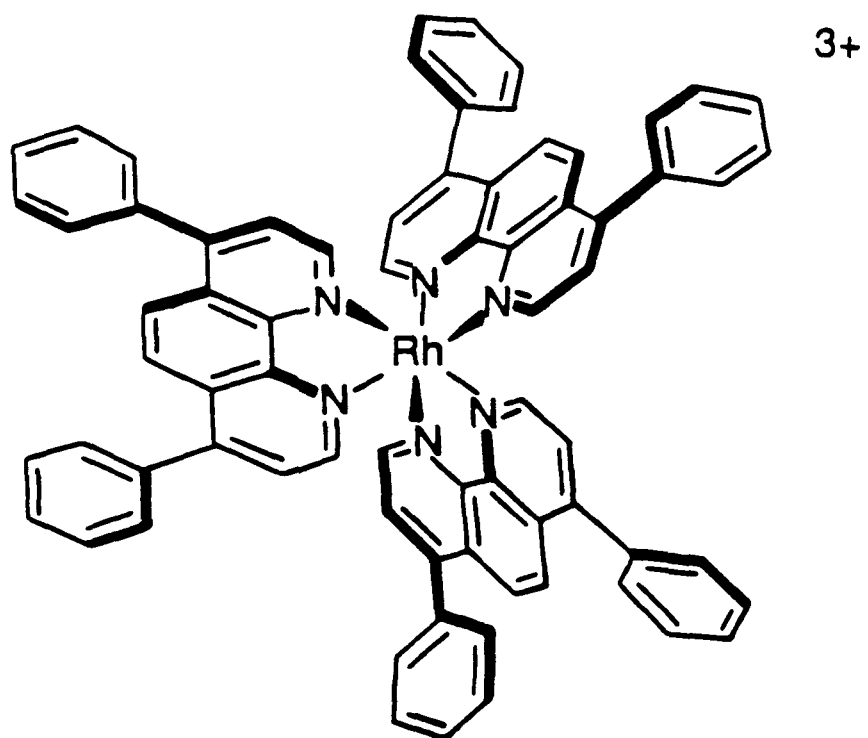


Figure 6.1. Schematic illustration of $\text{Rh}(\text{DIP})_3^{3+}$.

selectivity. It was unclear whether recognition of this site by the rhodium complex was particular to yeast tRNA^{Phe} or if recognition of G-U mismatches was a general feature of Rh(DIP)₃³⁺.

We have tested cleavage by Rh(DIP)₃³⁺ on a series of RNAs that contain G-U mismatches. In particular, we have examined cleavage by the rhodium complex on yeast tRNA^{Asp}, as well as on 5S rRNAs from *Xenopus* oocytes and *E. coli* with proposed G-U mismatches in helices I, II, and IV. In addition, a "microhelix" was synthesized, which consisted of seven base pairs of the acceptor stem of yeast tRNA^{Phe} connected by a six nucleotide loop. This microhelix contained a G-U mismatch involving residues G4 and U69. A U4:G69 variant of this sequence was also constructed. The goals of this work have been to delineate the specificity of Rh(DIP)₃³⁺ cleavage and attempt to correlate this specificity with the biological function of RNA.

6.2. Experimental

Materials: The reagents used in this study were obtained from the following suppliers: T4 RNA ligase (Pharmacia, Piscataway, NJ); Trizma base, NaOAc, NH₄OAc, NaCl, HEPES (free acid), MgCl₂, KCl, EDTA, polyacrylamide, N,N'-methylene-bis-acrylamide, urea, boric acid, and dimethyl sulfoxide (Molecular Biology Grade if available, Sigma, St. Louis, MO); dithiothreitol (DTT) (Boehringer Mannheim, Indianapolis, IN); solid supports and 5'-monomethoxytritylated 2'-silylated ribonucleoside phosphoramidites (BioGenex/ABN, San Ramon, CA); oligonucleotide purification cartridges (OPC) (Applied Biosystem, Inc., Foster City, CA); 1.0 M solution of tetrabutylammoniumfluoride in tetrahydrofuran (TBAF/THF), diethylpyrocarbonate (DEPC), dimethyl sulfate (DMS), hydrazine, sodium borohydride, and aniline (Aldrich, Milwaukee, WI); [γ -³²P]-ATP and [5'-³²P]-pCp (NEN/Du Pont, Wilmington, DE).

RNAs: tRNA^{Phe} from brewer's yeast was obtained from Boehringer Mannheim (Indianapolis, IN); tRNA^{Asp} from yeast was a gift from D. Moras (Institut de Biologie Moleculaire et Cellulaire du CNRS, Strasbourg, France); purified 5S rRNAs from *Xenopus* oocytes and *E. coli* were generously provided by P. W. Huber (Department of Chemistry and Biochemistry, University of Notre Dame, IN). The oligoribonucleotides (24-mers) were chemically synthesized on an Applied Biosystems 392 DNA/RNA Synthesizer using the phosphoramidite method.¹⁰ The oligoribonucleotides were deprotected with 1 mL of concentrated NH₄OH/95% EtOH (3/1) for 8 hours which was removed in a Speed-Vac evaporator. The resulting residues were treated with 0.5 mL of 1.0 M TBAF/THF for 5 hours. After concentrating in a Speed-Vac evaporator, the resulting oily brown residues were purified by the OPC desalting method (ABI) followed by polyacrylamide gel electrophoresis (12%, nondenaturing). To 10 OD units of RNA were added 20 µL of 10 mM Tris-HCl, pH 7.5 and 10 µL loading buffer containing TBE buffer (90 mM Tris, 90 mM boric acid, and 2.5 mM EDTA, pH 8.0) and 0.025% (w/v) each xylene cyanol and bromophenol blue, and the total 30 µL samples were loaded into single lanes on the polyacrylamide gel. Following electrophoresis, the gels were UV-shadowed using a fluorescent TLC plate. Once the presence of the desired sequences was established according to the electrophoretic mobility, the RNAs were excised and eluted from the gel in 45 mM Tris, 45 mM boric acid, and 1.25 mM EDTA, pH 8.0. The purified RNAs were stored in 10 mM Tris-HCl, pH 7.5 at -20°C.

Yeast tRNA^{Phe}, yeast tRNA^{Asp}, *Xenopus* oocyte 5S rRNA, *E. coli* 5S rRNA, and the synthetic oligoribonucleotides were 3'-end labeled with [5'-³²P]pCp and T4 RNA ligase (tRNAs and oligoribonucleotides were incubated on ice for 2.5 hours, 5S rRNAs were incubated on ice for 4 hours).¹¹ The labeled RNAs were gel purified on a 20% denaturing polyacrylamide gel (40 cm long, 0.8 mm thick), located by autoradiography, excised, and eluted from the gel in 45 mM Tris, 45 mM boric acid, and 1.25 mM EDTA,

pH 8.0. The eluted RNAs were precipitated twice with ethanol and stored in 10 mM Tris-HCl, pH 7.5.

Cleavage Reactions: [Rh(DIP)₃]Cl₃ was a gift from M. R. Kirshenbaum in our laboratory. Rh(DIP)₃³⁺ stock solutions were freshly prepared. The end-labeled tRNAs and oligoribonucleotides were renatured by heating to 70°C for 10 minutes in 10 mM Tris-HCl, pH 7.5 and slowly cooling to room temperature prior to use. Similarly, the end-labeled 5S rRNAs were renatured by heating to 65°C for 10 minutes in 10 mM Tris-HCl, 10 mM MgCl₂, 300 mM KCl, pH 7.5 and slowly cooling to room temperature. The 20 μL cleavage mixtures contained labeled RNA, 2.5 μM Rh(DIP)₃³⁺, Tris-HCl buffer (5 mM Tris, 50 mM NaCl, pH 7.0), and were brought to a final concentration of 100 μM in nucleotides with carrier tRNA^{Phe}. Irradiation for 6 minutes at 313 nm at ambient temperature using a 1000 W Hg/Xe lamp and monochromator yielded site-specific cleavage of the RNA samples only in the presence of the rhodium complex. The reaction mixtures were precipitated with ethanol, washed at least three times with 70% ethanol to remove buffer salts, and analyzed on 20% polyacrylamide 8 M urea gels. To test for authenticity, the synthetic RNAs were degraded by alkaline hydrolysis in 0.05M Na₂CO₃ in which the samples were heated to 90°C for 5 minutes and quickly chilled on ice. An equivalent amount of loading dye was then added and a small portion of the reaction mixture was loaded on the gel. The full-length RNAs and cleavage products were identified by coelectrophoresing with diethylpyrocarbonate (DEPC) (A-specific), dimethylsulfate (DMS) (G-specific), and hydrazine (U-specific) reactions¹² and viewed by autoradiography.

6.3. Results

6.3.1. Site-Selective Cleavage of Native tRNAs by $\text{Rh}(\text{DIP})_3^{3+}$

Cleavage of yeast tRNA^{Phe}: The sites of $\text{Rh}(\text{DIP})_3^{3+}$ induced strand scission of yeast tRNA^{Phe} were determined using 3'-end-labeled RNA. As can be seen in Figure 6.2. (lane 7), two specific sites of cleavage by the rhodium complex are evident. Strong cleavage occurs at residues $\Psi 55$ and C70. Identical sites of cleavage were observed in experiments conducted on 5'-end-labeled RNA. As discussed in Chapter 3, cleavage at $\Psi 55$ resembles the DNA cleavage observed by $\text{Rh}(\text{DIP})_3^{3+}$ on DNA cruciforms¹³, while cleavage at C70 is adjacent to a G-U mismatch on the 3'-side of U. The site at $\Psi 55$ is also cleaved by the complexes $\text{Ru}(\text{phen})_3^{2+}$, $\text{Rh}(\text{phen})_2\text{phi}^{3+}$, and $\text{Rh}(\text{phi})_2\text{bpy}^{3+}$, all of which may intercalate. Cleavage at C70 seems to depend on the neighboring G-U wobble pair, which causes structural distortions in the secondary structure of the acceptor stem of tRNA.²⁻³

Cleavage of yeast tRNA^{Asp}: The sites of $\text{Rh}(\text{DIP})_3^{3+}$ cleavage on yeast tRNA^{Asp} were determined on 3'-end-labeled RNA. In contrast to tRNA^{Phe}, Figure 6.2 (lane 22) reveals only weak cleavage by the rhodium complex on tRNA^{Asp} at residues G41 in the anticodon stem and G34 in the anticodon loop. No additional sites were revealed when 5'-end-labeled RNAs were employed for cleavage by $\text{Rh}(\text{DIP})_3^{3+}$. Cleavage induced by $\text{Rh}(\text{DIP})_3^{3+}$ at G34 may be related to cleavage by $\text{Rh}(\text{phen})_2\text{phi}^{3+}$ at $\Psi 32$ in the anticodon loop of this tRNA. As revealed by the crystal structure⁴, the anticodon loop in tRNA^{Asp} is single-stranded, yet structured through continued stacking interactions with the anticodon stem. The stacked residues in the anticodon loop may provide a favorable structure for interaction with both rhodium complexes. Cleavage at residue G41 is adjacent to a G-U mismatch. As with the C70 cleavage site on tRNA^{Phe}, G41 lies to the 3'-side of the wobble-paired U residue. Apparently, the rhodium complex can recognize a similar

Figure 6.2. Cleavage of ^{32}P 3'-end-labeled yeast tRNA^{Phe}, G4:U69 microhelix^{Phe}, U4:G69 microhelix^{Phe}, and yeast tRNA^{Asp} by Rh(DIP)₃³⁺. Cleavage was performed in 5 mM Tris, 50 mM NaCl, pH 7.0. Lanes 1-4: alkaline hydrolysis of tRNA^{Phe}, G4:U69 microhelix, U4:G69 microhelix, and tRNA^{Asp}, respectively. Lanes 5, 11, 16, and 21: controls without metal or irradiation; tRNA^{Phe}, G4:U69 microhelix, U4:G69 microhelix, and tRNA^{Asp}. Lane 6: light control; tRNA^{Phe} irradiated in the absence of metal. Lanes 7, 12, 17, and 22: specific cleavage by Rh(DIP)₃³⁺ on tRNA^{Phe}, G4:U69 microhelix, U4:G69 microhelix, and tRNA^{Asp}. Lanes 8-10: sequencing reactions on tRNA^{Phe}; A-, U-, and G-specific reactions, respectively. Lanes 13-15: sequencing reactions on G4:U69 microhelix; A-, U-, and G-specific reactions, respectively. Lanes 18-20: sequencing reactions on U4:G69 microhelix; A-, U-, and G-specific reactions, respectively. Lanes 23-25: sequencing reactions on tRNA^{Asp}; A-, U-, and G-specific reactions, respectively. Labels on the gels indicate the major Rh(DIP)₃³⁺ cleavage sites.

distortion, which is created by the G30-U40 mismatch in tRNA^{Asp} and a G4-U69 mismatch in tRNA^{Phe}.

6.3.2. Cleavage of Microhelix RNAs by Rh(DIP)₃³⁺

In order to define further the recognition by Rh(DIP)₃³⁺ and test whether the G4-U69 base pair retains its strong influence on rhodium cleavage in a smaller RNA, we have examined cleavage on synthetic RNAs representing the acceptor stem of tRNA^{Phe}. A "microhelix" was synthesized chemically on a solid support using the phosphoramidite method developed for RNA.¹⁰ This helix consists of the seven base pairs of the acceptor stem of tRNA^{Phe} from yeast, connected by a six-nucleotide loop. In the sequence of the G4:U69 microhelix^{Phe}, the sequence of the loop starts at U8 and continues into the 5'-side of the D-stem, such that C13 is joined to A66 of the acceptor helix. A U4:G69 variant of this microhelix sequence has also been synthesized to see if the directionality of the G-U mismatch is important for recognition by Rh(DIP)₃³⁺.

As shown in Figure 6.2 (lane 12), cleavage by Rh(DIP)₃³⁺ on G4:U69 microhelix^{Phe} is nearly identical to that observed on native tRNA^{Phe}. On 3'-end-labeled RNA, strong cleavage is apparent at C70, with minor cleavage occurring at G10. Once again, cleavage occurs at C70, which lies to the 3'-side of U69, which is wobble-paired with G4. Similarly, strong cleavage on U4:G69 microhelix^{Phe} occurs at A5; minor cleavage is apparent at G10 (Figure 6.2, lane 17). Residue A5 is also adjacent to a G-U mismatch. Consistent with cleavage on tRNA^{Phe}, tRNA^{Asp}, and G4:U69 microhelix^{Phe}, this site lies to the 3'-side of U4, which is wobble-paired with G69. Cleavage by Rh(DIP)₃³⁺ at G10 on both microhelices is consistent with the cleavage at G34 on tRNA^{Asp} in which the single-stranded loops following a helical stem are structured and interact favorably with the metal complex.

6.3.3. Cleavage of 5S rRNAs by $\text{Rh}(\text{DIP})_3^{3+}$

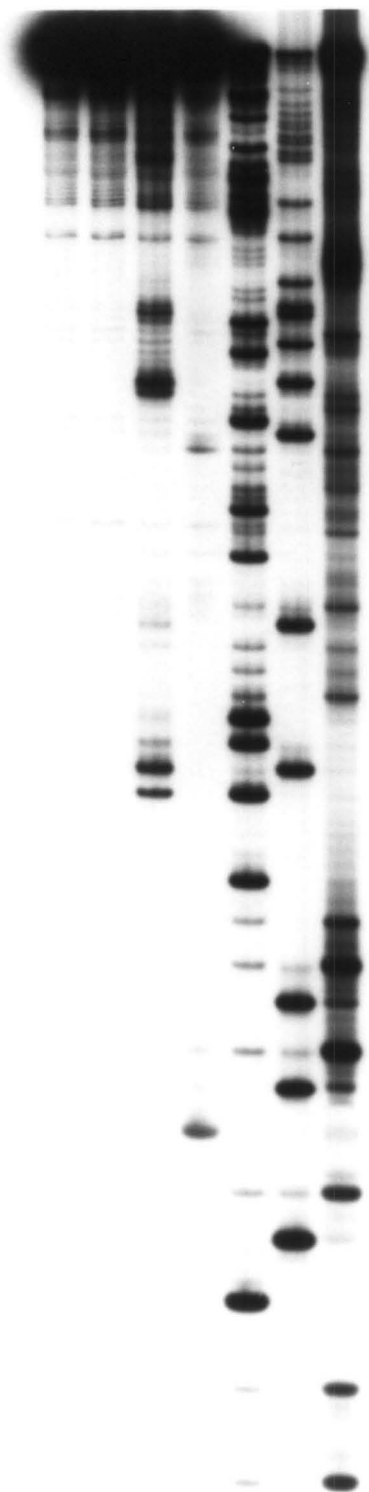
Comparison of the primary sequences of eukaryotic and prokaryotic 5S rRNAs led to the universal four-helix model that is now accepted to be the minimal secondary structure.¹⁴ For eukaryotic 5S rRNA, the model is extended to a five-helix model.¹⁵ These models have suggested the existence of G-U wobble pairs in helix I and helix IV of *Xenopus* oocyte 5S rRNA. A similar secondary structure model for *E.coli* 5S rRNA proposed the existence of a G-U mismatch in helix I, two in helix II, and two in helix IV.¹⁶ We have tested the recognition of $\text{Rh}(\text{DIP})_3^{3+}$ on both of these 5S rRNAs. As shown in Figure 6.3 (lane 4), strong site-selective cleavage by $\text{Rh}(\text{DIP})_3^{3+}$ occurs on *Xenopus* oocyte 5S rRNA at residues C112 and G85. These sites are different from those obtained with cleavage by $\text{Rh}(\text{phen})_2\text{phi}^{3+}$ (Figure 6.3, lane 3). As predicted, both C112 and G85 are located on the 3'-side of a U involved in G-U base pairing. Residue C112 is located in helix I adjacent to U111-G8, while G85 resides in helix IV next to U84-G93. Similarly, several of the proposed G-U mismatches in *E. coli* 5S rRNA are recognized by $\text{Rh}(\text{DIP})_3^{3+}$. In particular, strong cleavage is apparent at G112 (data not shown); weaker cleavage is observed at G81 in helix IV. The proposed secondary structure for *E. coli* 5S rRNA reveals that G112 is located on the 3'-side of U111, which base pairs with G9, while G81 lies on the 3'-side of U80-G96. It is interesting to note that G81 itself is involved in a G-U wobble pair with U95. However, no cleavage is apparent at G96, indicating that the adjacent G-U mismatches are not symmetric. Also, no cleavage is apparent at the other proposed G-U mismatches in helix II of *E. coli* 5S rRNA.

6.4. Discussion

The results for the cleavage by $\text{Rh}(\text{DIP})_3^{3+}$ on all the RNAs are summarized in Figure 6.4. As with $\text{Rh}(\text{phen})_2\text{phi}^{3+}$, the cleavage by $\text{Rh}(\text{DIP})_3^{3+}$ does not occur in standard double-helical nor single-stranded regions of the RNAs examined. Instead,

Figure 6.3. Cleavage of ^{32}P 3'-end-labeled 5S rRNA from *Xenopus* oocytes by $\text{Rh}(\text{DIP})_3^{3+}$. Cleavage was performed in 5 mM Tris, 50 mM NaCl, pH 7.0. Lane 1: RNA control without metal or irradiation. Lane 2: light control; 5S rRNA irradiated in the absence of metal. Lane 3: specific cleavage by $\text{Rh}(\text{phen})_2\text{phi}^{3+}$. Lane 4: specific cleavage by $\text{Rh}(\text{DIP})_3^{3+}$. Lanes 5-7: sequencing reactions on 5S rRNA; A-, U-, and G-specific reactions, respectively.

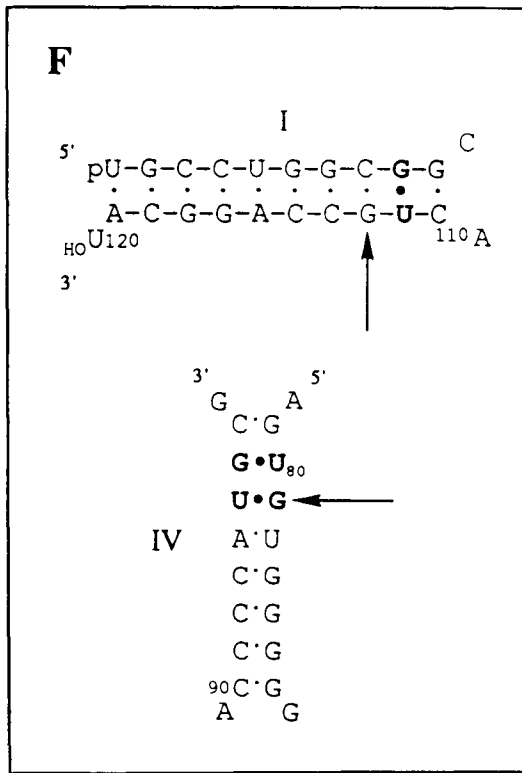
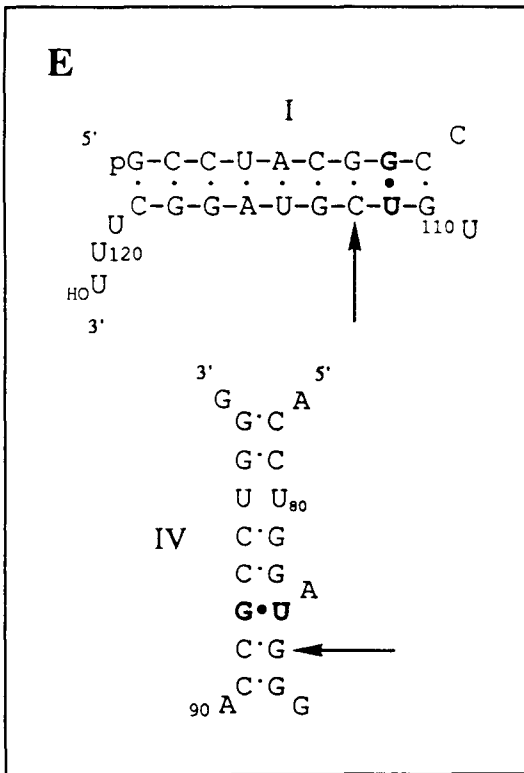
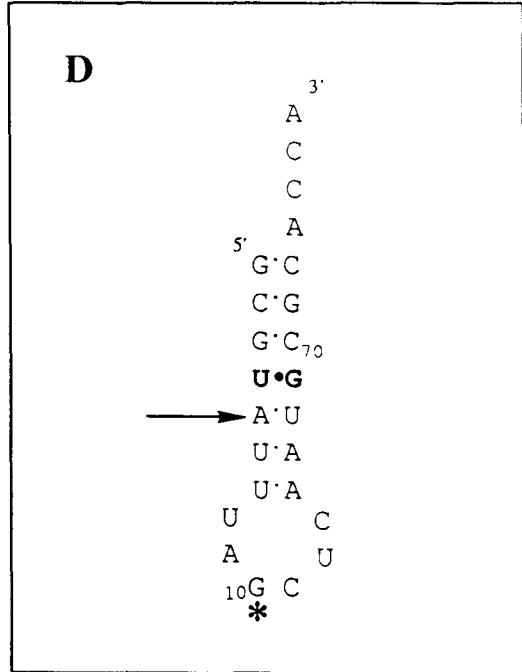
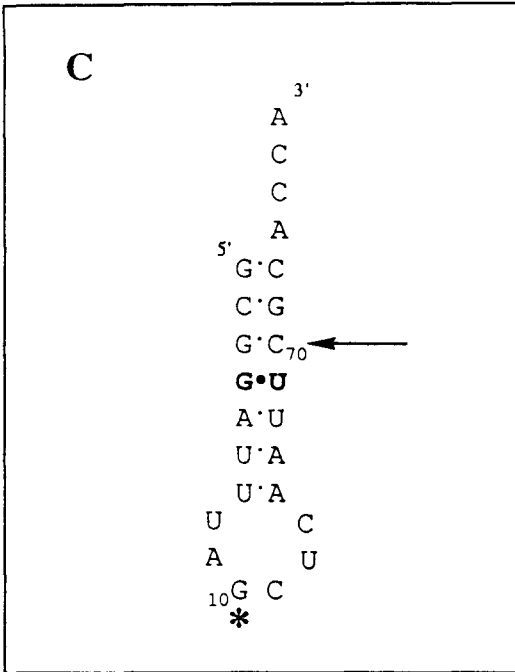
1 2 3 4 5 6 7



G85

C112

Figure 6.4. Schematic illustrations of yeast tRNA^{Phe} (A), yeast tRNA^{Asp} (B), G4:U69 microhelix^{Phe} (C), U4:G69 microhelix^{Phe} (D), helix I and helix IV of *Xenopus* oocyte 5S rRNA (E), and helix I and helix IV of *E. coli* 5S rRNA (F) with designations of Rh(DIP)₃³⁺ cleavage sites. The arrows indicate the positions of Rh(DIP)₃³⁺ promoted strand scission that lie adjacent to G-U mismatches. The large black dots represent G-U wobble pairs (and one G-Ψ mismatch in tRNA^{Asp}). The asterisks represent cleavage by Rh(DIP)₃³⁺ in loop regions.



cleavage is apparent at structured loop regions, such as the TΨC loop of yeast tRNA^{Phe} or the anticodon loop of yeast tRNA^{Asp}. We have also observed cleavage by Rh(DIP)₃³⁺ at a nucleotide adjacent to a G-U mismatch on yeast tRNA^{Phe}, yeast tRNA^{Asp}, G4:U69 microhelix^{Phe}, U4:G69 microhelix^{Phe}, *Xenopus* oocyte 5S rRNA, and *E. coli* 5S rRNA.

6.4.1. Recognition of Loop Structures in RNA by Rh(DIP)₃³⁺

Cleavage by Rh(DIP)₃³⁺ occurs at specific sites within the loop regions of RNA. In particular, strand scission is evident at Ψ55 in the TΨC loop of yeast tRNA^{Phe}, G34 in the anticodon loop of yeast tRNA^{Asp}, and G10 in the center of the six-nucleotide loop of both microhelix sequences. The crystal structures of the two tRNAs reveal that the TΨC and anticodon loops are single-stranded, yet the bases in the anticodon loop continue to stack in an A-like helical manner⁴ and the nucleotides in the TΨC loop are involved in long-range tertiary interactions with the D loop²⁻³. The nucleotides in the microhelix loop may stack in a similar manner as the anticodon loop residues in tRNA^{Asp}. Since not all loop residues are cleaved by the metal complex, the recognition of Rh(DIP)₃³⁺ is likely governed by specific tertiary structures within the RNA loops.

Cleavage at Ψ55 on yeast tRNA^{Phe} by Rh(DIP)₃³⁺ must depend on the precise folding of the D and TΨC loops, since no cleavage at this site is apparent on a tRNA^{Phe} transcript containing no modified bases¹⁷ (data not shown). Similarly, no cleavage was apparent by Rh(DIP)₃³⁺ at U55 on a series of tRNA^{Phe} mutants¹⁸ that were examined. These results are consistent with cleavage by the rhodium complex on DNA cruciforms¹³ and other unusual DNA structures¹⁹. The complex likely binds in a hydrophobic pocket between charged helices of the DNA or RNA. Results in our laboratory have indicated that the rhodium complex is very sensitive to small changes in the DNA structure, which depends upon exact salt concentrations, buffer conditions, and temperatures.¹⁹ Work is currently being conducted by I. Lee to examine the interaction of Rh(DIP)₃³⁺ with these

DNA structures in order to gain an understanding of the influences on recognition by the metal complex. In addition, in our laboratory K. Waldron is attempting to obtain a crystal structure of $\text{Rh}(\text{DIP})_3^{3+}$ bound to a double-stranded DNA oligonucleotide. Together these results may provide clues as to DNA, as well as RNA, recognition characteristics of the metal complex.

6.4.2. Recognition of G-U Mismatches in RNA by $\text{Rh}(\text{DIP})_3^{3+}$

We have observed cleavage by $\text{Rh}(\text{DIP})_3^{3+}$ at a nucleotide adjacent to a G-U mismatch on six different RNAs. As summarized in Figure 6.4, C70 in tRNA^{Phe} , C70 in G4:G69 microhelix^{Phe}, A5 in U4:G69 microhelix^{Phe}, C112 and G85 in 5S rRNA from *Xenopus* oocytes, and G112 in 5S rRNA from *E. coli* are strong cleavage sites; weak cleavage at G41 of tRNA^{Asp} is also apparent. Importantly however, not all G-U mismatches in these RNAs were recognized by the metal complex. No cleavage was apparent at the proposed G-U mismatches in helix II of *E. coli* 5S rRNA or at three of the four G-U mismatches in tRNA^{Asp} .

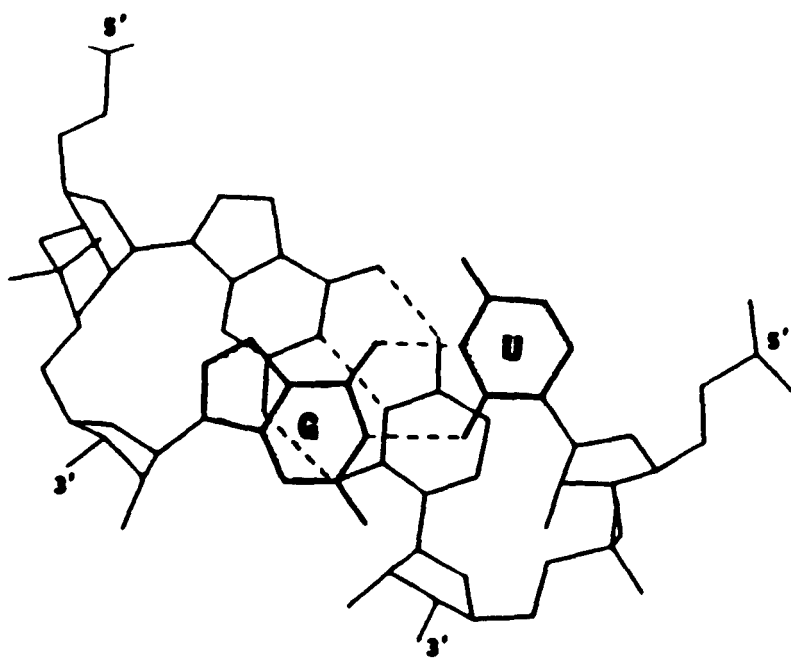
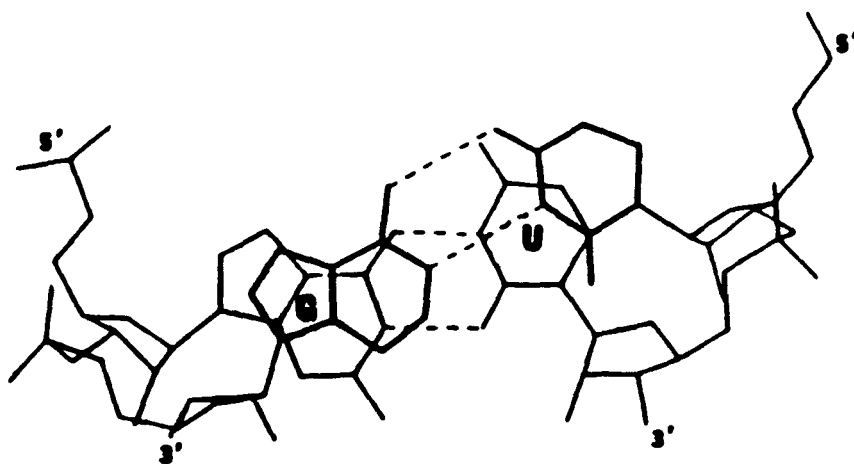
The cleavage by $\text{Rh}(\text{DIP})_3^{3+}$ also occurs specifically at C70 on a series of tRNA^{Phe} mutants (data not shown). Mutations in the D stem, D loop, or the T Ψ C loop of tRNA^{Phe} have no effect on cleavage at the G-U site in the acceptor stem. Also, the cleavage always occurs at the residue located on the 3'-side of U, regardless of the nucleotide composition of that site or the flanking sites. However, different intensities at the observed cleavage sites may reflect the subtle changes in structure associated with different bases at these sites. In addition, a double band is apparent at A5 of U4:U69 microhelix^{Phe}, suggestive of a secondary reaction mechanism, which is particular to this site. The different cleavage chemistry at this site may be a reflection of a different binding mode for the metal complex, which depends on this particular sequence of RNA. Our results indicate that the interaction of $\text{Rh}(\text{DIP})_3^{3+}$ with tRNA^{Phe} is dependent only upon a structure located within the

acceptor helix. RNA hairpin helices have been designed to correspond to this region of the molecule, and identical cleavage with $\text{Rh}(\text{DIP})_3^{3+}$ is observed. Furthermore, the recognition seems to depend only on the G-U mismatch. When the G4-U69 mismatch is switched to a U4-G69 mismatch, the cleavage occurs on the opposite side of the helix, just two nucleotides away from cleavage observed on the G4:U69 microhelix and consistently at the 3'-side of U.

The observed differences in the recognition of these sites by $\text{Rh}(\text{DIP})_3^{3+}$ may be rationalized because of the remarkably different base stacking interactions with the Watson-Crick base pairs situated on either side of the G-U mismatch. As shown in Figure 6.5, the G-U base pair exhibits greater stacking interactions with the Watson-Crick base pair following it on the 5'-side of U than the Watson-Crick pair preceding it on the 3'-side of U.⁵ The former corresponds to the "3'-end G-U" base pair, the latter to the "5'-end G-U" base pair. The 5'-end G-U exhibits stacking interactions similar to the stacking of two normal Watson-Crick base pairs. In contrast, the 3'-end G-U base pair does not stack well with the flanking base pair and the wobble paired U residue is pushed away from the helix interior into the major groove of the RNA. The $\text{Rh}(\text{DIP})_3^{3+}$ cleavage sites adjacent to the G-U mismatches all exhibit stacking of the 3'-end G-U base pair type, in which the G-U pair is offset from the adjacent Watson-Crick pair. Our results indicate that this stacking interaction is important for recognition by the rhodium complex. Perhaps, as seen in Chapters 4 and 5 with $\text{Rh}(\text{phen})_2\text{phi}^{3+}$, it is the extension of the normally deep and narrow major groove away from the normal base-pair stack that provides a favorable site for interaction with the metal complex. However, since $\text{Rh}(\text{phen})_2\text{phi}^{3+}$ does not exhibit cleavage at these sites, other factors involving the different shape of the molecule must be important in the unique recognition of G-U mismatches by $\text{Rh}(\text{DIP})_3^{3+}$.

In the case of tRNA^{ASP} , no cleavage is observed with $\text{Rh}(\text{DIP})_3^{3+}$ at any of the mismatch sites, U5-G68, G10-U25, or Ψ 13-G22. For the latter two mismatches, the base

Figure 6.5. Stacking of the G4-U69 wobble pair in the middle of the acceptor stem of yeast tRNA^{Phe} with the G3-C70 base pair and with the A5-U68 base pair. The former corresponds to the "3'-end G-U" base pair type, while the latter corresponds to the "5'-end G-U" base pair type. This figure is adapted from Reference 5.

**3'-end G-U****5'-end G-U**

pairs are located at either end of the D stem. Mizuno and Sundaralingam⁵ have shown that the unusual stacking properties of G-U mismatches have special repercussions at the ends of RNA helices. At a helix with a U-G pair stacked in a 5'-end G-U fashion with its neighboring base pair, the last two base pairs are stacked well. Both mismatches, Ψ13-G22 and G10-U25, are orientated in a 5'-end G-U manner, and therefore no interaction with the metal complex is expected. For the U5-G68 pair in the acceptor stem of tRNA^{Asp}, we would expect cleavage at G6. However, strand scission at this site does not occur. Perhaps this particular site is hindered from interaction with Rh(DIP)₃³⁺ since it lies only two base pairs away from the D and TΨC stems. The folding of these two arms may create a structure that will prohibit binding by Rh(DIP)₃³⁺ at G6.

No cleavage is apparent at the proposed G-U mismatches in helix II of *E. coli* 5S rRNA. It is difficult to rationalize the lack of cleavage at these sites, since little is known about the tertiary folding of this RNA. To better understand the influences of the rest of the molecule on binding the metal complex, it is necessary to consider cleavage by Rh(DIP)₃³⁺ on an oligoribonucleotide representing helix II as we have done with the tRNA acceptor stem. Without these experiments, no conclusions can be drawn as to the lack of cleavage of these particular G-U mismatched sites.

Finally, unusual cleavage by Rh(DIP)₃³⁺ is observed at G81 in helix IV of *E. coli* 5S rRNA. This residue lies to the 3'-side of U80-G96; however, G81 itself is involved in a G-U mismatch. No cleavage is apparent at G96, which lies to the 3'-side of U95-G81. Apparently, the stacking for adjacent mismatched base pairs is not the same as the stacking between a G-U mismatch and a Watson-Crick base pair. Our results indicate an asymmetry at this site since cleavage is observed at only one of the two G-U mismatches.

6.4.3. Implications for Protein Binding

Internal G-U mismatches are quite common features that occur in tRNA and in the proposed secondary structures of other RNAs. In studies of RNA-protein interactions, it has been established that G-U mismatches are important for specifying distinct functions in the RNA, such as determining the identity of tRNA in the aminoacylation reaction.⁶⁻⁹ A G-U wobble may influence the acceptor identity of certain tRNAs by introducing an irregularity in the acceptor helix of the molecule. It has been revealed by crystal structures of tRNA^{Phe} and tRNA^{Asp} from yeast that G-U mismatches can offer some polarity to the helical regions of an RNA molecule, although these particular G-U mismatches do not seem important in the recognition of the associated tRNA synthetases.

The stacking interactions on either side of the G-U mismatch differ greatly, with the base pair on the 3'-side of the U exhibiting highly destacked structures with the U extended into the major groove of the RNA. It seems that Rh(DIP)₃³⁺ is able to detect these differences in base stacking with the flanking Watson-Crick base pairs. In the case of a protein, a functional group on the G-U wobble pair may contribute to the specific interactions with amino acid side chains. However, Rh(DIP)₃³⁺ must recognize the G-U mismatches on the basis of shape considerations. The rhodium complex contains no hydrogen bonding groups, ruling out a hydrogen bonding interaction with O-4 of the U that protrudes into the major groove. It is possible that G-U mismatches may lead to a destabilization of the helical regions, which are important for protein recognition and similarly for recognition by Rh(DIP)₃³⁺. Nonetheless, it appears that variations in the secondary structure of RNA that result in tertiary base interactions, such as G-U mismatches, are important for recognition by the rhodium complex and likewise may be important for RNA-protein interactions.

References

1. Crick, F. H. C. *J. Mol. Biol.* **1966**, 19, 548-555.
2. Kim, S.-H.; Sussman, J. L.; Suddath, F. L.; Quigley, G. J.; McPherson, A.; Wang, A. H.; Seeman, N. C.; Rich, A. *Proc. Natl. Acad. Sci. U.S.A.* **1974**, 71, 4970-4974.
3. Quigley, G. J.; Rich, A. *Science* **1976**, 194, 796-806.
4. Westhof, E.; Dumas, P.; Moras, D. *J. Mol. Biol.* **1985**, 184, 119-145.
5. Mizuno, H.; Sundaralingam, M. *Nucleic Acids Res.* **1978**, 5, 4451-4461.
6. Hou, Y.-M.; Schimmel, P. *Nature* **1988**, 333, 140-145.
7. Hou, Y.-M.; Schimmel, P. *Biochemistry* **1989**, 28, 6800-6804.
8. Francklyn, C.; Schimmel, P. *Nature* **1989**, 337, 478-481.
9. McClain, W. H.; Foss, K. *Science* **1988**, 240, 793-796.
10. Usman, N.; Ogilvie, K. K.; Jiang, M.-Y.; Cedergren, R. J. *J. Am. Chem. Soc.* **1987**, 109, 7845-7854.
11. England, T. E.; Uhlenbeck, O. C. *Nature* **1978**, 275, 560-561.
12. Peattie, D. A. *Proc. Natl. Acad. Sci. U.S.A.* **1978**, 76, 1760-1764.
13. Kirshenbaum, M. R.; Tribolet, R.; Barton, J. K. *Nucleic Acids Res.* **1988**, 16, 7943-7960.
14. Fox, G. E.; Woese, C. R. *Nature* **1975**, 256, 505-506.
15. Luehrsen, K. R.; Fox, G. E. *Proc. Natl. Acad. Sci. U.S.A.* **1981**, 78, 2150-2154.
16. Pieler, T.; Erdmann, V. A. *Proc. Natl. Acad. Sci. U.S.A.* **1982**, 79, 4599-4603.
17. Sampson, J. R.; Uhlenbeck, O. C. *Proc. Natl. Acad. Sci. U.S.A.* **1988**, 85, 1033-1037; Hall, K. B.; Sampson, J. R.; Uhlenbeck, O. C.; Redfield, A. G. *Biochemistry* **1989**, 28, 5794-5801.

18. Sampson, J. R.; DiRenzo, A. B.; Behlen, L. S.; Uhlenbeck, O. C. *Biochemistry* **1990**, *29*, 2523-2532.
19. Lee, I., unpublished results.

Chapter 7:

Conclusions and Future Directions

This study presents an approach to understanding the three-dimensional folding of RNA molecules using transition metal complexes. A system is examined which entails the binding of inorganic coordination complexes that have been designed in our laboratory to the structurally well-characterized tRNA. These probes, derived from the parent tris(phenanthroline) metal complex, are involved in noncovalent interactions with RNA, which can be manipulated by changing the ligands on the metal center or by altering the ligand substituents. The concept underlying this work is that the metal complexes have fixed geometries and exhibit a variety of spectroscopic properties. The changes that occur in these properties upon RNA binding are well suited for investigations of the interactions of the complexes with RNA. We have shown that there are significant differences in the manner in which the metal complexes can bind to tRNA, which appear to be dependent upon the shape of the complex. Thus, a comparison of the spectroscopic properties of each of the different complexes bound to tRNA has afforded a basis for the development of structure-specific probes for RNA.

Furthermore, upon photoactivation the metal complexes have the ability to promote DNA or RNA strand scission at their binding sites. By coupling the photoreactivity to the shape of the metal complex, we have obtained a series of site-specific RNA cleaving agents. Evidence presented in this study indicates that the cleavage chemistry on RNA is likely the same as that found on DNA. RNA-induced cleavage by the complexes of rhodium(III) appears to occur through an oxidative pathway, while cleavage reactions by ruthenium(II) complexes are mediated by singlet oxygen. This work demonstrates that while changes in the ligand environment of the coordination complex can affect specific binding, changes in the metal center can affect the chemistry of strand scission. This is

important in order to identify all of the possible binding modes to structured RNA. For example, we have shown that complexes of rhodium(III) cleave by a direct abstraction of the C3'-H of the sugar moiety, which is accessible from the major groove of the RNA. In contrast, a metal complex bound on the surface of the minor groove of RNA cannot promote strand scission by this mechanism. However, a reaction mediated by a diffusible species, such as singlet oxygen that has been sensitized by complexes of ruthenium(II), can occur.

Finally, we have used shape-selective cleavage by transition metal complexes to explore the tertiary structures of a series of RNA molecules. In particular, we have found that the cleavage patterns produced by two complexes, $\text{Rh}(\text{phen})_2\text{phi}^{3+}$ and $\text{Rh}(\text{DIP})_3^{3+}$, are very different, despite the similar reactivity of the two complexes. Cleavage by $\text{Rh}(\text{phen})_2\text{phi}^{3+}$ appears to depend upon the tertiary folding of the RNA. This complex targets tertiary structures such as D-T Ψ C loop interactions, triply bonded regions, and helix-loop junctions in folded yeast tRNA^{Phe} and tRNA^{Asp} in which the major grooves are open and accessible for stacking. Nucleotide changes that either disrupt or maintain the tertiary interactions of tRNA reveal the dependence of site-recognition on tertiary structure rather than upon nucleotide composition. $\text{Rh}(\text{DIP})_3^{3+}$ has also been shown to target sites in tRNA involved in tertiary interactions. This complex has the unique ability to target G-U mismatches located in an RNA double-helix. With studies on tRNA as a foundation, we have explored the three-dimensional folding of 5S rRNA from *Xenopus* oocytes. Our results with $\text{Rh}(\text{phen})_2\text{phi}^{3+}$ support a model for 5S rRNA that involves independent helical domains containing structured loop regions. In 5S rRNA, stem-loop junctions, helix bulges containing more than one unmatched nucleotide, as well as base-pair mismatches, appear to provide open major grooves.

Overall, both $\text{Rh}(\text{phen})_2\text{phi}^{3+}$ and $\text{Rh}(\text{DIP})_3^{3+}$ have been shown to be useful reagents. In certain cases, their recognition properties may be related to the recognition of

RNA by proteins. However, more work is necessary to reveal the principles of binding to RNA by these complexes. With tRNA and 5S rRNA cleavage as a foundation, studies with model systems can be performed. For example, oligoribonucleotides can be synthesized, which represent specific structures found in native tRNA or 5S rRNA. The information gained from these studies may eventually lead to the rational design of biologically useful complexes. For example, certain metal complexes may be useful as chemotherapeutic agents if they can target specific sites along an RNA molecule. Alternatively, the complexes may serve as useful probes for the study of more intricate RNA structures and may offer information on how proteins interact with RNA.